The Dissertation Committee for Michael Joseph Maher Certifies that this is the approved version of the following dissertation:

Next Generation Materials for Block Copolymer Lithography

Committee:

C. Grant Willson, Supervisor

Christopher Ellison

Hung-wen Liu

Eric Anslyn

Chris Mack

Next Generation Materials for Block Copolymer Lithography

by

Michael Joseph Maher, B.A.

Dissertation

Presented to the Faculty of the Graduate School of

The University of Texas at Austin

in Partial Fulfillment

of the Requirements

for the Degree of

Doctor of Philosophy

The University of Texas at Austin

May 2016

Dedication

This dissertation is dedicated to my family and friends.

Acknowledgements

I would like to thank Professor Grant Willson for being the best advisor one could ask for. I would also like to thank my unofficial advisor, Professor Christopher Ellison, for guidance and support. I am thankful to have been a part of their research groups. I am honored to have worked side-by-side with such great coworkers, outstanding undergraduates, and friends. Much of the research presented here would not be possible without the contributions from Dr. Christopher Bates, Dr. William Durand, Gregory Blachut, Takehiro Seshimo, Kazunori Mori, Austin Lane, Sunshine Zhao, Yusuke Asano, Dr. Julie Cushen, Christopher Chen, Colin Hayes and Logan Santos. I thank the undergraduates that I have worked with: Matthew Carlson, Jeffrey Self, Summer Tein, and Andrew Dinhobl. I would like to thank our industrial collaborators: Dr. Steve Sirard from Lam, Dr. Ricardo Ruiz from HGST, Dr. XiaoMin Yang from Seagate, and Dr. Dan Sanders, Dr. Joy Cheng, and Dr. Charles Rettner from IBM.

I thank the rest of the Willson group for making everyday interesting and fun. I am especially thankful for all for their support, guidance, and friendship. I would also like to thank our secretaries, Donna Martin and Kathleen Sparks, whose efforts keep the group moving forward. I would like to thank IBM and the National Science Foundation for financially supporting my graduate studies.

Finally, I reserve the biggest acknowledgement for my wife, Leslie, for her continuous love and support.

Next Generation Materials for Block Copolymer Lithography

Michael Joseph Maher, Ph.D.

The University of Texas at Austin, 2016

Supervisor: C. Grant Willson

The electronics industry is a trillion dollar industry that has drastically changed everyday life. Advances in lithography have enabled manufacturers to continually shrink the dimensions of microelectronic components, which has resulted in devices that outperform previous generations. Unfortunately, conventional patterning techniques are approaching their physical resolution limits. The ability to economically pattern sub-10 nm features is necessary for the future growth of the industry. Block copolymer self-assembly has emerged as a leading candidate for next generation lithography and nanofabrication because block copolymers self-assemble into periodic nanostructures (e.g. cylinders and lamellae) on a length scale that exceeds the physical limits of optical lithography. However, for block copolymer lithography to be realized, the block copolymer domains need to form sub-10 nm features and display etch resistance for pattern transfer. Additionally, the orientation, alignment, and placement of block copolymer domains must be carefully controlled.

This dissertation discusses the synthesis, orientation and alignment of silicon-containing BCPs that are inherently etch resistant and provide access to nanostructures in the sub-10 nm regime. The orientation of domains is controlled by interactions between each block copolymer domain and each interface. Preferential interactions between the block copolymer domains and the either the substrate or air interface lead to a parallel

orientation of domains, which is not useful for lithography. Non-preferential ("neutral") interactions are needed to promote the desired perpendicular orientation. The synthesis of surface treatments and top coats is described, and methods to determine the preferential and non-preferential interactions are reported. Orientation control is demonstrated via rapid thermal annealing between two neutral surfaces. Combining orientation control of block copolymer domains with well established directed self-assembly strategies was used to produce perpendicular domains with long range order.

Chapter 1 provides an introduction to lithography and block copolymer self-assembly. Chapter 2 discusses the synthesis of silicon-containing block copolymers. Chapters 4-6 focus on controlling block copolymer domain orientation, and Chapter 7 focuses on directed self-assembly. Chapter 8 covers spatial orientation control of domains using photopatternable interfaces. Finally, Chapter 9 covers tin-containing polymers that are resistant to fluorine-containing etch chemistries and can be used to pattern silicon oxide.

Table of Contents

List of Tables

List of Figures

List of Schemes

Chapter 1: Patterning in Microelectronics

1.1 Historical Perspective

Programmable computers have fundamentally changed every aspect of modern society. One of the first programmable computers was developed in 1943. It was known as the Colossus (Figure 1.1) and was designed to help analyze enciphered German radio transmissions during World War II.[1] Far different than modern computers today, the Colossus was several meters tall, weighed over a ton, consumed large amounts of power, and relied on delicate vacuum tubes.[2] The computing power of early vacuum tube computers was very limited from today's perspective. Although they were far from practical, the potential and opportunities to advance the technology were great.

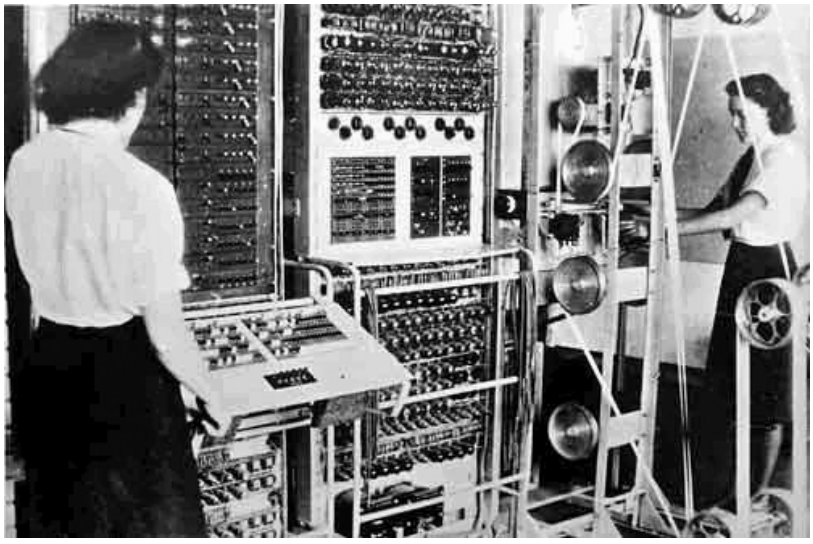

Figure 1.1: The Colossus Mark 2 assembled in 1944. Reproduced with permission from the National Archives under Open Government Licence v3.0. Catalogue reference: FO 850/234.

The invention of the transistor by Bardeen, Brattain, and Shockley at Bell labs in 1947 was a pivotal moment in history.[3] The point-contact transistor (Figure 1.2A) was made from germanium and was the first solid-state semiconductor device. It inspired the development of silicon transistors (Figure 1.2B), which quickly replaced vacuum tubes. These transistors were smaller and used less power than vacuum tubes, which allowed computers to become smaller, faster, and more reliable.

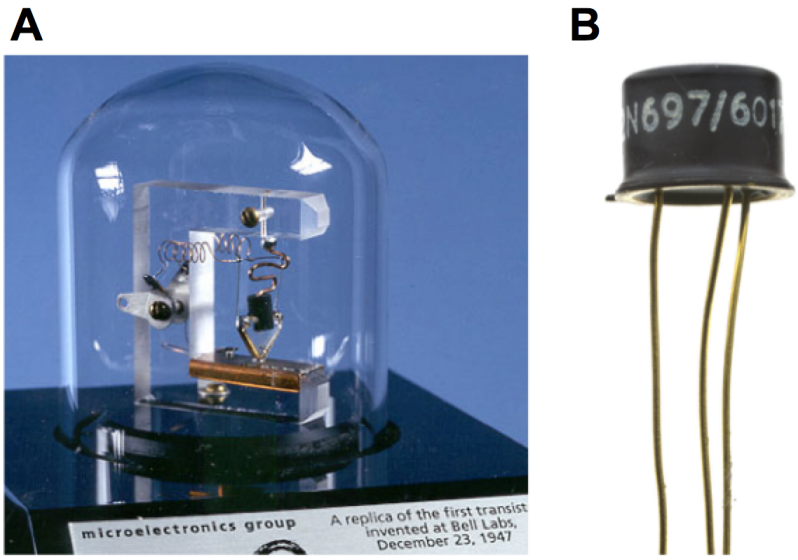

Figure 1.2: **A)** Replica of the Bell Lab's solid state point-contact transistor. **B)** Fairchild's 2N697 transistor

In 1958, the integrated circuit (IC) was independently co-invented by Robert Noyce at Fairchild Semiconductor and Jack Kilby at Texas Instruments (Figure 1.3).[4] The IC replaced individual transistor components with a design based on interconnecting several devices on a single piece of semiconducting material. Soon after Kilby, Robert Noyce and his team at Fairchild developed the planar transistor, which was more space efficient, cheaper to fabricate, and consumed less power. In 1960, the number of

transistors per IC was only four, a momentous achievement at the time. Exponential growth and innovation in the semiconductor field occurred throughout the 1960's, and on average, the transistor density in an IC doubled every year. Gordon Moore, a cofounder of Fairchild and Intel, predicted that this trend would continue. The device scaling as a function of time has become known as "Moore's Law".[5] Today, more than 50 years after the first IC, semiconductor companies are manufacturing microprocessors that contain more than 1 billion transistors (Figure 1.4).

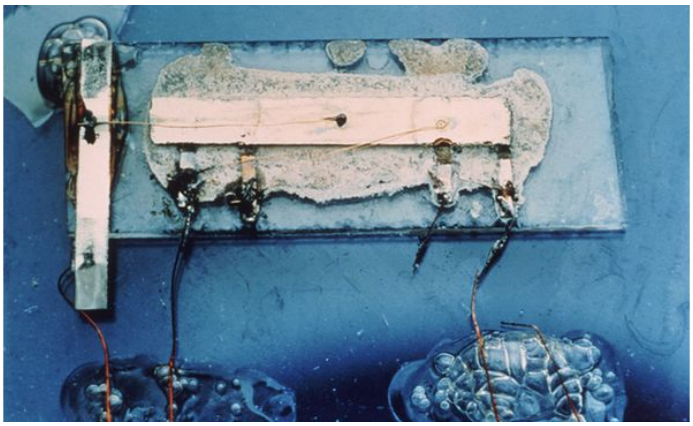

Figure 1.3: Jack Kilby's integrated circuit (Courtesy of Texas Instruments).

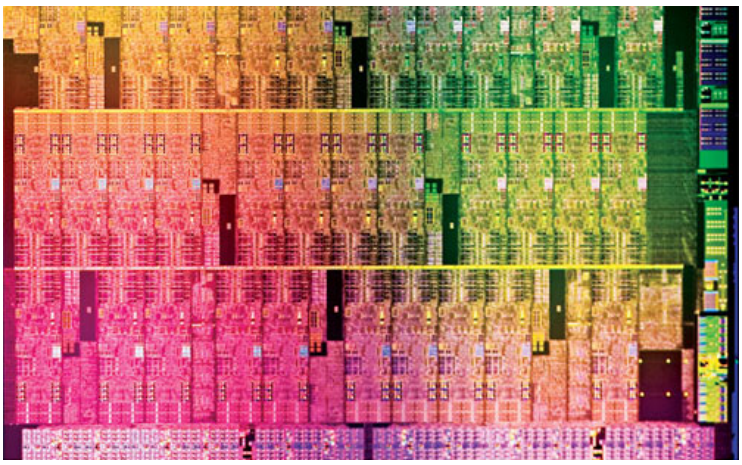

Figure 1.4: Modern Intel microprocessor.

To increase the density of transistors in ICs, the transistor size must become smaller. Figure 1.5 shows the transistor density and the feature size over time.[6] In the 1970s, transistors were on the order of microns in size. Today, the critical dimensions of transistors are on the order of 30 nm. Device scaling and semiconductor manufacturers' ability to make better products at the same price point is directly responsible for the computer-integrated modern society. Extending Moore's Law is required to continue device scaling, which hinges on the ability to pattern microelectronic devices with transistors and other semiconductor components on length scales less than 30 nm. Access to the sub-10 nm node is the "Holy Grail" of the microelectronics industry, but it is beyond the current physical limitations of high-volume manufacturing capabilities.

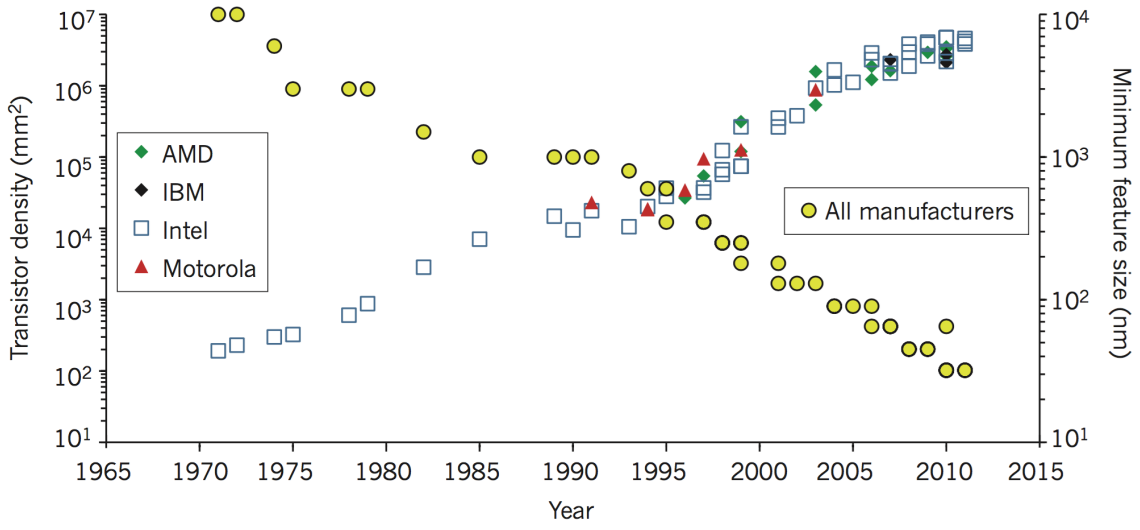

Figure 1.5: Transistor density and minimum feature size as a function of year. Reprinted by permission from Macmillan Publishers Ltd: Ferain *et al*. *Nature* **2011**, *479*, 310–316. Copyright 2011.

1.2 PHOTOLITHOGRAPHY

Optical photolithography is the state-of-the-art patterning technique that enables the patterning of complex microelectronic devices.[7] Photolithography uses polymer formulations known as photoresists, which contain photosensitive species or polymers with photolabile functional groups that change the solubility properties of the polymer upon exposure to UV-light (e.g. at a wavelength of 193 nm). Figure 1.6 illustrates the two common photolithographic processes, positive and negative tone development. First, a photoresist is spin coated as a thin film (50-100 nm thick) onto a substrate. Then, the photoresist is exposed to light in selected regions using a mask. In the exposed regions, a chemical change occurs that causes a solubility switch. In positive tone resists, the *exposed* regions are developed away by exposure to a selective solvent. In negative tone resists, the *unexposed* regions are developed. In both cases, the differences in solubility enable patterning topographical structures in an area-selective manner. The topographical pattern can be transferred into the underlying substrate by exploiting etch rate differences between the photoresist and substrate. Stripping the photoresist in developer yields a patterned substrate. Through many lithographic steps and other semiconductor manufacturing processes, complex three-dimensional transistors can be fabricated.

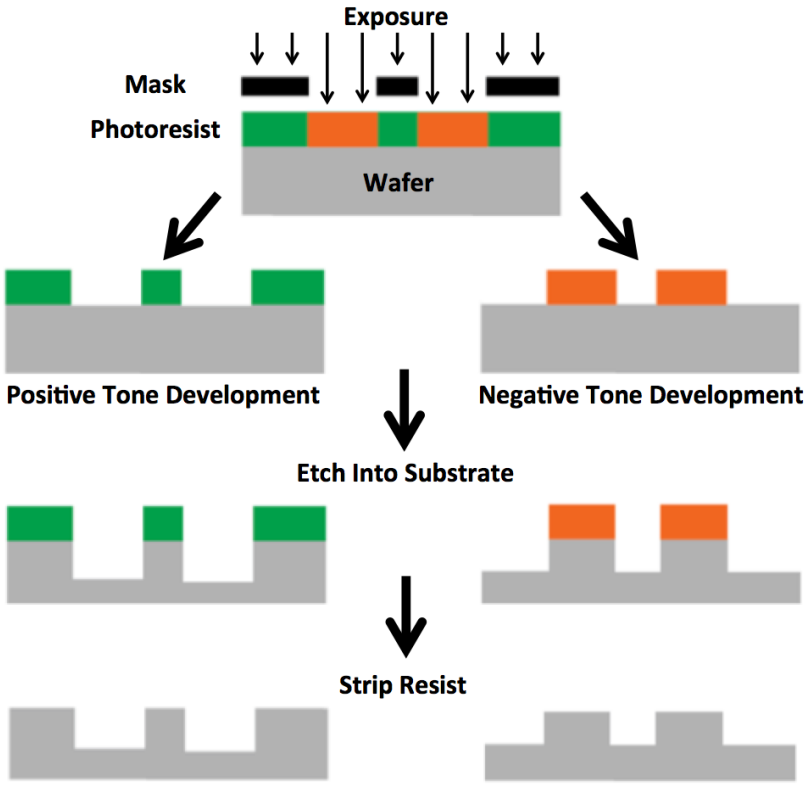

Figure 1.6: Schematic of the photolithographic process. The left side shows positive-tone development and the right side shows negative tone development.

The dimensions of the patterned features depend on the resolution limit, which is governed by the Raleigh's equation (Eq.1).[7]

$$R = k_1 \frac{\lambda}{NA} \qquad \text{Eq. 1}$$

In the equation, R is feature size, k_1 is an optimized process coefficient, λ is the wavelength of light, and NA is the numerical aperture. Extensive research in the field has optimized k_1 and NA to their physical limitations and they cannot be improved. Therefore, the only way to minimize R is to reduce the wavelength of light.[8] Currently, 193 nm light

is used for patterning microelectronics, which results in a resolution limit of about 40 nm (half-pitch). Patterning smaller features with optical lithography is becoming increasingly infeasible from an economics perspective. Next-generation tools that use 13.5 nm light (EUV lithography) are expected to cost over 100 million USD. It should also be noted that competitive fabrication facilities need several tools to keep production at volume high. Every process that uses EUV increases the overall cost.[9] EUV is not ready for high volume manufacturing because it does not have a powerful enough light source and simply cannot pattern enough wafers per hour to be profitable.[10]

In order to keep Moore's Law alive, alternative lithographic methods are required. Clever "engineering tricks" such as self-aligned double patterning have enabled semiconductor manufacturers to produce transistors below 40 nm (half-pitch). However, pattern multiplication schemes increase cost and complexity, both of which are currently precluding quadruple patterning and octuple patterning from being realized.[11] To date, there are no cost-effective ways to access features with dimensions below 10nm (half-pitch). The focus of this dissertation is on the self-assembly of block copolymers, which is currently one of the leading candidates to supplement 193nm lithography, because they form periodic nanostructures in the sub-10 nm regime that might be useful for production of semiconductor devices.

1.3 Block Copolymer Self-Assembly

1.3.1 Basics

The simplest block copolymers are AB diblock copolymers, which consist of two chemically incompatible polymers that are covalently bonded together at a junction. The most studied block copolymer, poly(styrene-*block*-methylmethacrylate) (PS-PMMA), is shown in Figure 1.7. Polystyrene and poly(methylmethacrylate) are immiscible, which creates a driving force for the blocks to phase-separate.[12] Phase-separation results in periodic structures on the nanoscale (3-100 nm), which far exceeds the resolution limit of optical lithography.

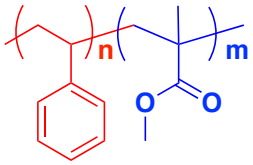

Figure 1.7: Poly(styrene-*block*-methylmethacrylate), the most studied block copolymer for lithography.

In bulk, block copolymers can form lamellae, cylinders, spheres, and gyroid networks.[12] The lamellar (line/space) morphology is particularly interesting for lithographic applications,[13] and is characterized by symmetric, alternating phases of block A and block B with a periodicity (i.e. pitch), L_0. The block copolymer morphology can be controlled by three synthetic variables: the overall degree of polymerization (N), the relative volume fraction of each block (f_A, f_B), and the block-block interaction parameter (χ). The degree of polymerization and volume fraction can be controlled by polymerization stoichiometry. The interaction parameter is determined by monomer choice and is difficult to predict *a priori*. As a general rule, χ increases as the blocks

become increasingly incompatible. For example, a block copolymer consisting of a hydrophilic block and hydrophobic block will likely have a higher χ value than a block copolymer consisting of two hydrophilic blocks. The interplay of N, f and χ can be seen in the phase diagram for an AB diblock copolymer (Figure 1.8),[14,15] which plots segregation strength (χN) against volume fraction (f). If the segregation strength is not greater than the order-disorder transition (ODT, χN = 10.5), the block copolymer is disordered and does not form well-defined, periodic structures. If χN is greater than the ODT, the block copolymer assumes one of the ordered morphologies depending on the volume fraction of each block (Figure 1.9). Since the lamellar morphology is preferred, the primary focus of this dissertation will be on block copolymers where $f_A \approx f_B$.

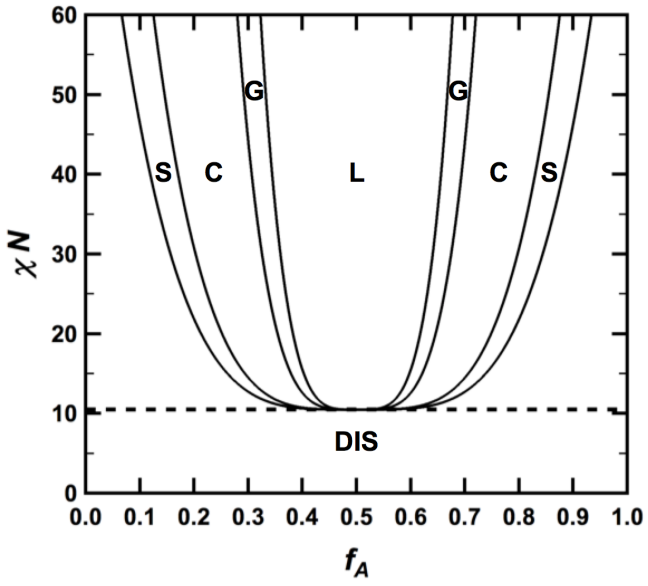

Figure 1.8: Phase diagram for a diblock copolymer. The ODT is at 10.5. Abbreviations: S=spheres, C=cylinders, G=gyroid, L=lamellae, DIS=disordered. Adapted from Cochran *et al*. *Macromolecules* **2008**, *39*, 2449-2451.[15]

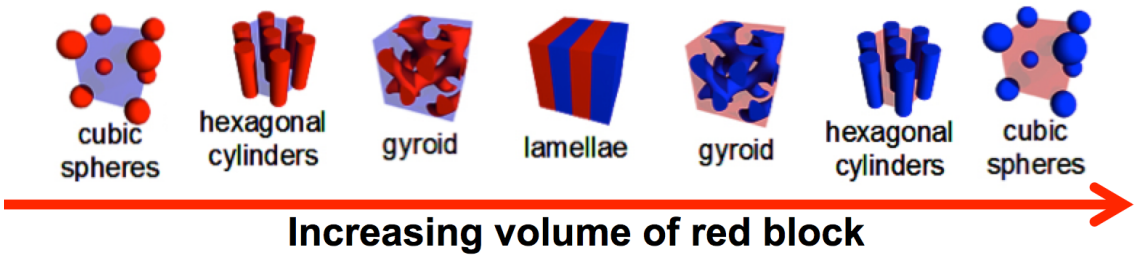

Figure 1.9: Block copolymer morphologies.

1.3.2 Thin Film Self-Assembly

The ideal lithographic process using block copolymers is shown in Figure 1.10. First, the block copolymer is spin coated onto a substrate. In the as-cast state, the block copolymer is not fully self-assembled and is kinetically trapped. Solvent annealing or thermal annealing can be used to induce phase separation. With all considerations equal, thermal annealing is preferred over solvent annealing because it is more controllable, uses existing equipment, accesses thermodynamically favored morphologies/orientations, and can be accomplished on the sub-minute time scale. For a review on solvent annealing of block copolymers, the reader is directed elsewhere.[16] Thermal annealing above the glass transition temperatures (T_g) of the blocks allows the block copolymer to phase separate into periodic domains. Selective removal of one of the domains *via* an etch process results in a topographical line/space image, which can be transferred into a functional substrate. Each line and space has a width of approximately 0.5 L_0.

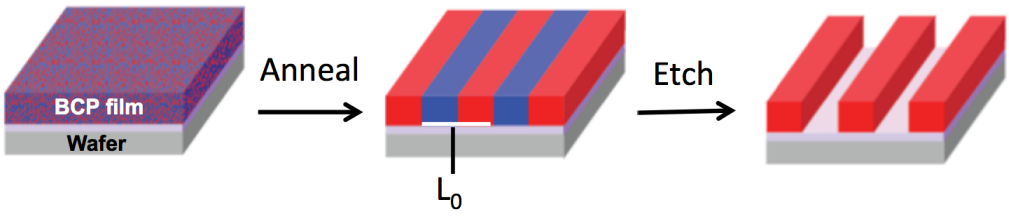

Figure 1.10: Block copolymer self-assembly in thin films.

1.3.3 Directed Self-Assembly

The self-assembly of block copolymer in thin films does not spontaneously yield structures that are useful for the microelectronics industry. For example, the orientation of PS-PMMA on a silicon wafer results in a "fingerprint pattern" (Figure 1.11a).[17] There is no driving force for the block copolymer to form well-aligned, useful arrays. To solve this problem, directed-self assembly (DSA) techniques have been developed to control the long-range alignment of block copolymer domains. To various degrees of success, this has been demonstrated by in-plane electric fields,[18] heterogeneous surfaces,[19] temperature gradients,[20] physical pre-patterns (grapho-epitaxy),[21,22] and chemical patterned surfaces (chemo-epitaxy).[17,23,24] The latter two methods are preferred because they are compatible with existing lithographic processes. Figure 1.11b shows a scanning electron microscopy (SEM) image of PS-PMMA annealed on a chemically patterned surface. The chemical patterns have a preference for one of the block copolymer domains, which creates a driving force for the fingerprint pattern to straighten out and follow the chemically patterned guidelines. The exclusive focus of Chapter 7 will be on DSA techniques.

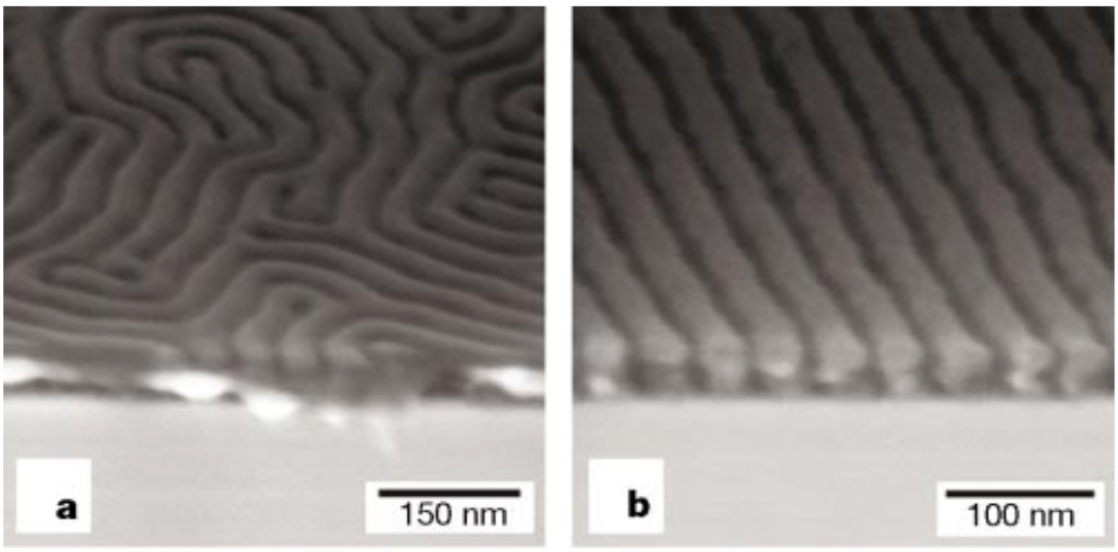

Figure 1.11: Cross-sectional SEM images of PS-b-PMMA films (L_0=48 nm) on **a)** unpatented and **b)** chemically nanopatterned surfaces. The samples were etched. Reprinted by permission from Macmillan Publishers Ltd: Kim *et al*. *Nature* **2003**, *424*, 411-414. Copyright 2003.

Controlling the long-range alignment of block copolymer domains *via* DSA of block copolymer films makes them useful in both the semiconductor and data storage industries. For example, the semiconductor industry can use DSA to design transistors[25] and shrink contact holes[26,27], and the data storage industry can use DSA to fabricate bit patterned media.[28] Excellent progress has been made over the past decade in making circuit-relevant structures from DSA such as jogs and T-junctions.[29,30] IBM has recently developed methods to create custom circuits and finFET transistors.[25] Figure 1.12 highlights an example of a fin circuit designed for logic. Ultimately, it shows that DSA can be used to form complex structures relevant to microelectronic architectures. Additionally, DSA patterns can also be used to create templates for nanoimprint lithography (NIL),[31] which the data storage industry needs to fabricate patterns for bit

patterned media.[32] Prototype templates with a high density of rectangular bits have already been demonstrated using DSA.[33,34] Figure 1.13 highlights an imprint template created from DSA and an imprinted copy with a density of 0.58 Tdot/in^2 where each dot represents one bit.[34] Improvements using more advanced block copolymers and DSA processes are anticipated to help the industry achieve goals of over 10 Tdot/in^2.[35]

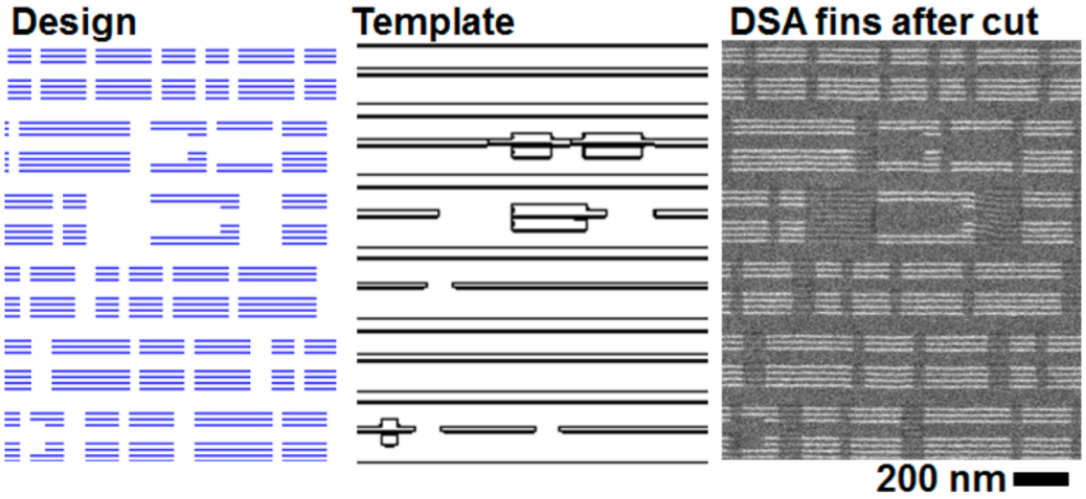

Figure 1.12: Fin circuit demonstrations for logic with DSA-patterns. The design, prepatterned template, and final etch transfer of PS-PMMA using the DSA of 28nm PS-PMMA. Reproduced with permission from Tsai *et al*. *ACS Nano*, **2014**, *8*, 5227-5232. Copyright 2014 American Chemical Society.

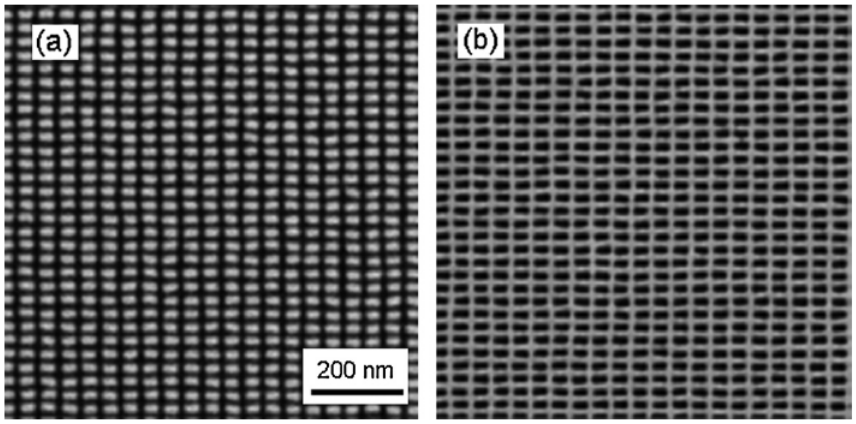

Figure 1.13: SEM images of **a)** nanoimprint master template with rectangular patterns fabricated from the DSA of PS-PMMA; **b)** Imprinted resist pattern from the master template. Reproduced with permission from Wan *et al*., *J. Micro/Nanolithography, MEMS, and MOEMS* **2012**, *11*, 031405.

1.4 Challenges in Block Copolymer Lithography

1.4.1 Necessity of High-χ Block Copolymers

The periodicity, L_0, for a given diblock copolymer is a function of N and χ. The relationship scales accordingly: $L_0 \sim \chi^{1/6}N^{2/3}$.[12] Intuitively, as the polymer becomes larger, L_0 increases. Additionally, as χ increases, the polymer chains stretch out more, which is entropically unfavorable, in order to minimize interfacial contact between the blocks. The periodicity is more strongly a function of N than χ. To minimize L_0 and still satisfy the ordering constraint, $\chi N > 10.5$, the ideal block copolymer should have a large χ value but a small N.

The importance of the segregation strength is demonstrated in Figure 1.14,[13] which shows the composition profile of a lamellar diblock copolymer in the strong ($\chi N >> 10.5$) and weak segregation regimes ($\chi N \approx 10.5$). The strong segregation regime is characterized by sharp interfaces, which is ideal for lithography. As the segregation

strength approaches the order-disorder transition (χN = 10.5, ODT), the phase composition profile becomes more sinusoidal. The sinusoidal phase profile obfuscates the interface between the A and B domains, which will likely increase line edge roughness and limit pattern transfer.

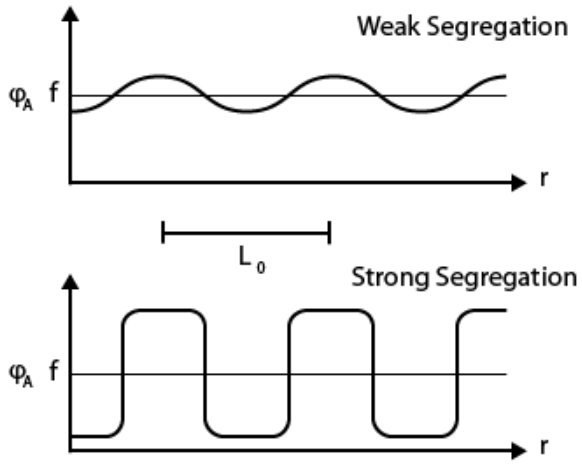

Figure 1.14: Theoretical composition profiles (ϕ_A) as a function of position (r) with periodicity, L_0. Reproduced with permission from Bates *et al*. *Macromolecules*. **2014**, *47*, 2–12. Copyright 2014 American Chemical Society.

PS-PMMA has been the current industry standard for block copolymer lithography, and it has been used to provide a detailed understanding of block copolymer thin film physics, material design, and processing. Unfortunately, a relatively low χ limits the resolution of domains to ca. 12 nm.[36] It will likely not be used to access the sub-10nm regime. Figure 1.15 shows the self-assembly of low molecular weight (small *N*) PS-PMMA (L_0 = 18.5 nm) on a patterned and unpatterned surface.[37] The segregation strength appears to be far too low to produce high quality patterns with sharp interfaces.

Next-generation block copolymers need to form 1) sharp interfaces, 2) sub-10 nm domains, and 3) display etch selectivity for pattern transfer.

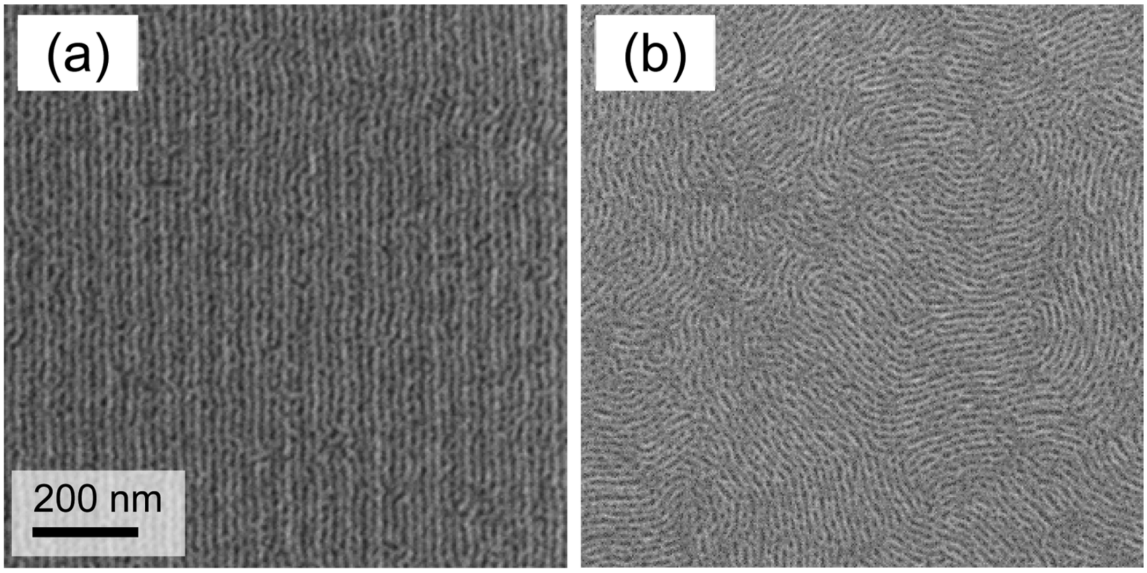

Figure 1.15: (a) Top-down SEM image of self-assembled lamellae-forming PS-PMMA with L_0 = 18.5 nm on a chemically patterned surface; **(b)** Fingerprint pattern PS-PMMA after O_2 etching. Reprinted with permission from Wan *et al*. *ACS Nano*, **2015**, *9*, 7506-7514. Copyright 2015 American Chemical Society.

1.4.2 Etch Contrast

The ability to selectively remove one of the domains is critical for the success of block copolymer lithography. In general, organic-organic block copolymers exhibit poor etch contrast. PS-PMMA is a special case because the PMMA domain is radiation sensitive and particularly sensitive to ion bombardment,[38] which enables its selective removal. Etch selectivity between other high-χ organic-organic block copolymers is not

guaranteed. Even for PS-PMMA, the etch selectivity drops significantly as the L_0 approaches 22 nm. The author is not aware of any reports of pattern transfer of PS-PMMA below 28 nm (full pitch).

Organic-inorganic block copolymer have much greater etch selectivity. For example, incorporating silicon[39] or metals[40,41] into one domain greatly increases etch contrast because oxidized metals are non-volatile under the etching conditions. Two general strategies have been developed to incorporate inorganic components. Sequential infiltration synthesis infuses metals into one of the block copolymer domains, which increases selectivity.[42] However, the process is slow, requires new production tools and alters the dimensions of the domains.[43] In the second approach, the synthesis of block copolymers containing inorganic monomers[44-49] imparts inherent etch contrast[50]. The latter technique is clearly preferable with all other considerations being equal.

This dissertation focuses on silicon containing block copolymers. Silicon imparts etch contrast as it is oxidized to silicon oxide during oxidative etch conditions. The oxide layer that is formed is essentially impervious to the etch process. The most studied silicon-containing polymer is poly(styrene-*block*-dimethylsiloxane). This polymer has a large-χ value and can form sub-10 nm features.[44,51] However, it is difficult to synthesize, and the siloxane block has a T_g over 100˚C below room temperature. Ideally, the block copolymer should have a T_g above room temperature so that block copolymer domains do not reflow after thermal annealing. This dissertation will primarily focus on poly(styrene-*block*-4-trimethylsilylstyrene) (PS-PTMSS),[52] which is shown in Figure 1.16. This polymer contains silicon, but it has T_g values greater than room temperature. Other silicon-containing polymers that are structurally similar to PS-PTMSS and can form sub-10 nm features will also be discussed.

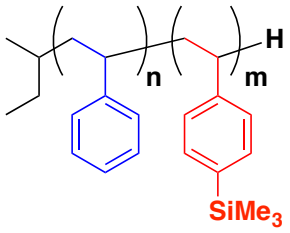

Figure 1.16: Poly(styrene-*block*-4-trimethylsilylstyrene).

1.4.3 Orientation Control

Block copolymer domain orientation relative to the substrate is critical for lithographic applications. Two possible domain orientations are shown in Figure 1.17: perpendicular and parallel. For lithography, the perpendicular orientation for lamellae is required.* The interfacial interactions between the block copolymer domains and each interface (substrate interface and top interface) control the block copolymer orientation.[53] In general, preferential interactions with one block and either the top or bottom interface drive a parallel orientation of domains. Non-preferential (neutral) interactions promote the perpendicular orientation. Many substrate modification methods have been developed to control the interactions at the substrate interface including polymeric brushes[54-57] and crosslinkable surface treatments[58-61]. Neutral surface treatments have been demonstrated to promote a perpendicular orientation of PS-PMMA. Again, PS-PMMA is a special case because the free interface is neutral at around 230°C.[62] Unfortunately, silicon-containing polymers have a strong preference to interact with the free interface. All attempts to thermally anneal silicon-containing block copolymers result in parallel oriented domains.

* It should be noted that parallel cylinders do not need orientation control and essentially look the same as perpendicular lamellae after etching. However, parallel cylinders are limited to 1 L_0 in film thickness. In general, the through-film uniformity of parallel cylinders and aspect ratio are poor.

Methods to control the interfacial interactions at the top and bottom interfaces for a series of silicon-containing block copolymers is a major theme in this dissertation.

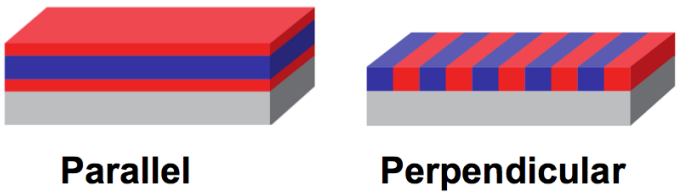

Figure 1.17: Two possible thin film orientations.

1.4.4 Defectivity in Directed Self-Assembly

It should be noted that one of the major concerns with block copolymer lithography is the number of defects per unit area.[63] Currently, DSA processes for integrating 28 nm PS-PMMA into high volume manufacturing are being explored.[64-66] However, these processes are not perfect and yield defects at greater than acceptable levels. Fortunately, calculations show that there is a large driving force to eliminate defectivity on chemically patterned surfaces[67] although the activation barrier for defect annihilation is predicted to be large for high-χ block copolymers.[68] The fundamental cause of defects is still not fully resolved, and defect quantification metrics are still not well defined. A deeper understanding of the DSA mechanism is needed in order to minimize defects. Recent data from IMEC suggests that the DSA mechanism is different than the current paradigm.[69] Defectivity studies are outside the scope of this dissertation. Future work by colleagues at IMEC is aimed at better understanding the DSA and defectivity of silicon-containing polymers.

1.5 Goals of this Dissertation

The goal of this dissertation is to present and solve some of the material design challenges in the field of block copolymer lithography. High-χ silicon-containing polymers that display etch-selectivity and form sub-10nm domains are described in Chapter 2. Orientation control strategies that enable thermal annealing on time scales consistent with industrial requirements are presented in Chapter 3-6. Demonstration that the aforementioned silicon-containing block copolymers are amenable to directed self-assembly is discussed in Chapter 7. Chapter 8 focuses on spatial control of domain orientation, which could be useful for creating customized self-assembled patterns. It is the author's goal that the principles and methods described herein will advance block copolymer lithography towards realization.

1.6 Acknowledgements

The work in this dissertation has been the result of largely collaborative efforts with graduate and undergraduate students in the Willson and Ellison groups. Additionally, strong industrial collaborations with Lam, IBM, IMEC, HGST, and Seagate have made it possible to advance the work presented herein. Acknowledgments to contributors will be stated at the end of every chapter.

Chapter 2: Silicon-Containing Block Copolymers

The purpose of this chapter is to detail the synthesis of the monomers and block copolymers used throughout this dissertation. The reader is directed to the works of Julia Cushen, Gregory Blachut, William Durand, and Yusuke Asano for a complete discussion on synthetic details and χ calculations. Portions of the chapter have been reproduced with permission from Bates, C. M.; Maher, M. J.; Janes, D.; Ellison, C. J.; Willson, C. G. "Block Copolymer Lithography." *Macromolecules* **2014**, *47*, 2–12 and Maher, M. J.; Bates, C. M.; Blachut, G.; Sirard, S.; Self, J. L.; Carlson, M. C.; Dean, L. M.; Cushen, J. D.; Durand, W. J.; Hayes, C. O.; Ellison, C. J.; Willson, C. G. "Interfacial Design for Block Copolymer Thin Films." *Chem. Mater.* **2014**, *26*, 1471–1479. Copyright 2014 American Chemical Society.[13,70]

2.1 Design of Silicon-Containing Block Copolymers

The block copolymers used in this dissertation were designed to have etch contrast, form sub-10 nm lamellar domains, and have glass transitions (T_g) above room temperature. Metal-containing block copolymers are etch resistant to oxidative etch conditions.[41,50] However, the microelectronics fabrication facilities prohibit metals because of contamination[71]; therefore, silicon-containing block copolymers were targeted. Previous studies have shown that only 10% silicon (by mass) is required to provide an etch barrier under oxidative etch conditions.[39] To obtain sub-10 nm domains, the block-block interaction parameter (χ) must be large. The value of χ is dependent on monomer choice, and it is difficult to predict *a priori* for a given pair of monomers. Obtaining high-χ block copolymers is guided by chemical intuition and empiricism. The segregation strength (χN) must be significantly larger than the order-disorder transition (ODT) so that

the block copolymer domains form features with well-defined interfaces between domains that are required for pattern transfer and low line edge roughness. The T_g of both blocks should be above room temperature. Poly(styrene-*block*-dimethylsiloxane) (PS-PDMS) has a large χ value and is over 30% silicon by mass, but PDMS has a T_g far below room temperature (-125°C).[72] There is speculation that T_g values below room temperature will compromise structural integrity because the polymer can flow, which could potentially lead to more defects. In this dissertation, the primary focus is on silicon-containing styrene derivatives, which have been reported to have the desired physical properties such as large χ values and T_g values above room temperature.[46,52,73]

2.2 Monomers for Anionic Polymerization

2.2.1 Silicon-containing Block

Several styrene derivatives that contain silicon were synthesized *via* the Grignard reaction between 4-chlorostyrene and a chlorosilane. Scheme 2.1 shows the synthesis of 4-trimethylsilylstyrene and 4-pentamethyldisilylstyrene. Each of these monomers contains greater than 10% silicon by weight, which imparts etch resistance. Presumably poly(4-pentamethylsilylstyrene) (PDSS) will have greater etch resistance than poly(4-trimethylsilylstyrene) (PTMSS) because it has more silicon by mass. The analogous styrene derivatives prepared from chlorosilanes containing three or four silicon atoms have been synthesized, but either do not successfully undergo anionic polymerization due to side reactions or have a very high boiling point.[74] Styrene-derivatives with high boiling points are difficult to purify for anionic polymerization and often polymerize when heated at elevated temperatures (>100°C). Both 4-trimethylsilylstyrene and 4-

pentamethylsilylstyrene are liquids with boiling points below 100˚C at 30 mTorr and can be more easily isolated than the analogous styrenes with three or more silicon atoms.

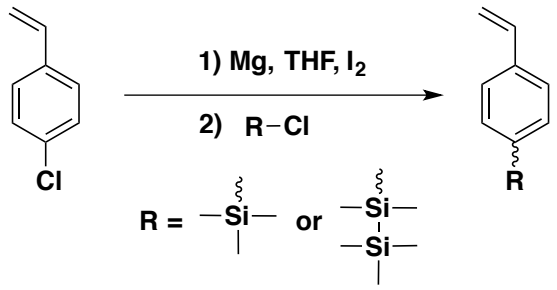

Scheme 2.1: Synthesis of 4-trimethylsilylstyrene and 4-pentamethyldisilylstyrene

2.2.2 Non-silicon-containing Block

The organic, non-silicon-containing block was designed to be highly incompatible with poly(4-trimethylsilylstyrene) (PTMSS) and poly(4-pentamethyldisilylstyrene) (PDSS). Since PTMSS and PDSS are hydrophobic, the monomer choice for the second block should be hydrophilic (relative to PTMSS and PDSS) and stable to anionic polymerization conditions. For example, poly(4-acetoxystyrene) would most likely be highly incompatible with PTMSS and PDSS, but the carbonyl group in 4-acetoxystyrene complicates anionic polymerization. Figure 2.1 shows several styrene derivatives that are amenable to anionic polymerization. Styrene and 4-methoxystyrene are commercially available. Styrenes C-F in Figure 2.1 were synthesized *via* the Wittig reaction (Scheme 2.2). The methoxy substituents in B-F increase the polarity of the organic block and should be even more incompatible with PTMSS than PS.

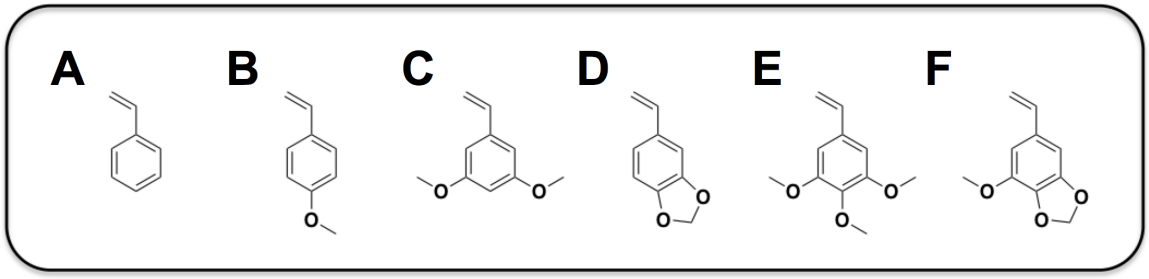

Figure 2.1: Various styrene monomers considered for the organic block.

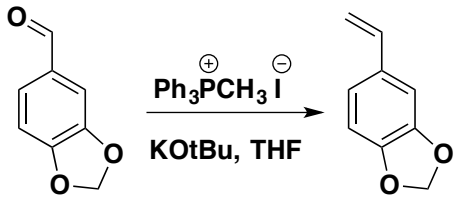

Scheme 2.2: Synthesis of 5-vinylbenzo[*d*][1,3]dioxole *via* the Wittig reaction.

2.3 HOMOPOLYMER ETCH SELECTIVITY

Block copolymer lithography hinges on the ability to selectively remove one of the domains to generate topographical images, and the incorporation of silicon into one block should provide etch selectivity.[75,76] The etch rates of homopolymer thin films under oxidative etch conditions were studied. Figure 2.2 shows the etch depth as a function of time for poly(methylmethacrylate) (PMMA), poly(4-methoxystyrene) (PMOST), PS, PTMSS, and PDSS. Interestingly, over the time range 0-10s, all of the polymers have the same etch rate. For PTMSS and PDSS, the initial loss of film thickness occurs while it is forming an etch stop. After losing an initial 4-7 nm, no further etching of PTMSS and PDSS was observed. Presumably, the film thickness is lost during the oxidation to silicon oxide. The non-silicon-containing polymers etch at a constant rate, which are

significantly greater than PTMSS and PDSS. This suggests that it should be possible to selectively remove the organic block from the silicon block. However, the initial film thickness loss for PTMSS and PDSS could pose a problem as the L_0 of the block copolymer scales down to 10 nm. For example, a 1 L_0 film cannot afford to lose 70% of the film before forming an etch stop; pattern transfer into the substrate is limited by thickness of the etch mask.[77] Thicker films can be used to overcome this problem, but there is an increased risk of through-film defects.

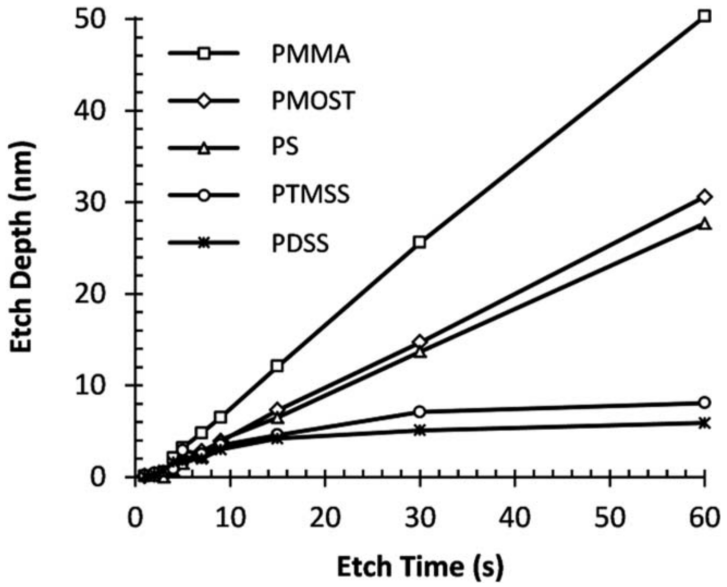

Figure 2.2: Homopolymer etch depth as a function of etch time when exposed to oxidative plasma. Reproduced with permission from Durand et al.[49] Copyright 2015 Wiley and Sons.

2.4 Block Copolymer Architecture

Two block copolymer architectures are commonly used in lithography: diblocks and triblocks. Figure 2.3 shows a comparison of L_0 in a triblock and diblock copolymer. The major difference is that two diblock chains comprise L_0 as opposed to a single chain (with double the molecular weight) for triblocks. The self-assembly behavior for AB diblocks and ABA triblocks is very similar. ABA triblocks have larger bulk domain spacing at all segregation strengths (χN) than their homologous AB diblocks (Figure 2.4A), but they exhibit narrower interfaces (Figure 2.4B).[78] The order-disorder transition (ODT) for lamellar diblocks is χN=10.5 while the ODT for lamellar ABA triblocks χN=9. Furthermore, there is theoretical[79] and experimental[80] precedence that triblocks more readily adopt a perpendicular orientation compared to diblocks as triblocks and are less sensitive to domain-pattern mismatch in directed self-assembly.[81,82] This dissertation will address orientation control of both silicon-containing triblocks and diblocks.

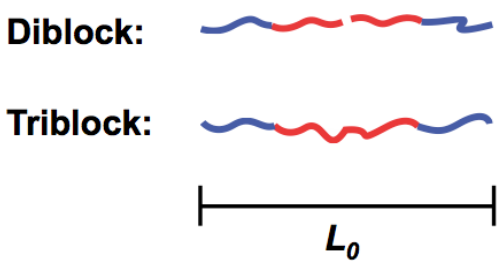

Figure 2.3: AB diblock and ABA triblock chain comparison.

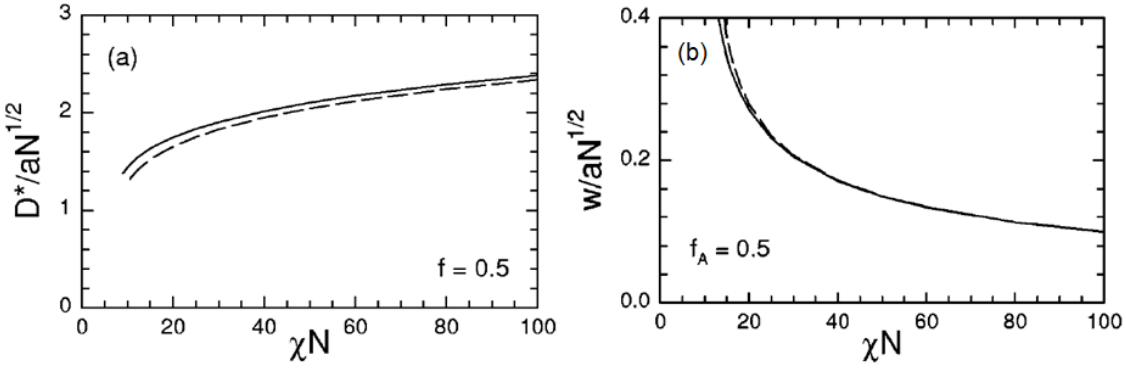

Figure 2.4: **a)** Normalized domain spacing ($D^*/aN^{1/2}$) and **b)** normalized interfacial width ($w/aN^{1/2}$) of a f_A=0.5 lamellar morphology as a function of χN for a triblock (solid curve) with degree of polymerization 2N and a diblock (dashed curve) with degree of polymerization N. Reprinted with permission from Matsen et al., *J. Chem. Phys.* **1999**, *111*, 7139-7146.

2.5 Block Copolymer Synthesis

This section provides an example of one of the block copolymer syntheses. Poly(styrene-*block*-4-trimethylsilylstyrene) (PS-PTMSS) was synthesized by Gregory Blachut using anionic polymerization according to Scheme 2.3. Anionic polymerization is very sensitive and must be performed under air/water free conditions using high-vacuum Schlenk lines. The first monomer (styrene) was added to a solution of organo-lithium initiator. The anionic polymerization of styrene goes to completion in THF at -78°C. Adding the second monomer (4-trimethylsilylstyrene) grew the PTMSS block. After complete reaction, the living anion can be quenched with a proton source such as methanol. The block copolymer was isolated by precipitation into methanol.

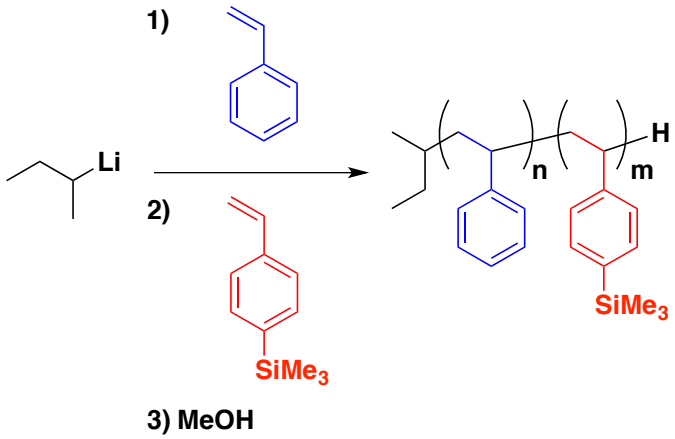

Scheme 2.3: Anionic polymerization of PS-PTMSS.

Two batches of different molecular PS-PTMSS were synthesized. Figures 2.5 and 2.6 shows the size exclusion chromatographs (SECs) of the first block and subsequent block copolymers. In both cases, the first block aliquot was monodisperse with $Đ < 1.05$. After complete growth of the second block, a shift to high molecular weights was observed in the SEC as expected. The dispersity of the block copolymer was less than 1.05 in both cases, which suggests controlled, living growth. The characterization data for the two block copolymers is listed in Table 2.1. Small angle x-ray scattering (SAXS) was used to calculate the periodic domain spacing (D) using the relationship $D=q/2\pi$ (Figure 2.6). For lamellar block copolymers, $D=L_0$. The periodicities of the block copolymer were 22 and 18 nm, respectively. The orientation control of these two polymers is the focus of Chapter 6.

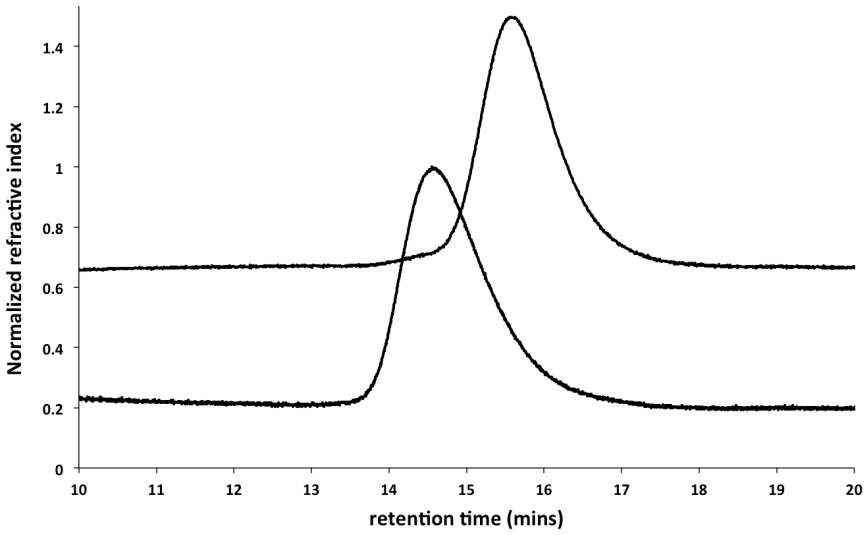

Figure 2.5: SEC traces of PS-PTMSS (L_0=22.0 nm, bottom) and the PS aliquot (top) with THF as the eluent. PS aliquot molecular weight data and dispersities were calculated relative to PS standards. PS aliquot: M_n = 16.7 kDa, $Đ$ = 1.02; PS-PTMSS: M_n = 34.1 kDa (^{1}H NMR), Đ = 1.03 (SEC).

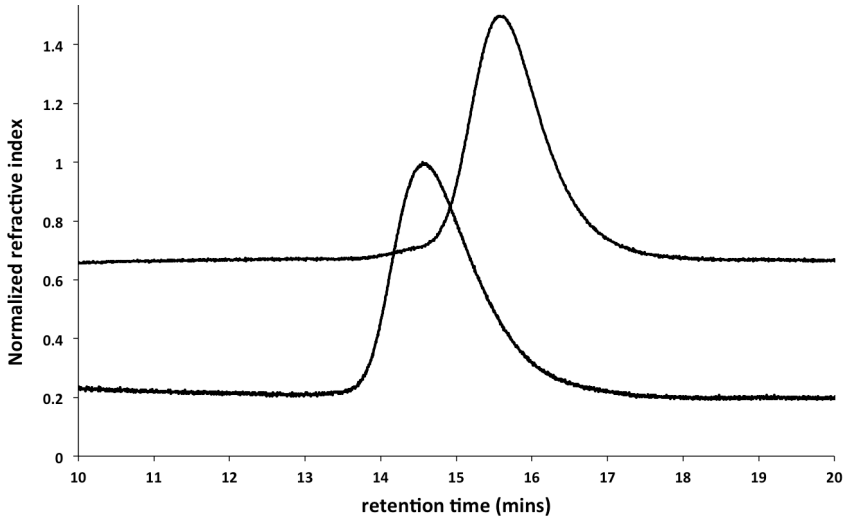

Figure 2.6: SEC traces of PS-PTMSS (L_0=18 nm, bottom) and the PS aliquot (top) with THF as the eluent. PS aliquot molecular weight data and dispersities were calculated relative to PS standards. PS aliquot: M_n = 14.8 kDa, $Đ$ = 1.04; PS-PTMSS: M_n = 29.0 kDa (^{1}H NMR), Đ = 1.04 (SEC).

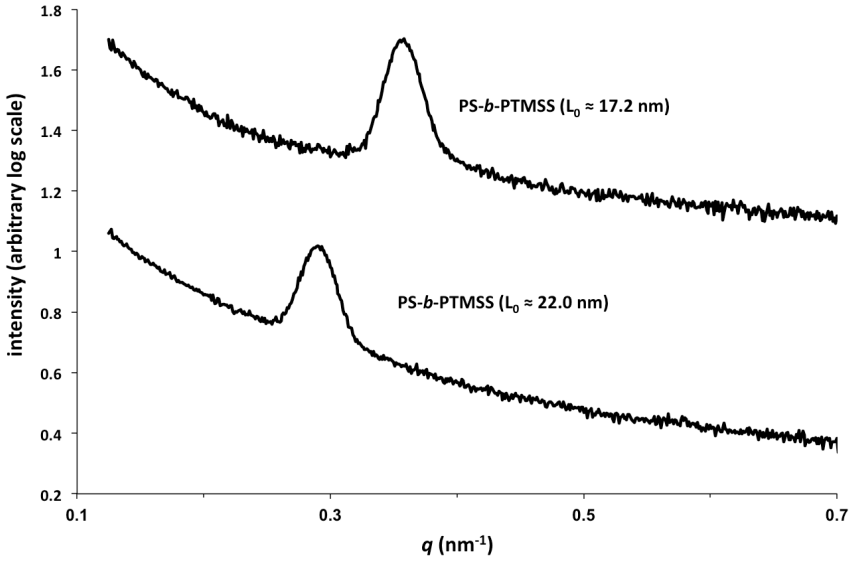

Figure 2.7: Block copolymer 1-D small angle X-ray scattering data (lab source) for PS-PTMSS at room temperature. Samples were annealed on a hot plate at 180 °C. Plots have been shifted vertically for clarity.

Table 2.1: Characterization data of PS-PTMSS

		PS Block			PTMSS Block		Block Copolymer		
Sample	**L_0[a]**	**M_n[b]**	**Đ[b]**	**T_g[c]**	**M_n[d]**	**T_g[c]**	**Đ[b]**	**T_{ODT}[e]**	**T_d[f]**
PS-PTMSS	22	16.7	1.02	105	17.4	134	1.03	N/A	331
PS-PTMSS	18	14.8	1.04	105	14.2	135	1.04	190	337

*L_0 in nm, M_n in kDa; T_g, T_{ODT}, and T_d in °C.
[a]Determined by small angle X-ray scattering. [b]Determined by SEC. [c]Determined by DSC. [d]Determined by ^{1}H NMR spectroscopy in $CDCl_3$. [e]Determined by rheology. [f]Determined by TGA.

2.6 Block Copolymer Summary

The χ parameter is used to determine the block-block compatibility. Members of the Willson and Ellison groups have measured the χ values for several of the block copolymers. Table 2.2 summarizes the structure and χ value of the silicon-containing polymers that appear throughout this dissertation. The χ values in Table 2.2 were measured using disordered samples and temperature dependent x-ray scattering. The characterization data for the ordered block copolymers will be referenced in the chapters they are used in. An extensive discussion on the numerical methods used for the χ calculations can be found in the dissertations of Julia Cushen[83] and William Durand.[84]

Table 2.2: Table of block copolymer χ values determined by SAXS.

Block Copolymer	χ	Block Copolymer	χ
PS-PMMA 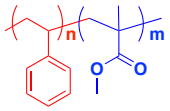	0.044	PS-PTMSM 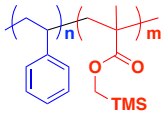	0.058
PS-PTMSS-PS 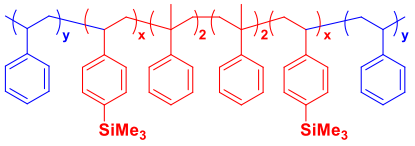	0.043	PS-PDSS 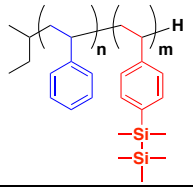	0.114
PS-PTMSS 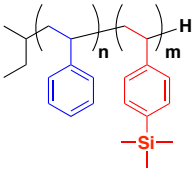	0.047	PMOST-PDSS 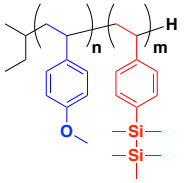	0.199
PMOST-PTMSS 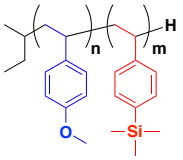	0.138	PVBD-PDSS 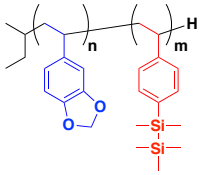	0.249
PTMOST-PTMSS 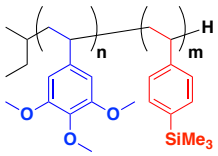	0.175	PTMOST-PDSS 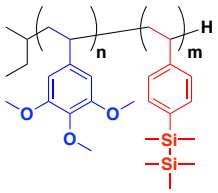	0.313
PTMSS-PLA 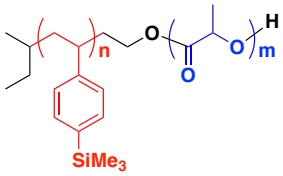	0.381		

There are several distinct features about the χ values in Table 2.2. PS-PTMSS and PS-PTMSS-PS have nearly the exact same χ value, which was expected because the block copolymer architecture should not impact the measurement of χ. It should be noted that PS-PMMA and PS-PTMSS have roughly the same χ value. Therefore, it is unlikely that PS-PTMSS will be the polymer to surpass PS-PMMA because it is likely to have the same resolution limits. However, PS-PTMSS serves as an excellent model polymer because it can form the same size features as PS-PMMA, but it contains silicon and should etch with a higher selectivity than PS-PMMA.

PS-PTMSS can be viewed as the baseline, lowest χ polymer used in this dissertation. The χ value of PMOST-PTMSS and PS-PDSS is greater than PS-PTMSS by slightly more than a factor of two. It is interesting to note that making PS more polar by inclusion of a methoxy group or PTMSS more hydrophobic through addition of a trimethylsilyl group has roughly the same impact on χ. Increasing the number of methoxy substituents from one to three significantly increases χ. The highest χ polymers such as PTMSS-PLA and PTMOS-PDSS are partially soluble in methanol, which is unfortunate because the top coat orientation strategy introduced in Chapter 6 requires that the block copolymer be insoluble in methanol. Orientation control of PTMSS-PLA is described in Chapter 3 using top coats albeit the top coat was cast from water, which does not affect PTMSS-PLA. The block copolymer made from the benzodioxole derivative (PVBD-PDSS) has a large χ value and can form sub-10 nm features, which is discussed in Chapter 6. Interestingly and fortuitously, this block copolymer is not soluble in methanol and is amenable to the orientation and alignment strategies discussed throughout this dissertation.

2.7 EXPERIMENTAL

2.7.1 Instrumentation

^{1}H NMR spectra were recorded on a Varian Unity Plus 400 MHz instrument. Chemical shifts are reported in ppm downfield from TMS using the residual solvent as an internal standard ($CDCl_3$, ^{1}H 7.26 ppm). SEC data were collected with an Agilent 1100 Series isopump and autosampler with a Viscotek VE 2001 triple detector and THF as an eluent at 23°C. Three I-series mixed bed high-MW columns were calibrated relative to PS standards. Small-angle x-ray scattering (SAXS) measurements were collected using a Molecular Metrology instrument equipped with a high brilliance rotating copper anode source (Kα radiation, λ = 1.5418 Å) and a two-dimensional 120 mm gas filled multiwire detector. Vertical focus was acquired with a single crystal germanium mirror, and horizontal focus and wavelength selection was made with an asymmetrically cut Si(111) monochromator. The beam was calibrated using silver behenate with its primary reflection peak set at 1.076 nm^{-1}.

2.7.2 Reagents

Styrene (S), *sec*-butyllithium (1.4 M in hexanes), di-*n*-butylmagnesium (1 M in heptane), calcium hydride (CaH_2, reagent grade powder, ca. 0-2 mm, 90-95%), 1,1-diphenylethylene, methanol, and lithium chloride were purchased from Sigma-Aldrich. Methyltrimethylsilyl methacrylate (TMSM) was purchased from Gelest. Uninhibited tetrahydrofuran (THF) was purchased from JT Baker. Basic alumina (Brockman activity I, 60-325 mesh) was purchased from Fischer. Ultrahigh purity argon was purchased from Airgas. Custom glassware was purchased from ChemGlass and made by the University of Texas at Austin Chemistry glass shop.

2.7.3 Monomer Syntheses

The following Grignard procedure is representative of all the Grignard reactions in this chapter.

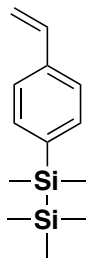

1,1,1,2,2-pentamethyl-2-(4-vinylphenyl)disilane- A three-neck round bottom flask was equipped with a condenser, three rubber stoppers, a stir bar, and magnesium (6.35 g, 261.6 mmol, 1.2 ee). The three-neck flask was flame dried three times under vacuum. Dry THF (240 mL) was added the flask under argon. A few crystals of catalytic iodine was added to the flask. The solution turned slightly yellow. The flask was placed in an oil bath at 65˚C. Then, the 4-chlorostyrene (30.2 g, 218 mmol, 1.0 eq.) was added dropwise via syringe. During the addition, the solution began to violently reflux and turn dark brown. After complete addition, the solution was refluxed for an additional 20 mins. The solution was cooled to 0˚C and 1-chloro-1,1,2,2,2-pentamethyldisilane (40.0 g, 240 mmol, 1.1 eq.) was added dropwise to the flask. The solution was stirred overnight (>12 hrs). Water (200 mL) was added to quench the reaction and ether (3x 200 mL) was used to extract the product. The ether layers were combined and washed with water (2x200 mL), 1 N HCl (1x200 mL) and brine (1x200 mL). The ether layer was dried over sodium sulfate, and the ether was evaporated via rotary evaporation. By GC, the crude product was approximately 90% pure. Further purification was achieved by distillation. Unfortunately, approximately 20-40% of the product is polymerized during this process. The pure product is a colorless liquid. B.P. 80˚C at 30 mTorr. ^{1}H-NMR (400 MHz; $CDCl_3$): δ 7.53-7.46 (m, 4H), 6.79 (dd, *J* = 17.6, 10.9 Hz, 1H), 5.86 (dd, *J* = 17.6, 1.0 Hz, 1H), 5.32 (dd, *J* = 10.9, 1.0 Hz, 1H), 0.44 (s, 6H), 0.16 (s, 9H). ^{13}C-NMR (101 MHz; $CDCl_3$): δ 139.5, 137.6, 137.1,

134.1, 125.6, 113.9, -2.1, -3.9. HRMS (CI) m/z for $[M]^+$ calcd for $C_{13}H_{22}Si_2$ 234.1260; found 234.1263.

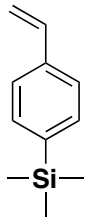

Trimethyl(4-vinylphenyl)silane- Isolated as a colorless liquid. ^{1}H-NMR (400 MHz; $CDCl_3$): δ 7.56-7.53 (m, 2H), 7.45-7.44 (m, 2H), 6.76 (dd, *J* = 17.6, 10.9 Hz, 1H), 5.83 (dd, *J* = 17.6, 1.0 Hz, 1H), 5.30 (dd, *J* = 10.9, 1.0 Hz, 1H), 0.33-0.31 (m, 9H). ^{13}C-NMR (101 MHz; $CDCl_3$): δ 140.3, 138.1, 137.0, 133.7, 125.6, 114.2, -0.99. HRMS (CI) m/z for $[M+H]^+$ calcd for $C_{11}H_{16}Si$ 177.1100; found 177.1086.

The following Wittig reaction is a representative procedure for the rest of the styrene syntheses.

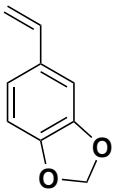

5-vinylbenzo[*d*][1,3]dioxole- A 1L round bottom flask was equipped with a stir bar and flame dried. Triphenylphosphonium iodide (119.0 g, 293.1 mmol, 1.1 eq.) and dry THF (300 mL) was added under nitrogen. The slurry was cooled to 0˚C in an ice bath. Potassium *tert*-butoxide (32.9 g, 293.1 mmol, 1.1 eq.) was added under nitrogen portionwise. The white slurry turned bright yellow. Piperonal (40.0 g) was dissolved in 100 mL of dry THF and added slowly via syringe needle. After 5 minutes, the slurry became white. After 1.5 hr, TLC showed that there was still unconsumed piperonal. An additional 10.7 g of triphenylphosphonium iodide and 3.0 g of *tert*-butoxide was added the reaction vessel. The reaction was stirred for an additional 3.5 hrs. TLC showed that that the piperonal was completely consumed. The reaction was then quenched with 5 mL of water. The solids were filtered off, and the solvent was removed *via* rotary evaporation. The crude product was passed through a

plug of silica using 1:9 ethyl acetate:hexanes as the eluting solvent. The solvent was removed using rotary evaporation and the product was dried *in vacuo*. The monomer was distilled (BP: 46-49˚C at 27 mTorr) prior to anionic polymerization to yield 33.9 g (86% yield) as colorless oil. ^{1}H-NMR (400 MHz; $CDCl_3$): δ 6.97 (d, *J* = 1.7 Hz, 1H), 6.85-6.83 (m, 1H), 6.77 (d, *J* = 8.0 Hz, 1H), 6.63 (dd, *J* = 17.5, 10.8 Hz, 1H), 5.96-5.95 (m, 2H), 5.58 (dd, *J* = 17.5, 0.8 Hz, 1H), 5.14 (dd, *J* = 10.8, 0.8 Hz, 1H). ^{13}C-NMR (400 MHz; $CDCl_3$): δ 147.9, 147.3, 136.3, 132.1, 121.1, 111.9, 108.2, 105.4, 101.0. HRMS (CI) m/z for $[M]^+$ calcd for $C_9H_8O_2$ 148.0524; found 148.0521.

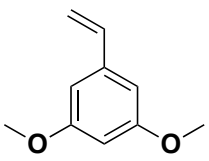

1,3-dimethoxy-5-vinylbenzene- Isolated at a colorless liquid. B.P. 85-90˚C at 30 mTorr. ^{1}H-NMR (400 MHz; $CDCl_3$): δ 6.70 (dd, *J* = 17.5, 10.8 Hz, 1H), 6.62 (d, *J* = 2.3 Hz, 2H), 6.44 (t, *J* = 2.3 Hz, 1H), 5.79 (dd, *J* = 17.5, 0.9 Hz, 1H), 5.30 (dd, *J* = 10.8, 0.9 Hz, 1H), 3.82 (d, *J* = 2.1 Hz, 6H). ^{13}C-NMR (101 MHz; $CDCl_3$): δ 160.9, 139.6, 136.9, 114.2, 104.3, 100.0, 55.2. (CI) m/z for $[M]^+$ calcd for $C_{10}H_{12}O_2$ 164.0837; found 164.0836.

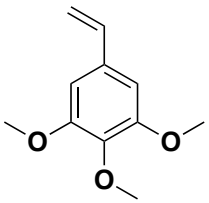

1,2,3-trimethoxy-5-vinylbenzene- Isolated as colorless oil. B.P. 110-115˚C at 30 mTorr. ^{1}H-NMR (400 MHz; $CDCl_3$): δ 6.58 (s, 2H), 6.57 (dd, *J* = 17.6, 10.8 Hz, 1 H), 5.61 (dd, *J* = 17.5, 0.8 Hz, 1H), 5.15 (dd, *J* = 10.9, 0.8 Hz, 1H), 3.80 (s, 6H), 3.79 (s, 3H). ^{13}C-NMR (101 MHz; $CDCl_3$): δ 153.1, 137.8 136.6, 133.1, 112.9, 103.0, 60.6, 55.7. (CI) m/z for $[M]^+$ calcd for $C_{11}H_{14}O_3$ 194.0943; found 194.0939.

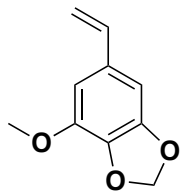

4-methoxy-6-vinylbenzo[*d*][1,3]dioxole- Isolated as an off yellow solid. Can be recrystallized in 90% n-hexanes: 10% diethyl ether. B.P. 105-110˚C at 30 mTorr. ^{1}H-NMR (400 MHz; $CDCl_3$): δ 6.64 (d, J = 1.4 Hz, 1H), 6.62-6.54 (m, 2H), 5.94 (s, 2H), 5.59 (dd, J = 17.4, 0.7 Hz, 1H), 5.14 (d, J = 10.8 Hz, 1H), 3.89 (s, 3H). ^{13}C-NMR (101 MHz; $CDCl_3$): δ 149.1, 143.5, 136.4, 135.0, 132.5, 112.4, 106.5, 101.4, 99.6, 56.4. (CI) m/z for $[M]^+$ calcd for $C_{10}H_{10}O_3$ 178.0630; found 178.0627.

2.7.4 Purification for Anionic Polymerization

Styrene and 4-trimethylsilylstyrene- Two 500 mL Schlenk flasks were loaded with di-*n*-butylmagnesium (ca. 1.5 mL for every 5 g styrene) in a glove box and the solvent was removed *in vacuo* on a Schlenk line. S or TMSS monomer was freeze-pump-thawed (3x) in a third 500 mL Schlenk flask. The styrene monomer was distilled trap-to-trap through a flame-dried short path into the first dry di-*n*-butylmagnesium Schlenk flask and the slurry was stirred for an hour at room temperature. S or TMSS was trap-to-trap distilled into the second di-*n*-butylmagnesium Schlenk flask and stirred for an hour at room temperature. Finally, S or TMSS was trap-to-trap distilled into a flame-dried and pre-weighed burette.

Tetrahydrofuran was passed through a Pure Solv MD-2 solvent purification system containing two activated alumina columns to remove trace water and a copper supported redox catalyst to remove oxygen. The purified THF was added to a 500 mL Schlenk flask directly from the purification system.

Methanol was degassed by sparging with ultrahigh purity argon for 30 min.

2.7.5 Block Copolymer Synthesis Polymerization

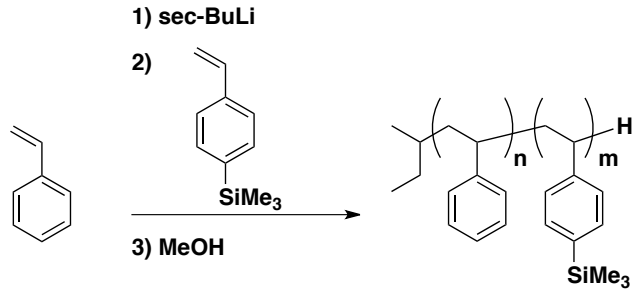

PS-PTMSS Polymerization- A 500 mL glass reactor, charged with a stir bar, was flame-dried under high vacuum and purged with argon gas (5x). Attached to the ports were a glass thermocouple well, a solvent flask, two glass blanks, and a glass arm with inlets to the Schlenk line, pressure gauge, and rubber septum. Purified THF (135 g) was added and the solvent was magnetically stirred. The reactor was cooled to -77 °C with a dry ice/IPA bath while maintaining a 3 psig overpressure of argon in the reactor. *sec*-BuLi (0.15 mL of a 1.4 M solution in hexanes, 0.21 mmol, 1.0 eq.) was then added via syringe. One hour later, styrene (3.75 g, 36.0 mmol, 171 eq.) was added via syringe. An aliquot of the resultant orange solution was taken after 2.5 hours. TMSS (3.70 g, 21 mmol, 100 eq.) was then added via syringe and the solution color changed to red after just a few drops. The reaction was run for one additional hour and terminated with degassed methanol. The solution was precipitated into methanol and the resultant white powder was dried *in vacuo*. The total recovered mass was 7.1 g.

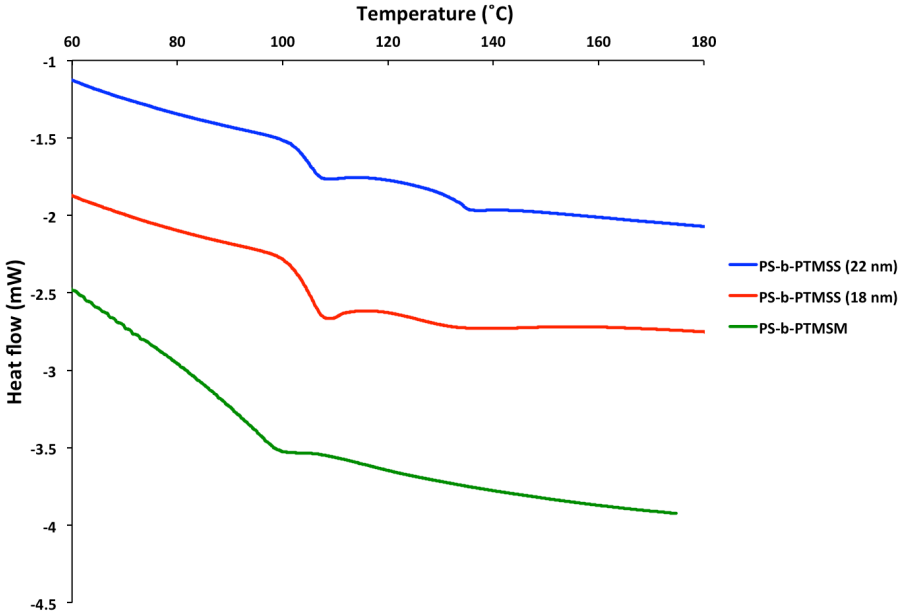

Figure 2.8: Block copolymer DSC data. Samples were heated to 180 ˚C at a rate of 20 ˚C/min for 3 cycles. The data shown correspond with the second heating leg.

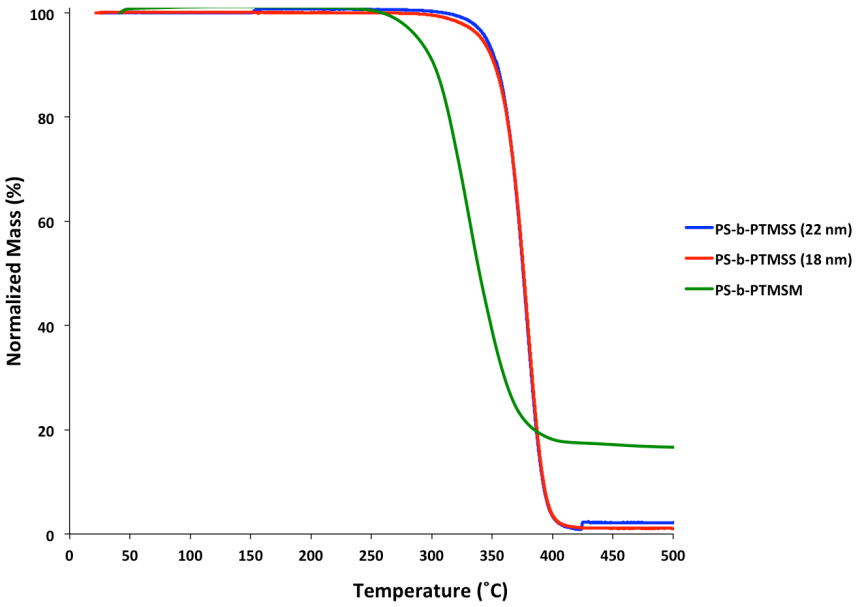

Figure 2.9: Block copolymer TGA data.

2.8 Acknowledgements

Julia Cushen, Gregory Blachut, Yusuke Asano, Yasunobu Someya and William Durand synthesized the block copolymers in this chapter. Monomers were synthesized with the help of Matthew Carlson, Yusuke Asano and Jeffrey Self.

Chapter 3: First Generation of Top Coats

The work in this chapter has been reported in Bates, C. M.; Seshimo, T; Maher, M. J.; Durand, W. J.; Cushen, J. D.; Dean, L. M.; Blachut, G.; Ellison, C. J.; Willson, C. G. "Polarity-Switching Top Coats Enable Orientation of Sub-10-nm Block Copolymer Domains." *Science* **2012**, *338*, 775–779.

3.1 Importance of Surface Energy in Block Copolymer Lithography

Interfacial surface energies control block copolymer orientation. Surface energy is the energetic penalty for the creation of a surface, and it is commonly expressed in units of mN/m. Consider a droplet of water. A water molecule in the interior of that droplet is free to interact and hydrogen bond with all of the surrounding water molecules. However, a water molecule at the air-interface of the droplet must also interact with the air, and the air-water interaction is less favorable than water-water interactions. The work per unit area associated with forming that water-air interface is the definition of surface energy. Surface energies of materials are commonly reported in reference to an air interface. For water, the surface energy is reported to be 73 mN/m.[85]

The surface energy of a given material is highly dependent on the intra- and inter-molecular forces. In general, higher intra/inter-molecular forces increase surface energy. Water has the ability to hydrogen bond, which contributes to its high surface energy. On the other hand, fluorinated materials typically have lower surface energies. Despite being polar, C-F bonds are not highly polarizable. There is not a strong driving force for fluorinated compounds to interact with other fluorinated species. As a result, the energetic penalty for fluorinated species forming a surface is much less than that of water, which is why fluorinated materials typically have "low-surface energy." For

example, poly(tetrafluoroethylene) is reported to have a surface energy of only 19 mN/m.[86]

The surface energy of silicon-containing polymers is typically lower than that of non-silicon-containing polymers. The reason why silicon-containing materials have lower surface energy is not 100% agreed upon. Silicon has a larger atomic radius than carbon, which means that it can be pack fewer atoms at a given surface than carbon. This would decrease the energetic penalty per area per atom. However, silicon is also more polarizable than carbon. It is possible that the low surface energy is due to what the silicon is bonded to in organosilicon polymers. For example, the methyl groups in poly(dimethylsiloxane) (PDMS) are not highly polarizable,[87] which could contribute to the low surface energy of PDMS, 20 mN/m.[44] For reference, the surface energy of polystyrene is 41 mN/m.

3.2 TOP INTERFACE PROBLEM

The orientation of block copolymer domains is controlled by interfacial interactions and the block copolymer film thickness relative to its natural periodicity, L_0.[53] Unconfined block copolymer films with an overall thickness of D tend to form layers commensurate with L_0 and adopt one of three orientations as shown in Figure 3.1. There are two arrangements of parallel domains, symmetric and asymmetric. Symmetric wetting occurs when one of the domains prefers to interact with both the top and bottom interfaces. Asymmetric wetting occurs when one block prefers to wet the top interface and the other block wets the bottom interface. As shown in Figure 3.1, the film thickness of the asymmetric wetting case is $D=(n+0.5)L_0$, and the film thickness of the symmetric wetting case is $D=nL_0$ where n is an integer. Unconfined block copolymer films annealed

at incommensurate film thicknesses [i.e. $D \neq (n+0.5)L_0$ for asymmetric wetting or $D \neq nL_0$ for symmetric wetting] can alleviate energetic frustration by forming island or hole topography, which minimizes the overall free energy of the system by forming layers that are all commensurate in thickness.[88-90] The consequences of island/hole formation will be covered extensively in Chapter 4.

The perpendicular orientation occurs when the interactions between each block and each interface is non-preferential (neutral). In other words, neither block prefers to interact with the top or bottom interface more than the other block. For lithography, a perpendicular orientation of domains is required to facilitate pattern transfer. Unfortunately, for silicon-containing block copolymer (and most high-χ block copolymers), there is a tendency for the lower surface energy silicon-containing block to migrate to the air interface during thermal annealing.[91] This drives the orientation to adopt a parallel arrangement even if the surface interactions at the substrate are neutral.*

* Parallel orientations on neutral surfaces are discussed in Chapter 4.

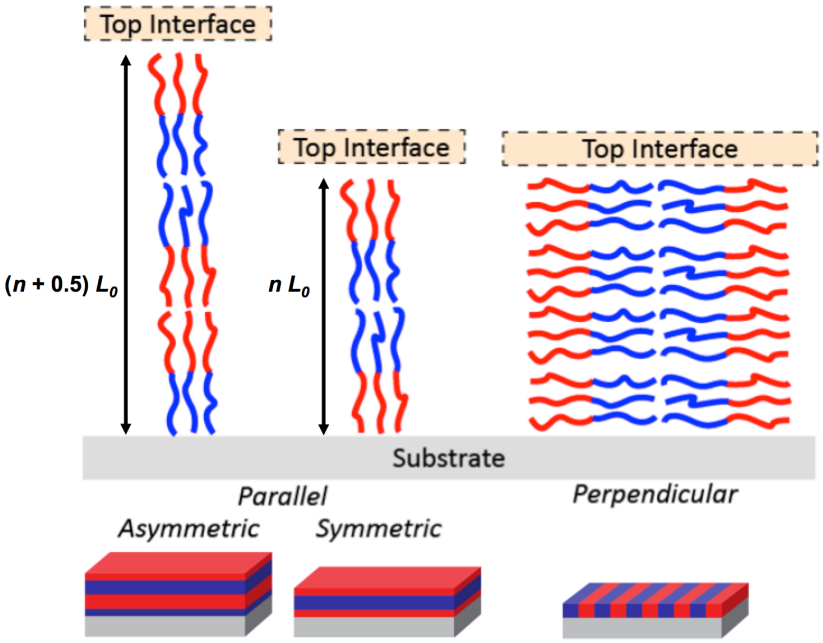

Figure 3.1: Illustration of parallel and perpendicular domains.

Turner[92] and Walton[53] have developed a model that calculates the free energy of the parallel and perpendicular orientations for block copolymers in the strong segregation regime. The free energy calculations determine the preferred orientation based on the interfacial surface tensions and the initial block copolymer film thickness. The interfacial interactions are described by the following variables: γ_{AB}, γ_{A-Top}, γ_{A-Bot}, γ_{B-Top}, and γ_{B-Bot}. In these terms, A and B refer to the blocks, and Top and Bot refer to either the top and bottom (substrate) interface, respectively. For example, γ_{A-Top} describes the interfacial interaction between block A and the top interface. By convention, $\gamma_{B-Top} \geq \gamma_{A-Top}$. The free energy of the perpendicular orientation (F_V), symmetric parallel orientation (F_{H-sym}), and asymmetric parallel orientation (F_{H-asym}) at any normalized film thickness ($d=D/L_0$) can be calculated. The free energy of each orientation can be described by Eq. 3.1-3.3. A full derivation of these equations can be found elsewhere.[93,94] Each free energy is

normalized to the bulk free energy (F_0), which is described in Eq. 3.4 where k is the Boltzmann constant, T is temperature, p is the number of copolymer chains, χ is the segment-segment interaction parameter and N is the degree of polymerization.

$$\frac{F_V}{F_0} = \frac{1}{3}\left[3 + \frac{1}{d}\left(\frac{\left(\gamma_{B-Bot} - \gamma_{A-Bot}\right) + \left(\gamma_{B-Top} - \gamma_{A-Top}\right)}{2\gamma_{AB}} + \frac{\gamma_{A-Top} + \gamma_{A-Bot}}{\gamma_{AB}}\right)\right] \quad \text{Eq. 3.1}$$

$$\frac{F_{H-sym}}{F_0} = \frac{1}{3}\left[\left(\frac{d}{n}\right)^2 + \frac{2n}{d} + \frac{1}{d}\left(\frac{\gamma_{A-Top} + \gamma_{A-Bot}}{\gamma_{AB}}\right)\right] \quad \text{Eq. 3.2}$$

$$\frac{F_{H-asym}}{F_0} = \frac{1}{3}\left[\left(\frac{d}{n+\frac{1}{2}}\right)^2 + \frac{2\left(n+\frac{1}{2}\right)}{d} + \frac{1}{d}\left(\frac{\gamma_{A-Top} + \gamma_{B-Bot}}{\gamma_{AB}}\right)\right] \quad \text{Eq. 3.3}$$

$$\frac{F_0}{kT} = \frac{3p}{2}\left(\frac{\chi}{2}\right)^{\frac{1}{3}} N^{\frac{1}{3}} \quad \text{Eq. 3.4}$$

It is more convenient to express the free energy equations as the differences between the free energies of the different orientations (Eq. 3.5-3.7). In this form, the lowest free energy orientation becomes completely dependent on the *differences* in the interfacial interactions ($\Delta\gamma_{Bot} = \gamma_{B-Bot} - \gamma_{A-Bot}$ and $\Delta\gamma_{Top} = \gamma_{B-Top} - \gamma_{A-Top}$) and not their absolute values. On a neutral bottom interface [$\Delta\gamma_{Bot}/\gamma_{AB} = (\gamma_{B-Bot} - \gamma_{A-Bot})/\gamma_{AB} = 0$], the orientation becomes only dependent on $\Delta\gamma_{Top}/\gamma_{AB}$ and the block copolymer film thickness.

$$\frac{F_{H-sym} - F_V}{F_0} = c - \frac{\Delta\gamma_{Bot} + \Delta\gamma_{Top}}{6d\gamma_{AB}} \quad \text{Eq. 3.5}$$

$$\frac{F_{H-asym} - F_V}{F_0} = c + \frac{\Delta\gamma_{Bot} - \Delta\gamma_{Top}}{6d\gamma_{AB}} \quad \text{Eq. 3.6}$$

$$c = \frac{d^3 + 2m^3}{3dm^2} - 1 \quad \text{where } m=n \text{ for } F_{H\text{-sym}}, m=(n+0.5) \text{ for } F_{H\text{-asym}} \quad \text{Eq. 3.7}$$

The equations can be used to study the effect of differing top interfacial interactions [$\Delta\gamma_{Top}/\gamma_{AB} = (\gamma_{B-Top} - \gamma_{A-Top})/\gamma_{AB} \neq 0$] on orientation on a neutral substrate [$\Delta\gamma_{Bot}/\gamma_{AB} = (\gamma_{B-Bot} - \gamma_{A-Bot})/\gamma_{AB} = 0$] . At different $\Delta\gamma_{Top}/\gamma_{AB}$ values, the orientation with the lowest free energy will be preferred. The ultimate effect of $\Delta\gamma_{Top}/\gamma_{AB}$ on orientation preference is shown in Figure 3.2 On the y-axis, the "normalized free energy" is plotted as the difference in free energy between the perpendicular and parallel orientation $(F_{H-min}-F_V)/F_0$. $F_{H\text{-min}}$ corresponds to the lower free energy between either F_{H-sym} or F_{H-asym} at any given film thickness. The difference $(F_{H-min}-F_V)/F_0$ is negative when the parallel orientation is favored and positive when the perpendicular orientation is favored. On the x-axis, the normalized film thickness (d/L_0) is plotted. Each curve in represents a different $\Delta\gamma_{Top}/\gamma_{AB}$. When the top interface is neutral ($\Delta\gamma_{Top}/\gamma_{AB} = 0$), the perpendicular ordination is favored at all film thicknesses. However, even small differences in surface interactions with the free interface ($\Delta\gamma_{Top}/\gamma_{AB} \neq 0$) result in a preference for the parallel orientation. For example, when $\Delta\gamma_{Top}/\gamma_{AB} = 0.25$, there is only a narrow thickness window in which the perpendicular orientation is preferred (d = 0.6-0.8 L_0). When $\Delta\gamma_{Top}/\gamma_{AB} = 0.5$, there are no film thicknesses that favor a perpendicular orientation.

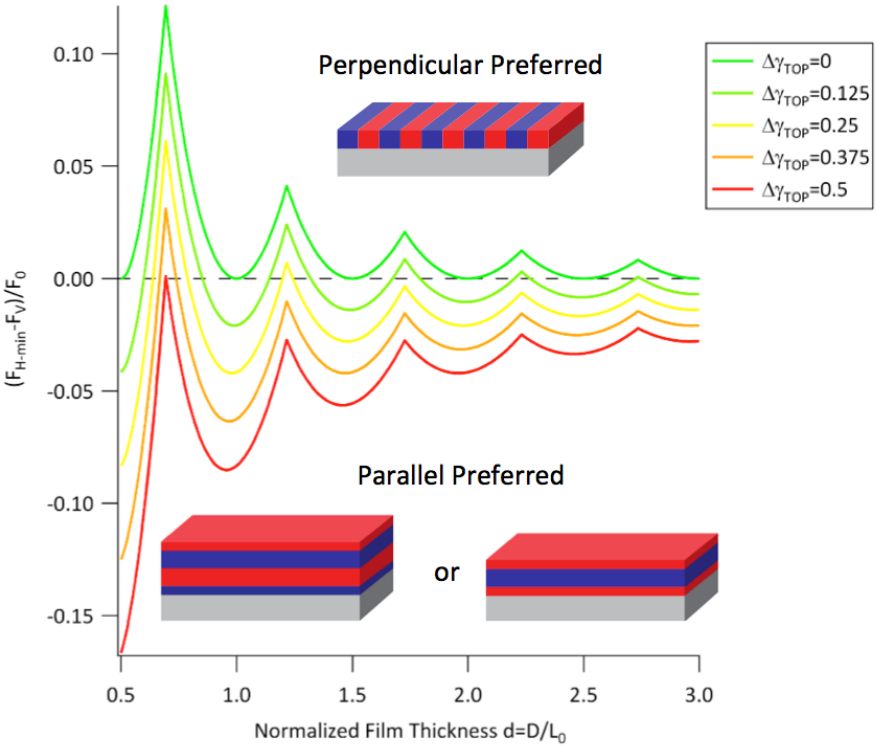

Figure 3.2: Free energy model.

The key point of the block copolymer orientation model is to demonstrate that the orientation is very sensitive to preferential interactions. Therefore, the surface treatments and top coats need to be as close to neutral as possible in order to achieve perpendicular domains.

3.3 Block Copolymers Used in this Chapter

Poly(styrene-*block*-4-trimethylsilylstyrene-*block*-styrene) (PS-PTMSS-PS)[52] and poly(4-trimethylsilylstyrene-*block*-D,L-lactide) (PTMSS-PLA)[46] shown in Figure 3.3 were both studied in detail. The silicon-containing blocks are shown in red while the

silicon free, organic domains are shown in blue. As discussed in Chapter 2, silicon imparts etch resistance, which is necessary for pattern transfer; however, neither of these polymers adopts a perpendicular orientation when thermally annealed. Thermal annealing attempts in vacuum, air, and nitrogen all resulted in a parallel orientation of domains. Therefore, the interactions at the top interface must be controlled to obtain a perpendicular orientation of domains.

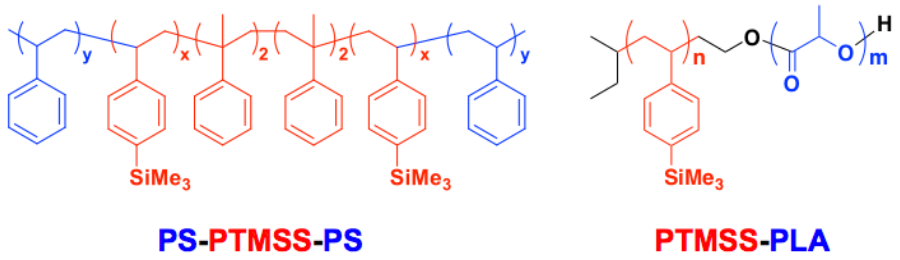

Figure 3.3: Silicon-containing block copolymers used in Chapter 3.

PS-PTMSS-PS (L_0 = 30 nm) was chosen for study because it contains silicon and has a relatively low interaction parameter, χ. It was hypothesized that lower χ block copolymers should have smaller differences in surface energies between the blocks and the top interface compared to high-χ block copolymers ($\Delta\gamma_{Top}$ close to 0). As a result, there should be a larger processing window for achieving a perpendicular orientation.* Additionally, PS-PTMSS-PS has a triblock architecture, and there is literature precedent suggesting that triblocks more readily adopt a perpendicular orientation compared to analogous diblocks.[79,95] PTMSS-PLA (L_0 = 16 nm) has a much larger χ value than PS-

* The assumption that lower χ block copolymers are easier to orient than higher χ block copolymers was never experimentally verified. It makes intuitive sense if surface energy is determined on a two-dimensional linear scale. However, surface energy is multidimensional.

PTMSS-PS and can form less than 10 nm features, which makes it more appealing for patterning applications than PS-PTMSS.

3.4 Proposed Solution Using Top Coats

The ideal solution to the top interface problem would be to spin coat a non-preferential, neutral polymeric layer on top of the block copolymer so that $\Delta\gamma_{Top} = 0$. Depositing the material *via* spin coating would be highly advantageous because the technique is ubiquitous in microelectronics facilities, can uniformly cover large areas, and is compatible with thermal processing. Spin coating a neutral material directly on the block copolymer is not simple, and the challenge can be best explained using an illustration. In Figure 3.4, the surface energies of the homopolymers in PS-PTMSS-PS are plotted on a linear scale.* For a symmetric block copolymers, the neutral surface treatment will likely have a surface energy that is intermediate between the two homopolymers. Unfortunately, neutral materials also have solubility properties similar to those of the block copolymer. In other words, spin coating a top coat onto the block copolymer from an organic solvent will dissolve or damage the block copolymer film.

* Surface energy is complex, nonlinear, and multidimensional. The linear scale shown in Figure 3.3 is for illustrative purposes.

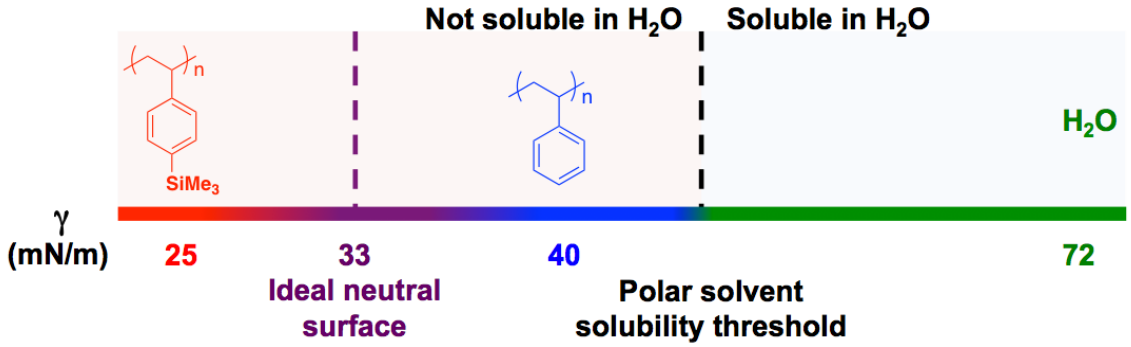

Figure 3.4: Linear surface energy scale of the homopolymers in PS-PTMSS-PS.

Higher surface energy materials become increasingly soluble in polar solvents such as alcohols or water. An arbitrary "polar solvent solubility threshold" is drawn in Figure 3.4. The high polarity solvents, such as water, do not damage the block copolymer thin film. Therefore, it would be ideal if the top coat material were soluble in water. Unfortunately, if the top coat is soluble in water, it is inherently in the non-neutral region according the scale in Figure 3.4. To counter this issue, a process enabling the orientation control of block copolymer domains using polarity switching top coats was invented.[96] This process is outlined in Figure 3.5. First, a neutral surface treatment that controls the interfacial interactions between the block copolymer and substrate is crosslinked, which renders the surface treatment completely insoluble. The block copolymer is spin coated from toluene to form a thin film over the surface treatment with an initial thickness between 1-3 L_0. The top coat is then spin coated over the block copolymer from water or methanol. Next, the film stack is thermally annealed. During the anneal, the top coat undergoes a polarity switch and becomes neutral. Simultaneously, the block copolymer phase separates into perpendicular lamellae. If the top coat polarity switch is reversible,

then the top coat can be stripped using an aqueous solvent. Then, an oxidative etch process can be used to remove the organic domains to create a topographical pattern.

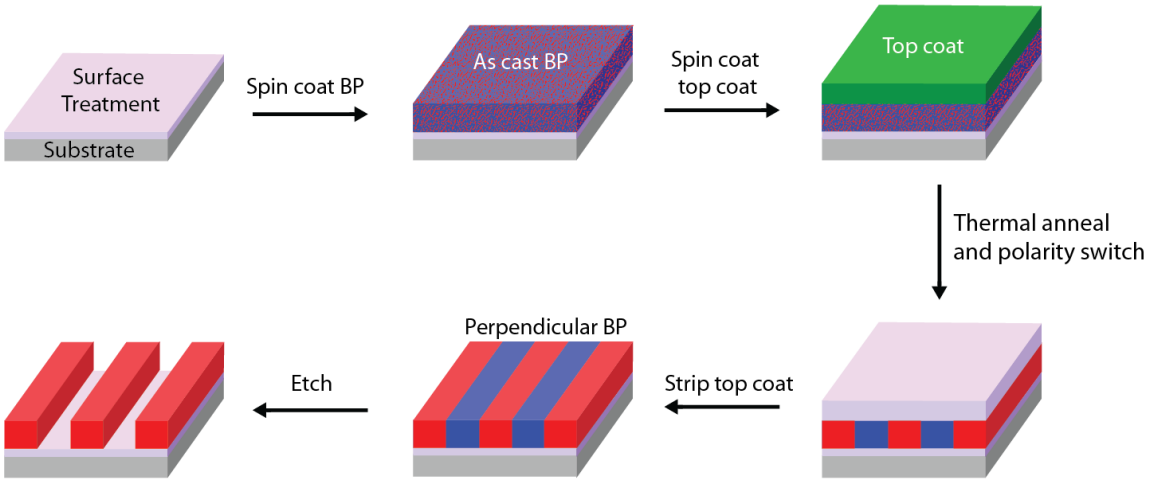

Figure 3.5: Process used to control the orientation of silicon-containing block copolymers *via* thermal annealing. reproduced with permission from Bates *et al*. "Block Copolymer Lithography." *Macromolecules* **2014**, *47*, 2–12. Copyright 2014 American Chemical Society.

3.5 Top Coat Criteria

The desired top coat must be spin coated from a solvent that does not interact with the block copolymer. Ideally, the material should have a reversible polarity switch, which will allow spin coating from water and become neutral upon thermal annealing. The glass transition temperature (T_g) of the top coat must be greater than the T_g of the blocks and annealing temperature. In theory, this will allow the block copolymer to phase separate and self-assemble while preventing any intermixing/dewetting of the top coat.[97] The T_g of PS, PTMSS, and PLA are roughly 106˚C, 131˚C, and 54˚C, respectively. The final

requirement is that the composition of the top coat needs to be tunable so that the surface energy can be appropriately adjusted to achieve neutrality.

3.6 TOP COAT DESIGN

All of the top coats were designed to contain maleic anhydride because it enables a polarity switch. The maleic anhydride moiety can exist in either a ring open or ring closed form, which greatly impacts the solubility properties of the polymer. Figure 3.6 shows the types of top coats that were synthesized in this chapter. Copolymers of maleic anhydride and norbornene are known to have T_g values exceeding 200˚C.[98] A wide variety of norbornene derivatives are available, which should enable surface energy control. It should be noted that norbornene derivatives are challenging to synthesize and purify because they are a mixture of endo/exo diastereomers. Other top coats include a third monomer such as a styrene, methacrylate, or methacrylamide derivative, which was hypothesized to enable capture of an even greater range of surface energies by judicious monomer choice.

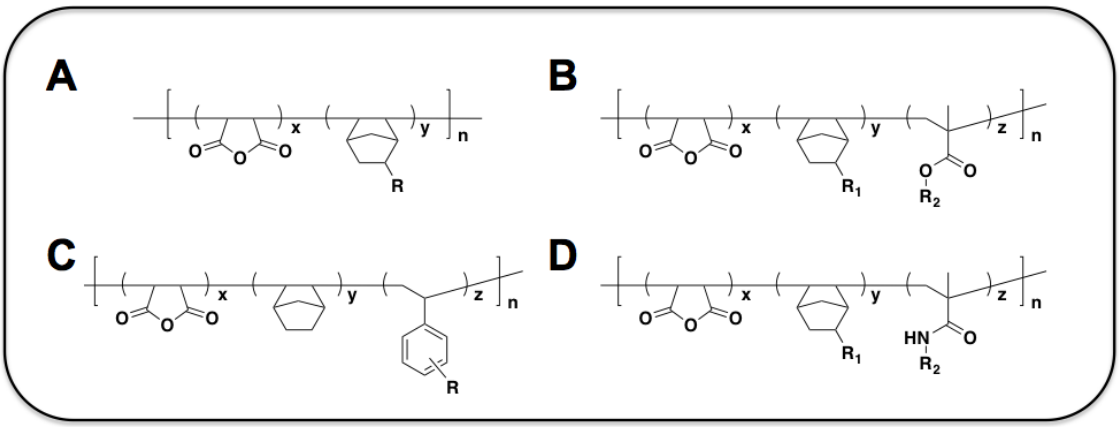

Figure 3.6: Possible sample space of top coats used in this chapter.

3.7 MONOMER AND POLYMER LIBRARY

Maleic anhydride is a relatively polar monomer that is preferential for the higher surface energy block. Therefore, the comonomers need to be preferential to the lower surface energy block to balance the interfacial interactions. Most of the polymers used in this chapter contain fluorinated monomers because fluorinated materials have low surface energies.[85] A large library of monomers that contain lower surface energy functional groups such as fluorine or hydrophobic *tert*-butyl groups were synthesized.

3.7.1 Styrene Derivatives

A wide variety of fluorinated styrene derivatives were synthesized according to Scheme 3.1. The hydroxyl group of 4-hydroxybenzaldehyde provides a synthetic handle for modification. Classical Williamson ether synthesis by nucleophilic substitution was used to create fluorinated ethers. Then, a Wittig reaction was used to convert the aldehyde into a vinyl group, which is suitable for polymerization.

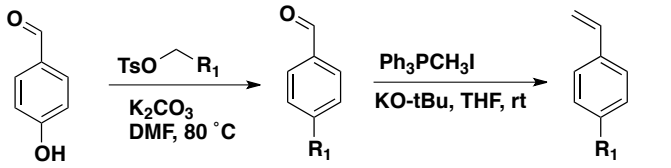

R_1	S_n2 % Yield	Wittig % Yield
–O–(CH2)3–F	76	89
–O–CH2–CF_3	78	79
–O–CH2–C_2F_5	40	41
–F	N/A	29
–CF_3	N/A	60

Scheme 3.1: Styrene of fluorinated styrene derivatives.

Synthesizing large quantities of styrene derivatives *via* the two-step synthesis in Scheme 3.1 was challenging because the Wittig reaction is not atom economical. The Heck coupling was used as an alternative approach to synthesize large quantities of fluorinated styrene derivatives.[99] Scheme 3.2 shows the palladium catalyzed coupling of a fluorinated aryl bromide with ethylene, which can be performed on a much larger scale (>50 g).

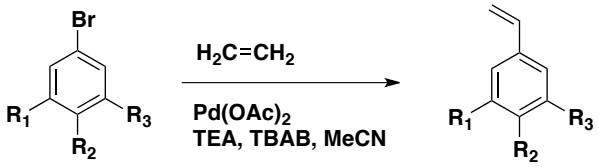

R_1	R_2	R_3	% Yield
—H	—CF_3	—H	88
—F	—H	—CF_3	85
—CF_3	—H	—CF_3	91

Scheme 3.2: Fluorinated styrene derivatives synthesized by the Heck coupling of an aryl bromide and ethylene gas.

3.7.2 Norbornene Derivatives

The norbornene derivatives used for alternating copolymerizations with maleic anhydride are shown below in Scheme 3.3. Since maleic anhydride is relatively polar and assumed to have high surface energy, the norbornene derivative should be lower in surface energy to balance the interfacial interactions. However, surface energy is difficult to measure and difficult to predict based on chemical structure. Therefore, some norbornene derivatives (e.g. R = OH) that were assumed to have higher surface energy

were also synthesized to provide access to a wide range of surface energies for testing. Unfortunately, the fine-tuning the surface energy of the norbornene-maleic anhydride top coats is tedious because the polymerization is alternating and a new monomer is needed for each copolymer. These monomers were difficult to synthesize and challenging to purify. Often, the endo/exo isomers could not be separated from one another using standard purification attempts (see experimental).

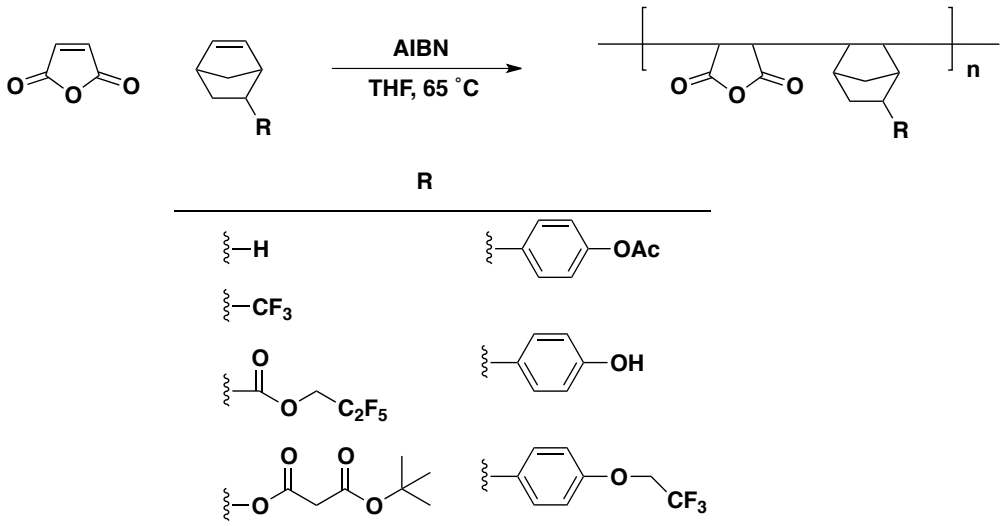

Scheme 3.3: Alternating copolymers of maleic anhydride and norbornene

3.7.3 Methacrylamide Derivatives

Methacrylamide derivatives were hypothesized to incorporate into norbornene-maleic anhydride copolymers similarly to acrylates.[100] Many aniline derivatives are commercially available, which can easily be transformed into the corresponding N-substitute methacrylamides by the reaction shown in Scheme 3.4. The methacrylamide derivatives used in this chapter are based on aniline and 2-fluoroaniline.

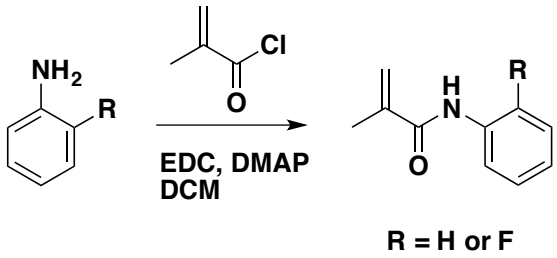

Scheme 3.4: Synthesis of methacrylamide derivatives

3.7.4 Polymer Characteristics

A large library of top coats was synthesized by several researchers in the Willson group to achieve the structures shown in Figure 3.6. All of the top coat polymers in this chapter were synthesized by free radical polymerization. An example of a top coat (TC-IR) synthesis that contains maleic anhydride, norbornene, and a fluorinated methacrylate derivative is shown in Scheme 3.5. The feed ratios and polymerization times were kept constant at 20 hrs. The mol percent in the polymer feed was always 60% maleic anhydride, 30% norbornene derivative, and 10% monomer 3 where monomer 3 was a styrene, methacrylate, or methacrylamide derivative. The glass transitions of these polymers are all greater than 175˚C. They are soluble in many common organic solvents but are not soluble in polar solvents such as water. However, all of the top coats are soluble in aqueous NH_4OH because the anhydride can ring open to form salts.

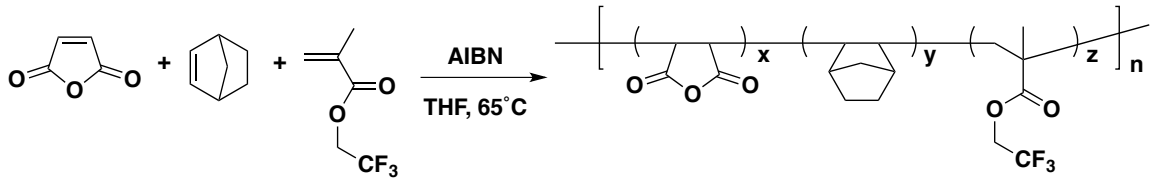

Scheme 3.5: Synthesis of a representative 3-monomer top coat. (TC-IR).

3.7.5 Polarity Switch Confirmation

An IR study was performed to confirm the maleic anhydride polarity switch. Figure 3.7 shows the thin film IR spectra of TC-IR. The blue curve corresponds to TC-IR spin coated onto a salt plate as a ca. 300 nm thick film from 2-butanone. The anhydride symmetric and asymmetric carbonyl stretches are observed at 1775 and 1850 cm^{-1}. The red curve corresponds to TC-IR cast from ammonium hydroxide.* During dissolution in ammonium hydroxide, the anhydride ring opens, and anhydride peaks completely disappear. Heating the ring-opened film at 210˚C for 1 min results in ring closure and ammonia gas and water vapor are evolved. The reappearance of the anhydride carbonyl stretching in the green curve bands confirms this observation.†

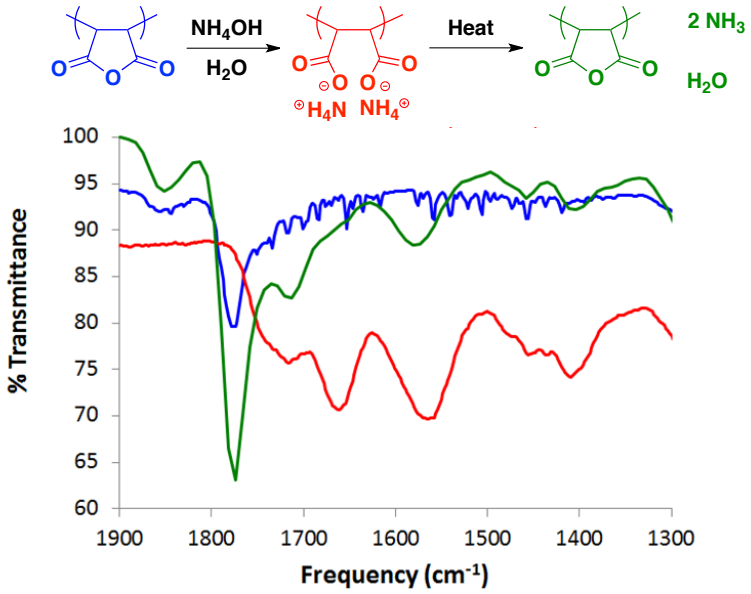

Figure 3.7: Blue: TC-IR spin coated from 2-butanone. Red: TC-IR spin coated from aqueous NH_4OH. Green: Subsequent heating at 210°C for 1 min.

* At the time this project was started, aqueous ammonium hydroxide was used as a solvent. Unfortunately, ammonium hydroxide reacts with maleic anhydride to form amide, and sequential heating results in some amide formation. See Chapter 5 for more in depth IR studies and interpretations.

† Notice in the green curve of Figure 3.5 that there is a peak at 1735 cm^{-1}. This peak most likely corresponds to imide. Second generation top coats discussed in later chapters eliminate imide formation.

3.8 Guess and Check Methodology

The major challenge associated with controlling the orientation of block copolymer domains is the seemingly infinite variable space. For example, the chemistry of the surface treatment, thickness of the block copolymer, chemistry and composition of the top coat, and annealing conditions must be all aligned for the orientation strategy to be successful. The first experiments were conducted with PS-PTMSS-PS. None of the parameters described beforehand were optimized for this block copolymer. To reduce the number of experiments, all of the variables were fixed save the top coat. The surface treatment was kept constant, which was poly(4-methoxystyrene-*random*-4-vinylbenzylazide) (XPMOST). This material was assumed to be neutral for PS-PTMSS-PS. Later experiments proved it to be preferential. However, at the time, no methodology existed to determine neutrality for silicon-containing block copolymers,* and previous work suggested that the orientation of block copolymers could be achieved solely on crosslinked homopolymers.[61] Large wafers were coated with the XPMOST and block copolymer. Then, the wafer was cut into many smaller pieces and different top coats were screened while keeping the surface treatment, block copolymer thickness, and annealing conditions constant. Screening the surface treatments, block copolymer film thicknesses, and annealing conditions exponentially grows the number of possible experiments.

At the time of these experiments, no methodology existed to determine the wetting preference of the top coat.† The only way to test the top coat was to carry out the entire process in presented in Figure 3.5 and inspect each sample by scanning electron microscopy (SEM). This method of testing was labor intensive and a null result did not

* Chapter 4 focuses on identifying neutral surface treatments for block copolymers. During these initial experiments, it was unclear how to apply surface evaluation methodologies developed for PS-PMMA to PS-PTMSS-PS.

† Chapter 6 focuses on strategies to determine top coat wetting.

necessarily mean the top coat was not neutral. A parallel orientation could have resulted from failure to optimized one of the aforementioned variables. The vast majority of the top coats were not successful because they did not result in a perpendicular orientation of domains, and the SEM micrographs often appeared as shown in Figure 3.8.

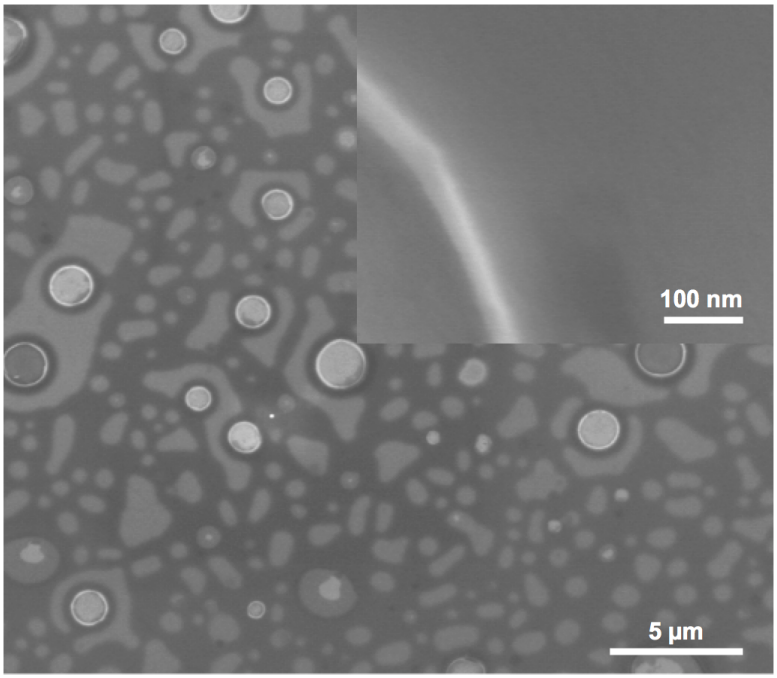

Figure 3.8: Representative SEM micrograph of the most common result of trial and error top coat testing. Large topography formed on the surface of the block copolymer.* Inset: zoomed in region at one of the interfaces of the topographical features.

* At the time, it was unknown what the topography meant. Later, these would be recognized as islands and holes, which are the basis of the top coat testing methodology. See Chapter 6.

3.9 First Success

After numerous unsuccessful orientation attempts, one set of materials showed promise. A special acknowledgement must be made here to Leon Dean, an undergraduate who worked extensively on screening surface treatments and block copolymer thicknesses. He ultimately found a condition where the block copolymer adopted a perpendicular orientation. Figure 3.9 shows the SEM of PS-PTMSS-PS (film thickness = 42 nm, 1.4 L_0) after annealing for 5 days at 130˚C confined between XPMOST and TC-IR. A majority of the domains appear to have the perpendicular orientation. However, there are large regions of parallel domains, which makes the SEM look "patchy." This patchy behavior is likely due to the fact that none of the processing parameters were optimized, including the top coat. Since this result was promising, the future experiments continued to use 42-nm-thick PS-PTMSS-PS on XPMOST, and the block copolymer thicknesses was kept constant at 42 nm.

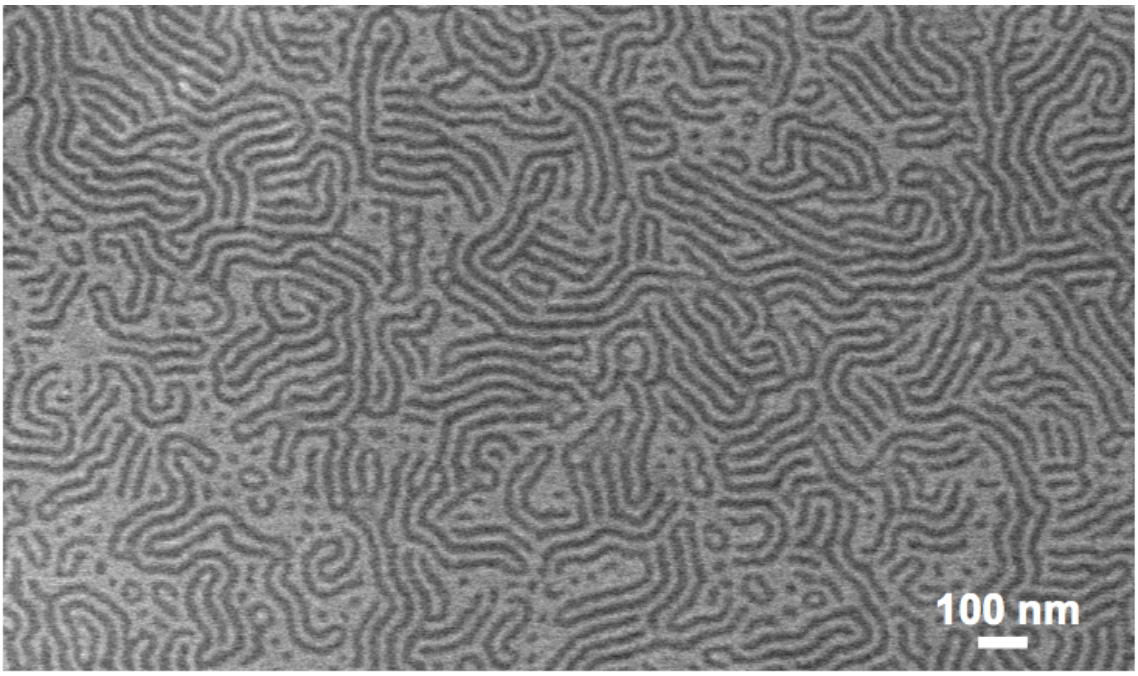

Figure 3.9: Fist "successful" orientation control over PS-PTMSS-PS. Sample was annealed for 5 days at 130˚C and etched using an oxidative plasma.

Other top coats were found to be successful in controlling the orientation of PS-PTMSS-PS soon after the initial success with TC-IR. A very similar result was observed using TC-OCF_3, which is shown in Figure 3.10A. Under processing conditions identical to those used for TC-IR, the block copolymer adopts a patchy orientation of perpendicular features (Figure 3.10B). The patchy behavior appeared to disappear as the annealing temperature was increased to 170˚C. However, black dots of unknown origin, colloquially known as "Durand Dots," began to appear. This could be the onset of dewetting as the sample was annealed near the T_g of TC-OCF_3, which is 180˚C. When the sample is annealed 10˚C above the T_g of TC-OCF_3, the top coat appears to dewet and a parallel orientation of domains was observed.

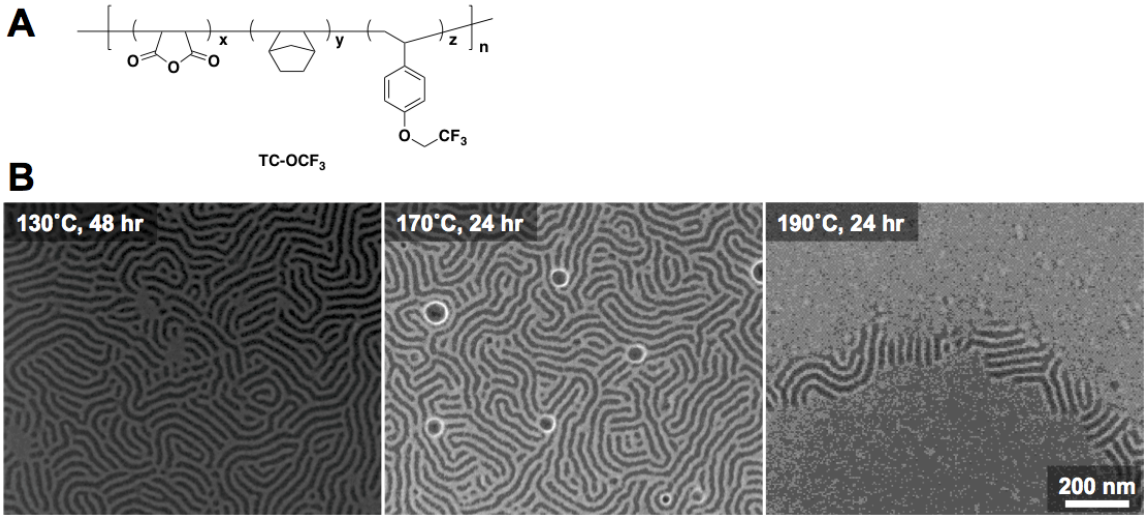

Figure 3.10: A) TC-OCF3. Top coat composition (mol%) x:y:z=56:17:27. T_g=180 °C. **B)** Scanning electron micrographs of 42 nm thick PS-PTMSS-PS annealed at various times and temperatures. Samples were stripped with a 3:1 mixture of IPA:aq. NH_4OH and etched with an oxidative plasma.

3.10 Orientation Control of PS-PTMSS-PS

During this period, another promising top coat was developed. This top coat is labeled TC-PS and is shown in Figure 3.11. It is similar in structure to TC-OCF_3 except that the 4-trifluoromethylstyrene can be synthesized in very large quantities *via* the Heck reaction in one step whereas 4-(2-trifluoroethoxy) styrene required two steps. Additionally, TC-PS has a T_g of 214˚C, which allows annealing of PS-PTMSS-PS at higher temperatures than TC-OCF_3.

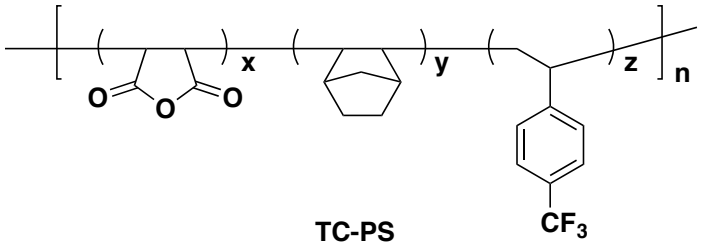

TC-PS

Figure 3.11: TC-PS. Top coat composition (mol%) x:y:z=57:17:26. T_g=214 °C.

Figure 3.12 shows the orientation results of PS-PTMSS-PS when annealed between XPMOST and TC-PS at 210˚C for 1 minute. Unlike previous results, the orientation control is seemingly perfect. No evidence of parallel domains is present after inspecting micron size areas in several locations of the wafer. The inset of Figure 3.12 shows the control sample without TC-PS. Only parallel domains are observed without a top coat. Top down SEM images only show the orientation at the top interface. However, for lithography, the domains need to adopt a perpendicular orientation throughout the entire film. A tilted SEM (Figure 3.13) confirms that the orientation of the domains spans the entire thickness of the film. Additionally, the image can be transferred into silicon (Figure 3.14), which would not be possible if the features did not persist throughout the entire film.

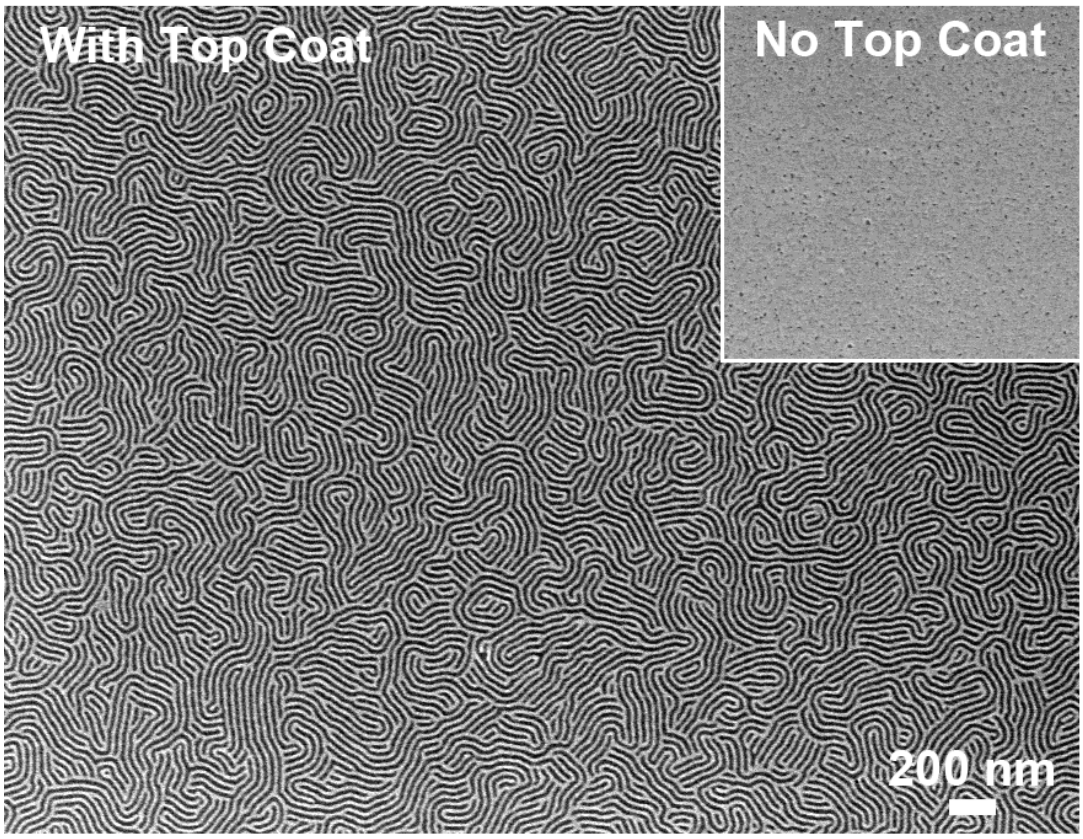

Figure 3.12: Scanning electron micrographs of PS-PTMSS-PS (L_0=30 nm) annealed on XPMOST at 210 °C for 1 minute on a hot plate open to air with top coat TC-PS without top coat (inset). The BCP film thickness was 43 nm (1.4 L_0). TC-PS was removed and the sample was etched prior to imaging. The scale bar is valid for both the images.

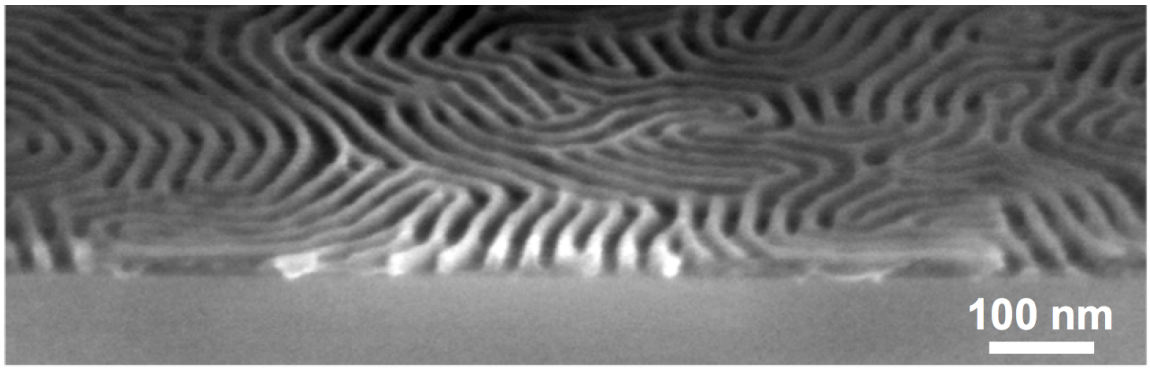

Figure 3.13: Tilted SEM demonstrating through-film perpendicular orientation of PS-PTMSS-PS. Annealing conditions are the same as Figure 3.12.

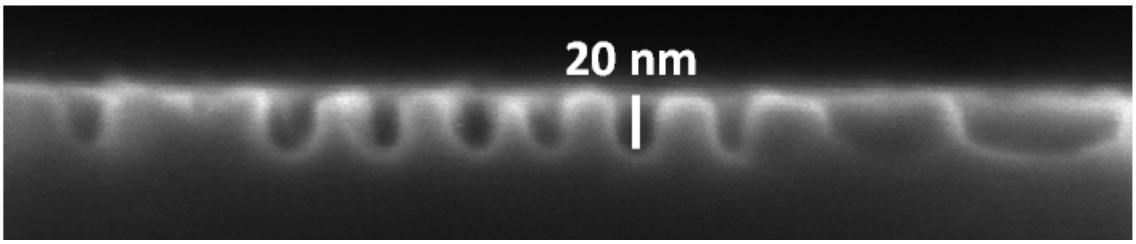

Figure 3.14: Cross-section SEM demonstrating pattern transfer of PS-PTMSS-PS into silicon.

The high T_g of TC-PS allowed for annealing at 210˚C. The annealing time of only 1 minute open to air rivals the fastest thermal annealing time reported for other block copolymers.[101] Discovering that the block copolymer can be annealed this quickly fundamentally transformed the process because it reduced the annealing conditions from 5 days under vacuum to 1 minute open to air. Increasing the annealing temperature well above the T_g of the block copolymer presumably makes the self-assembly much faster. At 210˚C, the self-assembly appears to be nearly perfect at 1 minute. Shorter annealing times at the same temperature and film thickness were investigated. Figure 3.15 shows the results of assembly after 10 and 30 seconds. After only 30 seconds, the assembly appears to be perfect. Even after 10 seconds of annealing, the majority of the self-assembly appears to be complete. However, there are defects present, which suggests that the orientation process is not completely finished at 10 seconds.

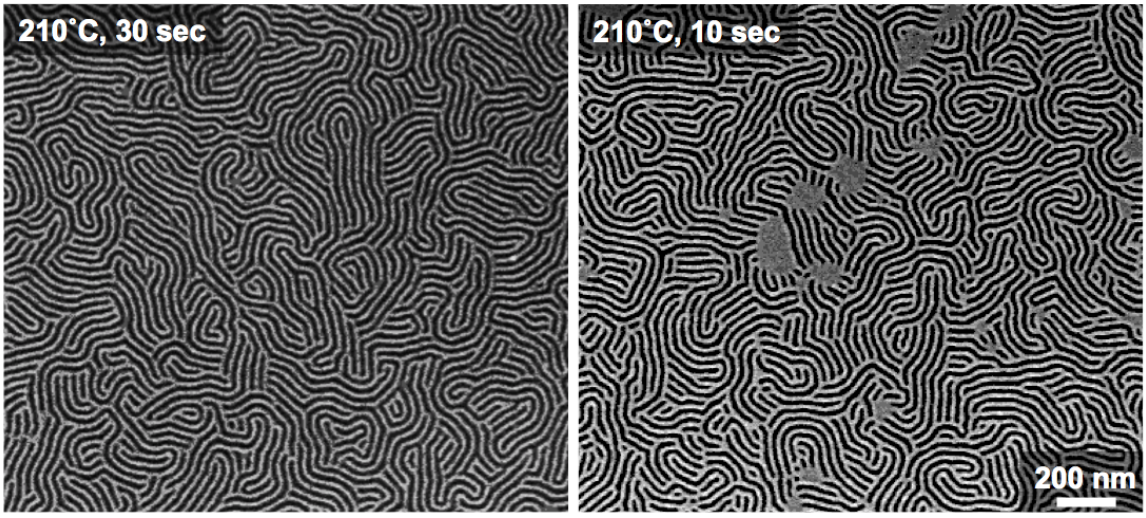

Figure 3.15: Top down SEMs of PS-PTMSS-PS annealed at 210˚C for 30s and 10s confined between XPMOST and TC-PS. The film thickness is 1.4 L_0. TC-PS was removed and the sample was stripped prior to imaging. The scale bar is valid for both images.

3.11 Orientation Control of PS-PLA

After successfully demonstrating the proof of concept that top coats can enable orientation control of low-χ block copolymers, attention was focused on higher-χ block copolymers. High-χ block copolymers can form smaller features and are more valuable to the lithography community. PTMSS-PLA used in this chapter has a L_0 of 15 nm in bulk and was synthesized by Julia Cushen.

As with PS-PTMSS-PS, different top coats were screened as candidates for controlling the orientation of PTMSS-PLA. No evidence of perpendicular orientation was observed except when a new top coat, TC-PLA, was used (Figure 3.16). Annealing PTMSS-PLA confined between XPMOST and TC-PLA produced perpendicular domains when annealed at 170˚C for 24 hrs (Figure 3.17). Interestingly, the thin film L_0 was measured to be closer to 19 nm as opposed to 15 nm in bulk. This discrepancy is likely

due to measurement error in the SEM metrology. No perpendicular domains were achieved without a top coat as demonstrated by the inset. It should be noted that this was one of the only times that orientation control was achieved with this PTMSS-PLA using top coats. The processing window was very narrow, and perpendicular domains were only observed when the film thickness was around 0.66 L_0. All other film thicknesses produced parallel domains when annealed under otherwise identical processing conditions.

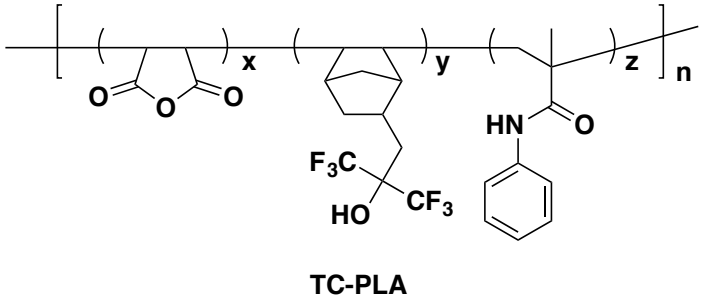

TC-PLA

Figure 3.16: TC-PLA. Maleic Anhydride:Norbornene:Methacrylate=61:19:20, T_g=180°C.

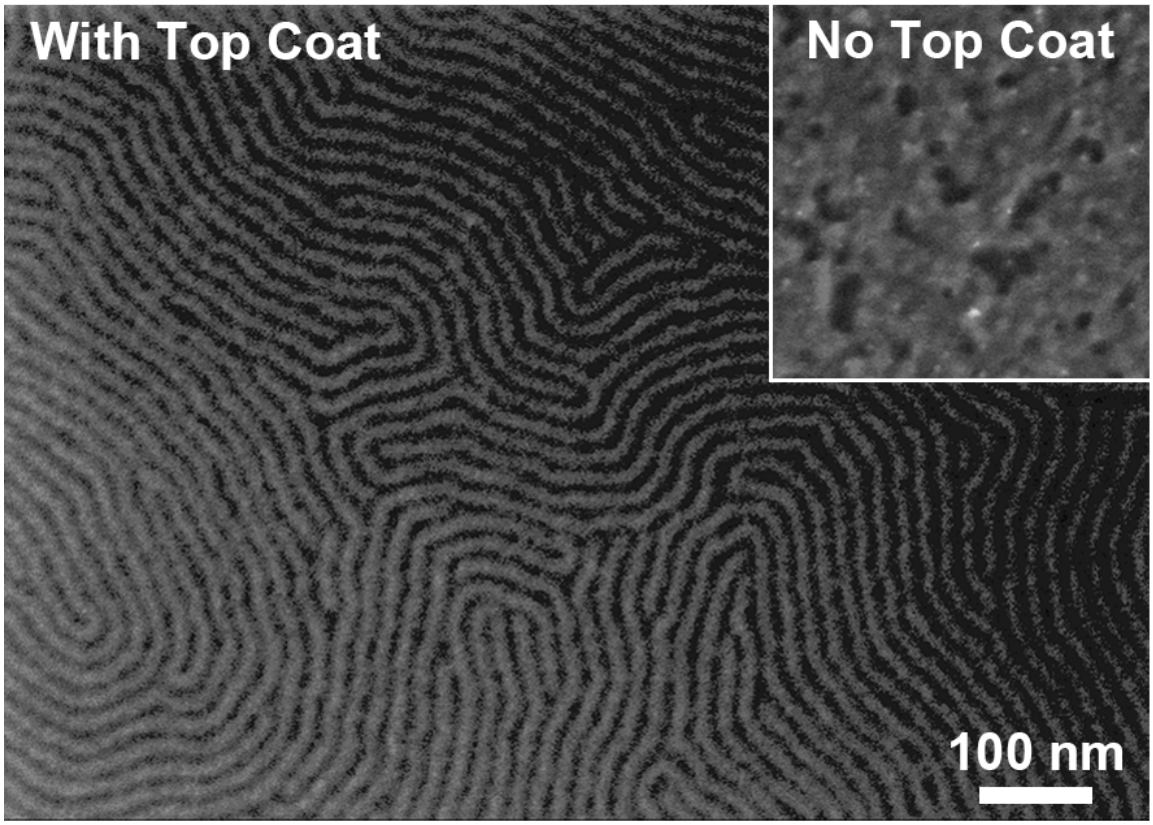

Figure 3.17: SEMs of PTMSS-PLA (L_0=19 nm as measured), annealed at 170 °C for 20h confined between top coat TC-PLA and without a top coat (inset). The BCP film thickness was 10 nm (0.66*L_0). This sample was not etched.

3.12 Problems With the Current System

In this chapter, orientation control of PS-PTMSS-PS and PTMSS-PLA was demonstrated using top coats comprised of maleic anhydride, a norbornene derivative, and a styrene or methacrylamide derivative. While this system worked, there are many problems associated with it. First, the process only worked at one film thickness. This suggests that both the top coat and XPMOST are not perfectly neutral. Recent theory developed by Durand *et al*. shows that non-neutral interfaces can favor the perpendicular orientations under some circumstances.[94] The equations in Section 3.2 can also be used to

study the effect of two preferential interfaces on block copolymer domain orientation. The model in Figure 3.18 shows the case where both the XST and top coat are equally preferential for the same block. Even though the interfaces are preferential, there are narrow thickness windows that favor the perpendicular orientation. On the graph, dashed lines correspond to the thicknesses where PTMSS-PLA and PS-PTMSS-PS were successfully oriented. If the free energy diagram in Figure 3.18 is assumed to be true for the results in this chapter, it explains why the orientation of the block copolymers oriented perpendicular on preferential interfaces, and why the results were so sensitive to film thickness.

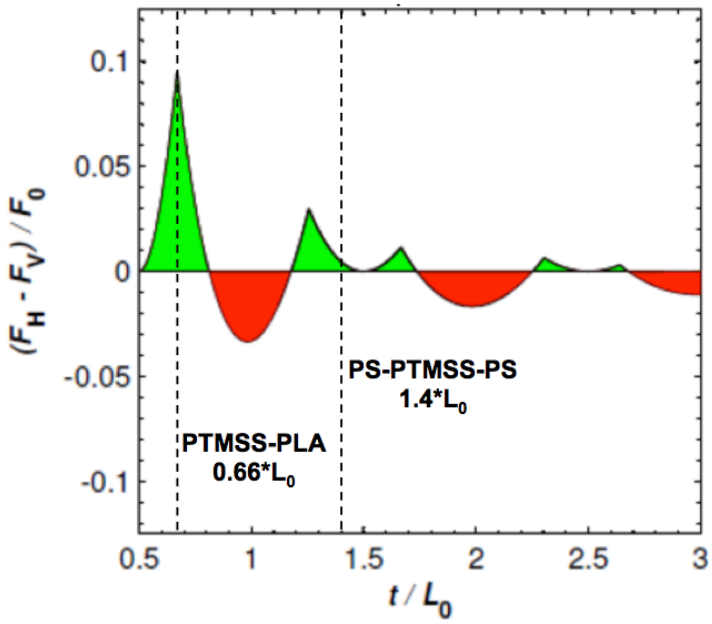

Figure 3.18: Free energy diagram for symmetric wetting interfaces. The dashed lines correspond to film thicknesses in which PS-PTMSS-PS and PTMSS-PLA were successfully oriented.

Another issue with the top coats described in this chapter is that they are largely irreproducible. This is demonstrated by Table 3.1, which lists the polymer feed ratios compared to the polymer composition for several experiments. These experiments were performed in an attempt to reproduce TC-PLA. Entries 1-3 have the exact same feed ratios. Unfortunately, all three polymers differ in composition and only entry 1 was able to control the orientation of PTMSS-PLA. Entries 4-7 examine the effect of changing the monomer feed ratio on the polymer composition. In general, adjusting the polymer feed ratio changes the polymer composition. However, complete control could not be obtained. Lastly, the size exclusion chromatographs (SEC) for these polymers show multimodal molecular weight distributions. The SEC for TC-PS and TC-PLA are shown in Figure 3.19. Obtaining the same polymer twice is nearly impossible.

Table 3.1: Attempts to reproduce TC-PLA

	Feed Ratio*			**Polymer Composition**		
Entry	**MA**	**Nor**	**NPMA**	**MA**	**Nor**	**NPMA**
1	0.60	0.30	0.10	0.65	0.22	0.13
2	0.60	0.30	0.10	0.61	0.22	0.17
3	0.60	0.30	0.10	0.69	0.21	0.10
4	0.60	0.35	0.05	0.69	0.25	0.06
5	0.60	0.30	0.10	0.68	0.21	0.11
6	0.60	0.25	0.15	0.66	0.14	0.20
7	0.60	0.20	0.20	0.62	0.12	0.26

*MA = maleic anhydride, nor = 2-(bicyclo[2.2.1]hept-5-en-2-ylmethyl)- 1,1,1,3,3,3-hexafluoropropan-2-ol, NPMA = N-phenylmethacrylamide

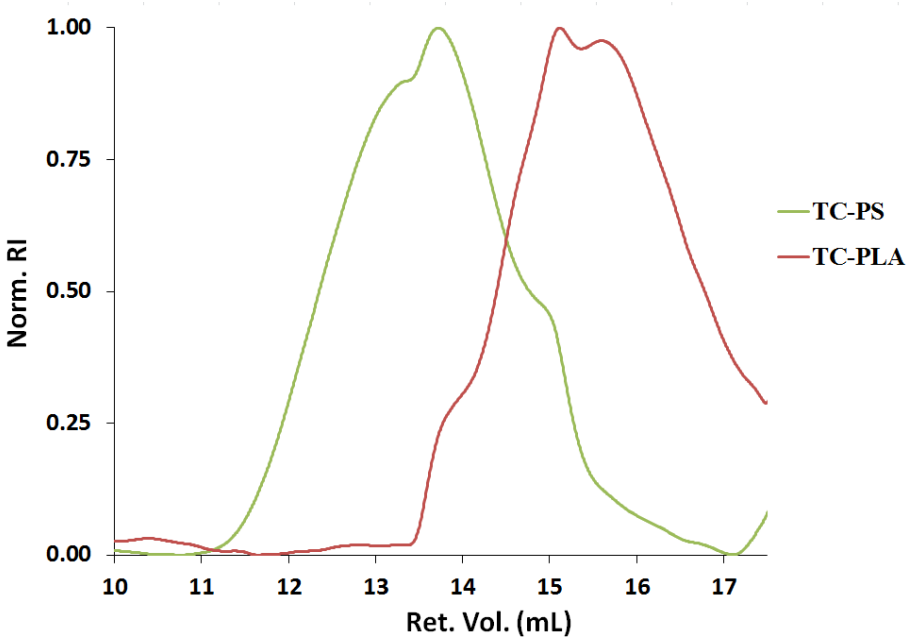

Figure 3.19: Top coat GPC data with DMF as an eluent. Molecular weight data calculated relative to PMMA standards. TC-PLA: M_n=4340 Da, M_w=8350 Da, Dispersity=1.92; TC-PS: M_n=19500 Da, M_w=42000 Da, Đ=2.16.

The future chapters of this dissertation address the weaknesses in this orientation control strategy. In Chapter 4, methodologies to create and characterize neutral surface treatments are explained. In Chapter 5-6, improved top coat synthesis is reported.

3.13 EXPERIMENTAL

Several figures and procedures within this experimental section have been reproduced with permission from "Advanced Materials for Block Copolymer Lithography." Copyright Christopher Bates 2013.

3.13.1 Instrumentation

^{1}H NMR spectra were recorded on a Varian Unity Plus 400 MHz instrument. Chemical shifts are reported in ppm downfield from TMS using the residual protonated solvent as an internal standard ($CDCl_3$, ^{1}H 7.26 ppm). Small molecule IR data were recorded on a Nicolet Avatar 360 FT-IR. Polymeric IR data were collected on a Nicolet Magna-IR 550 Spectrometer. Polymer gel permeation chromatography (GPC) data were measured using an Agilent 1200 Series Isopump and Autosampler with an Agilent Technologies 1100 RI detector equipped with one PLgel 5 μm, 100 Å column and one PLgel 5 μm, 1000 Å column using DMF as an eluent at 70 °C and a flow rate of 1 mL/min. GPC data were measured relative to seven PMMA standards (102, 2200, 4250, 12600, 23500, 41400, and 128000 Da). Films were spin-coated on a Brewer CEE 100CB Spincoater. Film thicknesses were determined with a J.A. Woollam Co, Inc. VB 400 VASE Ellipsometer using wavelengths from 382 to 984 nm with a 65° angle of incidence. Oxygen reactive ion etching was performed on an Oxford Instruments Plasmalab 80+ operating in inductively coupled plasma mode. Scanning electron microscopy was performed using a Zeiss Supra 40 VP at 3 kV with the in-lens detector. TGA data were collected on a TA Instruments Q500. DSC data were collected on a TA Instruments Q100. Combustion analysis was performed by Midwest Microlab LLC.

3.13.2 Materials

All starting reagents were purchased from commercial suppliers and were used as received unless otherwise noted. AIBN was recrystallized from methanol. 2-((1S,4S)-bicyclo[2.2.1]hept-5-en-2-ylmethyl)-1,1,1,3,3,3-hexafluoropropan-2-ol was generously provided by Central Glass Co. Inhibitors were removed using basic alumina prior to polymerization.

3.13.3 Monomer Syntheses

Styrene Derivatives:

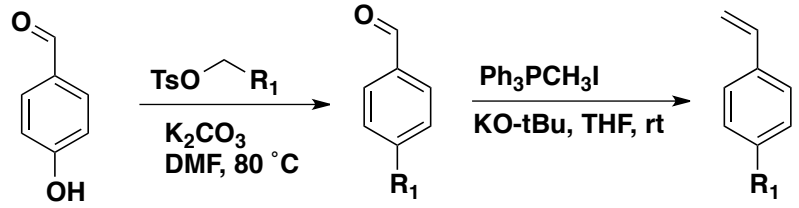

The following reaction is representative procedure for the S_n2 reaction:

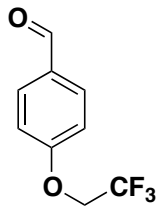

4-(2,2,2-trifluoroethoxy)benzaldehyde- A flame dried round bottom flask equipped with a magnetic stir bar and a rubber septum was charged with 2,2,2-trifluoroethyl 4-methylbenzenesulfonate (7.00 g, 27.5 mmol, 1.3 eq.), 4-hydroxybenzaldehyde (2.52 g, 20.6 mmol, 1 eq.), potassium carbonate (18.9 g, 137.6 mmol, 6.6 eq.), and 50 mL of dry DMF. The cloudy solution was heated to 120˚ C and stirred under a nitrogen atmosphere for 17 hrs. The solution was diluted with 400 mL of water, and the product was extract with 100 mL of ether (4x). The organic phases were combined and washed with 400 mL of water (3x) and 400 mL of brine (1x) and dried over Na_2SO_4. The solvent was removed by rotary evaporation to yield the crude product. Column chromatography (EtOAc/Hex) was used to yield 3.238 g (76.9%) of an off-white solid. MP: 48-51˚C. 1-H NMR (400 MHz; $CDCl_3$): δ 9.92 (s, 1H), 7.90-7.84 (m, 2H), 7.09-7.03 (d, 2H), 4.48-4.39 (q, J=7.9 Hz, 2H). HRMS (CI) m/z for $[M+H]^+$ calcd for $C_9H_8O_2F_3$ 205.0476; found 205.0475.

Representative procedure for the Wittig reactions:

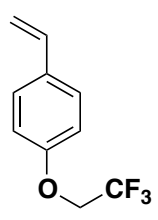

1-(2,2,2-trifluoroethoxy)-4-vinylbenzene- A flame dried round bottom flask equipped with a magnetic stir bar and a rubber septum was charged with methyltriphenylphosphonium iodide (5.4 g, 13.5 mmol, 1.3 eq.), potassium tert-butoxide (1.51 g, 13.5 mmol, 1.3 eq.) and dry THF (100 mL). The solution was bright yellow and cloudy, and was allowed to stir for 5 minutes. 4-(2,2,2-trifluoroethoxy)benzaldehyde (2.113 g, 10.35 mmol, 1 eq.) was dissolved in 25 mL of THF and was cannulated into the solution of ylide. The solution was allowed to stir for 6 hrs at room temperature. The white precipitate was filtered out of the solution, and the solvent was removed. The crude was purified via column chromatography (10% EtOAc/Hex) to yield 1.65 g (79.1%) of pure product as oil. ^{1}H-NMR (400 MHz; $CDCl_3$): δ 7.40-7.36 (m, 2H), 6.92-6.89 (m, 2H), 6.68 (dd, J = 17.6, 10.9, 1H), 5.66 (d, J = 17.6, 1H), 5.19 (d, J = 10.9, 1H), 4.38-4.32 (q, J = 8.1, 2H). ^{13}C-NMR (101 MHz; $CDCl_3$): δ 157.17, 135.94, 132.38, 127.72, 124.83, 115.08, 112.90, 66.02 (q). HRMS (CI) m/z $[M+H]^+$ calcd for $C_{10}H_{10}F_3O$ 203.0683; found 203.0684.

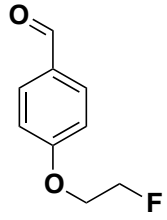

4-(2-fluoroethoxy)benzaldehyde- ^{1}H-NMR (400 MHz; $CDCl_3$): δ 9.89 (s, 1H), 7.86-7.82 (m, 2H), 7.05-7.01 (m, 2H), 4.85-4.83 (m, 1H), 4.74-4.71 (m, 1H), 4.34-4.32 (m, 1H), 4.27-4.25 (m, 1H).

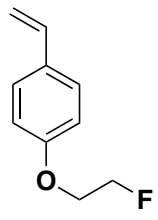

1-(2-fluoroethoxy)-4-vinylbenzene- ^{1}H-NMR (400 MHz; $CDCl_3$): δ 7.39 (q, *J* = 4.8 Hz, 2H), 6.91 (q, *J* = 4.8 Hz, 2H), 6.71 (dd, *J* = 17.6, 10.9 Hz, 1H), 5.67 (dd, *J* = 17.6, 0.9 Hz, 1H), 5.19 (dd, *J* = 10.9, 0.8 Hz, 1H), 4.82-4.69 (m, 2H), 4.24-4.15 (m, 2H).^{13}C-NMR (101 MHz; $CDCl_3$): δ 158.22,

136.15, 131.01, 111.95, 82.79, 81.10, 67.16 (d, J = 20.2 Hz). HRMS (CI) m/z for $[M]^+$ calcd for $C_{10}H_{11}OF$ 166.0794; found 166.0794

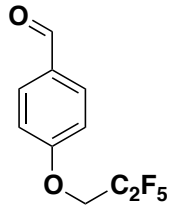

4-(2,2,3,3,3-pentafluoropropoxy)benzaldehyde- ^{1}H-NMR (400 MHz; $CDCl_3$): δ 9.93 (s,), 7.90-7.87 (m, 1H), 7.09-7.05 (m, 1H), 4.51 (tq, J = 12.1, 1.1 Hz, 1H). ^{13}C-NMR (101 MHz; $CDCl_3$): δ 190.73,161.92, 132.17, 131.57, 115.16, 65.07 (s, 1C), 64.79, 64.51. HRMS (CI) m/z for $[M+H]^+$ calcd for $C_{10}H_8F_5O_2$ 255.0444; found 255.044

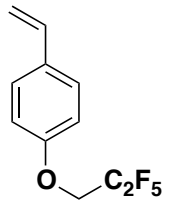

1-(2,2,3,3,3-pentafluoropropoxy)-4-vinylbenzene- ^{1}H-NMR (400 MHz; $CDCl_3$): δ 7.39-7.36 (m, 2H), 6.92-6.89 (m, 2H), 6.67 (dd, J = 17.6, 10.9 Hz, 1H), 5.65 (dd, J = 17.6, 0.9 Hz, 1H), 5.19 (dd, J = 10.9, 0.8 Hz, 1H), 4.42 (tq, J = 12.3, 1.1 Hz, 2H). ^{13}C-NMR (101 MHz; $CDCl_3$): δ 157.19, 135.93, 132.46, 127.71, 115.07, 112.97, 65.42, 65.15, 64.87. HRMS (CI) m/z for $[M+H]^+$ for $C_{11}H_{10}F_5O$ calcd 253.0652; found 253.0652

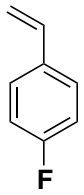

1-fluoro-4-vinylbenzene- ^{1}H-NMR (400 MHz; $CDCl_3$): δ 7.41-7.36 (m, 2H), 7.05-6.99 (m, 2H), 6.69 (dd, J = 17.6, 10.9 Hz, 1H), 5.68 (dd, J = 17.6, 0.5 Hz, 1H), 5.23 (d, J = 10.9 Hz, 1H).

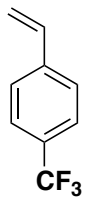

1-(trifluoromethyl)-4-vinylbenzene- ^{1}H NMR (400 MHz; $CDCl_3$): δ 7.58 (d, J = 8.3, 2H), 7.50 (d, J = 8.3, 2H), 6.75 (dd, J = 17.6, 10.9, 1H), 5.85 (dd, J = 17.6, 0.3, 1H), 5.39 (d, J = 10.9, 1H). HRMS (CI) m/z for $[M+H]^+$ calcd for $C_9H_7F_3$ 173.0578; found 173.0574

The following procedure is representative of the Pd-catalyzed reactions to form styrene derivatives:

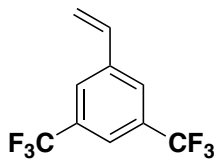

1-fluoro-3-(trifluoromethyl)-5-vinylbenzene - In a Parr reactor, 3,5-bis(trifluoromethyl)bromobenzene (126 g, 525 mmol), tetrabutylammonium bromide (27 g), and palladium acetate (170 mg) was dissolved in acetonitrile (540 mL) and triethylamine (107 mL). The solution was degassed by bubbling nitrogen for 15 minutes. The vessel was sealed and pressurized with 1000 psi of ethylene gas. The reactor was heated to 80˚C for 36 hrs. The vessel was cooled to room temperature and the excess gas was vented. The solution was diluted to 1.5 L and extracted with pentane (3 x 300 mL). The combined organic layers were washed with equivolume amounts of water (3x) and brine (3x). The organic layer was dried over sodium sulfate, filtered, and the solvent was removed via rotary evaporation to yield the product as a slightly yellow oil in 95% yield. ^{1}H-NMR (400 MHz; $CDCl_3$): δ 7.81 (t, J = 0.5 Hz, 2H), 7.75 (s, 1H), 6.77 (dd, J = 17.6, 10.9 Hz, 1H), 5.91 (dd, J = 17.6, 1.5 Hz, 1H), 5.50 (d, J = 10.9 Hz, 1H).

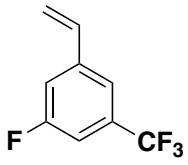

1,3-bis(trifluoromethyl)-5-vinylbenzene- ^{1}H-NMR (400 MHz; $CDCl_3$): δ 7.42 (d, J = 0.6 Hz, 1H), 7.29-7.19 (m, 2H), 6.69 (dd, J = 17.6, 10.9 Hz, 1H), 5.84 (d, J = 17.6 Hz, 1H), 5.42 (d, J = 10.9 Hz, 1H). ^{13}C-NMR (101 MHz; $CDCl_3$): δ 164.13 (s,), 161.66 (s,), 141.08 (d, J = 8.1 Hz,), 134.77 (d, J = 2.3 Hz), 119.14 (quintet, J = 3.5 Hz) 117.32, 116.24, 116.03, 111.98 (dq, J = 24.8, 3.8 Hz). HRMS (CI) m/z for $[M+H]^+$ calcd for $C_9H_7F_4$ 191.0484; found 191.0481

Methacrylamide derivatives:

Representative procedure for the acrylamide derivatives:

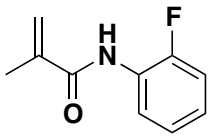

N-(2-fluorophenyl)methacrylamide- A flame dried three-neck round bottom flask equipped with a magnetic stir bar, glass stoppers, and a rubber septum was charged with methacrylic acid (1.26 mL, 14.8 mmol, 1.1 eq.), 2-fluoroaniline (1.30 mL, 13.5 mmol, 1 eq.), DMAP (0.329 g, 0.2 eq.) and dry DCM (15 mL). The solution was stirred under a nitrogen atmosphere, and EDAC·HCl (2.84 g, 14.8 mmol, 1.1 eq.) was added slowly. The resulting solution was stirred for 48 hours. The reaction was partitioned with water, and the organic phase was extracted and washed with equivolume amounts of water (2x), sat. $NaHCO_3$ (2x), sat. NH_4Cl (2x) and brine (1x). The organic phase was dried over Na_2SO_4. The organic phase was concentrated *in vacuo* and purified via column chromatography (5% EtOAc/Hex) to yield the desired product (0.722 g, 40% yield) as a yellow crystalline solid; 1-H NMR (400 MHz; $CDCl_3$): δ 8.40-8.35 (m, 1H), 7.76 (s, 1H), 7.17-7.03 (m, 3H), 5.85 (quintet, J = 0.8, 1H), 5.51 (qd, J = 1.6, 0.6, 1H), 2.08 (dd, J = 1.6, 0.9, 3H) ^{13}C-NMR (101 MHz; $CDCl_3$): δ 166.42, 153.86, 151.44, 140.53, 126.44 (d, *J* = 10.0 Hz), 124.71 (d, *J* = 3.7 Hz), 124.48 (d, *J* = 7.6 Hz), 121.77, 120.70, 114.82 (d, *J* = 18.9 Hz), 18.72. HRMS (CI) m/z for $[M+H]^+$ calcd for $C_{10}H_{11}NO_4F$ 180.0825; found 180.0834

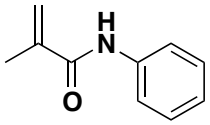

N-phenylmethacrylamide- ^{1}H-NMR (400 MHz; $CDCl_3$): δ 7.67-7.64 (m, 1H), 7.57-7.54 (m, 2H), 7.34-7.30 (m, 2H), 7.13-7.09 (m, 1H), 5.78 (s, 1H), 5.44 (t, *J* = 0.7 Hz, 1H). ^{13}C-NMR (101 MHz; $CDCl_3$): δ 166.85, 140.97, 137.86, 129.08, 124.53, 120.22, 119.99, 18.87. HRMS (CI) m/z for $[M+H]^+$ calcd for $C_{10}H_{12}NO$ 162.0919; found 162.0917

Norbornene derivatives:

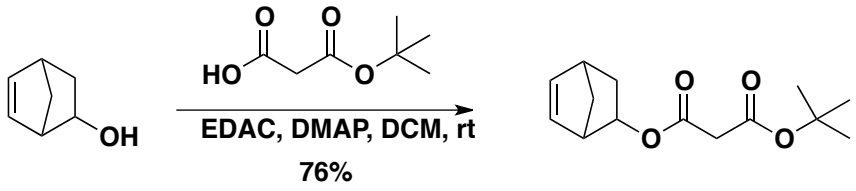

Bicyclo[2.2.1]hept-5-en-2-yl *tert*-butyl malonate . 5-Norbornen-2-ol (mixture of *endo* and *exo,* 5.00 g, 45.4 mmol, 1 eq.) was dissolved in 50 mL of dichloromethane. Under nitrogen, *N*-(3-Dimethylaminopropyl)-*N′*-ethylcarbodiimide hydrochloride (9.57 g, 49.9 mmol, 1.1 eq.) was added to the solution, and the reaction vessel was cooled to 0 ° C. 3-(*tert*-butoxy)-3-oxopropanoic acid (9.57 g, 49.9, 1 mmol) was added slowly to the solution. The vessel was warmed to room temperature and stirred for 3 days. The reaction was poured over an equivolume amount of saturated sodium bicarbonate. The organic layer was dried over sodium sulfate, and the solvent was removed via rotary evaporation. Column chromatography (10% ethyl acetate, hexanes) purified the product as a clear and colorless oil that smelled like watermelon (8.77 g, 76%).^{1}H-NMR (400 MHz; $CDCl_3$): δ 6.28 (ddd, *J* = 29.5, 5.7, 3.0 Hz, 1H), 5.96 (dd, *J* = 5.6, 2.9 Hz, 1H), 5.33-5.30 (m, 1H), 3.28-3.18 (m, 2H), 3.17-3.14 (m, 1H), 2.91-2.83 (m, 1H), 2.17-2.04 (m, 1H), 1.63-1.58 (m, 1H), 1.47 (s, 9H), 1.32-1.25 (m, 1H), 0.98-0.87 (m, 1H). ^{13}C-NMR (101 MHz; $CDCl_3$): δ 173.26, 138.42,138.35, 135.63, 132.11, 59.41, 59.13, 58.85, 49.82, 46.48, 45.93, 43.15, 42.95, 42.66, 41.81, 30.53,29.30. HRMS (EI) m/z for $[M+Na]^+$ calcd for $C_{14}H_{20}O_4Na$ 275.1253; found 275.1260

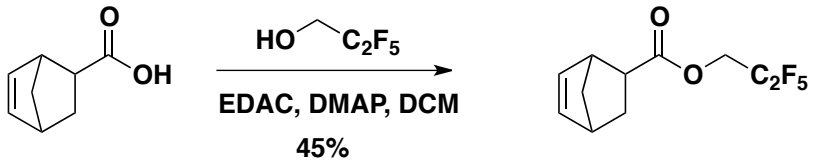

2,2,3,3,3-pentafluoropropylbicyclo[2.2.1]hept-5-ene-2-carboxylate

Bicyclo[2.2.1]hept-5-ene-2-carboxylic acid (mixture of *endo* and *exo,* 2.00 g, 14.47 mmol, 1 eq.) was dissolved in 150 mL of dichloromethane. Under nitrogen, *N*-(3-Dimethylaminopropyl)-*N′*-ethylcarbodiimide hydrochloride (3.05g,15.92 mmol, 1.1 eq.) was added to the solution, and the reaction vessel was cooled to 0 ˚ C. To the solution, 2,2,3,3,3-pentafluoropropanol (2.17 g, 14.5 mmol, 1 eq.) was added slowly to the solution. A catalytic amount of DMAP (0.35 g, 2.89 mmol 0.2 eq.) was also added. The vessel was warmed to room temperature and stirred overnight. The reaction was poured over an equivolume amount of saturated sodium bicarbonate. The organic layer was dried over sodium sulfate, and the solvent was removed via rotary evaporation. Column chromatography (10% ethyl acetate, hexanes) purified the product as a clear and colorless oil (1.75 g, 45%).^{1}H-NMR (400 MHz; $CDCl_3$): δ 6.19 (ddd, J = 19.6, 5.7, 3.0 Hz, 1H), 6.13-5.90 (m, 1H), 4.62-4.37 (m, 2H), 3.27-3.24, 2.34-2.30 (m, 1H), 3.09-2.93 (m, 2H), 1.98-1.92 (m, 1H), 1.51-1.39 (m, 2H), 1.32-1.29 (m, 1H). ^{13}C-NMR (101 MHz; $CDCl_3$): δ 173.26, 138.42, 138.35, 135.63, 132.11, 59.41, 59.13, 58.85, 49.82, 46.48, 45.93, 43.15, 42.95, 42.66, 41.81, 30.53, 29.30. HRMS (CI) m/z $[M+H]^+$: calcd for $C_{11}H_{12}F_5O_2$ 271.0757; found 271.0757.

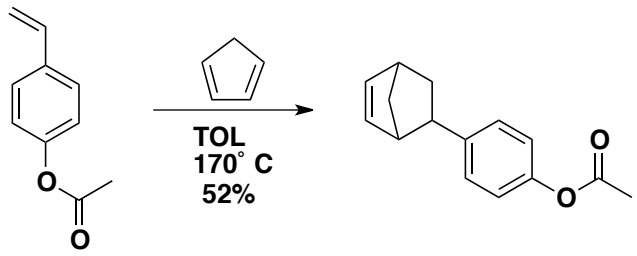

4-(bicyclo[2.2.1]hept-5-en-2-yl)phenyl acetate- In a Parr reactor, freshly cracked cyclopentadiene (18.6 g, 284 mmol, 1 eq.) was dissolved in 100 mL of toluene. To the reactor, hydroquinone (1.5 g) and 4-acetoxystyrene (46.0 g, 284 mmol, 1 eq.) was added, and the reactor vessel was sealed and heated to 170 ˚C. The reaction was heated for 16 hours. The vessel was opened, and the product was distilled to yield the desired product (bop. 125˚C at 46 mmHg, 33.547g, 52%) ^{1}H-NMR (400 MHz; $CDCl_3$): δ 7.30-7.13 (m, 2H), 7.04-6.93 (m, 2H), 6.27 (dd, *J* = 5.7, 3.1 Hz, 1H), 6.00 (ddd, *J* = 145.7, 5.7, 2.9 Hz, 1H), 3.38 (dt, *J* = 9.0, 4.4 Hz, 1H), 3.08-2.91 (m, 2H), 2.31-2.28 (m, 3H), 2.24-2.18 (m, 1H), 1.59-1.51 (m, 1H), 1.48-1.43 (m, 1H), 1.29 (ddd, *J* = 11.8, 4.8, 2.5 Hz, 1H). ^{13}C-NMR (101 MHz; $CDCl_3$): δ 169.88, 169.85, 148.66, 148.53, 143.84, 142.75, 137.54, 137.39, 137.32, 132.85, 129.07, 128.59, 121.28, 120.79, 116.19, 50.38, 48.73, 48.29, 45.82, 43.32, 43.12, 42.41, 33.89, 33.36, 21.28.HRMS (CI) m/z for $[M+H]^+$: calcd for $C_{15}H_{17}O_2$ 228.1150; found 228.1151

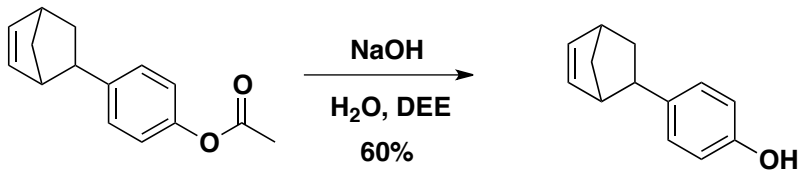

4-(bicyclo[2.2.1]hept-5-en-2-yl)phenol- In a round bottom flask 4-(bicyclo[2.2.1]hept-5-en-2-yl)phenyl acetate (43 g, 188 mmol) was dissolved in 400 mL of diethyl ether. To the

solution, 400 mL of 2M NaOH in water was added. The reaction was stirred vigorously overnight. The basic layer was separated from the organic layer. The organic layer was washed with 2 N NaOH 2 times, and the combined aqueous layers were acidified with concentrated sulfuric acid. Ethyl acetate was used to extract the product, and the solvent was removed. Column chromatography (20% ethyl acetate, hexanes) was used to purify the product as an off-white solid (mixture of *endo* and *exo,* 18.0 g, 60%). ^{1}H-NMR (400 MHz; $CDCl_3$): δ 7.16-6.99 (m, 2H), 7.16-6.99 (m, 2H), 6.81-6.69 (m, 2H), 6.81-6.69 (m, 2H), 6.26-6.16 (m, 1H), 6.26-5.78 (m, 2H), 6.00-5.78 (m, 1H), 4.72-4.67 (m, 1H), 4.72-4.67 (m, 1H), 3.34-2.69 (m, 3H), 3.05-2.84 (m, 2H), 2.31-2.15 (m, 2H), 2.21-2.12 (m, 1H), 2.03-1.87 (m, 1H), 1.72-1.40 (m, 2H), 1.51-1.43 (m, 1H), 1.29-1.21 (m, 1H), 1.27-1.21 (m, 1H). ^{13}C-NMR (101 MHz; $CDCl_3$): δ 169.88,169.85,148.66, 148.53, 143.84, 142.75, 137.54, 137.39, 137.32, 132.85, 129.07, 128.59, 121.28, 120.79, 116.19, 50.38, 48.73, 48.29, 45.82, 43.32, 43.12, 42.41, 33.89, 33.36, 21.28. HRMS (ESI) m/z for $[M-H]^-$: calcd for $C_{13}H_{13}O$ 185.0919; found 185.0972

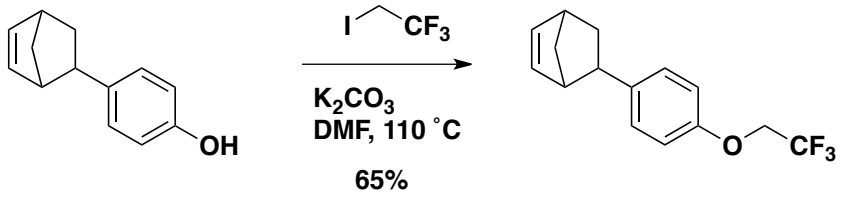

5-(4-(2,2,2-trifluoroethoxy)phenyl)bicyclo[2.2.1]hept-2-ene- In flame dried glassware, 4-(bicyclo[2.2.1]hept-5-en-2-yl)phenol (mixture of isomers, 3.72 g, 20 mmol, 1 eq.) was dissolved in 50 mL of dry DMF. To the solution, 1,1,1-trifluoro-2-iodoethane (3.0 g, 27 mmol, 1.4 eq.) was added along with potassium carbonate (4.14 g, 30 mmol, 1.15 eq.). The reaction was heated to 110 ˚C for 8 hours. The reaction vessel was cooled and

diluted with 500 mL of sat. aq. NH_4Cl. The solution was extracted with ethyl acetate (2 x 100 mL). The organic layers were combined and washed with water, brine, and dried over sodium sulfate. The solvent was removed via rotary evaporation, and the product was purified via column chromatography (5% ethyl acetate, hexanes) to yield a slightly yellow oil (mixture of *endo* and *exo*, 3.215 g, 60%). ^{1}H-NMR (400 MHz; $CDCl_3$): δ 7.25-7.09 (m, 2H), 6.95-6.84 (m, 2H), 6.25 (ddd, *J* = 35.3, 5.7, 3.0 Hz, 1H), 6.04-5.82 (m, 1H), 4.41-4.31 (m, 2H), 3.39 (dt, *J* = 9.0, 4.4 Hz, 1H), 3.10-2.90 (m, 2H), 2.38-2.20 (m, 2H), 1.39-1.27 (m, 2H). HRMS (CI) m/z for $[M+H]^+$: calcd for $C_{15}H_{16}F_3O$ 269.1153; found 269.1154

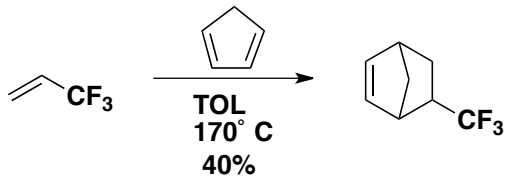

5-(trifluoromethyl)bicyclo[2.2.1]hept-2-ene- Freshly cracked cyclopentadiene (40.5 g, 612 mmol) was added to a Parr reactor with hydroquinone (1 g). The vessel was sealed and pressurized to 300 psi of 3,3,3-trifluoropropene and heated to 170 ˚C for 92 hours. The vessel was cooled to room temperature and excess gas was vented. The product was distilled from the mixture (4:1 endo:exo, b.p. 65 ˚C at 130 mmHg, 40.6 g, 40%). ^{1}H-NMR (400 MHz; C_6H_6): δ 6.20 (dd, *J* = 5.7, 3.1 Hz, 1H), 6.20 (dd, *J* = 5.7, 3.1 Hz, 1H), 6.17-6.16 (m, 1H), 6.17-6.16 (m, 1H), 5.99-5.95 (m, 1H), 5.99-5.95 (m, 1H), 3.11-3.08 (m, 1H), 3.11-3.08 (m, 1H), 3.00-2.92 (m, 2H), 3.00-2.92 (m, 2H), 2.73 (quintetdd, *J* = 9.9, 5.1, 3.3 Hz, 1H), 2.73 (quintetdd, *J* = 9.9, 5.1, 3.3 Hz, 1H), 2.03-1.93 (m, 2H), 2.03-1.93 (m, 2H), 1.73-1.67 (m), 1.73-1.67 (m), 1.56-1.36 (m, 3H), 1.56-1.36 (m, 3H), 1.31-1.25 (m, 3H), 1.31-1.25 (m, 3H), 1.13 (ddd, *J* = 12.0, 5.1, 2.6 Hz, 2H), 1.13 (ddd, *J* =

12.0, 5.1, 2.6 Hz, 2H), 0.90-0.84 (m, 1H), 0.90-0.84 (m, 1H). ^{13}C-NMR (101 MHz; C_6H_6): δ 138.18, 137.54, 136.38, 131.87, 129.40, 126.64, 50.00 (t, *J* = 1.4 Hz), 46.21 (t, *J* = 1.8 Hz), 43.55-43.43, 43.08-43.03, 42.77, 42.49 (d, *J* = 3.0 Hz), 41.34, 31.78, 27.77, 22.83. HRMS (CI) m/z for $[M+H]^+$ calcd for $C_8H_{10}F_3$ 163.0735; found 163.0734

3.13.4 Polymer Synthesis

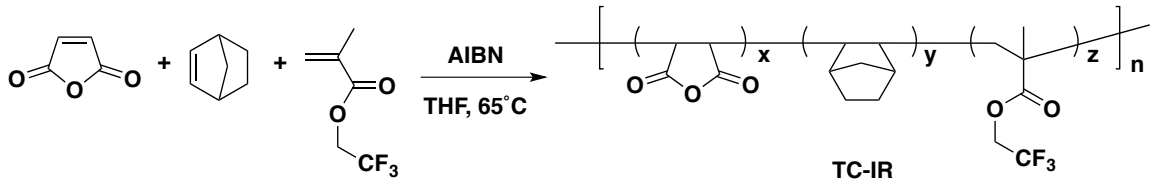

TC-IR: A 50 mL round bottom flask (RBF) was charged with a stir bar, maleic anhydride (6 eq., 1.575 g, 16.06 mmol), norbornylene (3 eq., 0.756 g, 8.03 mmol), 2,2,2-trifluoroethyl methacrylate (1 eq., 0.450 g, 2.68 mmol), and azoisobutyronitrile (0.1 eq., 0.044 g, 0.268 mmol). The RBF was fitted with a reflux condenser and 20 mL of dry THF was added, followed by three freeze-pump-thaw cycles to remove oxygen. The RBF was submerged in an oil bath at 60 °C under dry N_2 for 48 h, quenched at 0 °C, and precipitated in hexanes at room temperature. The product was filtered and dissolved in ethyl acetate, followed by 6 liquid-liquid extractions with H_2O to remove unreacted maleic anhydride monomer. The fine white powder was isolated by filtration and dried *in vacuo* to give ca. 50% yield. The top coat was analyzed by gel permeation chromatography. Molecular weight data calculated relative to PMMA standards. TC-IR: M_n=3490 Da, M_w=6700 Da, Dispersity=1.92. Composition (combustion): Maleic Anhydride:Norbornene:Methacrylate=50:34:16, T_g=137 °C.

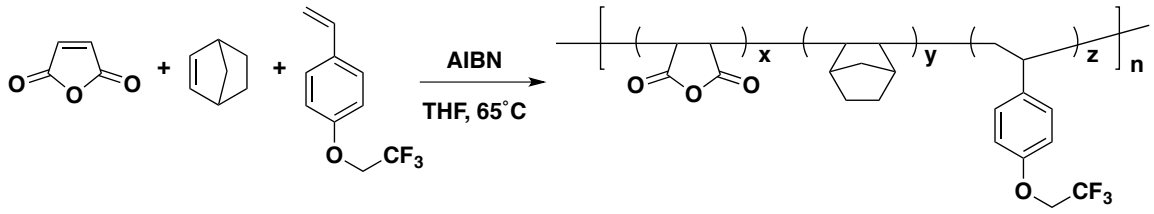

TC-OCF$_3$: A flame dried round bottom flask equipped with a magnetic stir bar and water condenser was charged with maleic anhydride (1.16 g, 11.8 mmol, 0.6 eq.), 1-(2,2,2-trifluoroethoxy)-4-vinylbenzene (0.40, 1.97 g, 0.1 eq.), norbornene (0.55 g, 5.9 mmol, 0.3 eq.), AIBN (6.5 mg, 0.039 mmol, 0.002 eq.), and dry THF (6 g). The solution was degassed by the freeze-pump-thaw method three times. The solution was heated and stirred at 60˚ C for 48 hours. The THF was removed and the polymer was dissolved in EtOAc (25 mL). It was washed with 25 mL (3x) of water. The solvent was removed until only about 2 mL of solution remained. The polymer was precipitated three times from EtOAc in hexane, 1:1 hexane/DCM, and DCM to remove any remaining monomer and impurities. The polymer was dried *in vacuo*, and 255 mg of polymer was obtained. Molecular weight data calculated relative to PMMA standards. M_n=6380 Da, M_w=18200 Da, Dispersity=2.85. Maleic Anhydride:Norbornene:Styrene=56:17:27, T_g=180°C.

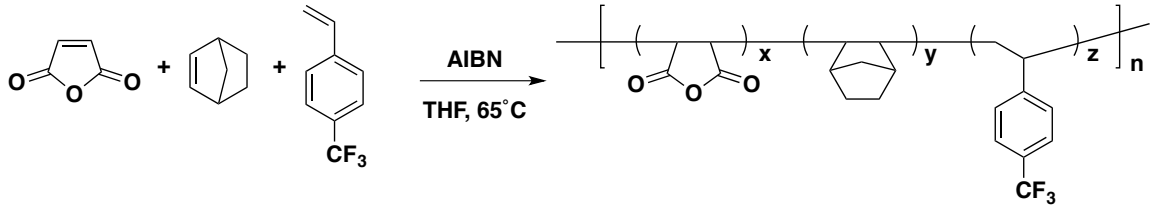

TC-PS: A flame dried round bottom flask equipped with a magnetic stir bar and water condenser was charged with maleic anhydride (1.16 g, 11.8 mmol, 0.6 eq.), norbornene (0.45 g, 6.94 mmol, 0.3 eq.), 1-(trifluoromethyl)-4-vinylbenzene (0.40 g, 2.32 mmol, 0.1 eq.), AIBN (7.6 mg, 0.046 mmol, 0.002 eq.), and dry THF (6.8 g). The solution was

degassed by the freeze-pump-thaw method three times. The solution was heated and stirred at 60˚ C for 48 hours. The THF was removed and the polymer was dissolved in EtOAc (25 mL). It was washed with 25 mL (3x) of water. The organic layer was added dropwise to hexane (~100 g) in order to precipitate out the polymer. The polymer was precipitated 2 more times in solutions of 1:1 hexane/DCM, and DCM to remove any remaining monomer and impurities. The polymer was dried *in vacuo*, and 200 mg of polymer was obtained. The top coat was analyzed by gel permeation chromatography. TC-PS: Composition (mol% from combustion): Maleic Anhydride:Norbornene:Styrene=57:17:26, T_g=214 °C.

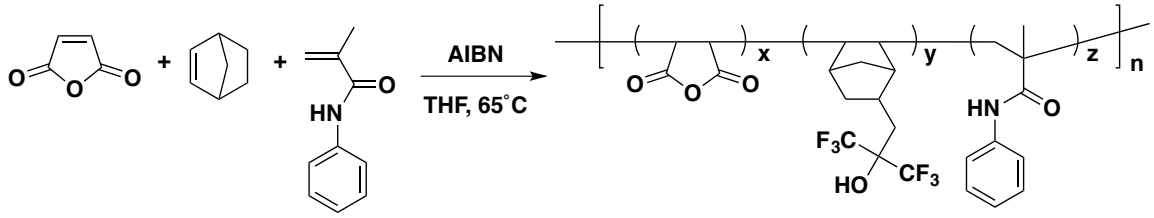

TC-PLA: A 50 mL round bottom flask was charged with a stir bar, maleic anhydride (6 eq., 1.130 g, 11.52 mmol), 3-(Bicyclo[2.2.1]hept-5-en-2-yl)-1,1,1-trifluoro-2-(trifluoromethyl)propan-2-ol (3 eq., 1.580 g, 5.762 mmol), N-Phenylmethacrylamide (1 eq., 0.310 g, 1.921 mmol), and azoisobutyronitrile (0.05 eq., 0.016 g, 0.096 mmol).The RBF was fitted with a reflux condenser and 8 mL of dry THF was added, followed by three freeze-pump-thaw cycles to remove oxygen. The RBF was submerged in an oil bath at 60 °C for 48 h, quenched at 0 °C, and precipitated in hexanes at room temperature. The product was filtered and redissolved in ethyl acetate, followed by 6 liquid-liquid extractions with H_2O to remove unreacted maleic anhydride monomer. The polymer solution was poured into hexane: DCM=6:4(wt/wt) mixture solvent. The fine white

powder was isolated by filtration and dried *in vacuo* to give ~30% yield. The top coat was analyzed by gel permeation chromatography (Figure 29). TC-PLA: Composition (mol% from combustion): Maleic Anhydride:Norbornene:Methacrylate=68:21:11, T_g=190 °C.

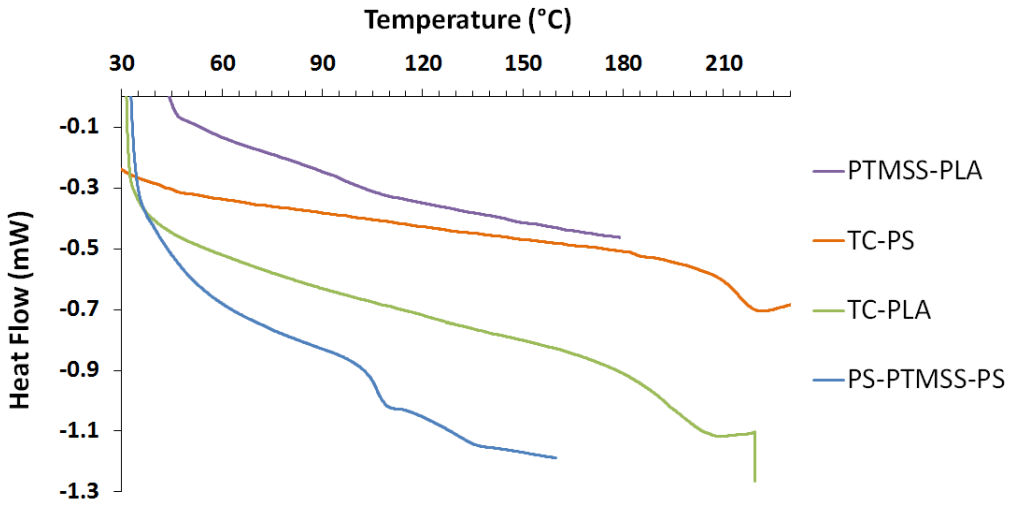

Figure 3.20: DSC data of block copolymers PS-PTMSS-PS and PTMSS-PLA and top coats TC-PS and TC-PLA. PS-PTMSS-PS: Heating rate=10 °C/min for PS-PTMSS-PS and 5 °C/min for PTMSS-PLA, TC-PS, and TC-PLA.

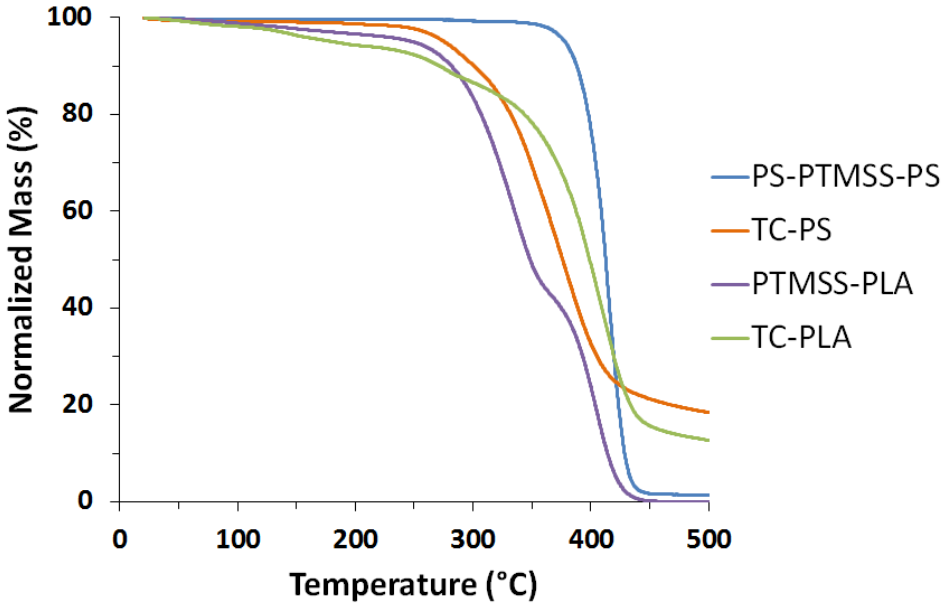

Figure 3.21: TGA data of block copolymers PS-PTMSS-PS and PTMSS-PLA and the top coats TC-PS and TC-PLA. The ramp rate for PS-PTMSS-PS was 5 °C/min from 20-300 °C and 20 °C/min from 300-500 °C; for PTMSS-PLA it was 10 °C/min from 0-500 °C; for TC-PS it was 10 °C/min from 20-500 °C; for TC-PLA it was 10 °C/min from 20-300 °C and 40 °C/min from 300-500 °C.

3.13.5 Substrate Surface Treatments

The substrate surface treatment poly(4-methoxystyrene-*random*-4-vinylbenzylazide) (XPMOST) was synthesized according to previously reported literature procedure.[59,61] Chapter 4 focuses on the synthetic details of these materials.

3.13.6 IR Study

The model topcoat containing maleic anhydride, norbornene, and a fluorinated methacrylate (TC-IR, Scheme 3.5) was used to generate thin film IR data, which were collected in transmission mode on thin films ca. 280 nm thick coated on NaCl salt plates

(Figure 3.7). The blue "no base" curve represents the top coat spin coated out of 2-butanone, which is unreactive towards the poly(maleic anhydride) moiety. The red "NH_4OH" curve was spin coated from a 30 wt% aq. NH_4OH solution and was subsequently heated at 210 °C for 1 min to produce the green curve.

3.13.7 Thin Film Preparation

A 0.5 wt% toluene solution of XPMOST was spin-coated at 3000 rpm for 30 sec onto a wafer that had been rinsed with acetone and isopropanol three times, respectively. The wafer was annealed at 250 °C for 5 min on a hot plate open to air to cross-link the film. Once removed from the hot plate and cooled to room temperature, the wafer was then submerged in toluene for 2 min and blown dry two times to remove uncrosslinked polymer. Typical film thicknesses were on the order of 13-15 nm, as determined by ellipsometry. Approximately 1 wt% toluene solutions of lamellar-forming PS-PTMSS-PS were applied to crosslinked XPMOST films at various spin speeds to produce different block copolymer film thicknesses as determined by ellipsometry. The top coat was then spin-coated out of a 3:1 by wt solution of MeOH:30 wt% aq. NH_4OH (for TC-PS) or just 30 wt% aq. NH_4OH (for TC-PLA) at various concentrations, giving top coat film thicknesses ca. 18 nm (TC-PLA) and ca. 60 nm (TC-PS). Methanol was used with the application of TC-PS to produce more uniform top coat thin films. Solutions of 3:1 by weight solution of MeOH:30 wt% aq. NH_4OH were found to have no effect on the block copolymer film thickness of both PS-PTMSS-PS and PTMSS-PLA as measured by ellipsometry. The film stacks were subsequently annealed at 170 °C (for PTMSS-PLA, in a vacuum oven) and 210 °C (for PS-PTMSS-PS, on a hot plate open to air) for 20 hr and one minute, respectively. Upon completion of annealing, the PTMSS-PLA sample

annealed in the vacuum oven was cooled down to room temperature under vacuum over the course of ca. 5 hr. The PS-PTMSS-PS sample annealed on a hotplate was removed and quickly cooled to room temperature on a room temperature solid metal block. The top coats were subsequently stripped with a 3:1 by weight solution of MeOH:30 wt% aq. NH_4OH by spinning the wafer at 3000 rpm and applying 20 drops of stripping solution by pipette. In most cases, less than 2 nm of residual top coat could be detected by ellipsometry. Stripped samples of PS-PTMSS-PS triblock copolymer were subsequently etched with oxygen reactive ion etching. Stripped samples of PTMSS-PLA were not etched. SEM images presented in the main body of the paper have had brightness and contrast enhanced with image editing software.

3.13.8 Etching

Oxygen plasma reactive ion etching performed on thin films of PS-PTMSS-PS used the following settings: pressure=20 mTorr, RF power=10 W, ICP power=50 W, O_2 flow rate=75 sccm, Ar flow rate=75 sccm, temperature=15 °C. These settings have previously been established as effective for at least partially removing one organic block relative to a PTMSS block. The etch rate of PS homopolymer using these conditions was measured with ellipsometry to be approximately 0.46 nm/sec; this corresponds with a targeted etch depth of 14 nm in 30 sec for the PS-PTMSS-PS triblock copolymer. The SF_6/C_4F_8 etch used for pattern transfer into single-crystal silicon used the following settings: pressure=55 mTorr, RF power=80 W, ICP power=150 W, SF_6 flow rate=20 sccm, C_4F_8 flow rate=50 sccm, temperature=15 °C. Etch times were variable and are specified in figure captions. Pattern transfer etch: The following sequence of etch times

was used, with the aforementioned formulas: 70 sec O_2, 5 sec SF_6/C_4F_8, 45 sec O_2, 75 sec SF_6. A piranha solution was used post-etch to remove residual surface treatment.

3.14 ACKNOWLEDGEMENTS

The synthesis of PS-PTMSS-PS and PTMSS-PLA was performed by Dr. Julia Cushen. Top coat design and synthesis was done in collaboration with Dr. Christopher Bates, Dr. William Durand, Gregory Blachut, and Takehiro Seshimo. Leon Dean made large contributions to the thin film processing. Dr. William Durand contributed to the theoretical sections.

Chapter 4: Substrate Surface Treatment Evaluation

4.1 Importance of Interfacial Interactions at the Substrate

In the previous chapter, the importance of neutral interfaces was discussed. The focus of this chapter is on controlling the interactions with the block copolymer domains and the substrate. Ignoring the air interface and complex morphologies, the lamellar domains of an AB diblock can adopt three distinct orientations as a result of surface interactions (Figure 4.1). If the substrate surface is preferential to either of the block copolymer domains, then a parallel orientation is preferred. However, if the surface is non-preferential (neutral), then the energetic penalty of each domain making contact with the substrate surface is perfectly offset. This allows both domains to touch the interface and adopt a perpendicular orientation. On a perfectly neutral substrate, the perpendicular orientation will be observed as long as the block copolymer-free interface is also neutral.[53] As discussed in previous chapters, this is not true for silicon-containing polymers as silicon tends to wet the air interface.[102]

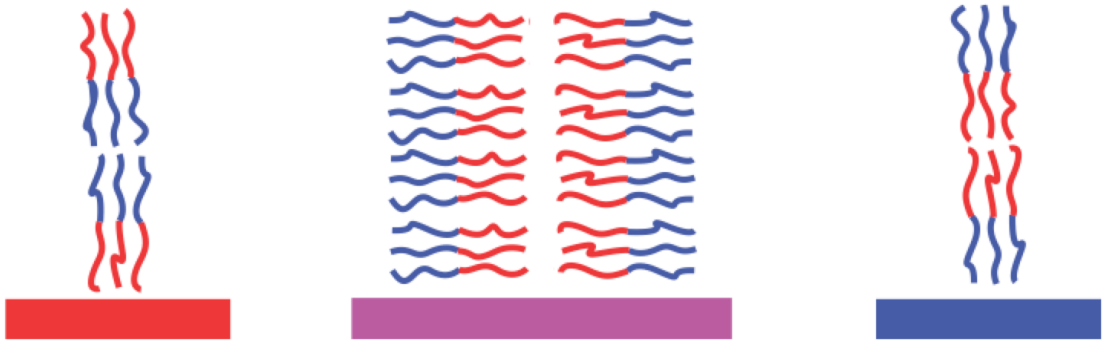

Figure 4.1: Illustration of parallel domains on preferential interfaces and perpendicular domains on a neutral surface.

4.2 CONTROLLING SUBSTRATE INTERACTIONS

On a silicon wafer, the native SiO_2 is inherently preferential and not neutral to most block copolymers. Therefore, this interaction needs to be shielded. Much of the early work focused on developing methods to shield this interaction by polymeric surface treatments,[54,55,58,59,103] which were designed to control the orientation of poly(styrene-*block*-methylmethacrylate) (PS-PMMA). The air interface for PS-PMMA is neutral at 230°C degrees,[104] but the SiO_2 is preferential towards the PMMA block and causes the domains to adopt a parallel orientation when annealed on a silicon wafer. Polymeric brushes and crosslinkable surface treatments (XSTs) have been developed to create neutral interfaces. These brushes and XSTs typically contain the monomers that comprise the block copolymer. For example, an XST that contains only styrene will be preferential to the PS block whereas an XST that only contains MMA will be preferential to the PMMA block. Somewhere between the two extremes, copolymers with both styrene and MMA can balance the interfacial interactions. At some ratio of the two monomers, the XST will be neutral and promote the perpendicular orientation.

4.3 SURFACE TREATMENT DESIGN

In the Willson group, efforts have been directed to making both brushes and XSTs to control the interfacial interactions of poly(styrene-*block*-4-trimethylsilylstyrene) (PS-PTMSS, L_0 = 22nm). This chapter focuses on XSTs because XSTs are easier to synthesize than hydroxy-terminated brushes, which rely on difficult to synthesize initiators and controlled radical polymerization techniques. The XSTs used herein were synthesized by uncontrolled free radical polymerization using three monomers according to Scheme 4.1. The three monomers that were chosen were 4-chloromethylstyrene, 4-*tert*-butylstyrene, and methyl methacrylate. The 4-*tert*-butylstyrene monomer is hydrophobic and should be preferential towards the hydrophobic, silicon-containing PTMSS block. Methylmethacrylate is much more polar and hydrophilic compared to 4-*tert*-butylstyrene and should preferentially interact with PS. 4-Chloromethylstyrene provides a functional handle for post-polymer modification. In scheme 4.2, the bimolecular nucleophilic substitution reaction with sodium azide is shown.[59,61] The azide can act as a thermal crosslinker at elevated temperatures (~250˚C).

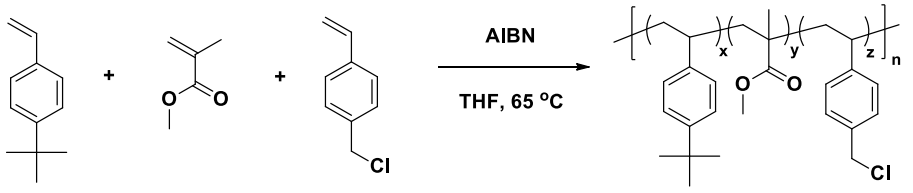

Scheme 4.1: Free radical copolymerization of the crosslinkable surface treatments.

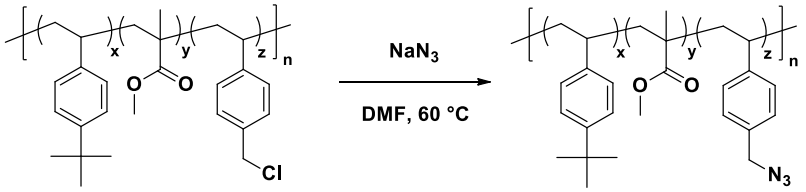

Scheme 4.2: Postpolymer modification to create thermally crosslinkable XSTs.

The decision to not incorporate the exact monomers in PS-PTMSS into the XST was done for several reasons. First, 4-trimethylsilylstyrene has silicon in it and because silicon is etch resistant, it was purposefully left out of the XST. Eventual pattern transfer requires etching through the XST. Therefore, 4-trimethylsilylstyrene was replaced with the carbonaceous analog, 4-*tert*-butylstyrene, in the XST. The XSTs were intended to control the orientation of more than one block copolymer. Therefore, MMA, which is more polar than styrene, was used as the hydrophilic component. This allows access to a wider range of surface energies than is needed for PS-PTMSS. By adjusting the ratio of the MMA and 4-*tert*-butylstyrene, any of the surface energies spanned by the extremes is theoretically obtainable as demonstrated by Figure 4.2.

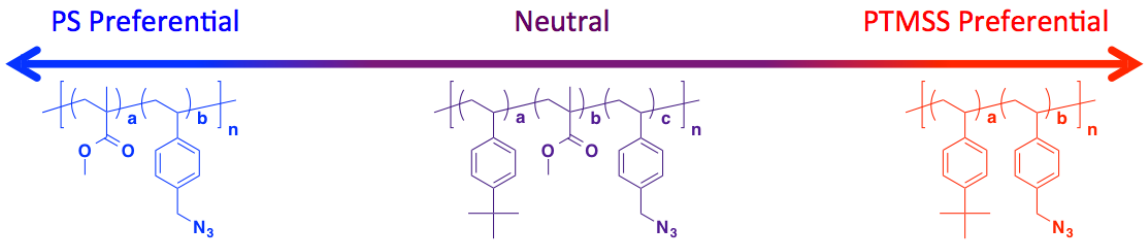

Figure 4.2: Range of accessible surface energies using the XSTs in this chapter.

Control over the XST composition is critical. A study on the reactivity ratios for these three monomers has been previously reported by Bates.[105] His results demonstrate that these three monomers can form statistical copolymers. A series of XSTs were synthesized by varying the monomer feed ratios. The copolymerizations were purposely run to low conversion to avoid monomer drift.[106] After synthesis, post-polymer modification converts the chloro-substituent to an azide. Confirmation of the transformation can be followed in the NMR as shown in Figure 4.3. Typically, the

azidation reaction in Scheme 4.2 goes overnight at 60˚C and goes to completion as indicated by a shift in the methylene protons from ~4.55 to ~4.25 ppm.

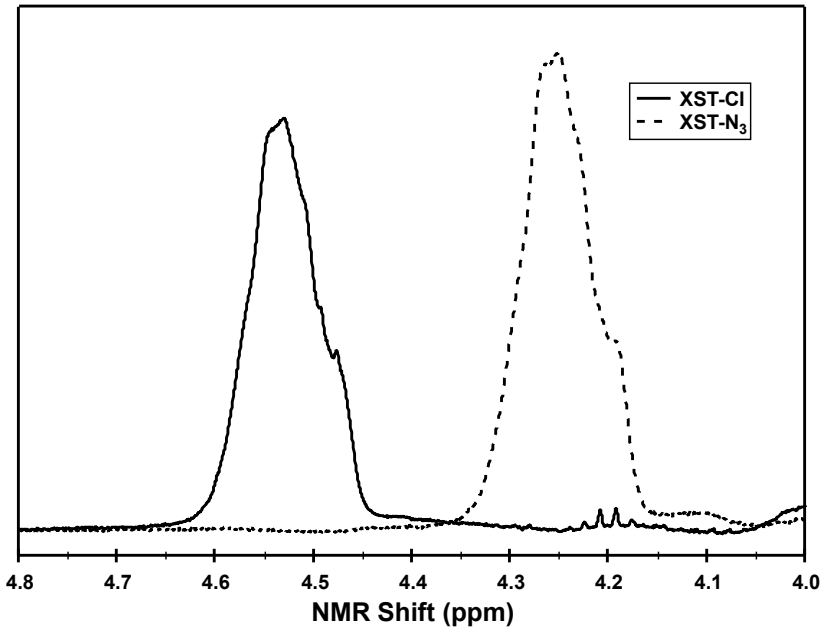

Figure 4.3: NMR of the XST before (XST-Cl) and after (XST-N_3) post-polymer modification.

Table 4.1 shows the characterization data of a series of XSTs. The XSTs have been labeled XST-xx where xx represents the percentage of 4-*tert*-butylstyrene incorporated into the XST. The actual composition of polymer correlates well with the monomer feed ratio, which demonstrates close control over composition. Additionally, each XST shows a monomodal distribution of molecular weights with dispersities below 2. The size exclusion chromatographs are shown in Figures 4.4 and 4.5.

Table 4.1: XST characterization summary.

	Feed Ratio			Actual Ratios			Molecular Weight (Da)		
XST	**tBuS**	**MMA**	**VBzCl***	**tBuS**	**MMA**	**VBzAz***	**M_n**	**M_w**	**Đ**
XST-22	16	81	3	22	72	6	31600	51300	1.62
XST-34	26	71	4	34	60	6	51400	71300	1.39
XST-48	48	49	3	48	48	4	36700	54100	1.49
XST-51	50	45	5	51	43	6	84800	120300	1.42
XST-52	58	38	4	52	44	4	36200	61800	1.71
XST-60	64	3	3	60	35	5	24600	36500	1.48
XST-64	67	30	3	64	30	6	34200	58300	1.70
XST-65	70	27	3	65	30	5	31000	52200	1.69

*Polymers were synthesized with vinylbenzyl chloride monomer and the resulting polymer was subsequently modified to vinylbenzyl azide.
Molecular weight data were calculated relative to a polystyrene standard in THF.
Abbreviations: tBuS= 4-*tert*-butylstyrene, MMA = methylmethacrylate, VBzCl = vinylbenzylchloride, VBzAz = vinylbenzylazide.

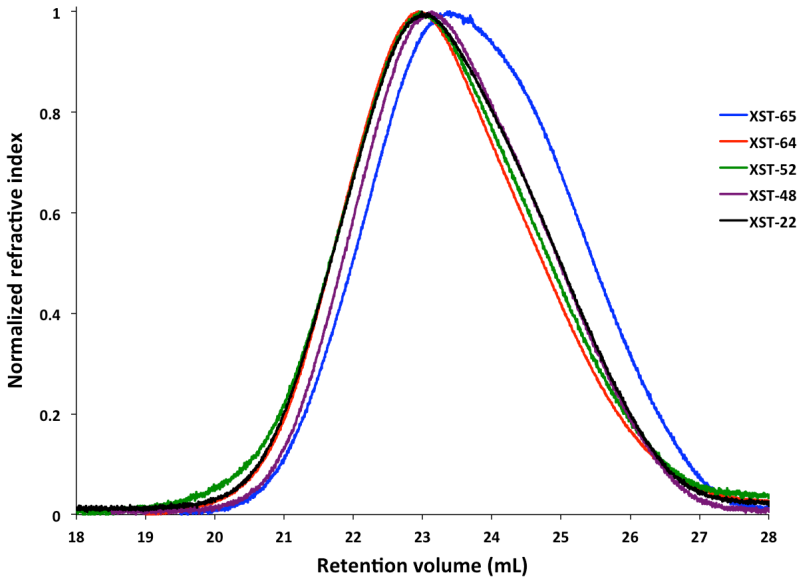

Figure 4.4: Size exclusion chromatograms of the XSTs reported in Table 4.1

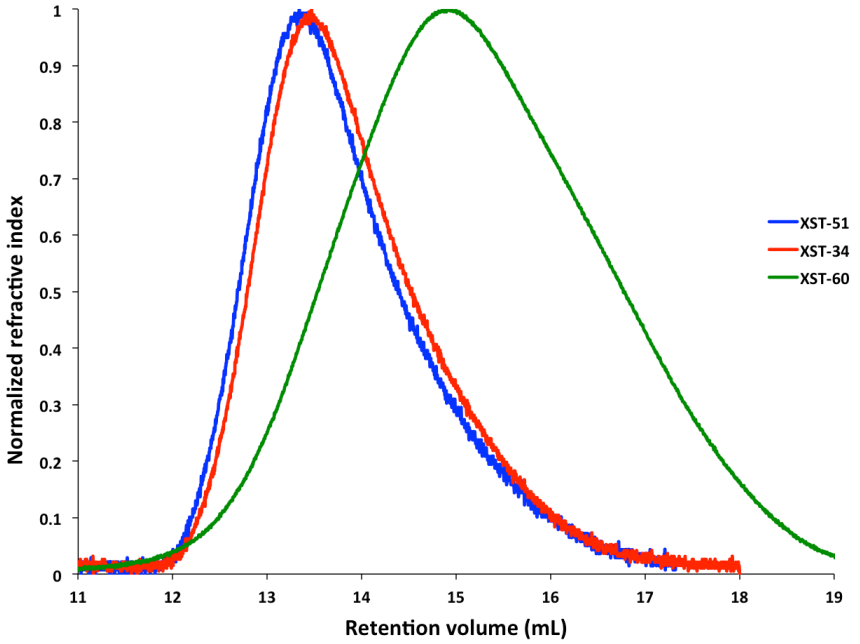

Figure 4.5: Additional size exclusion chromatograms of the XSTs reported in Table 4.1

4.4 THIN FILM PROCESSING

The XSTs are soluble in many good spin coating solvents such as toluene, PGMEA, MIBK, etc. To obtain films on the order of 10 nm, 0.5 wt% solutions were spin coated on silicon wafers at 3000 rpm. The resulting films were between 10-15 nm. Thermally annealing the film at 250˚C rendered the film insoluble to all solvents. An IR study of a thick film (~400nm) shows complete disappearance of the azide peak[107] at 2100 cm^{-1} after 5 mins of heating at 250˚C. This is consistent with the formation of nitrene that crosslinks the film.[108,109] The polymer before azidation does not crosslink, and a film annealed under the same crosslinking conditions is completely removed by exposure to solvent.

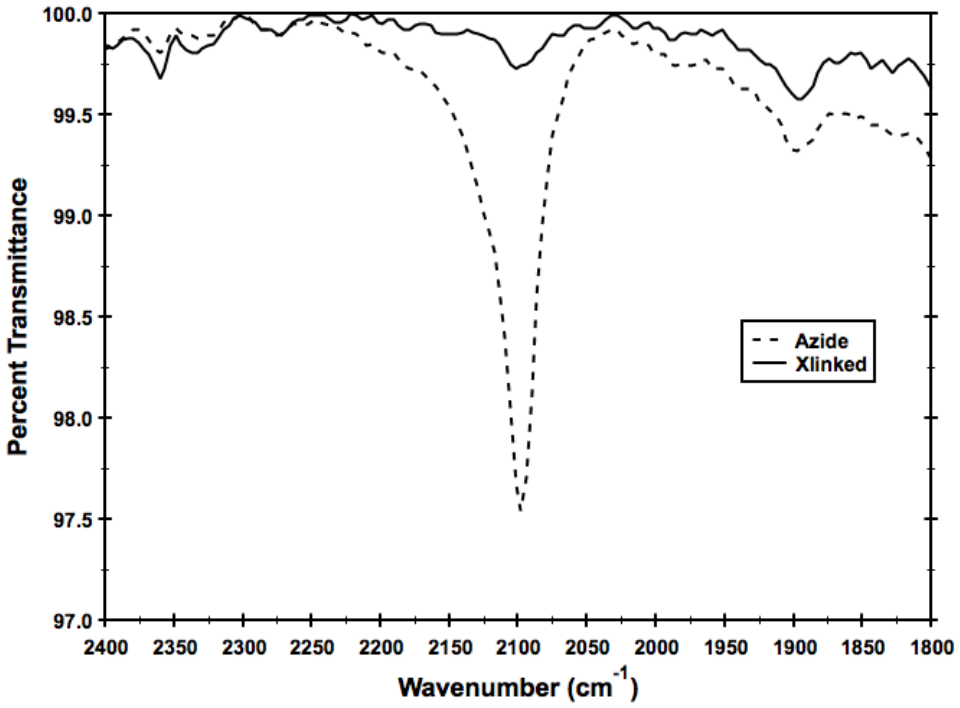

Figure 4.6: IR spectrum of a ~400 nm thick XST before (Azide, dashed lined) and after thermally crosslinking (Xlinked, solid line) at 250˚C for 5 min.

4.5 Island and Hole Methodology

It is important to determine the wetting preference of each XST in order to find a neutral composition. In previous literature, this was performed by spin coating PS-PMMA onto different surface treatments and thermally annealing the sample at 230-250˚C.[55,62,110] Since PS-PMMA has a neutral air interface, a perpendicular orientation of domains will be observed by AFM or SEM if the XST is also neutral. If it is not neutral, then a parallel domain orientation is observed. Islands and holes form if the block copolymer film thickness is not commensurate with the block copolymer periodicity.[89,111] Depending on whether or not islands or holes form, the wetting preference of an XST can be determined.

For silicon-containing block copolymers, the air interface is preferential to the silicon-containing domain, which causes the block copolymer to adopt parallel domains during thermal annealing. Because PTMSS migrates to the air interfaces, it is possible to determine which block wets the XST by using the well-established island/hole methodology.[110] There are two commensurate film thicknesses of parallel domains depending on which block wets the XST (Figure 4.7). If PTMSS wets both the air interface and the XST, then the block copolymer film thickness that minimizes the free energy of the system is nL_0 (symmetric wetting) where n is an integer. However, if PTMSS wets the air interfaces but PS wets the XST, then lowest energy film thickness is $(n+0.5)L_0$ (asymmetric wetting).

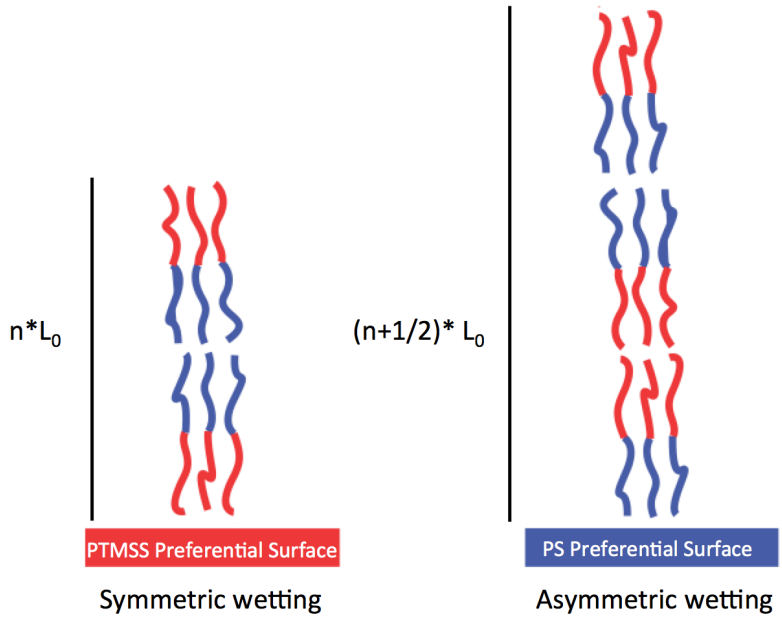

Figure 4.7: Commensurate film thicknesses for symmetric and asymmetric wetting conditions for PS-PTMSS. PTMSS and PS are depicted as the red and blue block, respectively. The free interface always prefers PTMSS.

If the initial block copolymer film thickness (L_{avg}) is incommensurate (e.g. 1.25 L_0), the block copolymer chains would have to either over stretch or over compress to satisfy the symmetric (nL_0) or asymmetric wetting cases (n+0.5)L_0, which effectively causes L_0 to deviate from its bulk periodicity. A change in L_0 due to frustration has been observed for block copolymers confined between two hard surfaces.[112,113] However, when there is a free interface, the block copolymer can alleviate frustration by forming topography instead of changing L_0.[114] For example, consider the situation where the block copolymer is spin coated at 1.25 L_0 on an XST where the wetting preference is unknown. Figure 4.8 shows the two possible topographical features that could form when the sample is annealed on XSTs that are either PTMSS or PS preferential. If the XST is PTMSS preferential, the film wants to satisfy the symmetric wetting conditions and be at thicknesses that are nL_0. During thermal annealing, the bulk of the film decreases in thickness to 1 L_0 if the initial film thickness is 1 $L_0 < L_{avg} < 1.5$ L_0. The entire film cannot shrink to 1 L_0 because there is "extra" material, and this extra material forms islands on top of film. If the XST is PS preferential, then the bulk of the BCP film grows to 1.5 L_0. In this case, there is not enough material for the entire film to grow to 1.5 L_0 and holes form to satisfy the asymmetric wetting condition. The step heights of the island and holes correspond to 1 L_0. Island and holes are microns in diameter, form quickly (<10 minutes at 180˚C for PS-PTMSS), and can be easily observed using optical microscopy and AFM. Therefore, XSTs and their wetting preference can be quickly determined using these methods.

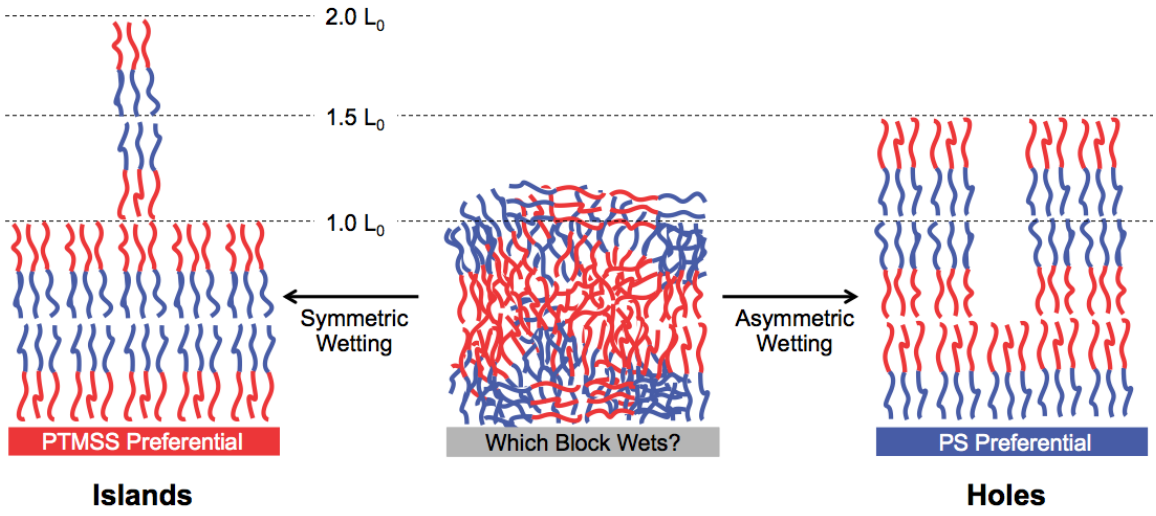

Figure 4.8: Island and hole formation on preferential interfaces.

4.6 Neutral Surface Analysis

Island and hole topography that have step heights of 1 L_0 indicate that both the bottom and free interface are preferential. A simultaneous discovery in the Willson/Ellison labs at the University of Texas at Austin and Frank Bates Lab at the University of Minnesota Twin Cities showed that the island and hole behavior on neutral surfaces is different. If one of the interfaces is neutral and the other is preferential, then "half" L_0 features are observed that become highly sensitive to film thickness.[115] Consider the example in Figure 4.9 for PS-PTMSS. Again, the air interface is highly preferential to PTMSS but the XST is neutral. The XST can wet either PS or PTMSS to satisfy the symmetric or asymmetric wetting conditions. In other words, 1 L_0 and 1.5 L_0 are commensurate film thicknesses. If the initial block copolymer film thickness is 1 $L_0 < L_{avg}$ < 1.25 L_0, then the closest commensurate film thickness is 1 L_0. Annealing the sample will cause the majority of the block copolymer to shrink down to 1 L_0 to satisfy the

symmetric wetting condition. The extra material in the film forms islands to satisfy the asymmetric wetting condition. As a result, these islands have step heights that are 0.5 L_0 in contrast to the full 1 L_0 features observed with preferential interfaces. This is only possible because the XST wets both PS *and* PTMSS. If the initial block copolymer film thickness is 1.25 L_0 < L_{avg} < 1.5 L_0, then the closest commensurate film thickness is 1.5 L_0. Annealing the sample will cause the majority of the film to grow in thickness 1.5 L_0 to satisfy the asymmetric wetting condition. Since there is not enough material for the entire film to grow to 1.5 L_0, holes are left in the film. These "half holes" have step heights of 0.5 L_0 to satisfy the symmetric wetting condition. Again, this is only possible because the XST prefers to wet both the PS and PTMSS block. In the optical microscope, the "half features" appear lighter in contrast relative to the "full features." Intuitively, this makes sense because the full features have step heights that are 1 L_0 whereas the half features have step heights that are 0.5 L_0.

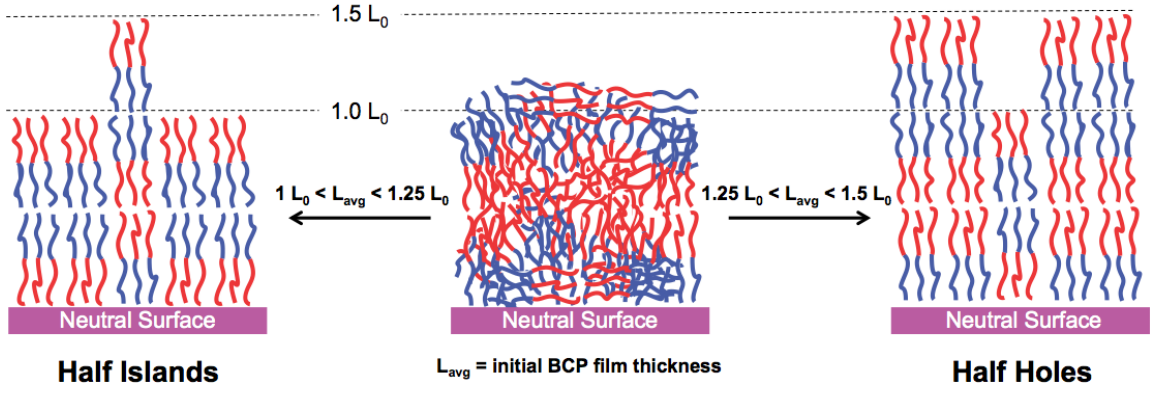

Figure 4.9: Island and hole evaluation for neutral interfaces. Half (0.5) L_0 features are observed if the one interface is preferential and the other neutral. The red block is PTMSS and the blue block is PS.

4.7 XST EVALUATION

The consequence of the island/hole behavior and *a priori* knowledge that PTMSS wets the air interface means that the XSTs can be quickly screened to determine their wetting preference. Figure 4.10 summarizes the four possible outcomes that may be observed during the XST screening. If the BCP film is 1 L_0 < L_{avg} < 1.5 L_0, either full islands (PTMSS wetting), full holes (PS wetting) or half features (neutral wetting) can occur.

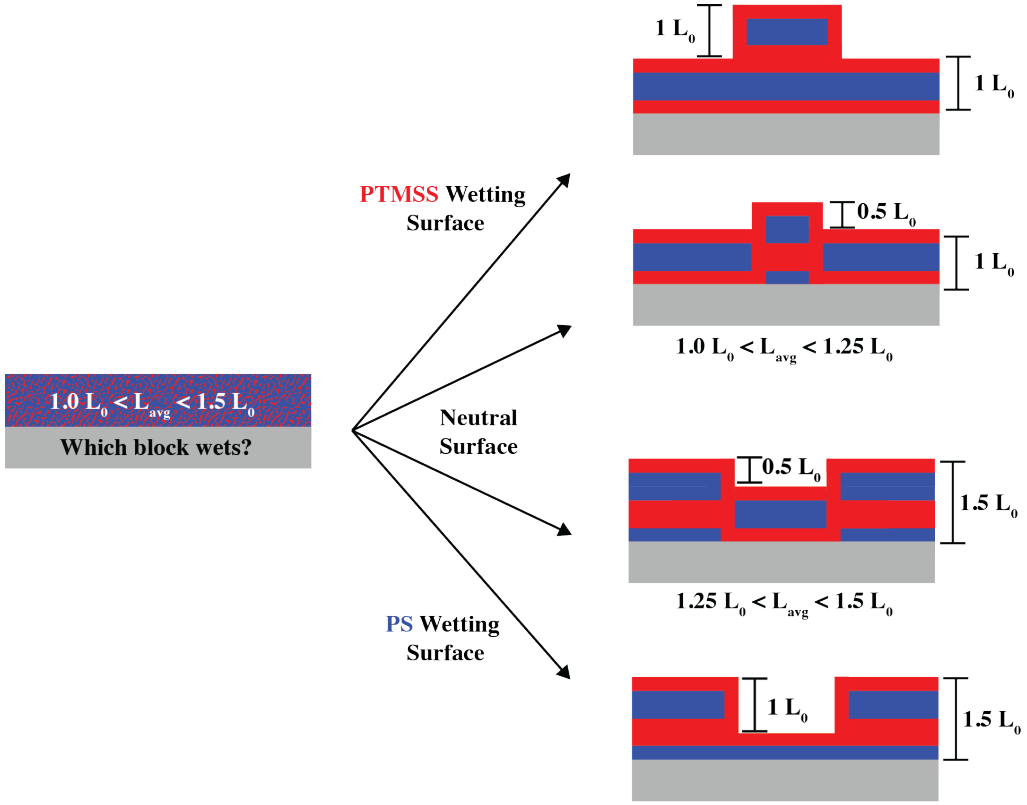

Figure 4.10: Island and hole evaluation for neutral interfaces. Half (0.5) L_0 features are observed if the one interface is preferential and the other neutral. The red block is PTMSS and the blue block is PS.

The island and hole test was performed on various XSTs. The island and hole results are shown in Figure 4.11 for XST-48, XST-52, and XST-65. The initial film thicknesses are all between 1 L_0 and 1.5 L_0. For XST-48, after annealing the sample, light colored holes appear that are visible on the optical microscope. The 1 L_0 holes can be confirmed using AFM. The full holes suggest that XST-48 is PS wetting. XST-65 is slightly more hydrophobic because it has more 4-*tert*-butylstyrene in the XST. The same island/hole experiment on XST-65 results in islands, which appear as dark colored spots (opposite contrast to holes) when viewed on the optical microscope. AFM confirms that the islands have 1 L_0 step heights, which suggests that XST-65 is PTMSS wetting. Since XST-48 wets PS and XST-65 wets PTMSS, there should be a composition between those two that is neutral. When the same island/hole experiment is performed on XST-52 with a block copolymer thickness of 1.18 L_0, islands are observed in the optical microscope. However, these islands are noticeably fainter than the islands observed for XST-65. AFM confirms that the features are 0.5 L_0 islands, which suggests that XST-52 is neutral. Increasing the film thickness to 1.4 L0 on XST-52 results in holes. Again, these features are fainter than the full holes observed with XST-48, and AFM confirms that the step height is 0.5 L_0. The flip from half islands to half holes about 1.25 L_0 suggests that XST-52 is neutral to PS-PTMSS.

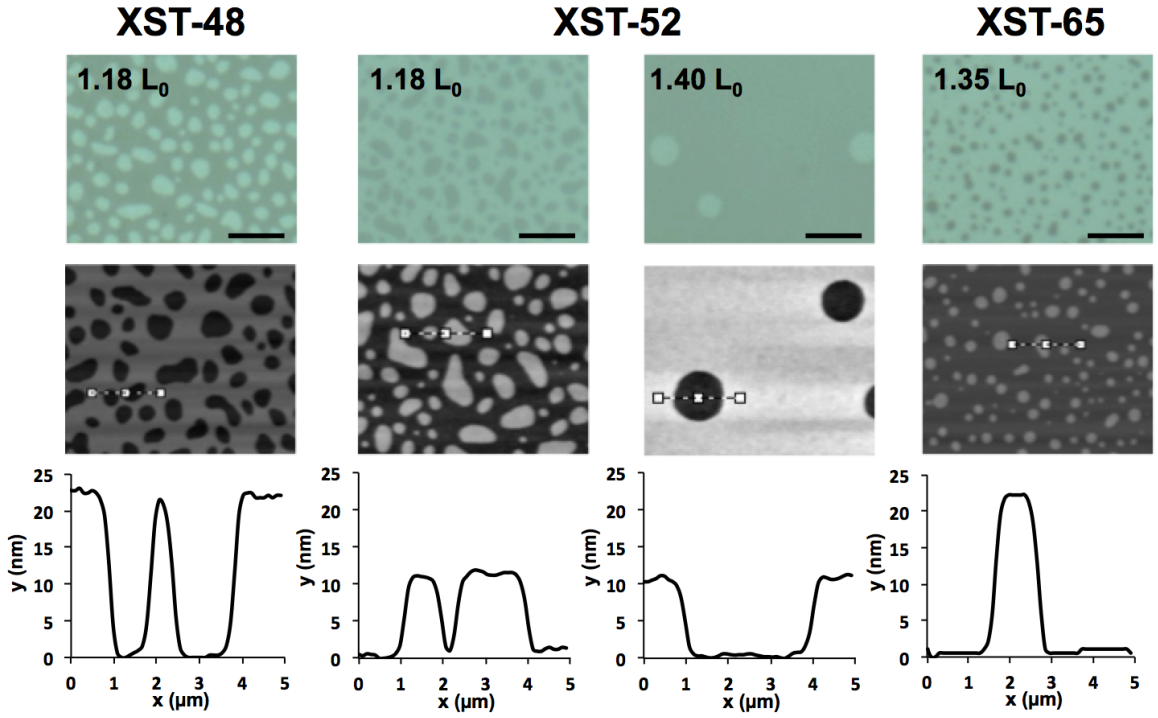

Figure 4.11: Island and hole test for several XSTs. **Top Row)** Optical microscope images. Scale bar = 5 μm. **Middle Row)** AFM images. **Bottom Row)** Height traces corresponding the AFMs in the middle row.

4.8 Internal Structure of Islands and Holes

The island and holes are a convenient way to determine the wetting preference of the XSTs. However, the cartoons that are drawn do not accurately depict the through film structure, which is unstudied for half features. Since the AFM only looks at the top interface, there is no physical data to suggest that both PS and PTMSS wet the neutral XST. The goal of this section is to study the through film structure of islands and holes using cross-sectional SEM. Studying island and holes by cross-sectional SEM is difficult considering the periodicity of the polymer is only 22nm. Thicker films are easier to image and were used to study the internal structure of the full and half features.

4.8.1 Full Features

Both islands and holes were generated by spin coating films between 3-4 L_0 onto SiO_2, which is preferential to the PS. Figure 4.12 shows the cross-sectional SEM of a hole along with a corresponding cartoon schematic and AFM micrograph. Figure 4.13 shows the analogous data for a full island. The cartoons that have been drawn throughout this chapter are not drawn to scale. The cartoon makes the transition between thicker and thinner film appear abrupt. The real data shows that transition regions are gradual and occur over the course of 100 nm or more. The transition regions for the island and hole sample are similar to one another and no distinction can be made between the two. The transition points occur when one layer bifurcates into two layers to create the additional layers in the island and hole samples, in good agreement with theoretical predictions.[116] This transition point can occur anywhere in the film. In Figure 4.14, an entire island is captured and two distinct bifurcation points can be seen in the two different transition regions. It should be noted that the PTMSS domain was always observed bifurcating into the added layer during in these transition regions. This could be because PTMSS is lower surface energy than PS or it could be because the volume fraction of PTMSS is higher than PS.

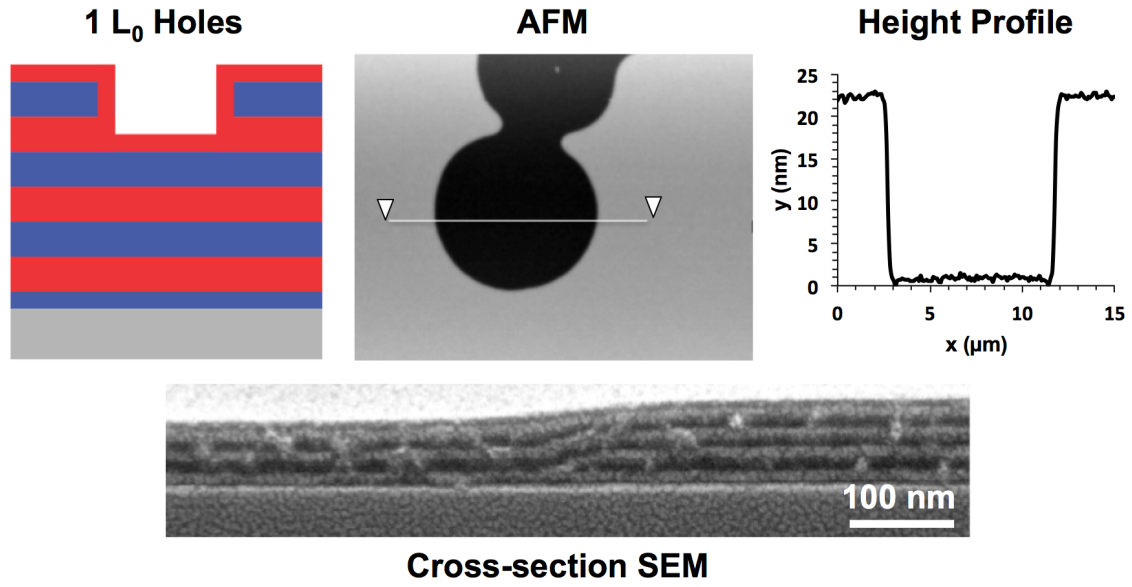

Figure 4.12: Cartoon, AFM, height profile, and cross-sectional SEM of a full hole.

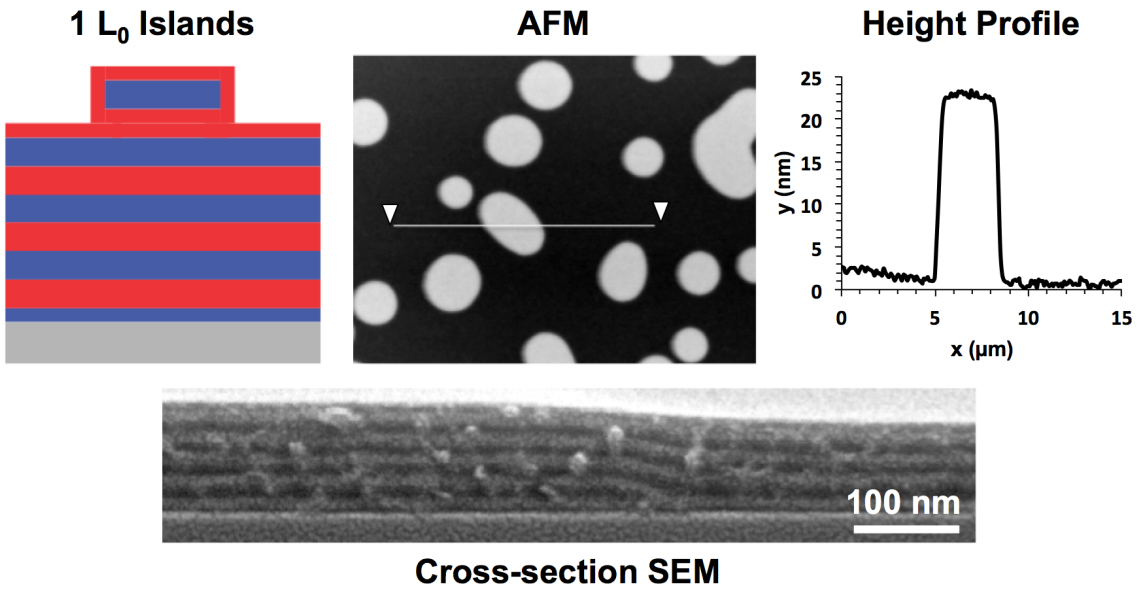

Figure 4.13: Cartoon, AFM, height profile, and cross-sectional SEM of a full island.

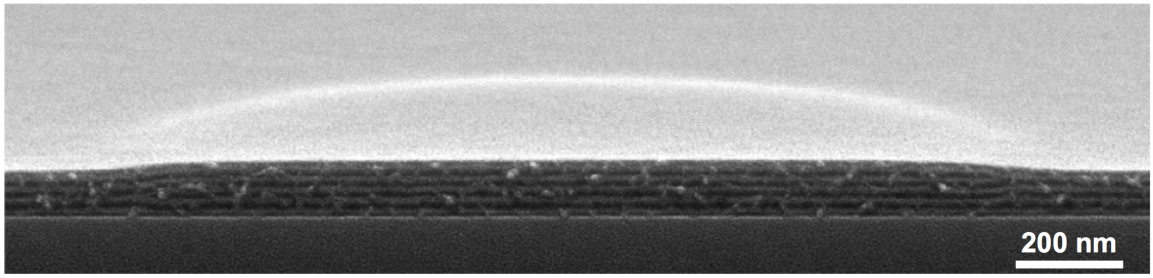

Figure 4.14: Full cross-section of an entire island. Notice that the bifurcation points occur in two layers at the two different transition regions.

4.8.2 Half Features

In the previous sections, the half features were assumed to be the result of a neutral XST wetting both the PS and PTMSS blocks. To confirm the speculation that both domains touch the neutral interface, cross-sections on a neutral grafted surface treatment were examined.* The neutral grafted treatment was 3 nm thick as measured by ellipsometry; it is too thin to be observed as a distinct layer in the cross-sectional SEMs. PS-PTMSS was annealed on the neutral surface, cross-sectioned, and imaged. Half islands (Figure 4.15) and half holes (Figures 4.16) and their corresponding AFMs are shown. The half islands and half holes look identical by cross-section. In both figures, it appears that both PS and PTMSS are in contact with the interface. The additional 0.5 L_0 layer is added due to a transition at the interface. It is hypothesized that this transition must be confined to the substrate surface because the XST wets both PS and PTMSS. It would not make sense if the additional 0.5 L_0 layer was added anywhere else but the substrate surface. All of the experiential data is in agreement with this conclusion. To confirm that the surface does indeed wet both blocks, a thick block copolymer sample (~300 nm) was annealed on the neutral surface. At this film thickness, no topography was

* Neutral grafted surface treatments are the focus of Chapter 8.

observed by optical microscope or AFM. The cross-section SEM (Figure 4.17) shows that both domains are in contact with the substrate surface and adopt a perpendicular orientation in the bottom half of the film. At the free interface, the domains begin to adopt a parallel orientation because PTMSS migrates to the air interface.

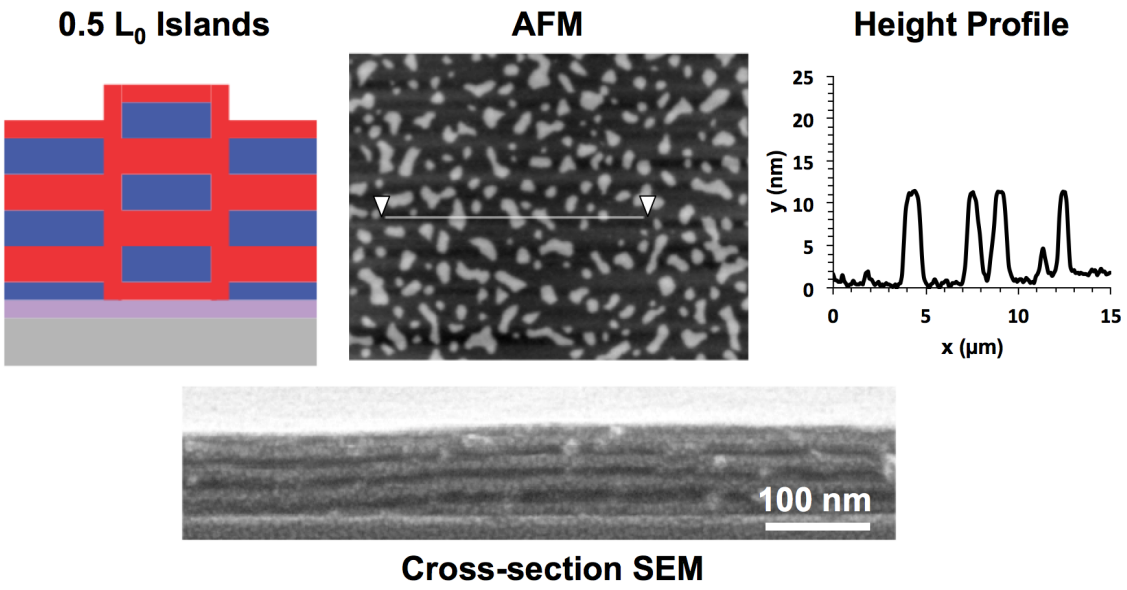

Figure 4.15: Cartoon, AFM, height profile, and cross-sectional SEM of a half island.

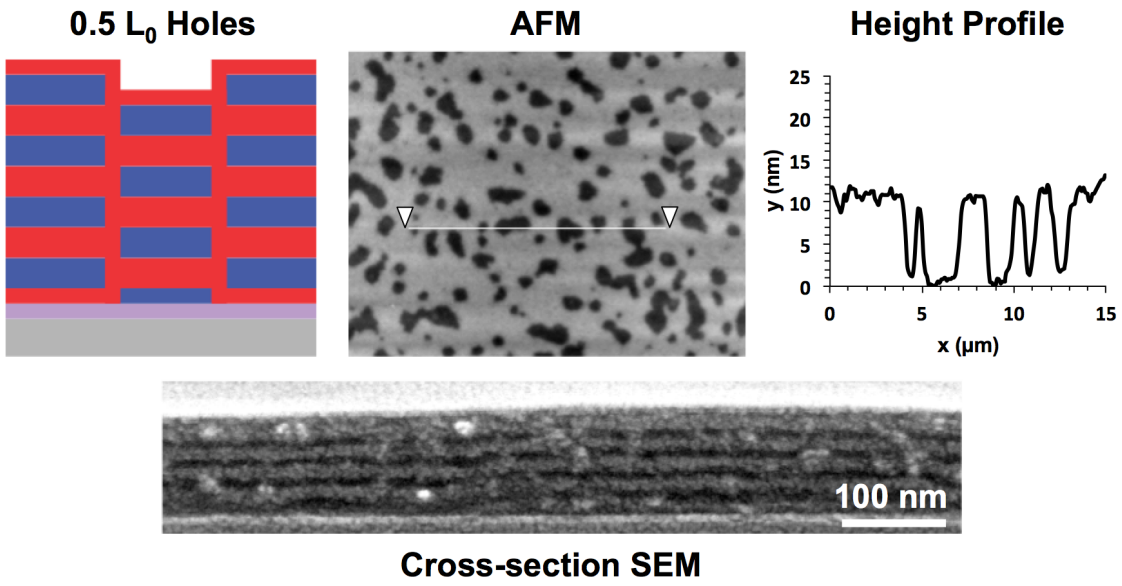

Figure 4.16: Cartoon, AFM, height profile, and cross-sectional SEM of a half hole.

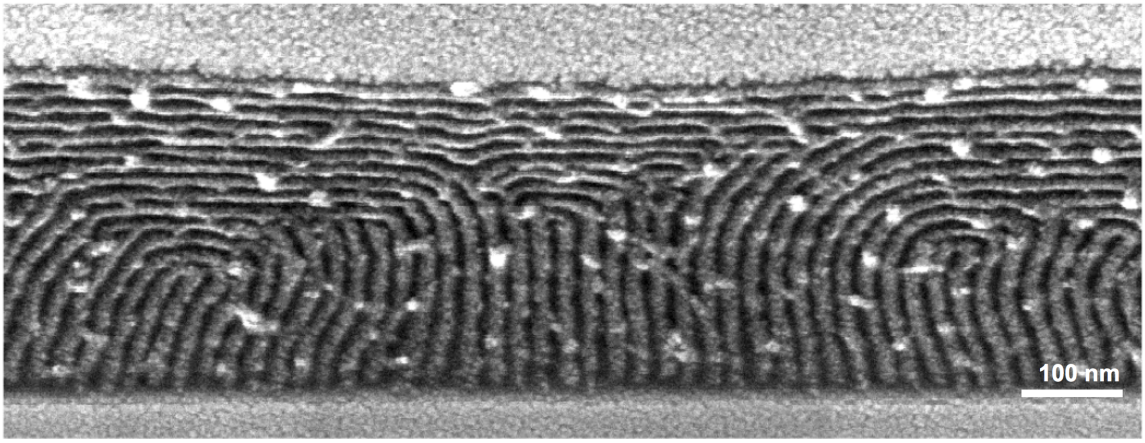

Figure 4.17: Cross-section of a thick block copolymer film annealed on a neutral surface treatment.

4.9 CONCLUSIONS

In this chapter, a library of XSTs with controlled compositions and various surface energies was synthesized. Crosslinking the XST on a silicon wafer can systematically modulate the surface energy of a substrate. An island/hole technique was implemented to determine the wetting preferences of the XSTs. Full islands and full holes appear when both interfaces are preferential. Half island and half holes appear when one interface is neutral and the other preferential. Half features are possible because the neutral XST wets both block copolymer domains. Cross-sectional microscopy was used to confirm the internal structure of full and half features.

4.10 EXPERIMENTAL

4.10.1 Instrumentation

Size exclusion chromatography (SEC) data for the top coats were collected on an Agilent 1200 Series Isopump and Autosampler with an Agilent Technologies 1100 RI detector. One PLgel 5 μm, 100 Å column and one PLgel 5 μm, 1000 Å column were used with DMF as an eluent at 70°C and a flow rate of 1 mL/min. Substrate surface treatment SEC data were collected with an Agilent 1100 Series isopump and autosampler with a Viscotek Model 302 TETRA detector platform and THF as an eluent at 23°C. Three I-series mixed bed high-MW columns were calibrated relative to PS standards. Brewer CEE 100CB Spincoater was used to coat all thin films. Ellipsometry was performed with a J.A. Woollam Co, Inc. VB 400 VASE Ellipsometer with wavelengths from 382 to 984 nm and a 65° angle of incidence. The elemental analysis used to calculate XST was performed by Midwest Microlab, LLC.

4.10.2 Materials

4.10.3 Substrate Surface Treatments

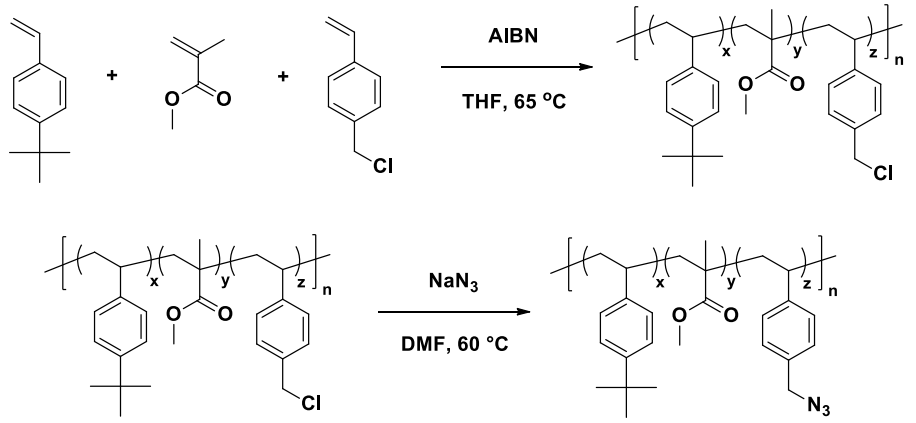

The following procedure was used for XST-52 and is representative of all other XSTs described herein. Methyl methacrylate, 4-*tert*-butylstyrene, and 4-vinylbenzylchloride were stirred with basic alumina for 30 minutes and filtered prior to use. 4-vinylbenzylchloride was passed through an additional basic alumina plug to yield a clear and colorless liquid before use. Methyl methacrylate (8.86 g, 88.6 mmol, 0.38 eq.), 4-*tert*-butylstyrene (21.60 g, 134.8 mmol, 0.58 eq.), vinylbenzylchloride (1.20 g, 7.8 mmol, 0.034 eq.), and AIBN (0.38 g, 2.31 mmol, 0.01 eq.) were added to a 100 mL 3-neck round bottom flask equipped with a stir bar, condenser, and three rubber septa. The reagents were dissolved in THF (23 mL) and the solution was deoxygenated by vigorously bubbling nitrogen through the solution for 30 minutes. The reaction vessel, under positive nitrogen pressure, was immersed in an oil bath at 65 ˚C. The reaction was heated and stirred for 45 minutes and quenched at 0 ˚C. Conversion was intentionally kept low (<10%) to minimize monomer drift. The viscous liquid was precipitated into methanol (350 mL) and filtered. The polymer was dissolved in 15 mL of THF and reprecipitated into methanol two additional times. The polymer was dried *in vacuo* overnight at 100 ˚C to yield 2.072 g of dry polymer. The polymer was placed in a 100 mL

round bottom flask and dissolved in 35 mL of DMF. Sodium azide (0.690 g, 33 wt% with respect to the polymer) was added to the flask and the reaction was heated to 60 ˚C for 12 hours. The reaction was cooled to room temperature and the polymer was precipitated into methanol (3x). Drying the polymer overnight *in vacuo* at 100 ˚C afforded 1.460 g of XST-52. The broad benzyl position resonance in the ^{1}H NMR completely shifted from ~4.5 (VBzCl) to ~4.3 (VBzAz) and the infrared spectrum indicates the presence of azide with a sharp peak ca. 2100 cm^{-1}.

4.10.4 Thin Film Preparation

A 0.5 wt% solution of XST in toluene was filtered with a 0.2 micron Chromafil® filter and spin coated at 3500 rpm for 30 sec to yield a smooth film ca. 15 nm. The film was heated at 250 °C on a hot plate for 5 minutes to crosslink the azide functionality and subsequently rinsed with toluene 3 times at 3500 rpm to remove uncrosslinked material. The final film thickness after rinsing was ca. 13 nm as measured by ellipsometry. Various concentration solutions (1~2.5 wt%) of block copolymer (either PS-*b*-PTMSS or PS-*b*-PTMSM) in toluene or amyl acetate were filtered with a 0.2 micron Chromafil® filter and cast onto the XST films at various spin speeds to produce relatively smooth films with various thicknesses. Samples were annealed on a Thermolyne HP-11515B hot plate between 170 °C and 190 °C for various lengths of time and quickly cooled to room temperature on a solid metal block. Samples were analyzed for topography by optical microscopy and atomic force microscopy.

4.11 ACKNOWLEDGMENTS

The XSTs in this chapter were synthesized in collaboration with Dr. Christopher Bates, Anthony Thio, Matthew Carlson, Litan Lee, and Jeffrey Self. PS-PTMSS was synthesized by Gregory Blachut. The internal structures of the full and half features were imaged at the IBM Almaden Research Center in collaboration with Dan Sanders and Joy Cheng. Amy Bauer helped with etching and Elizabeth Lofano helped with imaging.

Chapter 5: Second Generation Top Coats and Evaluation

5.1 Problems with Previous Designs

In Chapter 3, three criteria were established for the ideal top coat platform. 1) The top coat needs a polarity switch, which was accomplished using maleic anhydride-containing polymers. 2) The T_g of the top coat must be greater than the T_g of the blocks in the block copolymer. A large T_g was obtained *via* incorporation of norbornene into the top coat. 3) The surface energy of the polymer must be precisely tuned to neutralize the interfacial interactions between the block copolymer domains and the top coat. While the norbornene-maleic anhydride-styrene containing polymers accomplished the goals of controlling the orientation of poly(styrene-*block*-4-trimethylsilylstyrene-*block*-styrene) (PS-PTMSS-PS, L_0 = 30 nm), the synthesis of these top coats is very difficult to control and reproduce. For example, the top coats have highly disperse, multi-modal molecular weight distributions, and the composition of the polymers could not be controlled *via* monomer feed ratio. This chapter focuses on the design of second-generation of top coats that meet the same criteria but have controlled composition. The block copolymer used in this chapter is PS-PTMSS-PS (L_0 = 30 nm), which was previously used in Chapter 3.

5.2 Alternating Polymerization of Maleic Anhydride and Styrene

Maleic anhydride and styrene are known to undergo an alternating copolymerization as shown in Scheme 5.1. The free radical monomer reactivity ratios for styrene and maleic anhydride are $r_1 = r_2 = 0$, which means that neither monomer has the tendency to homopolymerize in the presence of the other monomer.[117] Therefore, the resulting polymers tend to be alternating.[106] For maleic anhydride and styrene, the instantaneous polymer composition is insensitive to feed ratio and is alternating, which results in a highly predicable and reproducible polymers.

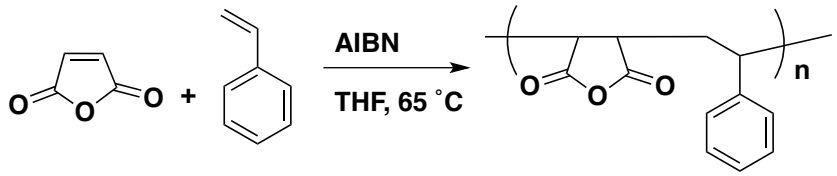

Scheme 5.1: Alternating copolymerization of styrene and maleic anhydride

Maleic anhydride is also known to form alternating copolymers with other styrenic derivatives. However, to the best of the author's knowledge, there are no studies on the simultaneous copolymerization of maleic anhydride with two different styrene derivatives as shown in Scheme 5.2. It was hypothesized that two styrene derivatives polymerized with maleic anhydride should yield polymers with a controlled composition. This hypothesis assumes that the reactivity ratios between the two-styrene derivatives are similar enough that they will incorporate into the polymer at the same rate (weighted by the feed ratios).

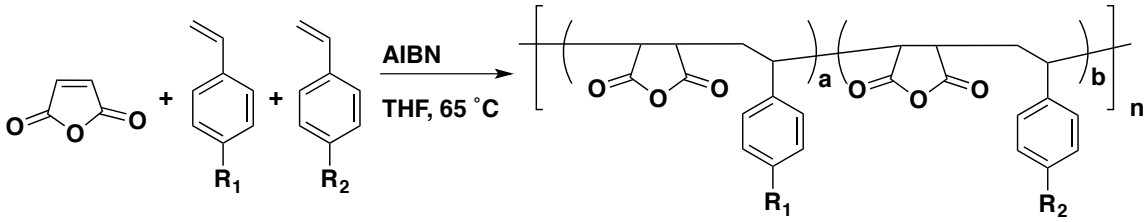

Scheme 5.2: Copolymerization between two styrene derivatives and maleic anhydride.

5.3 TOP COAT DESIGN

Assuming that the reactivity ratios of different styrenes and maleic anhydride are similar, the composition of the resulting copolymers from maleic anhydride and two styrene derivatives should be entirely controlled by the monomer feed ratio. By adjusting the ratio of the styrene derivatives in the copolymer, control over top coat surface energy should be obtainable. In order for this design to be successful, the range of surface energies captured by the extreme compositions (50% styrene1 and 50% styrene2) need to include the neutral surface energy for the block copolymer. Since low surface energy and often contain fluorinated groups or hydrophobic *tert*-butyl containing groups, a series of monomers that could have "low surface energy" were synthesized and are shown below in Figure 5.1.[85]

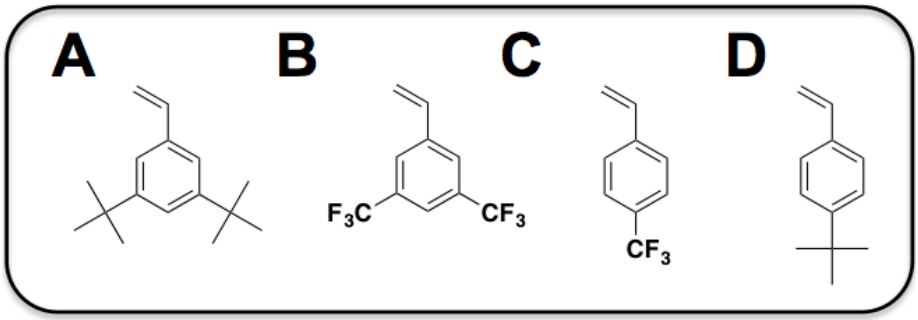

Figure 5.1: Hydrophobic styrene monomers.

The first top coats of this design were synthesized using maleic anhydride, styrene and 4-trifluoromethylstyrene (CF_3S). If the composition can be controlled, the possible surface energies that can be achieved should be within the range captured by the extreme compositions as shown in Figure 5.2. This is not an unreasonable assumption as copolymers of fluorinated styrenes and acrylates have shown that surface energy decreases as a function of increasing fluorinated monomer incorporation.[118]

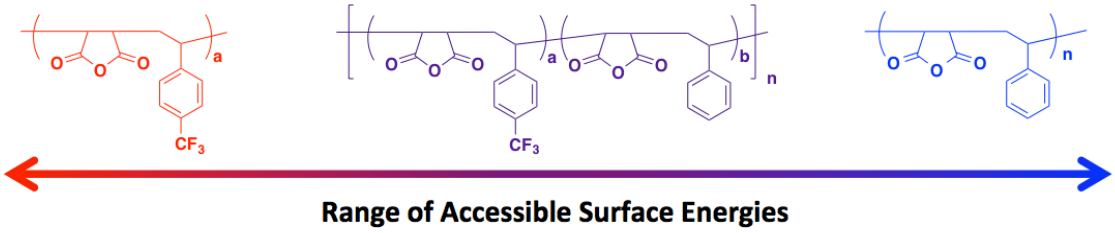

Figure 5.2: Range of surface energies that can be captured by the copolymers of maleic anhydride, styrene, and 3,5-di-*tert*-butylstyrene.

5.4 SYNTHESIS OF SECOND GENERATION TOP COATS

It was hypothesized that poly(4-trifluoromethylstyrene-*alt*-maleic anhydride) would preferentially wet PTMSS while poly(styrene-*alt*-maleic anhydride) would preferentially wet PS.* Copolymers were synthesized by uncontrolled radical polymerization as shown in Scheme 5.3. In all of the polymerizations, the maleic anhydride monomer was kept constant at a mol feed ratio of 0.5. The ratio of the two styrene derivatives was the only variable that was changed.

* At this point in time, no methodology for testing the top coat wetting preference existed. Chapter 6 focuses on methodology to characterize top coat wetting.

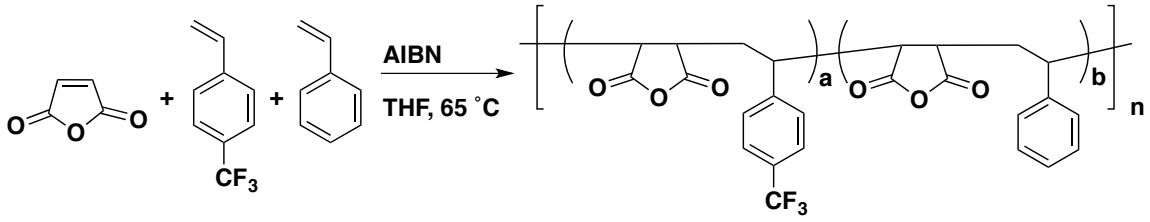

Scheme 5.3: Free radical copolymerization of maleic anhydride, 4-trifluoromethylstyrene, and styrene.

The polymer feed ratios and compositions are shown in Table 5.1. The actual polymer compositions were determined by combustion analysis (see experimental section 5.7.4) and are in excellent agreement with the feed ratio,* which demonstrates that the *average* polymer composition can be controlled. The individual top coats are named based on how much CF_3S was incorporated into the final polymer. For example TC-7 contains 7% CF_3S.

Table 5.1: Feed ratios and polymer compositions for CF_3S top coats.

		Feed Ratio (mol%)			Actual Ratio (mol%)**			
Entry	**Top Coat**	**MA**	**CF_3S**	**S**	**MA**	**CF_3S**	**S**	**Yield**
1	TC-7	50	7	43	50	7	43	79
2	TC-22	50	25	25	49	22	29	69
3	TC-35	50	33	17	46	35	19	84
4	TC-37	50	40	10	48	37	15	55
5	TC-53	50	47	3	46	53	1	49

**Determined by combustion analysis

* These polymerizations were run to full conversion. According to theory, polymers that are run to full conversion should converge to the feed ratio. With a slightly different top coat system, high and low conversion top coats have the same composition that is equal to the initial feed ratio. This is reported in Chapter 6.

The top coat characterization data is summarized in Table 5.2. The molecular weight distributions are fairly disperse, which is expected of uncontrolled free radical polymerization. However, the size exclusion chromatographs (SECs, Figure 5.3) show that the polymers are monomodal, which is significantly better than the multimodal top coats presented in Chapter 3. The CF_3S top coats are thermally stable to temperatures greater than 300˚C (Figure 5.4). Surprisingly, the T_g of these top coats are all greater than 190˚C (Figure 5.5). In previous literature, the T_g of poly(styrene-*alt*-maleic anhydride was reported to be only 170˚C.[119] These polymers are soluble in saturated ammonium hydroxide and could be spin coated as thin films. Therefore, the two-styrene maleic anhydride, second-generation top coat system meets all of the desired material properties.

Table 5.2: Top coat characterization data.

Top Coat	M_n*	M_w*	Đ	T_g (˚C)	T_d (˚C)
TC-7	15400	44900	2.93	190	288
TC-22	15000	40200	2.67	199	307
TC-35	38500	85300	2.21	200	303
TC-37	14000	33500	2.38	198	298
TC-53	31300	71500	2.28	196	312

*Molecular weights relative to PMMA standards in DMF at 70˚C. Units are in Da.

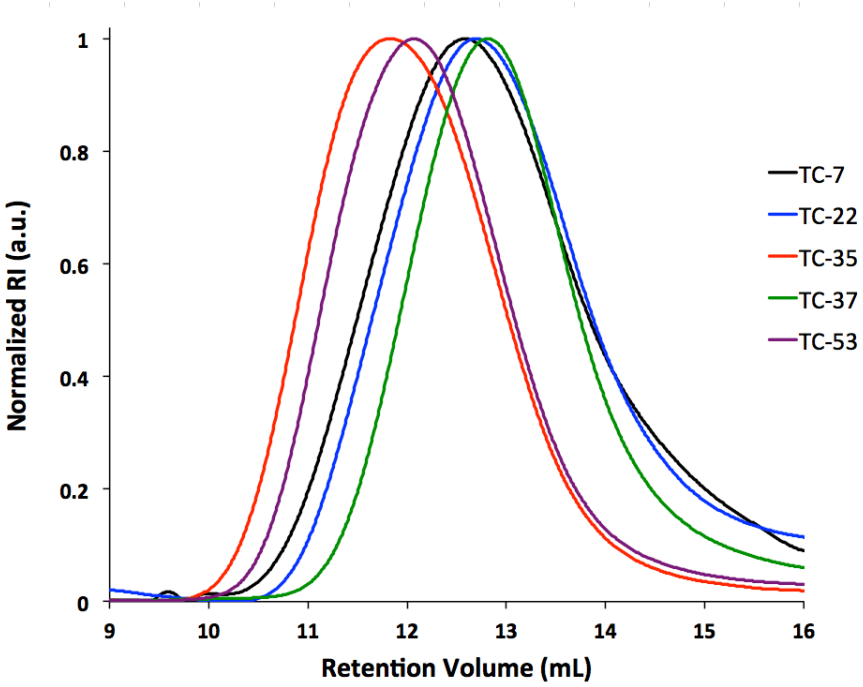

Figure 5.3: Size exclusion chromatographs for CF_3S top coats.

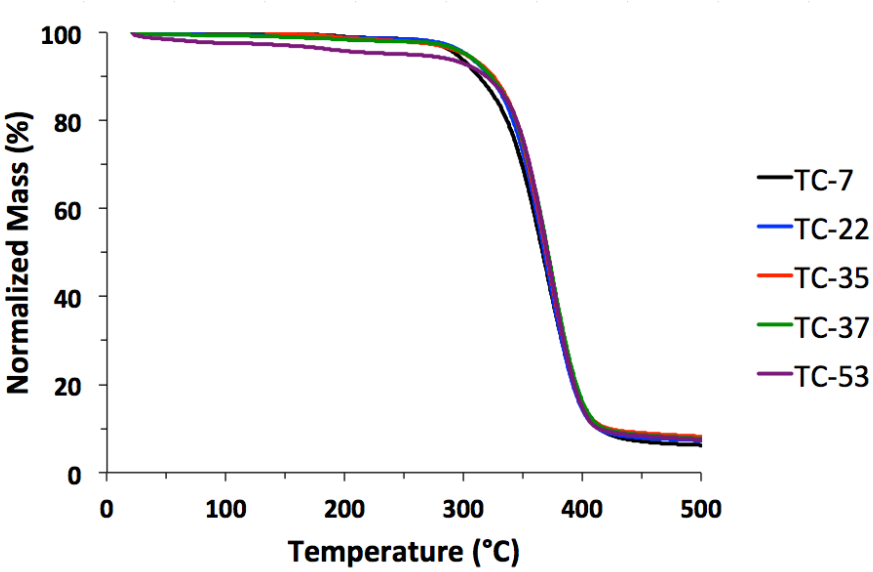

Figure 5.4: TGA data collected for CF_3S top coats. Heating rate: 10 °C/min under nitrogen.

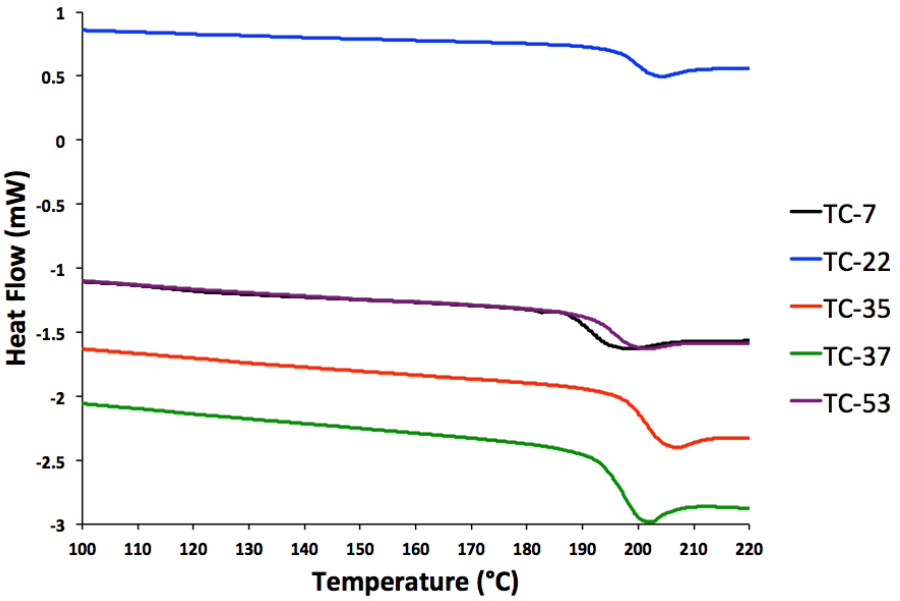

Figure 5.5: DSC data for CF_3S top coats. Data shown is the third heating cycle at rate of 10 °C/min.

5.5 Thin Film Evaluation

The CF_3S-containing copolymers were tested as top coats for PS-PTMSS-PS. The first orientation experiments were performed on poly(4-methoxystyrene-*random*-4-vinylbenzylazide) (XPMOST) as the crosslinkable surface treatment (XST) for comparison to the results in Chapter 3. XPMOST was crosslinked on a silicon wafer to produce a thin film that was ca. 15 nm thick. PS-PTMSS-PS was spin coated as a 44 nm (1.4 L_0) thick film. The sample was split into multiple pieces and different top coats were spin coated onto the wafer coupons. The samples were annealed at 175°C for 10 minutes, quenched, stripped, and etched prior to inspection by scanning electron microscopy (SEM). Figure 5.6 shows the orientation results of the CF_3S top coat system on XPMOST. At the extremes compositions (TC-53 and TC-7), a parallel orientation of

domains was observed by SEM. However, a perpendicular orientation was observed with TC-37 and TC-22. There are many defects when TC-37 was used relative to TC-22, which yielded nearly perfect orientation. The results with TC-22 appear identical to those in Chapter 3 using the norbornene-maleic anhydride-styrene system. These results do not necessarily mean that TC-22 is a neutral material. It could be that TC-22 provides the correct surface energy to favor the perpendicular orientation at this particular block copolymer film thickness.[94] Nonetheless, this result is highly significant because it demonstrates that the surface energy of the top coat system can be changed in a systematic fashion depending on polymer composition. The CF_3S top coat system is much more efficient than the systems in Chapter 3 because it uses the same monomers for each polymer. Changing the monomer feed ratio fine-tunes the top coat composition and thus surface energy.

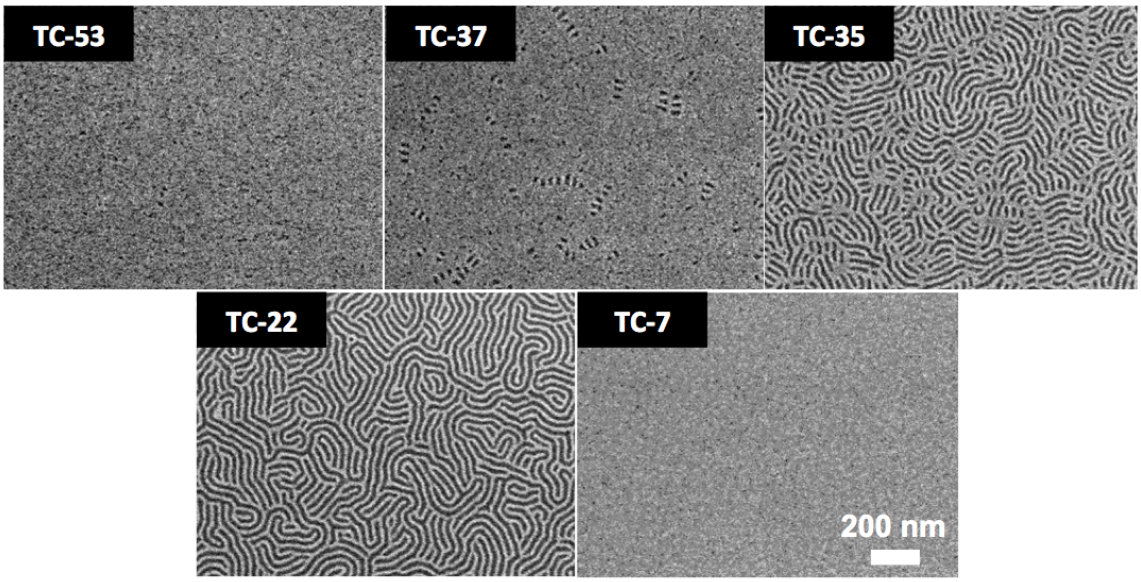

Figure 5.6: SEM micrographs of PS-PTMSS-PS (41 nm, 1.4 L_0) annealed at 175˚C for 10 minutes confined between XPMOST and various CF_3S top coats. The top coats were removed and the samples were etched prior to imaging. The scale bar is valid for all images.

The result in Figure 5.6 provided an excellent comparison to the results in Chapter 3. However, XPMOST is not a neutral surface treatment, and in Chapter 4, a convenient method was used to determine neutral crosslinkable surface treatments (XSTs). The same island and hole methodology was used with PS-PTMSS-PS, and XST-46* was identified as neutral. PS-PTMSS-PS was spin coated at film thickness of 1 L_0 and confined between XST-46 and the CF_3S top coats. Figure 5.7 shows the orientation results after annealing, removing the top coat, and etching. All of the top coats except for TC-7 and TC-29 produced perpendicularly oriented domains. At all film thicknesses tested (1-2 L_0), TC-53, TC-37, and TC-35 provided a perpendicular orientation of the domains. It is unclear

* See Chapter 4 for XST nomenclature and structure.

which TC is perfectly neutral as the range of potentially neutral materials spans approximately 20% in CF_3S composition.

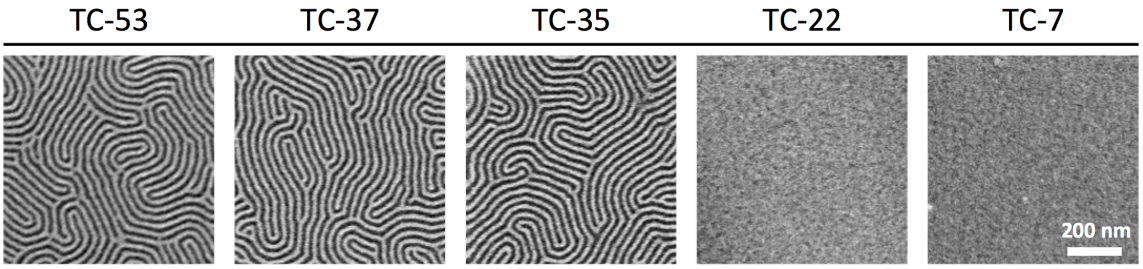

Figure 5.7: Effect of varying top coat composition and BCP thickness on the neutral substrate surface treatment with composition. XST-46. Samples were annealed at 175°C for 10 minutes, stripped, and etched before imaging.

The effect of block copolymer thickness on the orientation of domains was studied using XST-46 and TC-37, which was presumed to be close to neutral. Figure 5.8 shows the orientation results from varying film thicknesses ranging from 1-3.2 L_0. A perpendicular orientation at all of the film thicknesses was observed with no sign of parallel domains. The thickness independence suggests that TC-37 is either perfectly neutral or very close to neutral. Interestingly, TC-37 induced a parallel orientation of domains when annealed on XPMOST. Additionally, TC-22 resulted in a perpendicular orientation of domains when XPMOST was used but resulted in parallel domains when neutral XST-46 was used. This suggests that TC-22 is not actually neutral. It controlled the orientation on XPMOST only because of the complex interplay between all of the interfacial interactions that favored the perpendicular orientation at that particular film thickness.[94]

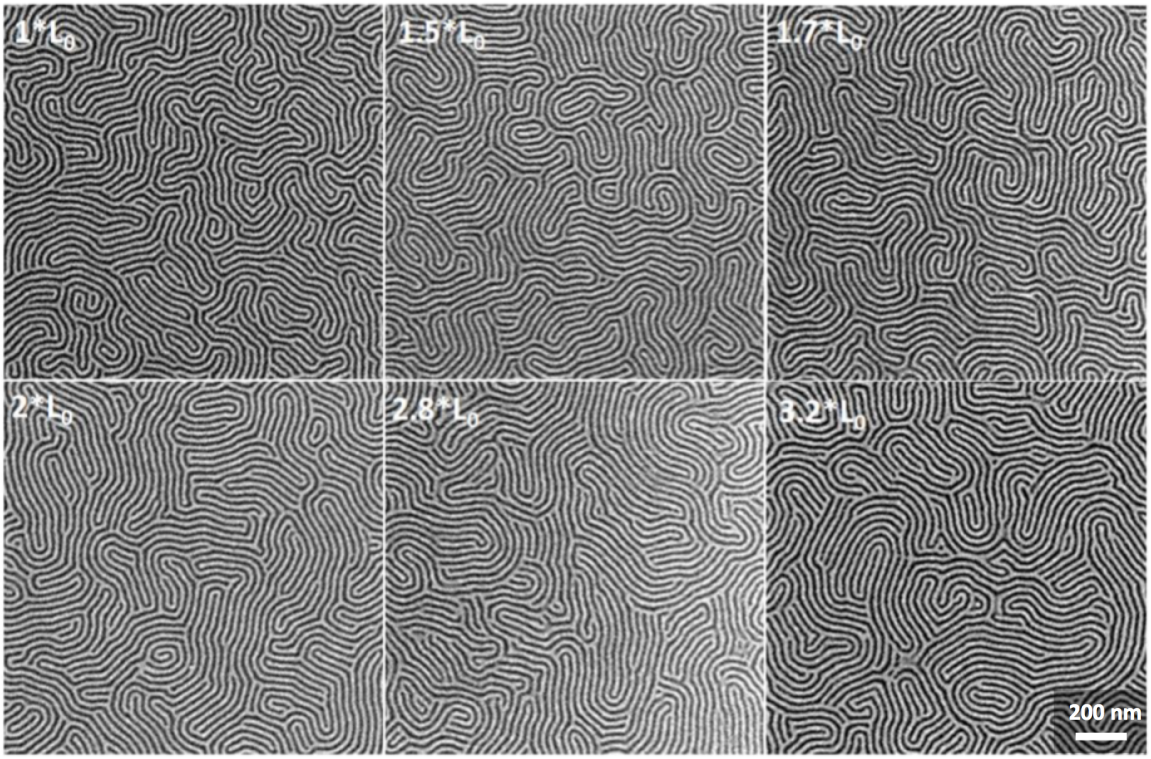

Figure 5.8: The effect of film thickness on PS-PTMSS-PS orientation when annealed confined between XST-46 and TC-37. Samples were annealed at 190°C for 11 min and etched prior to imaging.

The SEM micrographs show the orientation of the domains from a top-down point of view. In order to observe the through film structure, a cross-sectional image of PS-PTMSS-PS at a thickness of 3.2 L_0 was generated by Hiroshi Yoshida at Hitachi. The sample was cross-sectioned using an advanced argon milling technique.[120] A majority of the domains span the entire thickness. However, through-film defects such as domain tilting and bifurcations were observed. Defects of this sort are unacceptable for lithographic applications because they would limit pattern transfer. The reason why these defects occurred could be due to the large film thickness. It is not clear whether these

defects would be present if the original film thickness were between 1-2 L_0. These types of through film defects are predicted to be minimized when orientation control is combined with directed self-assembly processes.[68,101]

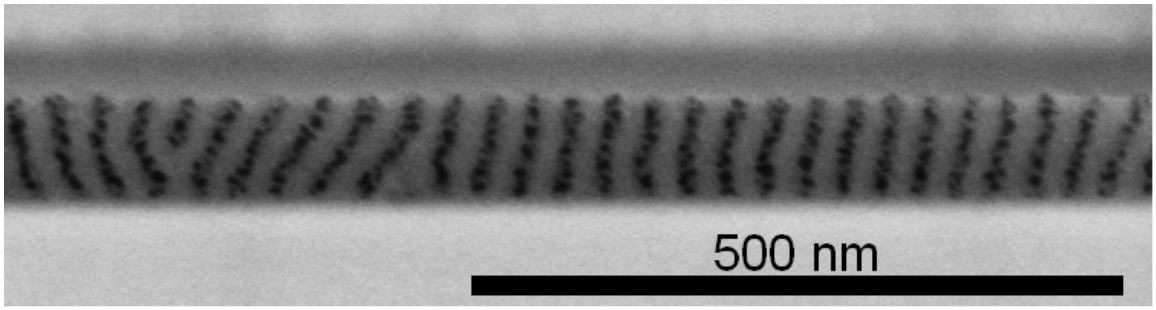

Figure 5.9: Cross-sectional SEM of PS-PTMSS-PS. The initial film thickness was 96 nm (3.2 L_0).

5.6 CONCLUSIONS

A new top coat system based on maleic anhydride, styrene, and CF_3S was introduced. The composition of these top coats can be controlled by adjusting the monomer feed ratio. Top coats with different compositions display different interfacial properties, which have been exploited to control the orientation of PS-PTMSS-PS. When coupled with a neutral XST, a parallel orientation of block copolymer domains was achieved independent of film thickness.

5.7 EXPERIMENTAL

5.7.1 Materials

Azoisobutyronitrile (Sigma Aldrich) was recrystallized from methanol. Maleic anhydride (Sigma Aldrich) and tetrahydrofuran (Fischer Scientific, uninhibited) were used as received. Styrene (Sigma Aldrich), 4-*tert*-butylstyrene (Sigma Aldrich), methyl methacrylate (Sigma Aldrich), and 4-trifluoromethylstyrene (Chapter 3) were stirred with basic alumina for 30 minutes to remove inhibitor and filtered.

5.7.2 Instrumentation

Size exclusion chromatography (SEC) data for the top coats were collected on an Agilent 1200 Series Isopump and Autosampler with an Agilent Technologies 1100 RI detector. One PLgel 5 μm, 100 Å column and one PLgel 5 μm, 1000 Å column were used with DMF as an eluent at 70°C and a flow rate of 1 mL/min. The refractive index response of the top coats was compared to nine PMMA standards (1660, 2200, 4250, 6370, 12600, 23500, 41400, 89300, and 201000 Da), which were used to calibrate the instrument by refractive index response (conventional calibration). Thermogravimetric analysis was performed on a TA Q500. Digital scanning calorimetry was performed on a TA Instruments Q100. Combustion analysis was performed by Midwest Microlab, LLC. A Brewer CEE 100CB Spincoater was used to cast all thin films. Ellipsometry was performed with a J.A. Woollam Co, Inc. VB 400 VASE Ellipsometer with wavelengths from 382 to 984 nm and a 65° angle of incidence. A Zeiss Supra 40 VP scanning electron microscope operating at 3 kV was used to collect all SEM data. Brightness and contrast for all SEMs were uniformly enhanced using commercial image editing software.

5.7.3 Polymer Synthesis

PS-PTMSS-PS: The block copolymer synthesis and characterization can be found elsewhere.[52,83]

Top Coats:

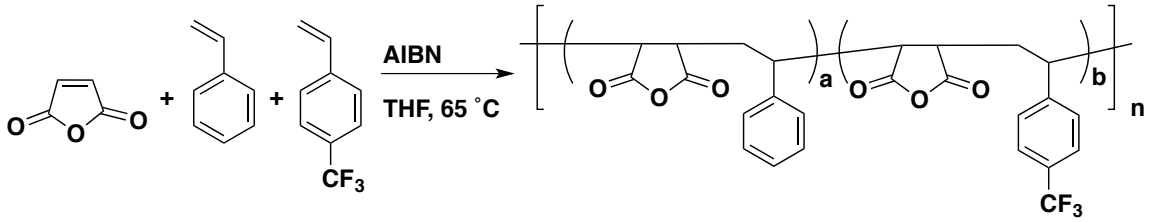

The following procedure is representative for the CF_3S-containing top coats. A round bottom flask fitted with a reflux condenser was charged with a stir bar, maleic anhydride (0.50 eq., 1.00 g, 10.2 mmol), styrene (0.25 eq., 0.531 g, 5.1 mmol), and 4-trifluoromethylstyrene (0.25 eq., 0.878 g, 5.1 mmol), azoisobutyronitrile (0.005 eq., 16.7 mg, 0.102 mmol), and tetrahydrofuran (10 mL). Feed ratios were varied as described in Table 5.1. The reaction mixture was degassed by sparging with dry N_2 for 15 min and heated at 65°C for 24 h. The reaction was quickly cooled to 0°C and precipitated into a 3:1 (by vol) mixture of hexanes:DCM. The polymer was isolated by vacuum filtration, redissolved in THF and reprecipitated two more times into a 3:1 (by vol) mixture of hexanes:DCM. The resulting white powder was dried *in vacuo* at 100°C and analyzed by SEC, DSC, and TGA.

XST-46: XST was synthesized according to the procedure in Chapter 4. Feed ratio: 4-*tert*-butylstyrene: methyl methacrylate: 4-vinylbenzylchloride = 0.475: 0.475: 0.05. Actual composition: 4-*tert*-butylstyrene: methyl methacrylate: 4-vinylbenzylazide = 0.46: 0.48: 0.06. M_n = 26.1 kDa, M_w = 45.2 kDa relative to PS standards in THF.

5.7.4 Combustion Analysis Calculations

Combustion analysis was used to determine the composition of the surface treatments in Chapter 4 and top coats in Chapters 3, 5, 6, and 8. Elemental analysis was presumed to be more accurate than NMR analysis for determining polymer composition. In the ^{1}H-NMR of the top coats, there is significant peak overlap, which makes it difficult to determine the contributions from individual monomers. The composition by combustion analysis was calculated using Solver in Microsoft Excel. In this technique, a theoretical mol fraction of the polymer's monomers (x_1 = maleic anhydride, x_2 = styrene, x_3 = CF_3S and $x_1 + x_2 + x_3 = 1$) was used to calculate a theoretical wt% of carbon ($\%C_{theo}$), hydrogen ($\%H_{theo}$), fluorine ($\%F_{theo}$), and oxygen ($\%C_{theo}$). The theoretical weight percent of each element is dependent on the molecular formula of each monomer (maleic anhydride: $C_4H_2O_3$, styrene: C_8H_8, CF_3S: $C_9H_7F_3$) and the mol fraction of the incorporated monomers. The total mass of each element (C_{tot}, H_{tot}, F_{tot}, and O_{tot}) is the sum of contributions from all three monomers. Dividing the total mass of each element by the mass contributions from all the elements ($C_{tot} + H_{tot} + F_{tot} + O_{tot}$) yields the wt% of each element. The equations for theoretical wt% of each element are as follows:

$$\%C_{theo} = \frac{C_{tot}}{C_{tot} + H_{tot} + F_{tot} + O_{tot}}$$

$$\%C_{theo} = \frac{12.01(4x_1 + 8x_2 + 9x_3)}{12.01(4x_1 + 8x_2 + 9x_3) + 1.01(2x_1 + 8x_2 + 7x_3) + 19(3x_3) + 16(3x_1)}$$

$$\%H_{theo} = \frac{H_{tot}}{C_{tot} + H_{tot} + F_{tot} + O_{tot}}$$

$$\%H_{theo} = \frac{1.01(2x_1 + 8x_2 + 7x_3)}{12.01(4x_1 + 8x_2 + 9x_3) + 1.01(2x_1 + 8x_2 + 7x_3) + 19(3x_3) + 16(3x_1)}$$

$$\%F_{theo} = \frac{F_{tot}}{C_{tot} + H_{tot} + F_{tot} + O_{tot}}$$

$$F_{theo} = \frac{19(3x_3)}{12.01(4x_1 + 8x_2 + 9x_3) + 1.01(2x_1 + 8x_2 + 7x_3) + 19(3x_3) + 16(3x_1)}$$

$$\%O_{theo} = \frac{O_{tot}}{C_{tot} + H_{tot} + F_{tot} + O_{tot}}$$

$$\%O_{theo} = \frac{16(3x_1)}{12.01(4x_1 + 8x_2 + 9x_3) + 1.01(2x_1 + 8x_2 + 7x_3) + 19(3x_3) + 16(3x_1)}$$

The actual combustion data for each element ($\%C_{act}$, $\%H_{act}$, $\%F_{act}$, and $\%O_{act}$) is compared to the theoretical wt% for each element. The sum of the squared differences is defined as:

$$Sum = (\%C_{act} - \%C_{theo})^2 + (\%H_{act} - \%H_{theo})^2 + (\%F_{act} - \%F_{theo})^2 + (\%O_{act} - \%O_{theo})^2$$

The actual polymer composition was presumed to be the mol fractions that minimize the sum of the square differences. For example, the actual combustion results for TC-22 is:

C: 64.76%, H: 4.49%, F: 10.73%, O: 20.02%. By substitution, the sum of the squared differences becomes:

$$
\begin{aligned}
Sum = & \left(64.76 - \frac{12.01(4x_1 + 8x_2 + 9x_3)}{12.01(4x_1 + 8x_2 + 9x_3) + 1.01(2x_1 + 8x_2 + 7x_3) + 19(3x_3) + 16(3x_1)} \right)^2 \\
& + \left(4.49 - \frac{1.01(2x_1 + 8x_2 + 7x_3)}{12.01(4x_1 + 8x_2 + 9x_3) + 1.01(2x_1 + 8x_2 + 7x_3) + 19(3x_3) + 16(3x_1)} \right)^2 \\
& + \left(10.73 - \frac{19(3x_3)}{12.01(4x_1 + 8x_2 + 9x_3) + 1.01(2x_1 + 8x_2 + 7x_3) + 19(3x_3) + 16(3x_1)} \right)^2 \\
& + \left(20.02 - \frac{16(3x_B)}{12.01(4x_1 + 8x_2 + 9x_3) + 1.01(2x_1 + 8x_2 + 7x_3) + 19(3x_3) + 16(3x_1)} \right)^2
\end{aligned}
$$

Solver in Excel was used to adjust the mol fractions in order to minimize the sum of the square differences. In the case of TC-22, the mol fractions that minimize the sum are:

$$x_1 = 0.49, \;\; x_2 = 0.29, \;\; x_3 = 0.22$$

These mol fraction values derived from the combustion data are in excellent agreement with the feed ratios. The compositions of the top coats and surface treatments have been calculated using this method.

5.7.5 Thin Film Preparation

A 0.5 wt% solution of XST in toluene was filtered with a 0.2 micron filter and spin coated at 3000 rpm to provide a film of ~15 nm thick. The film was heated at 250°C on a hotplate for 5 minutes to crosslink and was rinsed with toluene to remove

uncrosslinked chains. PS-PTMSS-PS solutions in toluene (1-2.5 wt%) were spin coated onto the XST to produce films between 30-100 nm thick. Top coats were spin coated onto PS-PTMSS-PS from 1 wt% solutions of a 3:1 (by mass) MeOH:aq. 30 wt% NH_4OH solution. TC-7 was cast from 1:3 (by mass) MeOH:aq. 30 wt% NH_4OH. 3:1. Samples were annealed on a hot plate at 175°C (or 190°C) for various lengths of time. They were quickly removed and cooled to room temperature. The top coat was stripped with the same casting solvent. Stripped samples contained little (< 3 nm) residual top coat.

5.7.6 Reactive Ion Etching

Etching was performed on an Oxford Plasmalab 80+ in inductively coupled plasma mode with the following formula: pressure=20 mTorr, RF power=10 W, ICP power=80 W, Ar flow rate=75 sccm, O_2 flow rate=75 sccm.

5.8 Acknowledgements

Dr. Christopher Bates and Anthony Thio helped synthesize top coats. Dr. William Durand and Gregory Blachut contributed to second-generation top coat design. Leon Dean helped test and analyze the top coats in this chapter.

Chapter 6: Top Coat Evaluation

The material reported in this chapter has been reproduced in part with permission from Maher, M. J.; Bates, C. M.; Blachut, G.; Sirard, S.; Self, J. L.; Carlson, M. C.; Dean, L. M.; Cushen, J. D.; Durand, W. J.; Hayes, C. O.; Ellison, C. J.; Willson, C. G. "Interfacial Design for Block Copolymer Thin Films." *Chem. Mater.* **2014**, *26*, 1471–1479. Copyright 2014 American Chemical Society.[70]

6.1 The Need for a Top Coat Wetting Test

In the previous chapter, top coats with a controlled composition were reported. Fine-tuning top coat surface energy was achieved by changing the monomer feed ratio in a three monomer system consisting of maleic anhydride, styrene, and 4-trifluoromethylstyrene. However, there was no real way of predicting whether or not any of those top coats would exhibit neutral interfacial interactions with the block copolymer. Despite having a top coat system with composition control, all of the top coats had to be tested using an Edisonian approach; the "success" of each top coat was determined by examining block copolymer orientation *via* scanning electron microscopy (SEM). This type of approach is labor intensive, and negative results do not provide the feedback necessary to improve the experimental design. In this chapter, new top coats with a wider range of surface energies and methods for evaluating coat wetting are reported. The block copolymers used to demonstrate these concepts are poly(styrene-*block*-4-trimethylsilylstyrene) (PS-PTMSS, L_0 = 18 and 22 nm) and poly(styrene-block-trimethylsilylmethyl methacrylate) (PS-PTMSM, L_0 = 15 nm). The last portion of the chapter shows that the orientation strategy can be applied to multiple high-χ block copolymers, including one with L_0 = 10 nm.

6.2 More "Hydrophobic" Top Coats

In Chapter 5, the top coats based on 4-trifluoromethylstyrene (CF_3S) were reported to be successful in controlling the orientation of PS-PTMSS-PS. Top coats with low amounts of CF_3S (<20%) produced a parallel orientation whereas compositions with intermediate amounts of CF_3S (37%) produced a perpendicular orientation. Even the most extreme top coat with 53% CF_3S produced a perpendicular orientation at all film thicknesses tested (1-3 L_0). These data suggest that TC-53 is neutral. It would be more satisfying if the top coat system spanned a larger range of surface energies so that one extreme would be preferential to PS and the other would be preferential to PTMSS. It was hypothesized that a more hydrophobic monomer, such as 3,5-di-*tert*-butylstyrene (di-t-BS) would be enable access to a larger range of surface energies relative to CF_3S top coats (Figure 6.1).

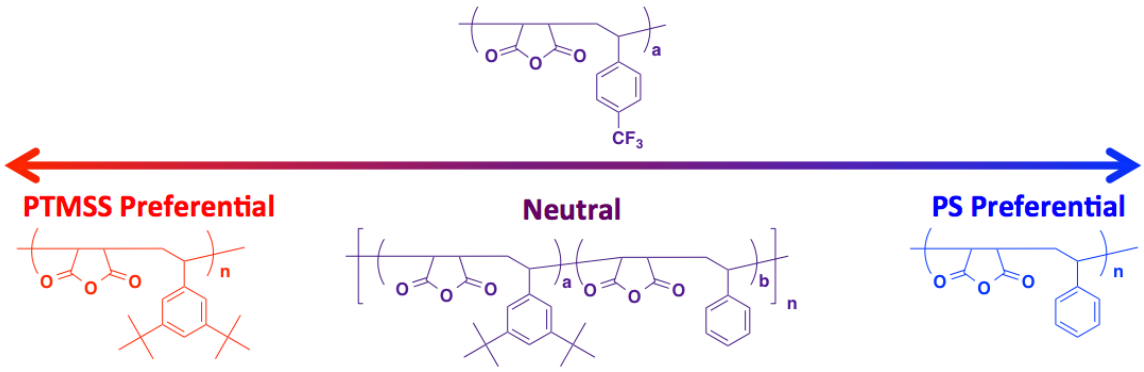

Figure 6.1: Range of surface energies that can be captured by the copolymers of maleic anhydride, styrene, and 3,5-di-*tert*-butylstyrene.

The top coats based on di-t-BS were synthesized according to Scheme 6.1. Similarly to the CF_3 top coats, composition was controlled *via* monomer feed ratio. The polymer composition was found to be the same at low and high conversions for this system (see 6.10.4), which suggests that the reactivity ratios of the two styrene derivatives are similar. The new top coats and their properties are summarized in Tables 6.1 and 6.2. The top coats have been named TC-S-xx where xx represents the amount of di-t-BS incorporated into the top coat.

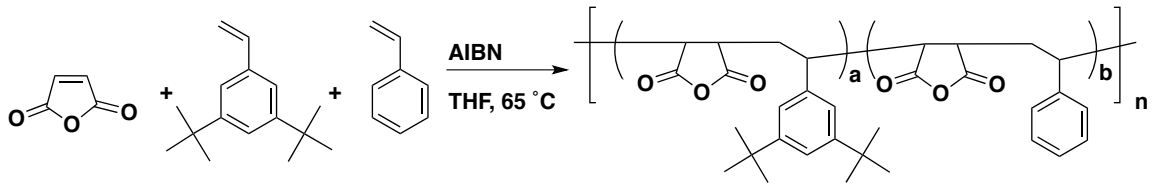

Scheme 6.1: Top coat synthesis using styrene, maleic anhydride and di-t-BS.

Table 6.1: Summary of top coat composition

		Feed Ratio (mol%)			Actual Ratio (mol%)[a]		
Entry	**Top Coat**	**MA**	**di-t-BS**	**S**	**MA**	**di-t-BS**	**S**
a	TC-S-6	50	5	45	52	6	42
b	TC-S-12	50	10	40	52	12	36
c	TC-S-25	50	26	24	51	25	24
d	TC-S-49	50	50	0	51	49	0

* Abbreviations: MA (maleic anhydride), di-t-BS (3,5-di-*tert*-butylstyrene), S (styrene), [a]Calculated by combustion analysis.

Table 6.2: TC-S characterization data.

TC	M_n*	M_w*	Đ	T_g (˚C)	T_d (˚C)	Yield
TC-S-6	4710	12100	2.56	196	269	76
TC-S-12	4600	14500	3.15	197	261	25
TC-S-25	5050	15200	3.02	195	275	52
TC-S-49	6230	12090	1.94	208	278	42

*Molecular weights relative to PS standards in DMF at 70˚C. Units are in Da.

The di-t-BS top coat system meets all of the desired top coat property requirements. They have a controlled composition and glass transition temperatures above 200˚C. Unfortunately, some of these top coats with large amounts of di-t-BS are not soluble in aqueous ammonium hydroxide. This problem is addressed in the following section by creating trimethylammonium salts.

6.3 TRIMETHYLAMMONIUM SALTS

For the di-t-BS containing topcoats, there were two major problems. Most of the di-t-BS top coats were not soluble in ammonium hydroxide solution, which prevented spin coating directly onto the block copolymer. Secondly, further IR studies showed that imide was forming during the thermal ring closure. Figure 6.2 shows the bulk IR spectra of a model top coat, poly(4-*tert*-butylstyrene-*alt*-maleic anhydride) (TC-S-IR). The blue curve corresponds to TC-S-IR as synthesized. The red curve corresponds to the NH_4 salt of the TC-S-IR, which was obtained by dissolving TC-S-IR in aqueous ammonium hydroxide and subsequently removing the solvent. The green curve shows the result of thermal annealing. The green curve mirrors the blue curve perfectly with one major

exception: a new peak emerges at around 1715 cm^{-1}. The new peak is characteristic of imide formation, which means that upon dissolution in ammonium hydroxide, a substantial amount of amide was formed. This was problematic because the ratio of anhydride to imide cannot be controlled, which makes the top coat surface energy vary from trial to trial.

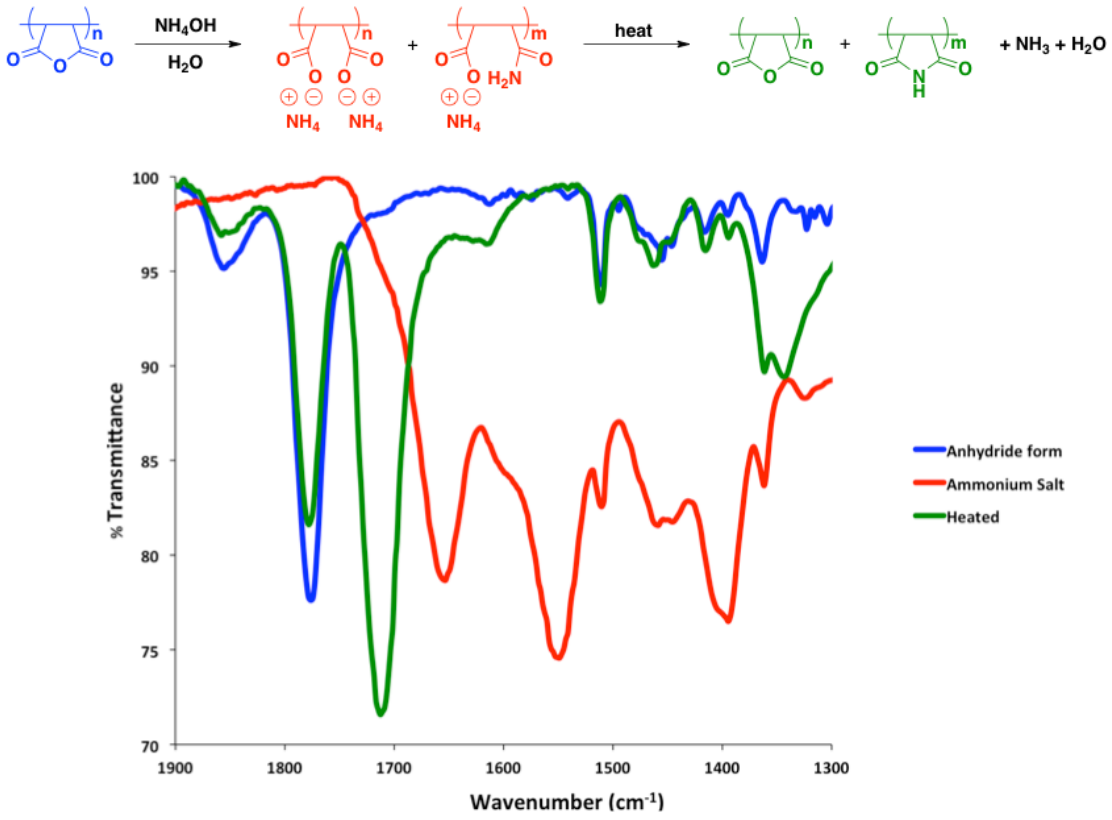

Figure 6.2: Bulk IR spectra of TC-S-IR (blue curve), the corresponding NH_4 salt (red curve), and the product of heating the NH_4 salt to 200 ℃ at a rate of 10 ℃/min (green curve). All IR spectra were obtained in the solid state using FT-ATR.

It was hypothesized that amide/imide formation could be avoided by switching spin coating solvents from ammonium hydroxide to a tertiary amine since tertiary amines cannot form imides. Trimethylamine (TMA) was used because it is the simplest tertiary amine and is commercially available in aqueous solution. The TMA salt of TC-IR was isolated and the analogous IR experiment in bulk was performed (Figure 6.3). The blue and red curves show the as synthesized TC-IR and the corresponding TMA salt, respectively. The green curves shows the result after heating. No new peaks are formed, and the IR matches the blue curve almost exactly, which suggests that the TMA salt prevents imide formation.

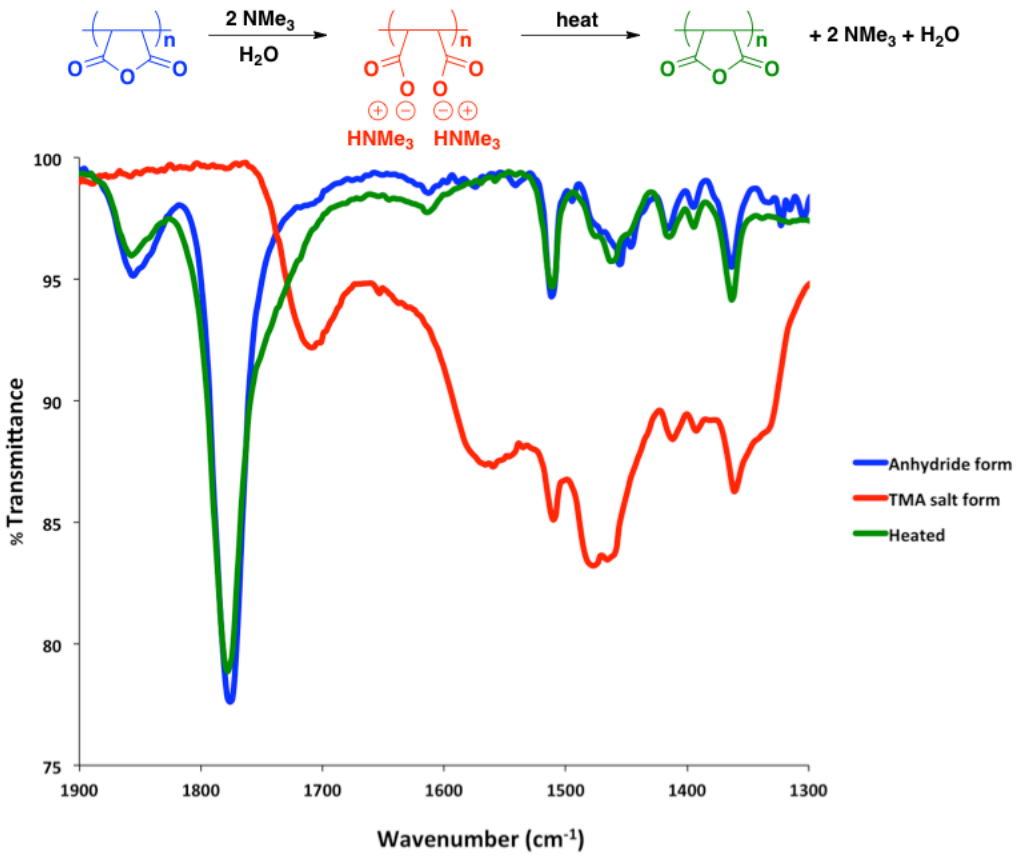

Figure 6.3: IR spectra of TC-IR (blue curve), the corresponding TMA salt (red curve), and the product of heating the TMA salt to 200 ℃ at a rate of 10 ℃/min (green curve). All IR spectra were obtained in the solid state using FT-ATR.

It was important to check the IR of the TMA salt in thin film, which could deviate from results observed in bulk. Fortunately, the TMA salt of TC-S-IR is highly soluble in water and methanol, which enables spin coating. The IR study is shown in Figure 6.4. The blue curve represents the top coat as cast from amyl acetate. The asymmetric and symmetric C=O stretching bands were observed at 1853 cm^{-1} and 1774 cm^{-1}, respectively.[121] The TMA salt cast from methanol (red curve) shows no anhydride peaks; instead, carboxylate peaks at 1560 cm^{-1} and 1463 cm^{-1} are present. A new peak at 1708

cm^{-1} was also observed, which is attributed to the free carboxylic acid carbonyl stretch. After heating at 190 ˚C for 30 seconds (green curve), the carboxylate and free carboxylic acid peaks diminish, and the reemergence of the anhydride peaks was observed. No other new peaks were formed.

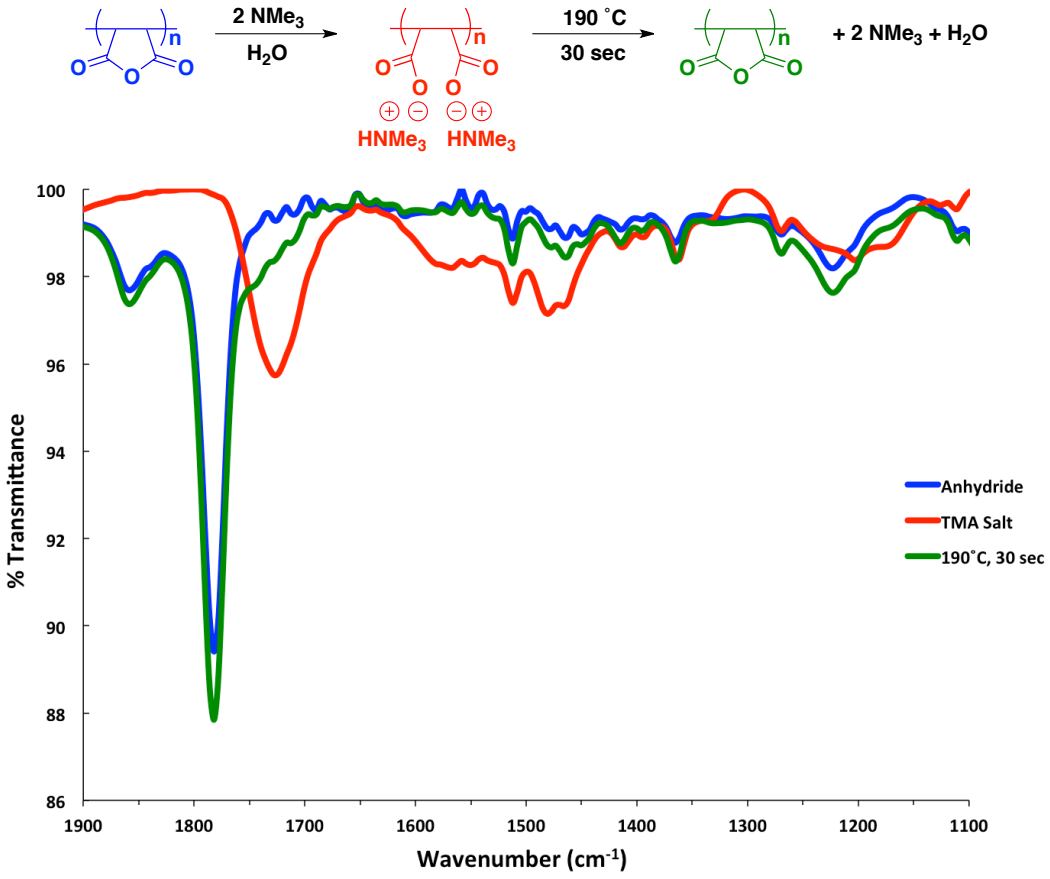

Figure 6.4: Thin film IR spectra of TC-IR as cast from amyl acetate (blue curve), the corresponding TMA salt cast from methanol (blue curve), and the TMA salt after heating at 190 ˚C for 30 seconds (green curve).

A combustion analysis study was performed to determine if any nitrogen containing species were being formed after thermal annealing. This was performed in bulk by isolating the NH_4 and TMA salts, annealing them, and measuring their elemental composition. Table 6.3 shows the results of the study. TC-S-IR is the control, non-salt form. In the case of the NH_4 salt, 3.64% nitrogen is detected. This translates to 65% of the maleic anhydride units being converted to the imide after dissolution in ammonium hydroxide and subsequent heating. For the TMA salt, no nitrogen was detected, which suggests that no nitrogen-containing species are formed. This is consistent with complete elimination of trimethylamine during the thermal closing of the anhydride.

Table 6.3: Combustion analysis results.

Sample	%C	%H	%N
TC-S-IR	74.12	6.97	0.00
NH_4 Salt After Heating	74.16	7.28	3.64
TMA Salt After Heating	75.04	7.04	0.00

Fortuitously, all top coats reported in Table 6.1 are soluble in aq. TMA. The polymeric salts of each top coat was generated by dissolution in TMA and were isolated by removing the solvent. Even the TMA salt of the most hydrophobic top coat, TC-S-49, is soluble in methanol. The top coat films of TMA salts spin-coated from methanol produce significantly more uniform films than those coated from solutions containing water. The enhanced solubility of TMA salts in methanol greatly broadens the scope of processable top coats.

6.4 CROSSLINKABLE TOP COATS

Up until this point, testing the top coats was an Edisonian process guided by chemical intuition and imprecise structure-property relationships. The guess and check methodology must be repeated for each block copolymer. Techniques that simplify the optimization of top coat materials are necessary. In this section, crosslinkable top coats (XTCs) are introduced. These top coats contain benzocyclobutenestyrene (BCB), which thermally crosslinks at 250˚C.[58] This allows the XTC to behave like a surface treatment. The top coat wetting can be evaluated using the same island/hole test that was previously used to identify neutral surface treatments (see Chapter 4). This is very valuable because it can identify if the monomers chosen for the top coat system will be neutral for a given block copolymer. To further illustrate, consider a top coat with 25% styrene, 25% di-t-BS, and 50% maleic anhydride. If a parallel orientation of domains results after SEM inspection, what does the result say about the top coat composition? Does the top coat need to have more di-t-BS or styrene? The island/hole test provides insight into which block the top coat is wetting, which guides how the top coat composition should be adjusted. Two XTCs were synthesized according to Schemes 6.2 and 6.3. The XTC-A is the styrene extreme, and XTC-Ω is the di-t-BS extreme. The composition of XTC-A is 52:41:7 maleic anhydride: styrene: BCB, and XTC-Ω contains 50:42:8 maleic anhydride: di-t-BS: BCB.

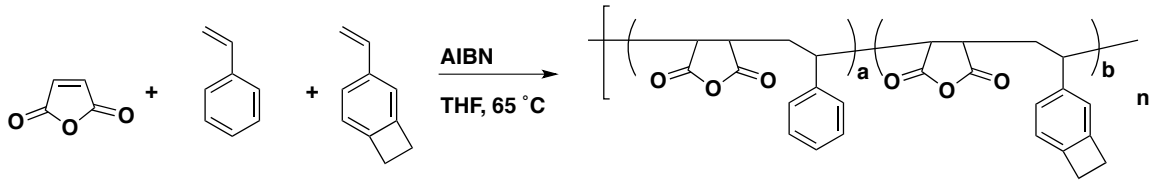

Scheme 6.2: Synthesis of XTC-A.

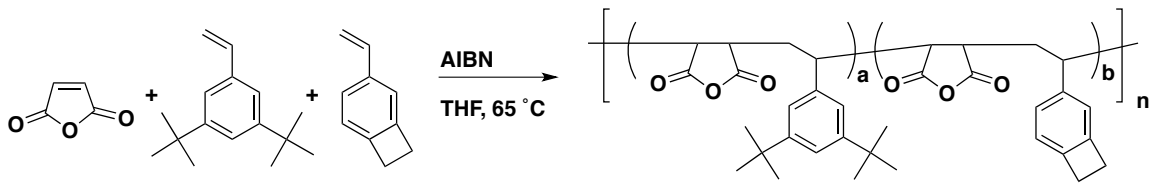

Scheme 6.3: Synthesis of XTC-Ω.

The wetting preference of the XTCs was examined using PS-PTMSS-PS (L_0 = 19 nm).[83] XTCs were crosslinked into ~30 nm films by annealing at 250˚C for 15 minutes. Then, the block copolymer was spin coated at an incommensurate thickness (~1.2 L_0) and thermally annealed at 190˚ for 1 minute. The optical microscope images of the films are shown in Figure 6.5. Holes appeared when the block copolymer was annealed on XTC-A, which suggests asymmetric wetting. Since the PTMSS wets the air interface, this means that XTC-A wets the PS block. When the same experiment was performed with XTC-Ω, islands appeared, which suggests symmetric wetting. Therefore, XTC-Ω wets the PTMSS block. These island and hole results suggest that there should be a composition in the di-t-BS top coat system that is neutral for PS-PTMSS block copolymers. This is only true because the extreme compositions wet different blocks. If the wetting results in Figure 6.5 were identical, then a new top coat system would be needed. Fortunately, this is not the case. PS-PTMSS-PS triblock was used in this study, and it is reasonable to assume that wetting characteristics would have been the same for the homologous diblock.

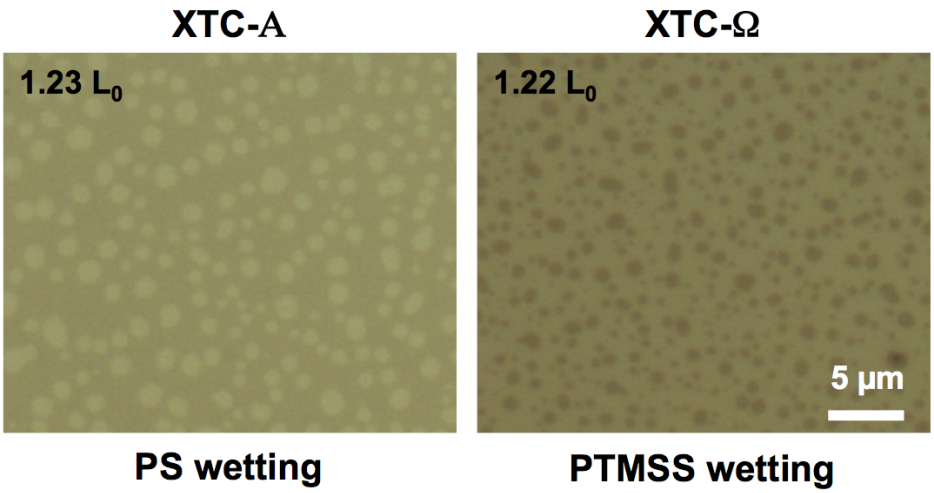

Figure 6.5: Optimal microscope images of PS-PTMSS-PS (L_0=19nm) annealed on two different XTCs.

XTCs can be made to test various compositions for neutrality. Unfortunately, this is not a practical approach because BCB is made by a multistep synthesis in low yields. Additionally, the XTC will not be crosslinked when it is applied as a top coat. The crosslinked structure incorporates a small amount of BCB thermolysis products, which could cause it to have slightly different wetting characteristics than the non-crosslinked top coat. Therefore, while this strategy is good for testing composition extremes for different top coat systems, it is not a direct method for testing the top coat wetting preference or finding the condition of perfect neutrality.

6.5 Confined Island Hole Test

Shortly after the development of XTCs, a direct method for testing top coat wetting was discovered. Recall from Chapter 3 that Figure 3.8 had micron-sized topography that resulted from choosing the "wrong" top coat. Upon further examination,

the topography was actually due to island/hole formation. This led to the discovery that the top coats do not suppress island and hole generation. If the substrate interface is highly preferential (e.g. SiO_2 for PS), then the BCP can alleviate incommensurability by forming island hole topography even when confined by a top coat. Essentially, the top coat can be directly tested by an "inverse" or "confined" island hole test. All of the same island hole principles discussed for surface treatments in Chapter 4 still apply here. The major difference is that the top coat wetting is unknown whereas in Chapter 4, the crosslinkable surface treatment (XST) wetting was unknown. For the classical island/hole test, it was known that the air was preferential to PTMSS. For the confined island/hole test, a PS-preferential XST such poly(styrene-*random*-4-vinylbenzyl azide) (X-PS) can be used. As long as the wetting preference for one interface is known, the island/hole test (classic or confined) can be used to determine the wetting preference of the other interface.

Figure 6.6 illustrates the "confined" island and hole test that was developed to evaluate (non-)preferential wetting at the block copolymer-top coat interface. PS-PTMSS with an as-cast thickness $1\ L_0 < L_{avg} < 2\ L_0$ is coated on X-PS. PS is depicted in blue and PTMSS is depicted in red. A top coat TMA salt is then coated onto the block copolymer film from methanol. The film stack is annealed on a hot plate and subsequently examined with optical and/or atomic force microscopy. In principle, the topography that forms only depends upon the as-cast block copolymer thickness and the (non-)preferential interactions between the block copolymer and the top coat. First consider the film thickness range $1\ L_0 < L_{avg} < 1.5\ L_0$. If holes are observed, asymmetric wetting implies that the PTMSS block wets the top coat. In contrast, if islands are observed, symmetric wetting implies that the PS block wets the top coat. Half islands (if $1\ L_0 < L_{avg} < 1.25\ L_0$) or half holes (if $1.25\ L_0 < L_{avg} < 1.5\ L_0$) indicate the presence of the desired neutral top

coat.[115] With a PS-wetting substrate, the film thickness range 1.5 $L_0 < L_{avg} < 2\ L_0$ produces islands if the top coat wets the PTMSS block, holes if the top coat wets the PS block, and half islands (if 1.5 $L_0 < L_{avg} < 1.75\ L_0$) or half holes (if 1.75 $L_0 < L_{avg} < 2\ L_0$) if the top coat is neutral.

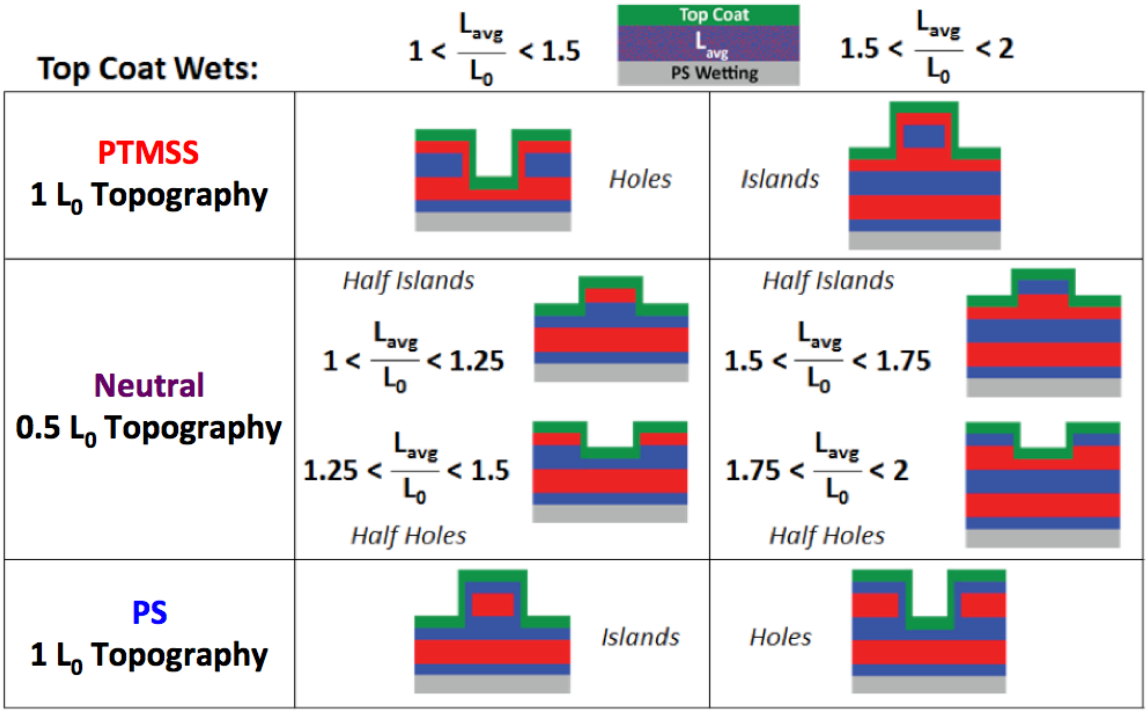

Figure 6.6: Illustration of the "confined" island and hole test. Block copolymer annealed between a strongly preferential substrate surface and a top coat produces topography that depends only upon the preferential wetting at the block copolymer-top coat interface. Note the block(s) that contact the top coat in each scenario.

The confined island and hole test was performed on PS-PTMSS (L_0 = 18 nm) with 1.0 $L_0 < L_{avg} < 1.5\ L_0$ using three top coats, TC-S-49, TC-S-25, and TC-S-6 on X-PS. After application of the block copolymer and top coat, the resulting film was uniform and

featureless before annealing. The film stacks were annealed at 180 °C for 5 min on a hot plate and subsequently examined with an optical microscope (Figure 6.7). Note that with these film thicknesses, thicker regions appear darker (islands) and thinner regions are lighter (holes). The top coats were not removed before imaging. TC-S-49 produced holes consistent with asymmetric wetting. The density of holes correlates with L_{avg}: a high density of spinodal-like features was observed near the most incommensurate film thickness $L_{avg} \approx 1\ L_0$ and slowly decreased as L_{avg} approached the 1.5 L_0 commensurate condition. TC-S-6 exhibited the opposite quantization behavior. Islands consistent with symmetric wetting were observed; their density correlates inversely with the TC-S-49 sample, as expected. Films near the commensurate thickness $L_{avg} \approx 1\ L_0$ exhibited very sparse features that became denser and finally spinodal-like near the most incommensurate thickness $L_{avg} \approx 1.5\ L_0$. TC-S-25 produced features with markedly lower optical contrast than either the TC-S-49 or TC-S-6 samples. Topography inverted surrounding $L_{avg} \approx 1.25\ L_0$; half islands formed when $1.0\ L_0 < L_{avg} < 1.25\ L_0$ and half holes when $1.25\ L_0 < L_{avg} < 1.5\ L_0$. Additionally, spinodal-like features were produced in the vicinity of $L_{avg} \approx 1.25\ L_0$.

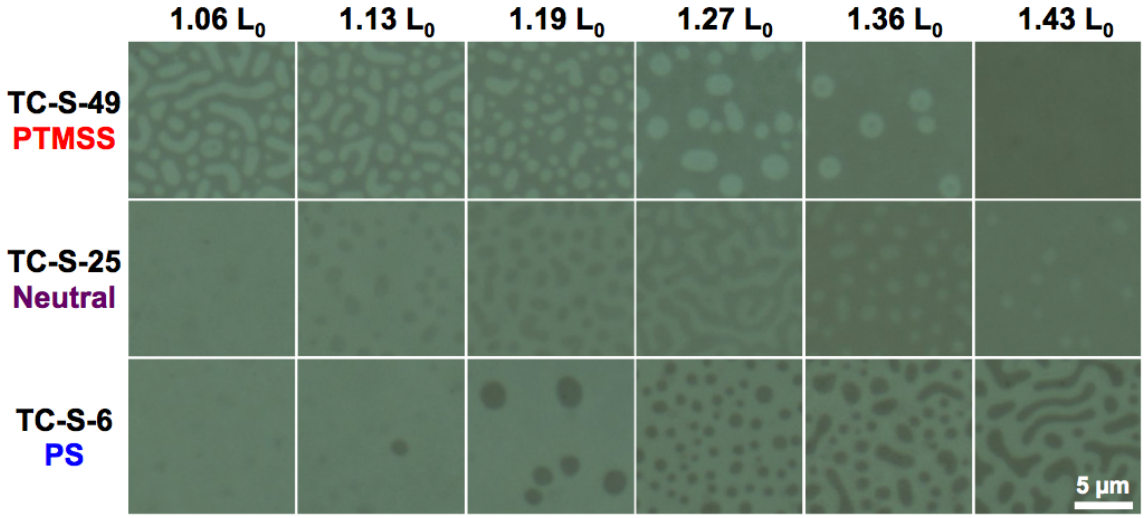

Figure 6.7: Optical micrographs of PS-PTMSS (L_0≈18 nm) confined between a top coat and a PS surface treatment, annealed at 180 °C for 5 min. Implied top coat preferential wetting is listed in color. Note: at these film thicknesses, dark spots are thicker (islands) and light spots are thinner (holes). The scale bar is valid for all micrographs and represents 5 μm.

Atomic force micrographs (AFMs, Figure 6.8) of select data from Figure 6.7 confirmed the conclusions drawn from the optical micrographs. TC-S-49 and TC-S-6 produced topography with 1 L_0 step heights, consistent with block copolymer thickness quantization in the presence of preferential interfaces. TC-S-49 wets PTMSS and TC-S-6 wets PS. In contrast, TC-S-25 produced half islands and half holes with 0.5 L_0 step heights. TC-S-25 is neutral for PS-PTMSS (L_0 = 18 nm). The confined island and hole test was repeated using PS-PTMSS with L_0 = 22 nm (Figure 6.9). Remarkably, identical wetting trends were observed. TC-S-25 is neutral for PS-PTMSS with both L_0 = 18 nm and L_0 = 22 nm.

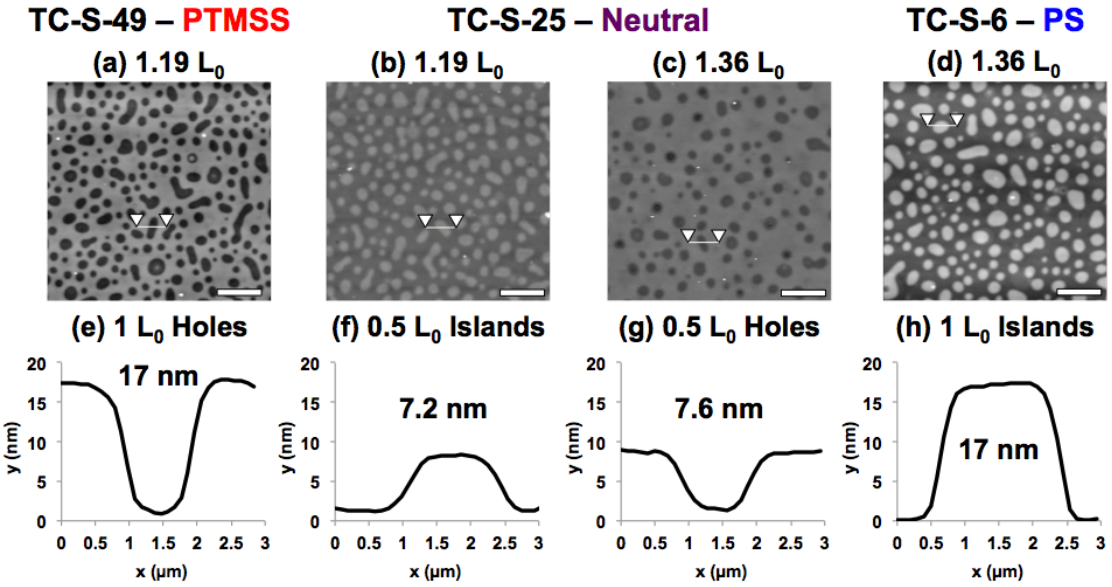

Figure 6.8: (a-d) AFM height and (e-h) height traces of select PS-PTMSS (L_0 =18 nm) samples from Figure 3, confined between a top coat and a PS surface treatment, annealed at 180 °C for 5 min. Implied top coat wetting is listed in color. The scale bars represent 5 μm.

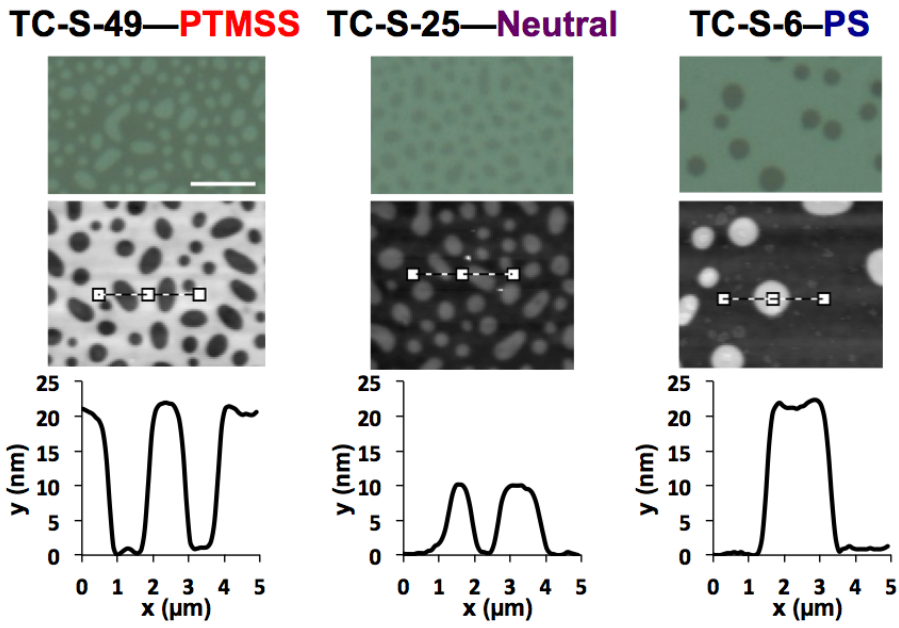

Figure 6.9: Confined island and hole test with PS-PTMSS (L_0 = 22 nm). Optical micrographs, AFM micrographs, and AFM height traces of the topography formed when confined between a top coat and X-PS. Samples were annealed at 180 °C for 6 min. Scale bars represent 5 μm.

6.6 Thin Film Evaluation

Orientation control of PS-PTMSS (L_0 = 22nm) was attempted using TC-S-49 (PTMSS preferential), TC-S-25 (Neutral), and TC-S-6 (PS preferential). Figure 6.10 shows the orientation results after thermally annealing a 1 L_0 thick film at 190˚C for 30 seconds. The extremes induce a parallel orientation while the neutral material results in a perpendicular orientation. This demonstrates that the di-t-BS top coats span a larger surface energy than the CF_3S top coats (see Chapter 5). Additionally, it demonstrates that different types of monomers can be used to control the block copolymer orientation.

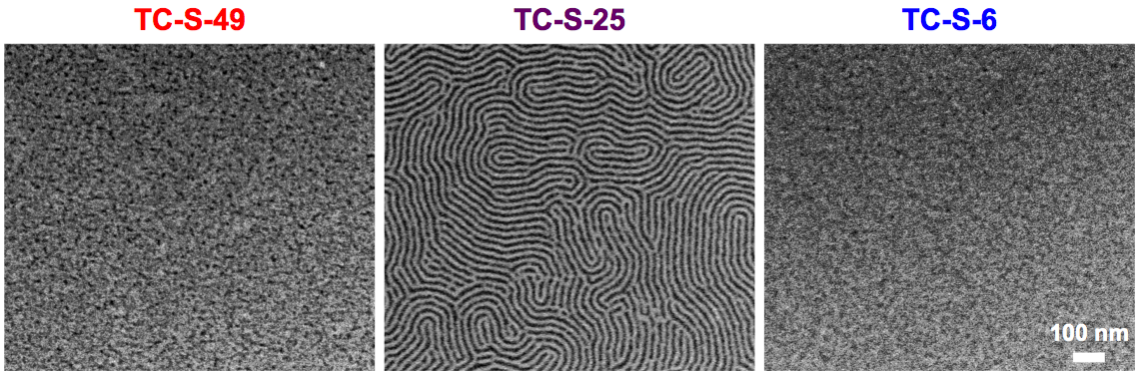

Figure 6.10: Orientation of PS-PTMSS (L_0 = 22 nm) after stripping the top coat and etching. The samples were originally annealed between XST-52 and one of the top coats listed above the SEM image. The scale bar is valid for all images.

The presence of two neutral interfaces theoretically decouples block copolymer orientation from block copolymer thickness as discussed in Chapter 3. The perpendicular orientation at any block copolymer thickness becomes favorable with two perfectly neutral materials.[53,94] Complete interfacial neutrality was achieved for PS-PTMSS with the combination of top coat TC-S-25 and either XST-52* (for L_0 = 22 nm) or XST-51 (for L_0 = 18 nm). PS-PTMSS samples annealed at 190 °C for 30 sec produced perpendicular lamella independent of block copolymer film thickness. Scanning electron micrographs (SEMs) of PS-PTMSS with L_0 = 22 nm (Figure 6.11a-e) and L_0 = 18 nm (Figure 6.11f-j) demonstrate perpendicular lamellae at all block copolymer film thicknesses between 1-3 L_0.

* See Chapter 4 for XST nomenclature and structure.

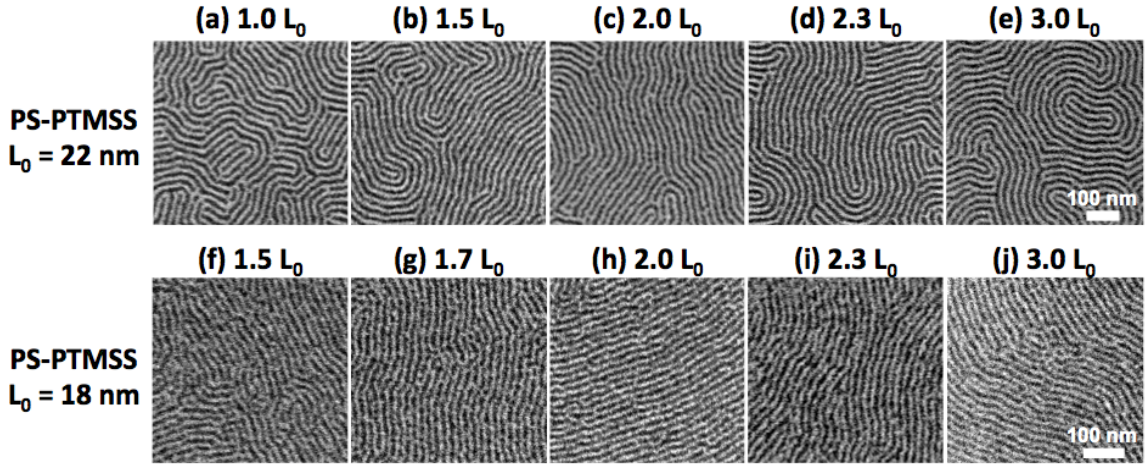

Figure 6.11: SEM annealed between two neutral interfaces. (a-j) PS-PTMSS at 190 °C for 30 sec. (a-e) $L_0 \approx 22$ nm, (f-j) $L_0 \approx 18$ nm. Samples (a-j) were etched with O_2 plasma. The scale bars are valid for the micrographs in a given row.

The perpendicular lamellae produced by PS-PTMSS ($L_0 = 22$ nm) span the entire thickness of a 1.68 L_0 film (Figure 6.12). A generalization of this result suggests that perpendicular lamellae formed in the presence of neutral interfaces exhibit excellent through-film uniformity. Presumably, there is some threshold thickness above which the lamellae produce through-film defects such as dislocations or bifurcation, which have been observed in thicker lamella-forming[13] block copolymer films. However, in the presence of surface directing pre-patterns, defectivity significantly improves.[101,122,123] These experimental observations are reinforced by theoretical calculations that reveal a large thermodynamic driving force for the removal of thin film defects in the presence of substrate surface chemical patterns.[67,68] Directed self-assembly induced defect reduction also translates to improved through-film uniformity, as evidenced by experiments on thin[120] and thick[124] PS-PMMA films.

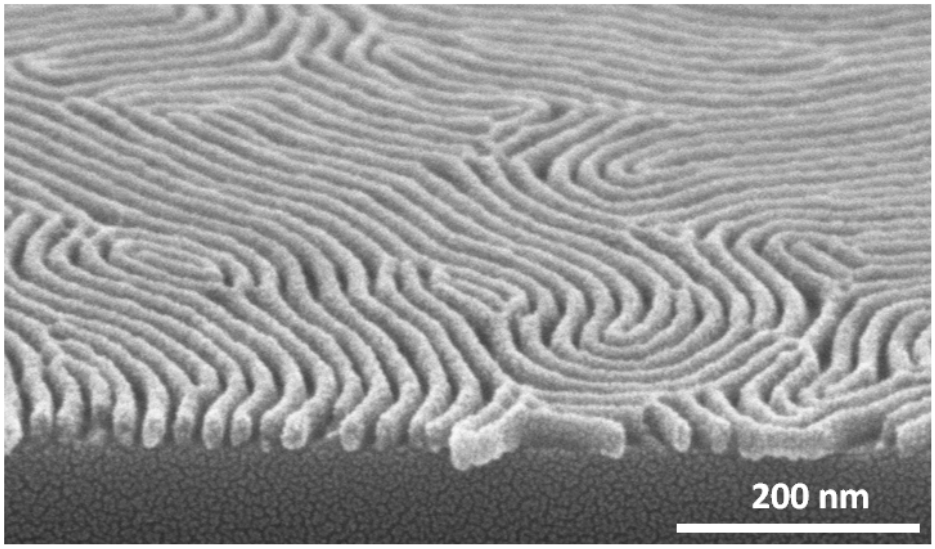

Figure 6.12: Tilted SEM of PS-PTMSS (L_0 = 22 nm) with an as-cast film thickness of 37 nm (1.68 L_0), annealed between neutral top and bottom interfaces at 190 °C for 60 sec. The top coat was stripped with TMA/MeOH and the film was etched. The perpendicular lamellae span the entire thickness of the film.

6.7 MALEIMIDE TOP COATS FOR PS-PTMSM

The di-t-BS-containing top coats all failed in controlling the orientation of poly(styrene-*block*-methyltrimethylsilylmethacrylate) (PS-PTMSM, L_0 = 15 nm). During the confined island/hole test, all of the TC-S top coats were PTMSM wetting. This result was highly puzzling. Recall that surface energy is complex, multi-dimensional, and is dependent on a combination of intramolecular forces.[125] It was suspected that there might be some interaction with PTMSM and maleic anhydride that makes top coats based on maleic anhydride prefer to wet PTMSM. Therefore, it was hypothesized that top coats with less maleic anhydride might wet the PS block. A new top coat design was introduced that holds the styrene component constant at 50 mol% and varies the relative ratio of maleic anhydride and a functionalized maleimide. Both maleimide derivatives

and maleic anhydride are known to form alternating copolymers with styrene.[126] N-methylmaleimide (MM) was chosen as the functionalized maleimide because it is commercially available. These top coats are named as TC-M-xx, where the M signifies use with the PS-PTMSM block copolymer and the xx represents the mol% of MM in the copolymer. These polymers were synthesized according to Scheme 6.4 and the respective characterization data is listed in Tables 6.4 and 6.5. These top coats also meet all of the desired requirements and can be converted into TMA salts for testing.

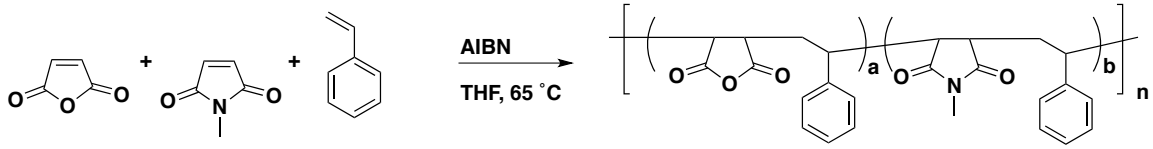

Scheme 6.4: Synthesis of TC-M top coats.

Table 6.4: Summary of top coat composition

		Feed Ratio (mol%)			Actual Ratio (mol%)[a]		
Entry	**Top Coat**	**MA**	**MM**	**S**	**MA**	**MM**	**S**
1	TC-M-31	20	30	50	23	31	46
2	TC-M-29	25	25	50	25	29	46
3	TC-M-23	30	20	50	30	23	47
4	TC-M-19	35	15	50	34	19	47
5	TC-M-14	40	10	50	38	14	48

* Abbreviations: MA (maleic anhydride), MM(N-methylmaleimide), S (styrene)
[a]Calculated by combustion analysis.

Table 6.5: Summary of top coat composition

TC	M_n*	M_w*	Đ	T_g	T_d	Yield
TC-M-31	11700	38500	3.29	200	315	85
TC-M-29	10800	33600	3.11	198	282	80
TC-M-23	7866	28300	3.60	195	292	83
TC-M-19	8286	28700	3.46	196	271	87
TC-M-14	7082	24100	3.40	196	275	87

*Molecular weights relative to PS standards in DMF at 70˚C. Units are in Da.

The confined island/hole test for PS-PTMSM with the new TC-M top coats was performed. Optical micrographs of PS-PTMSM annealed between X-PS and a top coat produced topography that signals top coat wetting (Figure 6.14). TC-M-19 induced asymmetric wetting and is thus PTMSM preferential. In contrast, TC-M-31 preferentially wets PS as evidenced by symmetric wetting. This confirms the hypothesis that reducing the amount of maleic anhydride increases the wetting preference for PS. An intermediate composition, TC-M-29 exhibited incommensurability at 1.25 and 1.75 L_0, as expected for a single neutral interface. AFM confirmed the step heights associated with TC-M-19 and TC-M-31 are 1 L_0, while TC-M-29 formed 0.5 L_0 islands and holes (Figure 6.14). TC-M-29 is thus neutral for PS-PTMSM with L_0 = 15 nm.[115]

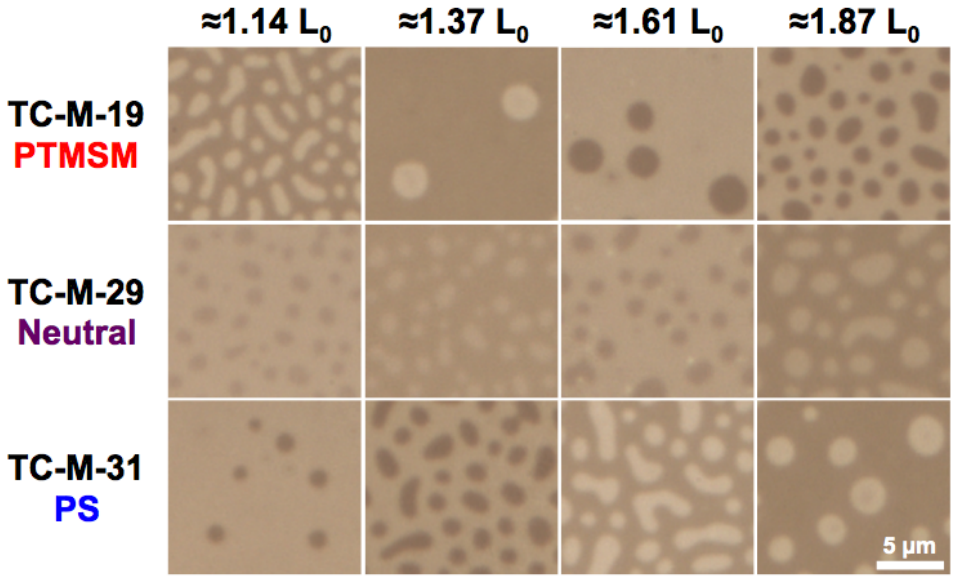

Figure 6.13: Optical micrographs of PS-PTMSM (L_0≈15 nm) confined between a top coat and X-PS, annealed at 170 °C for 10 min. Implied top coat wetting is listed in color. At these film thicknesses, dark spots are thicker (islands) and light spots are thinner (holes). The scale bar is valid for all micrographs.

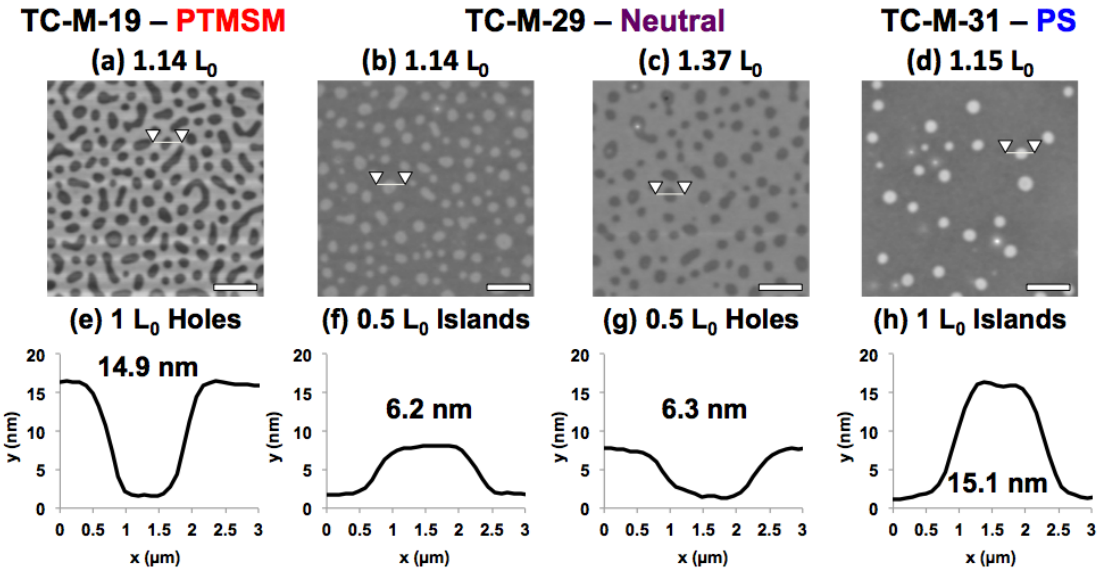

Figure 6.14: (a-d) AFM height and (e-h) height traces of select PS-PTMSM (L_0 =15 nm) samples from Figure 6.14, confined between a top coat and a PS surface treatment, annealed at 170 °C for 10 min. Scale bars represent 5 μm.

PS-PTMSM confined between neutral interfaces (TC-M-29 and XST-34) and annealed at 170 °C for 60 sec also produced perpendicular lamellae. A large SEM of the first successful orientation attempt is shown in Figure 6.15. A perpendicular orientation can be seen with no sign of parallel domains. A thickness study (Figure 6.16a-d) shows perpendicular orientation independent of film thickness, which suggests that TC-M-29 is neutral. These samples were imaged after stripping the top coat but without reactive ion etching. The presence of perpendicular features without etching suggests the absence of a block copolymer wetting layer at the block copolymer/top coat interface during annealing. Such wetting layers are not expected to arise in the presence of neutral interfaces. PS-PTMSM features exhibit low contrast by SEM. Three possible explanations could account for the imaging difficulties: 1) the SEM is operating very near its resolution limit for soft materials with low electron density differences, 2) the electron beam damages the block copolymer during imaging, and 3) the polymer is near the order-disorder transition temperature, which could blur the interface between domains. Regardless, uniform coverage of perpendicular features across the entire substrate is evident.

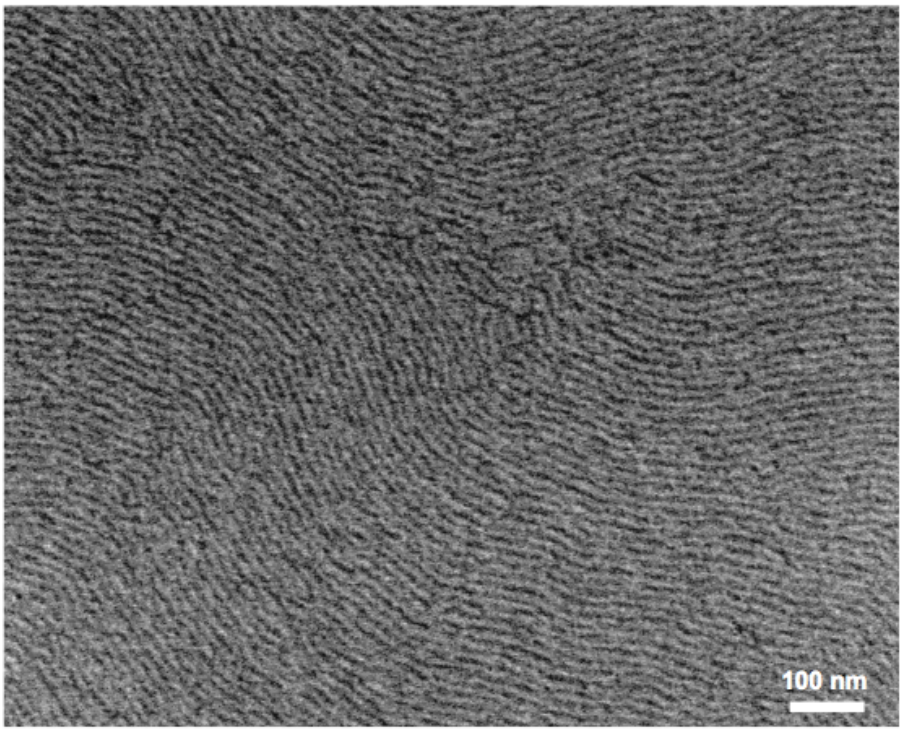

Figure 6.15: Orientation of PS-PTMSM annealed at 180˚C for 1 minute confined between XST-34 and TC-M-29. Sample was briefly etch with O_2 plasma after removing the top coat.

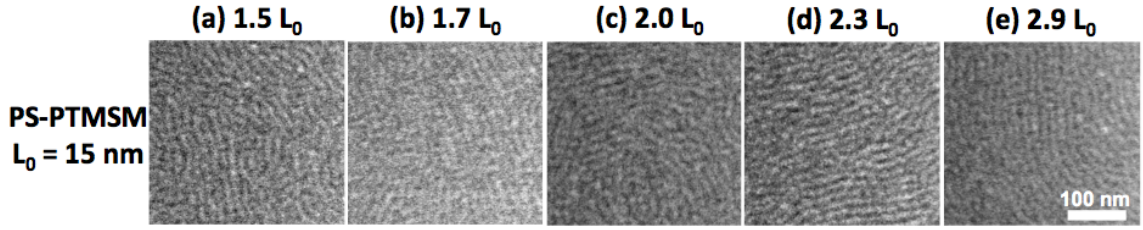

Figure 6.16: PS-PTMSM (L_0 = 15 nm) annealed at 170 °C for 60 sec while confined between XST-34 and TC-M-29. Samples are unetched. The scale bar is valid for all of the micrographs.

6.8 Application to Other Silicon-containing Block Copolymers

The orientation strategy in this chapter has been demonstrated using two different silicon-containing block copolymers. Recent work has shown that the XST and TC-S system can control the orientation of even higher χ block copolymers. In a report by Durand *et al*,[49] the orientation PS-PTMSS was compared to poly(4-methoxystyrene-*block*-4-trimethylsilylstyrene) (PMOST-PTMSS) and poly(styrene-*block*-4-pentamethyldisilylstyrene) (PS-PDSS). Through film etch results are shown in Figure 6.17. In the top row, all three block copolymers have L_0 values of 20 nm (subscript 20 nm). In the bottom row, PMOST-PTMSS and PS-PDSS have L_0 values of 14 nm (subscript 14 nm). At a pitch of 20 nm, the higher χ block copolymers (PMOST-PTMSS and PS-PDSS) appear to have much stronger phase separation, less defects, and less bridging. PMOST-PTMSS and PS-PDSS can also be used to access the sub-10 nm (half pitch) regime. Notice in Figure 6.17 that PMOST-PTMSS$_{14}$ and PS-PDSS$_{14}$ appear to have the same bridging issues as PS-PTMSS$_{20}$. This suggest that the χ values of these polymers are not large enough to form crisp features when L_0 = 14 nm. This is presumably because the polymers are approaching the order-disorder transition. Even higher χ block copolymers are needed in order to be useful in patterning half-pitch lines/spaces on the order of 5 nm.

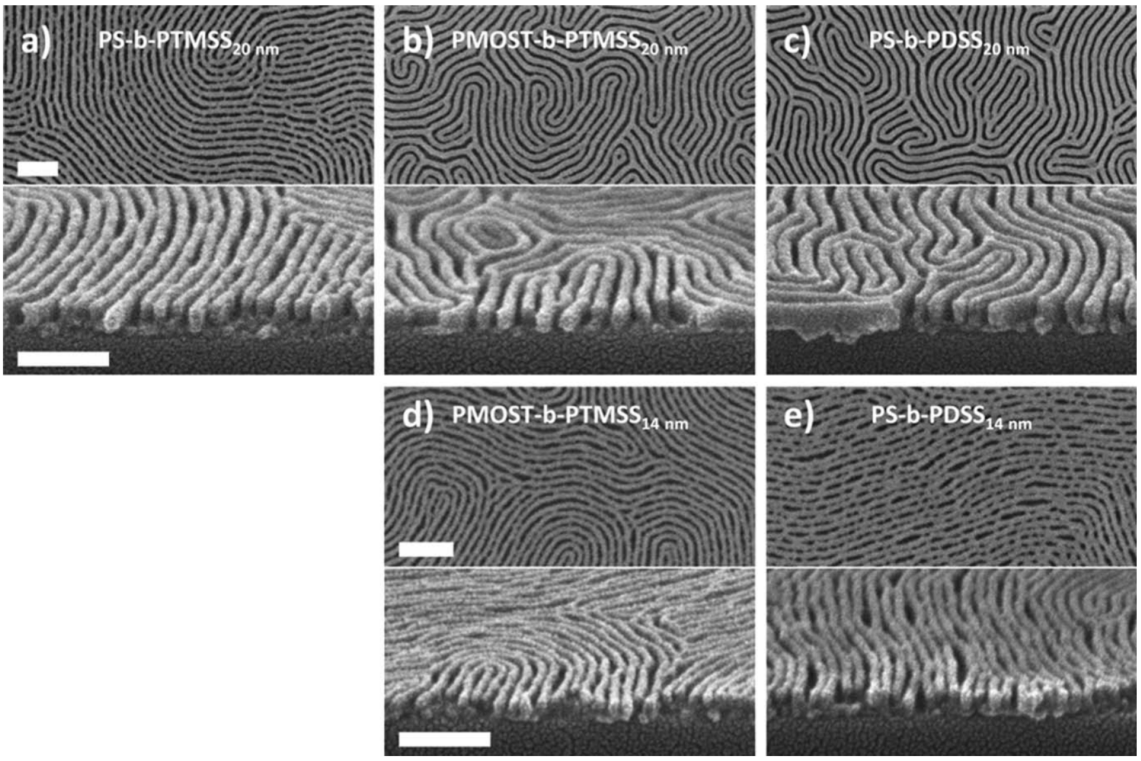

Figure 6.17: Top-down and angled SEM of **a)** PS-PTMSS$_{20\ nm}$, **b)** PMOST-PTMSS$_{20\ nm}$, **c)** PS-PDSS$_{20\ nm}$, **d)** PMOST-PTMSS$_{14\ nm}$, and **e)** PS-PDSS$_{14\ nm}$ after etching. As cast film thicknesses are ca. 1.75 L_0. Scale bars are all 100 nm and apply to each row of figures, respectively. Reproduced with permission from Durand et al. *J. Polym. Sci., Part A: Polym. Chem.*, **2015**, 53, 344-352. Copyright 2014 Wiley Periodicals.

Very recently, the highest χ block copolymer in the Willson and Ellison groups was oriented using the TC-S and XST interfaces. The block copolymer was poly(5-vinylbenzo[d][1,3]dioxole)-*block*-poly(pentamethyldisilylstyrene) (PVBD-PDSS). PVBD-PDSS with L_0 = 10 nm appears to form strongly segregated, crisp line/space patterns with high etch contrast (Figures 6.18 and 6.19). To the best of the author's knowledge, this is the smallest thermally annealed block copolymer sample in the world.

Well-defined line/space patterns with critical dimensions of 5 nm are expected to be pattern transferred in the near future.

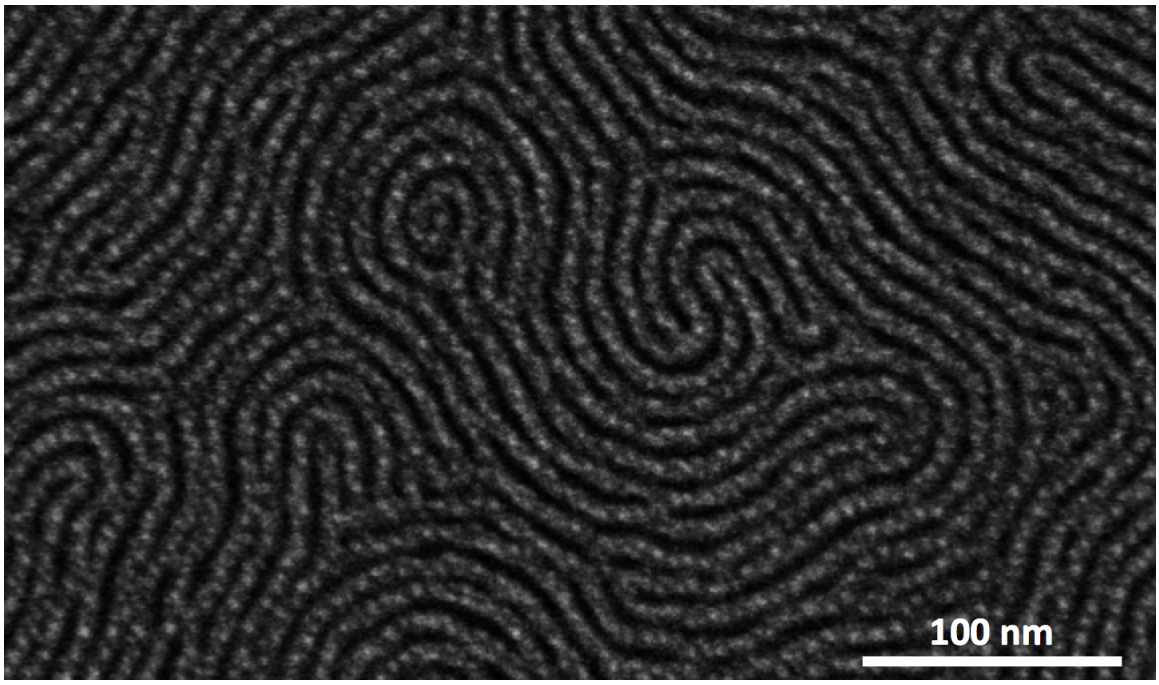

Figure 6.18: Orientation control of PVBD-PDSS. Sample was annealed at 190˚C for 1 minute.

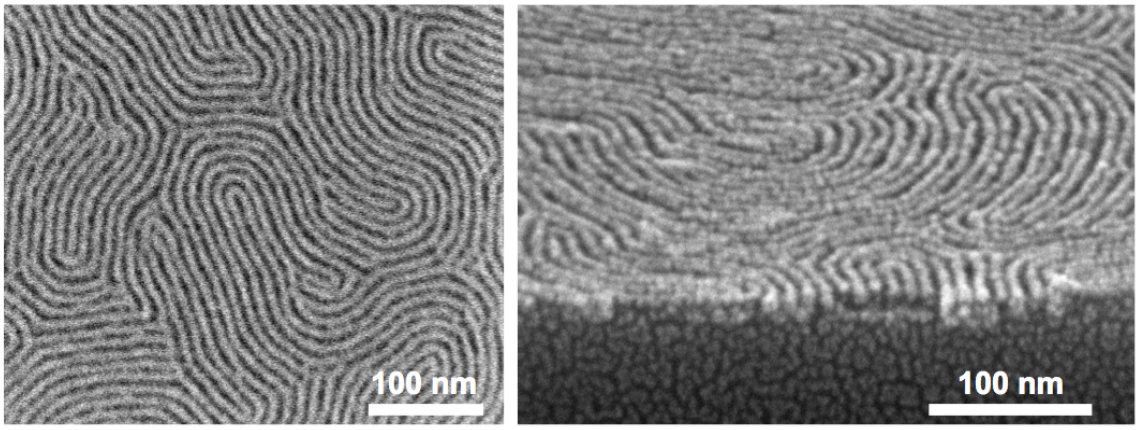

Figure 6.19: Top-down and angled SEM of PVBD-PDSS. Sample was annealed at 190˚C for 1 minute and etched prior to imaging.

6.9 CONCLUSIONS

New top coat design, coating, and optimization methods were introduced that facilitated the synthesis, application, and identification of neutral top coats for PS-PTMSS (L_0 = 18 and 22 nm) and PS-PTMSM (L_0 = 15 nm) thin films. Top coat composition, controlled via synthesis, determined interfacial wetting characteristics. The isolation of trimethylammonium top coat salts provided solubility in polar solvents and afforded high quality thin film coatings. Analysis of the topography formed by PS-PTMSS and PS-PTMSM films confined between a preferential substrate surface and a top coat reported (non-)preferential wetting at the top coat/block copolymer interface. Neutral top coats were readily synthesized and identified for both block copolymers. Perpendicular lamellae were quickly (≤ 60 sec) generated independent of block copolymer film thickness (1-3 L_0) at elevated temperatures when either block copolymer was confined between neutral top and bottom interfaces. A 1.68 L_0 PS-PTMSS sample formed perpendicular lamellae that penetrate the entire thickness of the thin film. The materials and methodologies introduced herein should greatly facilitate the orientation of high-χ block copolymers that are otherwise impossible to orient by thermal annealing alone. The orientation control of a 10 nm full pitch block copolymer with high etch contrast was demonstrated, which highlights the power of the orientation strategy.

6.10 EXPERIMENTAL

6.10.1 Instrumentation

Size exclusion chromatography (SEC) data for the top coats were collected on an Agilent 1200 Series Isopump and Autosampler with an Agilent Technologies 1100 RI

detector. One PLgel 5 μm, 100 Å column and one PLgel 5 μm, 1000 Å column were used with DMF as an eluent at 70°C and a flow rate of 1 mL/min. The refractive index response of the top coats was compared to polystyrene (PS) standards, which were used to calibrate the instrument by refractive index response (conventional calibration). Solid state IR spectra were recorded on a Nicolett 380 FT-IR diamond ATR. Thin film IR transmission spectra were collected on a Nicolet Avatar 360 FT-IR. A Brewer CEE 100CB Spincoater was used to coat all thin films. Ellipsometry was performed with a J.A. Woollam Co, Inc. VB 400 VASE Ellipsometer with wavelengths from 382 to 984 nm and a 65° angle of incidence. A Zeiss Supra 40 VP scanning electron microscope operating at 3 kV with the in-lens detector was used to collect all SEM data. Brightness and contrast for all SEMs were uniformly enhanced using commercial image editing software.

6.10.2 Reagents:

Maleic anhydride, N-methylmaleimide, and 50% aq. TMA, potassium *tert*-butoxide were purchased from Acros; styrene (99%), 4-*tert*-butylstyrene, magnesium, and azobisisobutyronitrile (AIBN) were purchased from Sigma-Aldrich. 3,5-Di-*tert*-butylbromobenzene was purchased from Combi-Blocks. All materials were used without further purification unless otherwise stated. AIBN was recrystallized from methanol. Magnesium turnings were successively washed with 1 M HCl, deionized water, acetone, and dried *in vacuo* before use. Test grade silicon wafers with ca. 1.5 nm native oxide were purchased from Addison Engineering. Methanol (HPLC grade) and dimethylformamide (DMF) were purchased from Fisher Scientific. Tetrahydrofuran (THF) was purchased from J.T. Baker.

6.10.3 Top Coat Monomer Synthesis

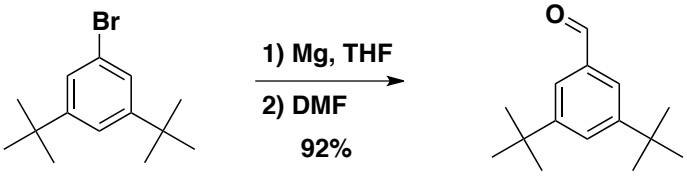

3,5-di-*tert*-butylbenzaldehyde. Acid-washed magnesium turnings (1.35 g, 55.7 mmol, 1.5 eq.) were added to a 3-neck flask equipped with a reflux condenser and magnetic stir bar. The vessel was flamed dried under vacuum and purged with dry argon. Dry THF (40 mL) was added and heated to reflux. A small amount of dibromoethane (0.05 mL) was added to the refluxing solvent. After 5 minutes, 1-bromo-3,5-di-*tert*-butylbenzene (10.0 g dissolved in 10 mL dry THF, 37.1 mmol, 1 eq.) was added to the solution dropwise over a 15 minute period. Vigorous boiling was observed. After complete addition, the mixture was refluxed for an additional 30 minutes. The reaction vessel was cooled to 0 ˚C in an ice bath, and dry DMF (5.4 g, 74.3 mmol, 2 eq.) was added dropwise. A white precipitate became visible during the addition. After complete addition of DMF, the solution was heated back to reflux for 20 minutes and subsequently poured into ice water. The mixture was filtered, and extracted with ethyl acetate (3x150 mL). The organic layers were combined and washed with equivolume amounts of water (2x) and brine (1x). The organic layer was dried over sodium sulfate, and the solvent was removed by rotary evaporation to yield the desired product as a white solid (7.65 g, 92%). M.P. 80-82°C. 81-^{1}H-NMR (400 MHz; $CDCl_3$): δ 10.01 (s, 1H), 7.73-7.71 (m, 3H), 1.36 (s, 18H). ^{13}C-NMR (101 MHz; $CDCl_3$): δ 193.32, 151.96, 136.33, 129.01, 124.27, 35.11, 31.32. HRMS (CI) m/z for $[M+H]^+$ calcd for $C_{15}H_{22}O$ 219.1749; found 219.1749.

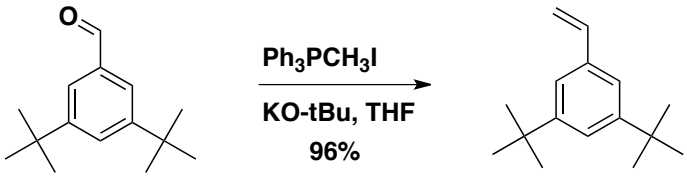

1,3-di-*tert*-butyl-5-vinylbenzene. Methyltriphenylphosphonium iodide (20.09 g, 49.5 mmol, 1.2 eq.) and potassium *tert*-butoxide (5.55 g, 49.5 mmol, 1.2 eq.) were added to a flame dried round bottom flask. Dry THF (100 mL) was added at room temperature and stirred to form a bright yellow slurry. The slurry was cooled to 0 ˚C in an ice bath. A solution of 3,5-di-*tert*-butylbenzaldehyde (9.00 g in 20 mL of THF, 41.2 mmol, 1 eq.) was added slowly over 5 minutes. The solution changed from yellow to pale white as the reaction proceeded forward. The reaction vessel was warmed to room temperature and monitored by thin layer chromatography. After 30 minutes, no starting material was present. The solution was filtered and the THF was removed via rotary evaporation to yield a viscous yellow-orange oil that was opaque. The oil was passed through a silica plug using pentane as the eluent. Removal of the pentane via rotary evaporation yielded the desired product as a clear and colorless oil (8.567 g, 96%). ^{1}H-NMR (400 MHz; $CDCl_3$): δ 7.41 (t, *J* = 1.8 Hz, 1H), 7.33 (d, *J* = 1.8 Hz, 2H), 6.79 (t, *J* = 8.8 Hz, 1H), 5.80 (dd, *J* = 17.6, 1.0 Hz, 1H), 5.27 (dd, *J* = 10.9, 1.0 Hz, 1H), 1.39 (s, 18H). ^{13}C-NMR (101 MHz; $CDCl_3$): δ 151.00, 137.96, 136.92, 122.30, 120.66, 113.23, 34.97, 31.61. HRMS (CI) m/z for $[M]^+$ calcd for $C_{16}H_{24}$ 216.1878; found 216.1875.

6.10.4 Top Coat Syntheses

TC-S Synthesis:

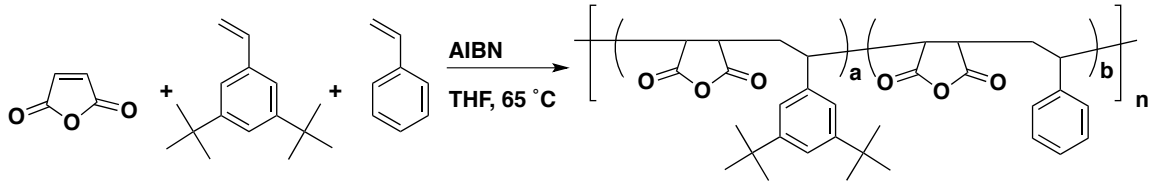

The following procedure was used for TC-S-6 but is representative of all TC-S top coat syntheses (TC-S-49 did not contain any styrene in the feed). Maleic anhydride (1.36 g, 13.9 mmol, 0.50 eq.), 3,5-di-*tert*-butylstyrene (0.333 g, 1.54 mmol, 0.05 eq.), styrene (1.30 g, 12.5 mmol, 0.45 eq.), and AIBN (0.045 g, 0.38 mmol, 0.01 eq.) were added to 100 mL 3-neck round bottom flask equipped with a condenser, stir bar, and 3 rubber septa. The contents of the flask were dissolved in 60 mL of uninhibited THF. Nitrogen was vigorously bubbled through the stirring solution for 30 minutes. The vessel was kept under positive nitrogen pressure and was immersed into an oil bath at 65 ˚C for 16 hours. The reaction was quenched at 0 ˚C, and the solvent was reduced *in vacuo* to yield a viscous liquid. The viscous liquid was precipitated into either 400 mL of methanol and filtered. The resulting polymer was dissolved in 20 mL of THF and reprecipitated into methanol two more times. The white solid was dried at 100 ˚C *in vacuo* overnight.

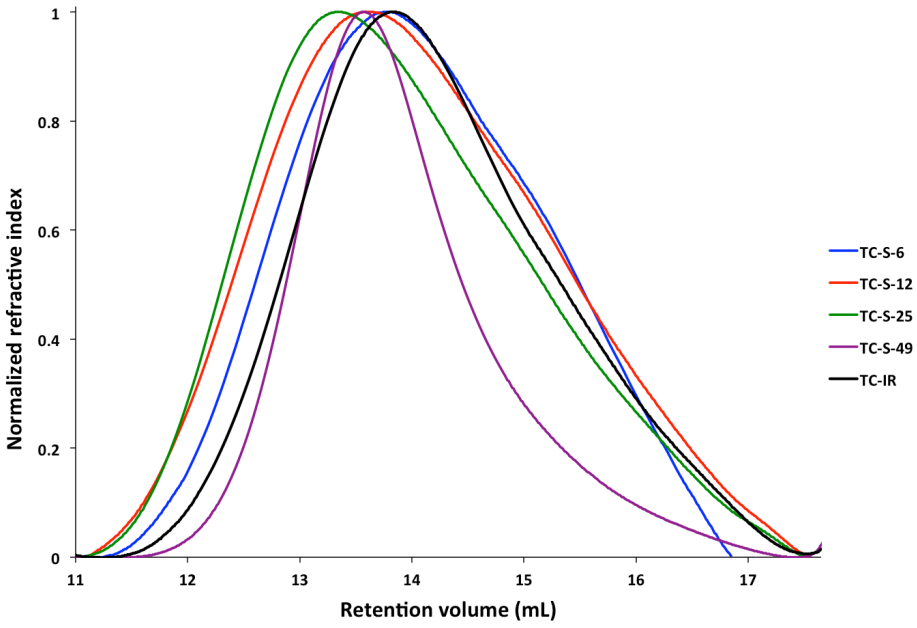

Figure 6.20: TC-S top coat SEC traces.

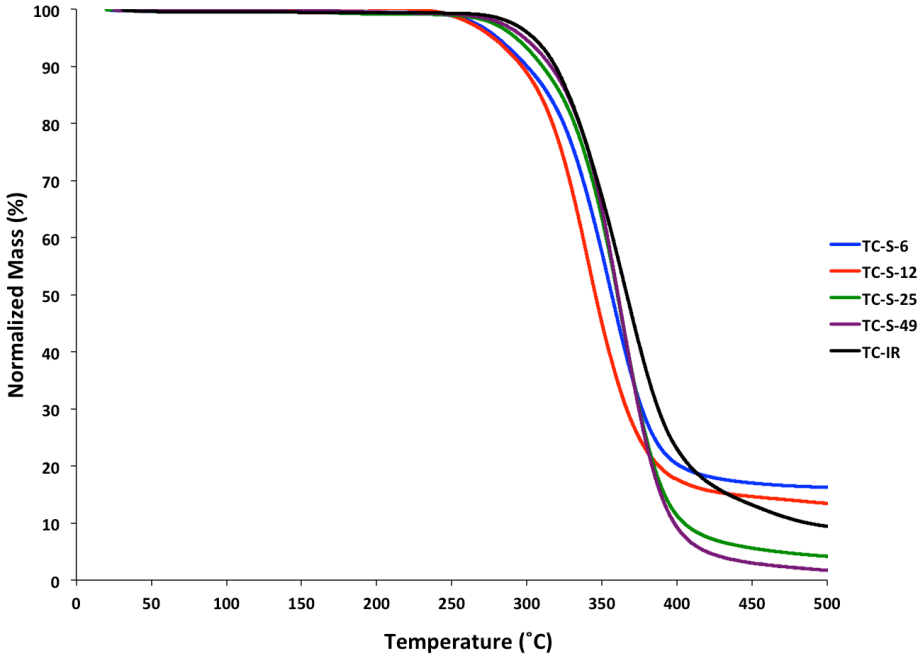

Figure 6.21: Thermal gravimetric analysis (TGA) of TC-S top coats and TC-IR heated from 25 ˚C to 500 ˚C at a rate of 10˚C/min.

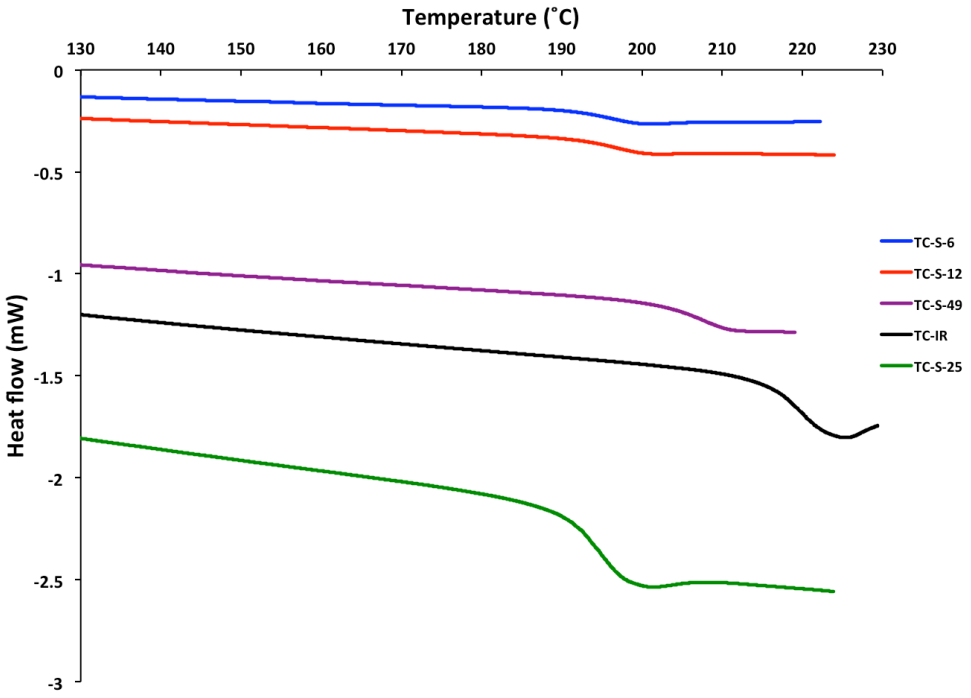

Figure 6.22: Differential scanning calorimetry (DSC) data for TC-S top coats and TC-IR. Samples were heated at a rate of 10 ˚C/min for 3 cycles. The heating leg of cycle 2 is shown in the graph.

TC-M Synthesis:

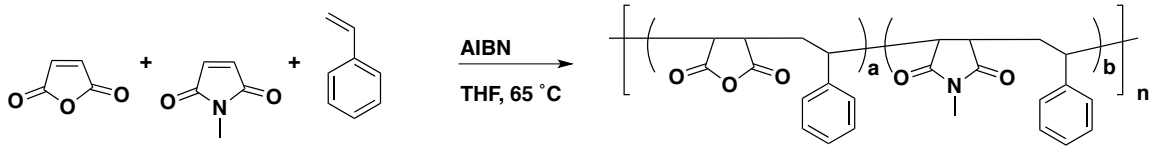

The following procedure was used for TC-M-31 but is representative of all TC-M top coat syntheses. Maleic anhydride (1.176 g, 12 mmol, 0.20 eq.), N-methylmaleimide (2 g, 18 mmol, 0.30 eq.), styrene (3.125 g, 30 mmol, 0.50 eq.), and AIBN (0.099 g, 0.60 mmol, 0.01 eq.) were added to 100 mL 3-neck round bottom flask equipped with a condenser, stir bar, and 3 rubber septa. The contents of the flask were dissolved in 60 mL of

uninhibited THF. Nitrogen was vigorously bubbled through the stirring solution for 30 minutes. The vessel was kept under positive nitrogen pressure and was immersed into an oil bath at 65 ˚C for 14 hours 30 min. The reaction was quenched at 0 ˚C and precipitated into 400 mL of 4:1 (by volume) hexanes:dichloromethane or methanol (depending on composition) and filtered. The resulting polymer was dissolved in 20 mL of THF and reprecipitated into methanol two more times. The white solid was dried at 100 ˚C *in vacuo* overnight.

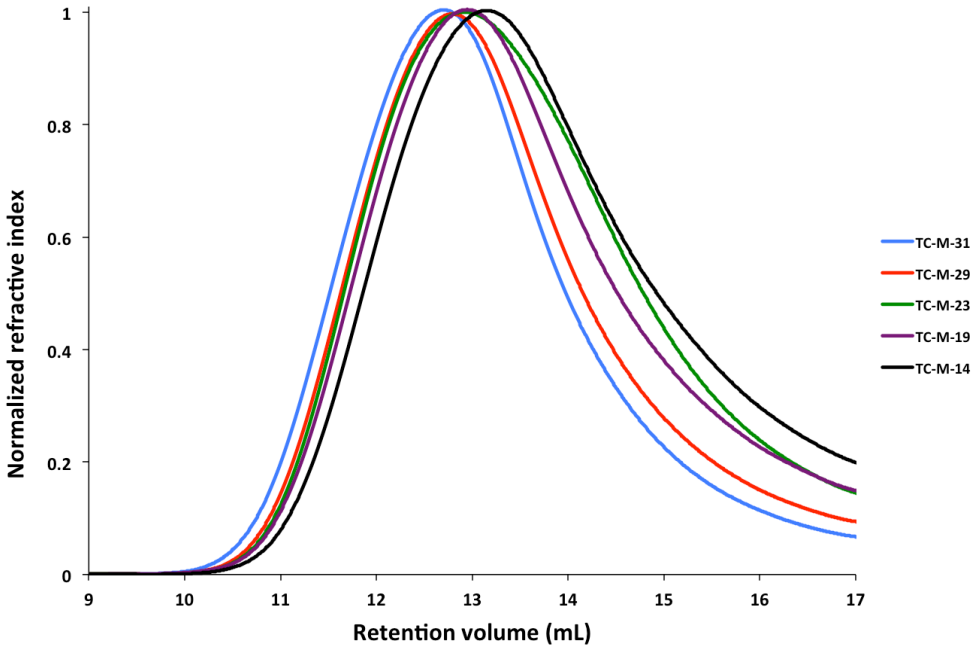

Figure 6.23: TC-M top coat SEC traces.

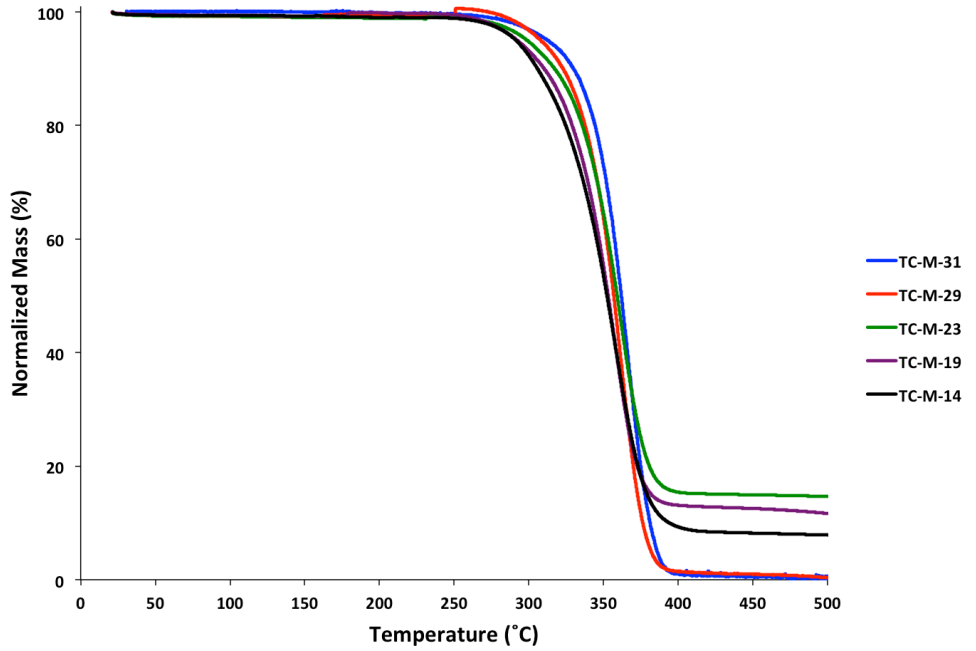

Figure 6.24: TGA of TC-M top coats heated from 25 ˚C to 500 ˚C at a rate of 10˚C/min.

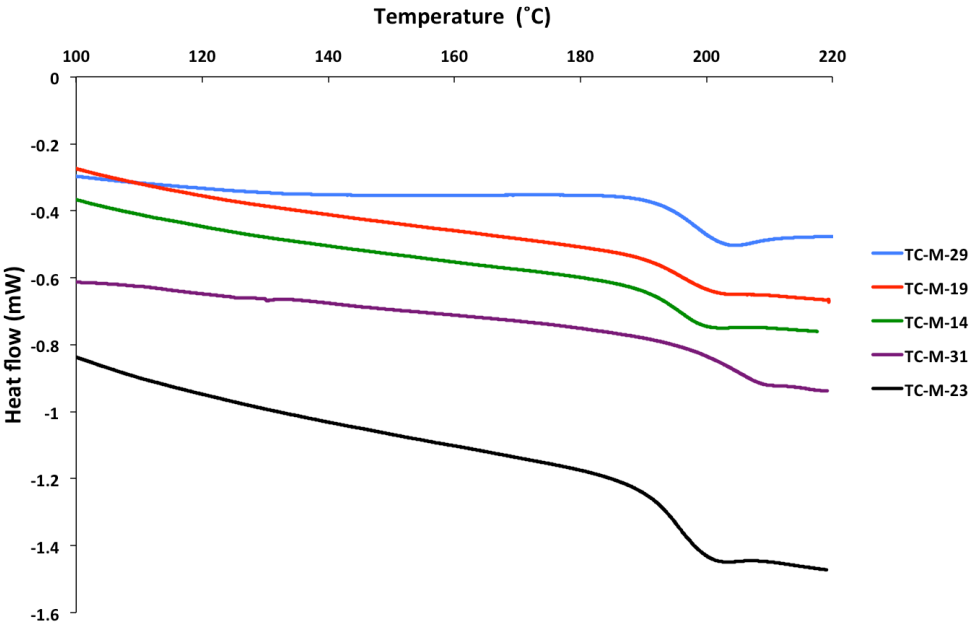

Figure 6.25: DSC data for TC-M top coats. Samples were heated at a rate of 10 ˚C/min for 3 cycles. The heating leg of cycle 2 is shown in the graph.

Low/High Conversion Study of TC-S and TC-M

Table 6.6: Summary of top coat compositions as a function of conversion for representative TC-S and TC-M top coats.

			Feed (mol%)			Actual (mol%)		
Top coat	**Batch**	**% Conversion**	**di-tBS or MA**	**MM**	**S**	**di-tBS or MA**	**MM**	**S**
TC-S	1	~10	50	30	20	46	32	22
	1	~90				49	29	22
	2	~90				50	33	17
TC-M	1	~10	25	25	50	22	28	50
	1	~90				27	27	46
	2	~90				25	29	46

*Abbreviations: MA = maleic anhydride, di-tBS = 3,5-di-*tert*-butylstyrene, MM = n-methylmaleimide

Synthesis of model top coat for IR (TC-S-IR)

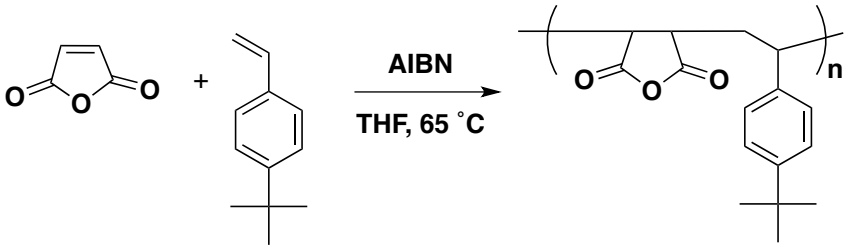

A three-neck round bottom flask fitted with a reflux condenser was charged with a stir bar, maleic anhydride (0.50 eq., 5.196g, 53.0 mmol), 4-*tert*-butylstyrene (0.50 eq., 8.642 g, 53.9 mmol), azoisobutyronitrile (0.01 eq., 174 mg, 1.05 mmol), and tetrahydrofuran (100 mL). The reaction mixture was degassed for 15 min with dry N_2 and heated at 65 °C for 24 hr. The reaction was quenched at 0 °C and precipitated into a 3:1 (by vol) mixture of hexanes:DCM. The polymer was isolated by vacuum filtration, redissolved in acetone and reprecipitated two more times into a 3:1 (by vol) mixture of hexanes:DCM. The white powder was dried *in vacuo* at 100 °C and the isolated yield was

24%. The polymer was analyzed by size exclusion chromatography (SEC), differential scanning calorimetry (DSC), thermal gravimetric analysis (TGA), infrared spectroscopy (IR), and combustion analysis. Composition: 52% maleic anhydride: 48% *tert*-butylstyrene. $T_g = 222^{\circ}C$.

6.10.5 TMA Salt Preparation

In a 10 mL scintillation vial, 1.5 g of polymer was added to circa 10 mL of 50% aqueous trimethylamine. The vial was sealed and stirred until the polymer was completely dissolved. Isolation of the salt was achieved in one of two ways, depending on the top coat composition. **NOTE: The second method is the current standard.**

1) Precipitation into THF or THF/pentane (4:1 by volume) solution. The solution of polymer in aq. TMA was slowly added to the precipitation solution. The precipitate was filtered and dried *in vacuo* at room temperature. Occasionally, the precipitate formed a sticky residue that stuck to the glassware. In this case, the solvent was decanted and the salt was dried with a gentle stream of air. The resulting solid was further dried *in vacuo* at room temperature.
2) Rotary evaporation. The solution of polymer in aq. TMA was diluted with 200 mL of THF and the solvent was removed *in vacuo*. This is the preferred process.

6.10.6 Thin Film IR Study

Thin film IR study procedure:

A 5 wt% solution of TC-IR in amyl acetate and 5 wt% of TC-IR TMA salt in methanol were prepared and filtered through a 0.20 μm filter. TC-IR was spin-coated from amyl acetate at 1500 rpm onto a double polished silicon wafer. The resulting film thickness was 162 nm as measured by ellipsometry. A transmission IR spectra was obtained and labeled "anhydride" (blue curve) in Figure 6.3. The TC-IR TMA salt was spin-coated onto a double polished silicon wafer at 1500 rpm to yield a 305 nm film as measured by ellipsometry. A transmission FT-IR spectra was obtained and labeled "TMA salt" (red curve). The wafer containing the film of TC-IR TMA salt was placed on a hot plate at 190 ˚C for 30 seconds and was immediately quenched to room temperature. A subsequent IR spectrum was obtained and labeled "190 ˚C, 30 sec" (green curve) in Figure 6.3.

6.10.7 Crosslinkable Monomer Synthesis

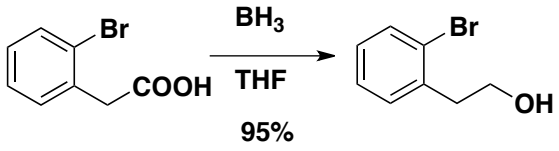

2-(2-bromophenyl)ethanol-A 2L 3-neck round bottom flask, equipped with a magnetic stir bar, condenser and addition funnel, was flame dried and purged with dry argon. To the vessel, 2-(2-bromophenyl)acetic acid (100 g, 465 mmol, 1 eq.) was added. The solid was dissolved in 300 mL of dry THF, and 600 mL of 1M borane (1.3 eq.) in THF was added dropwise over 4 hours. The solution was stirred overnight. The solution was then refluxed for 3 hours, cooled to room temperature, and quenched with 100 mL of water.

The THF was removed by rotary evaporation, and the solution was diluted to 500 mL with water. The aqueous phase was extracted with 200 mL of ethyl ether three times. The organic phases were combined and washed with equivolume amounts of water, sat. aq. $NaHCO_3$ (2x), and twice with brine. The ether was filtered through a short plug of silica, and the ether was removed via rotary evaporation to yield 2-(2-bromophenyl)ethanol (88 g, 95% yield) as a colorless oil. ^{1}H-NMR (400 MHz; $CDCl_3$): δ 7.55 (dd, *J* = 7.9, 1.0 Hz, 1H), 7.29-7.23 (m, 2H), 7.10 (ddd, *J* = 8.0, 6.7, 2.4 Hz, 1H), 3.87 (s, 2H), 3.05-3.01 (m, 2H), 7.55 (dd, *J* = 7.9, 1.0 Hz, 1H), 7.29-7.23 (m, 2H), 7.10 (ddd, *J* = 8.0, 6.7, 2.4 Hz, 1H), 3.88 (d, *J* = 13.4 Hz, 2H), 3.05-3.01 (m, 2H), 1.57-1.54 (m, 1H). ^{13}C-NMR (101 MHz; $CDCl_3$): δ 137.92, 133.10 , 131.41, 128.35, 127.60, 124.82, 62.21, 39.46. HRMS (CI) m/z for $[M-H]^-$ calcd for $C_8H_9O^{79}Br$ 198.9759; found 198.9760.

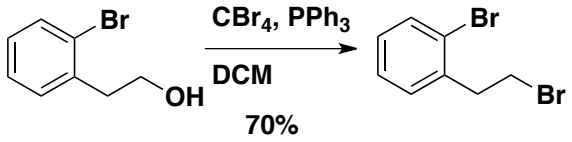

1-bromo-2-(2-bromoethyl)benzene- Under argon, 2-(2-bromophenyl)ethanol (23.0 g, 115 mmol ,1 eq.) was added to a round bottom flask equipped with a magnetic stir bar and was dissolved in 350 mL of dry dichloromethane. The resulting solution was cooled to 0 ˚C in an ice bath. Triphenylphosphine (30.0 g, 115 mmol , 1 eq.) was added to the solution. Carbon tetrabromide (38 g, 115 mmol, 1 eq.) was added portionwise to the solution, and the solution was warmed to room temperature and stirred overnight. The solvent was reduced by rotary evaporation, and the yellow oil was passed through a short plug of silica with DCM as the eluent. Removal of the solvent and purification via distillation yield the product as a clear and colorless oil (21.1 g, 70% yield). ^{1}H-NMR

(400 MHz; $CDCl_3$): δ 7.56 (dt, *J* = 7.8, 0.7 Hz, 1H), 7.29 (t, *J* = 0.8 Hz, 1H), 7.28 (d, *J* = 0.9 Hz, 1H), 7.16-7.12 (m, 1H), 3.60 (td, *J* = 7.6 Hz, 2H), 3.31 (t, *J* = 7.6 Hz, 2H). ^{13}C-NMR (101 MHz; $CDCl_3$): δ 138.20, 133.16, 131.30, 128.86, 127.68, 124.44, 39.71, 31.17. HRMS (CI) m/z for $[M]^+$ calcd for $C_8H_8{}^{79}Br_2$ 261.8993; found 261.8994.

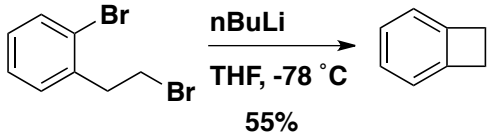

Bicyclo[4.2.0]octa-1,3,5-triene- In a 2 L flask equipped with a stir bar, 1-bromo-2-(2-bromoethyl)benzene (61.5 g, 233 mmol, 1 eq.) was dissolved in 760 mL of dry THF. The vessel was cooled to -78˚ C and 102 mL of n-butyllithium (2.5 M in hexanes, 1.1 equivalents) was added dropwise. The reaction vessel was warmed to room temperature over the course of 1 hour after complete addition of n-butyllithium. The reaction was quenched with 400 mL of water. The solution was extracted with ether (3x 250 mL), and the combined ether layers were dried over $MgSO_4$. The ether was removed via rotary evaporation and a pale yellow oil was obtained. Distillation was used to yield the desired product (b.p. 60˚C at 65 mmHg). All spectral data was identical to the reported literature values.

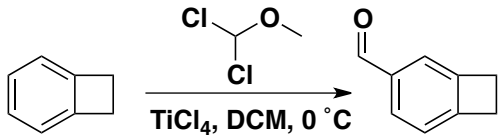

Bicyclo[4.2.0]octa-1,3,5-triene-3-carbaldehyde- In a flame dried round bottom flask equipped with a stir bar, benzocyclobutene (4.776 g, 45.8 mmol, 1 eq.) was dissolved in 60 mL of dry dichloromethane under argon. The reaction vessel was cooled to 0 ˚C in an

ice bath. Titanium tetrachloride (17.5 g, 91.9 mmol, 2 eq.) was added slowly over the course of 10 minutes. A solution of 1,1-dichloromethyl methyl ether (5.5 g in 12 mL of dry DCM, 47.8 mmol, 1.05 eq.) was added dropwise, and the reaction was stirred at 0 ˚C for 1.2 hours. The contents of the reaction vessel were poured over 100 mL of ice water and the product was extract with ethyl acetate (3x 100 mL). The combined organics were washed with water, brine, and dried over Na_2SO_4. Removal of the solvent yielded 5.2 g of crude product that was purified using flash chromatography (10% ethyl acetate/hexanes). The purified product was obtained as a slight yellow oil (2.95 g, 49%). ^{1}H-NMR (400 MHz; $CDCl_3$): δ 9.93 (d, *J* = 1.2 Hz, 1H), 7.72 (d, *J* = 7.5 Hz, 1H), 7.57 (s, 1H), 7.20 (d, *J* = 7.5 Hz, 1H), 3.25-3.21 (m, 4H).^{13}C-NMR (101 MHz; $CDCl_3$): δ 192.74, 153.97, 146.79, 135.88, 130.57, 123.09, 123.03, 30.16, 29.45. HRMS (CI) m/z for $[M]^+$ calcd for C_9H_8O 132.0575; found 132.0573.

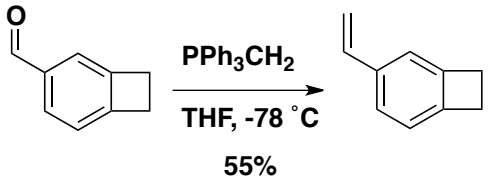

3-vinylbicyclo[4.2.0]octa-1,3,5-triene. In a flame dried round bottom flask equipped with a stir bar, triphenylphosphonium iodide (11.3 g, 27.8 mmol, 1.2 eq.) was added to 50 mL of dry THF. The slurry was cooled to -78 ˚C and 12.7 mL of n-butyllithium (2.5 M in hexanes, 1.2 eq.) was added dropwise. The slurry turned bright yellow, and was warmed to room temperature. The solution became dark orange after complete dissolution, and the reaction vessel was cooled back to -78 ˚C. Bicyclo[4.2.0]octa-1,3,5-triene-3-carbaldehyde (3.44 g, 23.2 mmol, 1 eq.) dissolved in 13 mL of dry THF and was added slowly to the solution. A gummy precipitate appeared during the addition. The reaction

was warmed to room temperature and stirred for 2 hours. The solution was filtered, and the solvent was removed via rotary evaporation. Then, the crude material was passed through a short column of silica and further purified by column chromatography (pentanes) to yield the product (1.88, 55% yield). ^{1}H-NMR (400 MHz; $CDCl_3$): δ 7.22 (dd, *J* = 7.6, 1.3 Hz, 1H), 7.16 (s, 1H), 7.01 (dd, *J* = 7.5, 0.8 Hz, 1H), 6.70 (dd, *J* = 17.6, 10.9 Hz, 1H), 5.67 (dd, *J* = 17.6, 1.0 Hz, 1H), 5.15 (dd, *J* = 10.9, 1.0 Hz, 1H), 3.17-3.16 (m, 4H). ^{13}C-NMR (101 MHz; $CDCl_3$): δ 146.18, 145.84, 137.93, 136.64, 125.70, 122.67, 119.92, 112.51, 29.60, 29.43. HRMS (CI) m/z for $[M]^+$ calcd for $C_{10}H_{10}$ 130.0783; 130.0783

6.10.8 Block copolymer synthesis

The synthesis of the PS-PTMSS has been reported in Chapter 2. PTMSM synthesis can be found elsewhere.[70] The block copolymer characterization data is listed below in Table 6.7. The periodicity was measured by small angle x-ray scattering. The molecular weight of the PS block and second block was measured by SEC and ^{1}H NMR, respectively. T_g and T_d were measured by DSC (TA Q100) and TGA (TA Q500).

Table 6.7: Block Copolymer Characterization Data

		PS Block			PTMSS / PTMSM Block		Block Copolymer		
Sample	**L_0**	**M_n [a]**	**Đ**	**T_g [b]**	**M_n [c]**	**T_g [b]**	**Đ**	**T_{ODT} [b]**	**T_d [b]**
PS-PTMSS	22	16.7	1.02	105	17.4	134	1.03	N/A	331
PS-PTMSS	17	14.8	1.04	105	14.2	135	1.04	190	337
PS-PTMSM	15	11.9	1.05	97	9.8	N/A	1.02	181	250

a: Units are kDa. Measured relative to PS standards in THF at 23°C
b: Reported in °C
c: Units are kDa. Measured by ^{1}H-NMR

6.10.9 XST Synthesis

The XSTs were synthesized and characterized as reported in Chapter 4.

6.11 Acknowledgements

The work in this chapter was due to a very collaborative effort in the Willson and Ellison groups. Dr. Christopher Bates contributed to top coat design and synthesis. Colin Hayes helped synthesize BCB for the XTCs. Dr. William Durand, Gregory Blachut, Dr. Julie Cushen, and Yusuke Asano contributed to the block copolymer design and synthesis. Matthew Carlson, Leon Dean, and Jeffrey Self helped synthesis neutral XSTs for the block copolymers in this chapter and helped with the thin film studies. Steve Sirard from Lam developed etch recipes and is responsible for Figure 6.12.

Chapter 7: Directed Self-Assembly

The work in this chapter has been reproduced in part with permission from Maher, M. J.; Rettner, C. T.; Bates, C. M.; Blachut, G.; Carlson, M. C.; Durand, W. J.; Ellison, C. J.; Sanders, D. P.; Sanders, D. P.; Cheng, J. Y.; Willson, C. G. "Directed Self-Assembly of Silicon-Containing Block Copolymer Thin Films." *ACS Appl. Mater. Interfaces* **2015**, *7*, 3323–3328 and Cushen, J.; Wan, L.; Blachut, G.; Maher, M. J.; Albrecht, T. R.; Ellison, C. J.; Willson, C. G.; Ruiz, R. "Double-Patterned Sidewall Directed Self-Assembly and Pattern Transfer of Sub-10 nm PTMSS-*b*-PMOST." *ACS Appl. Mater. Interfaces* **2015**, *7*, 13476–13483. Copyright 2015 American Chemical Society.

7.1 Background

Nanofabrication applications using block copolymer templates, such as bit patterned media for hard disk drives[127] and semiconductor device manufacturing, require establishing methods for patterning sub-10 nm features (e.g. lamellae or cylinders). This length scale is beyond the resolution limit of both photolithography and block copolymer self-assembly using poly(styrene-*block*-methyl methacrylate) (PS-PMMA). High-χ block copolymers (i.e. polymers with a large interaction parameter, χ) can form sub-10 nm domains,[128-131] but the low etch contrast of typical organic-organic block copolymers becomes a challenge as the dimensions approach 10 nm. Organic polymers that contain inorganic constituents, such as silicon,[44,46,73,132] are inherently etch resistant.[39] Hence, incorporation of one such block in high-χ block copolymers affords exceptional etch

contrast. However, the directed self-assembly (DSA) of lamella-forming, Si-containing block copolymers have not been studied in detail because the lower surface energy Si-containing block segregates to the top interface during thermal annealing and thereby drives a parallel orientation of the domains.[91] For patterning applications, a perpendicular orientation of the lamellae is required along with controlled lamella placement and alignment. In this chapter, orientation refers to the direction normal to the substrate interface and alignment refers to the direction relative to the plane of the film. Thermal annealing is preferred because it can rapidly orient the block copolymer domains and is compatible with existing industrial processes. Therefore, orientation and alignment control *via* thermal annealing is preferred for high-resolution patterning.

To various degrees of success, achieving the long-range order of block copolymer domains has been reported through use of in-plane electric fields,[18] heterogeneous surfaces,[19] temperature gradients,[20] topographic pre-patterns (grapho-epitaxy),[21,22] and chemical pre-patterns (chemo-epitaxy).[17,23,24] These latter two methods are the leading candidates for DSA because: 1) registration of the block copolymer domains with low placement error is possible,[133] 2) self-aligned customization can afford complex device-oriented patterns[29,134,135] of the sort required to produce fully-functioning Fin-FET devices,[25] and 3) both processes are compatible with 193 nm immersion lithography[136,137] and can be integrated with 300 mm state-of-the-art processes for high-volume manufacturing.[64,66,123,138]

Either chemo-epitaxy, grapho-epitaxy or a combination of both can be used to accomplish various patterning goals within the microelectronics industry. Each method

has certain advantages and disadvantages. Chemo-epitaxy has much stricter patterning requirements and relies on the ability to pattern chemical guide lines on the order of block copolymer periodicity, L_0. Typically, these guidelines are between 0.5-1.5 L_0. Patterning guide lines will be a major challenge as the block copolymer periodicity is reduced to sub-15 nm. Grapho-epitaxy has less strict patterning requirements than the chemo-epitaxy approach because it subdivides a larger patterned area. However, the physical pre-patterns occupy valuable space on the wafer, which makes chemo-epitaxy more attractive for certain applications.

The majority of DSA research and development has been done with PS-PMMA because the free surface (in air, nitrogen, or vacuum) is energetically neutral to the components of the block copolymer at elevated temperatures,[139] which enables the formation of perpendicular features when annealed on a neutral layer alone. PS-PMMA also has acceptable etch selectivity because the PMMA component is particularly sensitive to ion bombardment.[38] Unfortunately, PS-PMMA has a relatively small χ and can only form a minimum half-pitch of approx. 10-12 nm.[38] High-χ block copolymers that contain only organic components are unlikely to have the same intrinsic etch selectivity as PS-PMMA. Recently, Durand *et al*. introduced a family of silicon-containing block copolymers including poly(styrene-*block*-trimethylsilylstyrene) (PS-PTMSS), poly(styrene-*block*-pentamethyldisilylstyrene) (PS-PDSS), and poly(4-methoxystyrene-*block*-trimethylsilylstyrene) (PMOST-PTMSS) as candidates for lithographic applications.[49] These block copolymers can be oriented using top coats. They are highly etch resistant and can form features as small as 7 nm. The first DSA work on

this class of block copolymers is reported in this chapter using lamella-forming PS-PTMSS (L_0 = 22 nm) as a model. DSA was accomplished by combining well-established chemo- and grapho-epitaxy techniques in conjunction with top coats for orientation control. Hydrogen silsesquioxane (HSQ) was used to direct the self-assembly because it is a negative-tone e-beam resist compatible with sub-10 nm patterning[140] and has been previously used for both chemo[133,141]and grapho[25]-epitaxy of PS-PMMA. At the end of the chapter, the DSA using two high-χ silicon-containing polymers is reported.

7.2 CHEMO-EPITAXY

Chemo-epitaxy relies on chemical contrast in thin guidelines on the surface of a silicon wafer to direct self-assembly. Figure 7.1A illustrates the materials used in this chapter. Full characterization of these materials is reported in previous chapters and the literature.[70] Figure 7.11B shows the process flow used for the chemo-epitaxy approach. A polymeric surface treatment (XST) comprised of a random copolymer of 4-*tert*-butylstyrene, methyl methacrylate, and vinylbenzyl azide was thermally crosslinked on a substrate. HSQ was spin coated on the neutral surface, patterned using e-beam lithography, and developed to achieve lines of approx. 0.5 L_0 (11 nm) in width. In the figure, a 2 L_0 HSQ full pitch (0.5 L_0 HSQ line + 1.5 L_0 space) pattern is illustrated. The block copolymer was spin coated onto the chemically patterned surface, and the trimethylamine salt of a poly(4-*tert*-butylstyrene-*alt*-maleic anhydride) top coat (TC) was spin coated on top of the block copolymer using methanol, an orthogonal solvent.[70]

Thermal annealing induces a polarity switch in the TC, which produces a neutral top interface and facilitates the formation of perpendicular lamellae.[93] Interestingly, the HSQ lines have a higher affinity for the PS block than the PTMSS block, which causes the PS domains to segregate over the HSQ covered regions. This directing interaction induces the alignment of the PS domains and the adjacent domains overlaying the non-preferential region (XST region that is not covered by HSQ) of the substrate. After annealing, the TC was removed by washing with tetramethylammonium hydroxide (TMAH) developer. Finally, for inspection purposes, O_2 reactive ion etching was performed to selectively remove the PS domains, enabling observation of the line/space pattern by SEM.

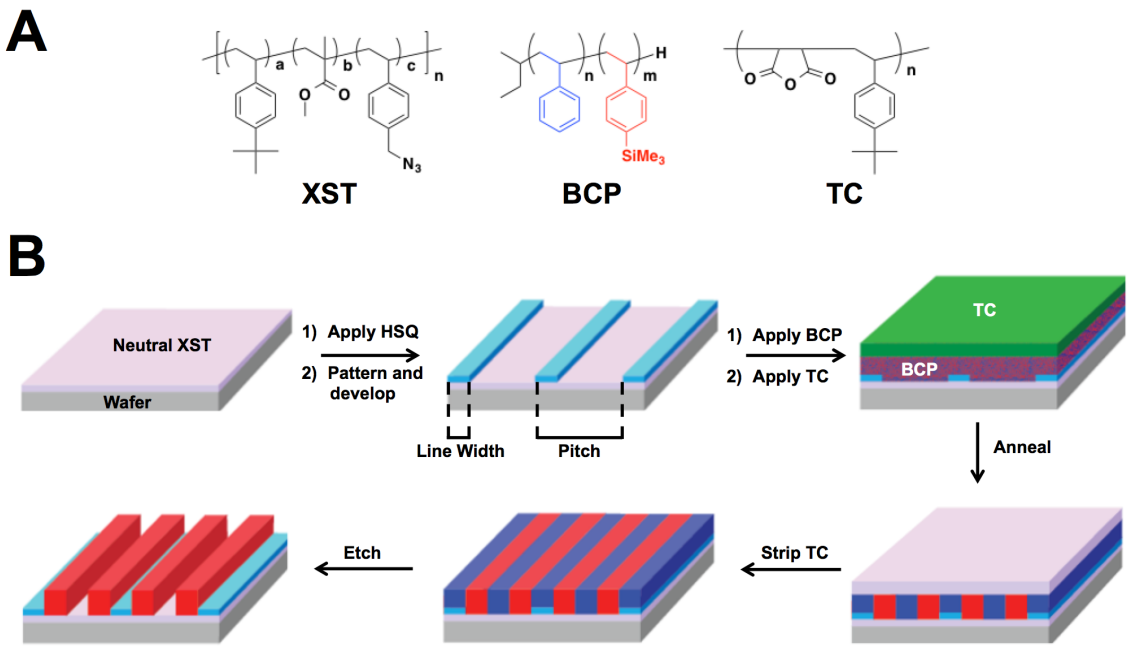

Figure 7.1: A) The materials used in the present study. B) Schematic of the chemo-epitaxy strategy using HSQ directing lines.

Three parameters were varied to optimize the DSA process shown in Figure 7.1B: HSQ line width, HSQ pitch, and the composition of the XST. It was found that integer (n) multiples of 22.5 nm (within 3% of L_0) successfully induced alignment. The range of HSQ line widths that successfully directed assembly was found to be between 10-12 nm (approx. 0.5 L_0). Additionally, the composition of the XST was varied, and a slightly off-neutral composition was found to minimize defectivity (Figure 7.2). There was unequal block coverage in the interstitial regions between HSQ guidelines. Since HSQ is preferential for the PS block, the interstitial region contained excess PTMSS block. Therefore, a slightly PTMSS preferential XST was chosen, which produced optimum alignment. This phenomenon has been reported in the chemo-epitaxy of PS-PMMA.[120]

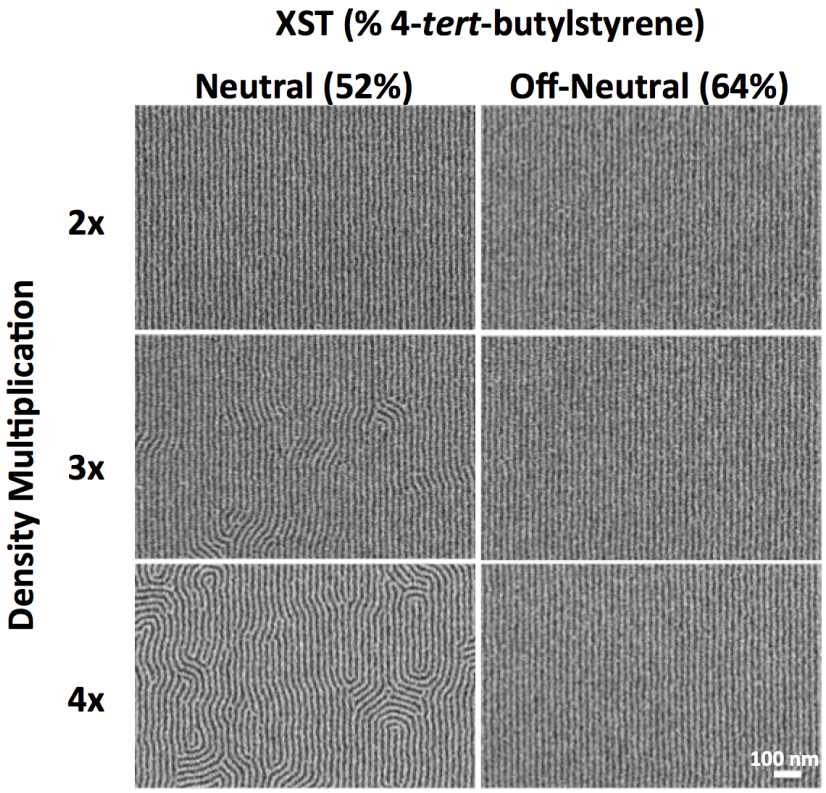

Figure 7.2: Comparison of chemo-epitaxy using a neutral and slightly off-neutral surface treatment. The block copolymer was approx. 22 nm thick, and the samples were annealed for 10 minutes at 190˚C. The scale bar is valid for all the micrographs.

Figure 7.3 (top row) shows the HSQ guidelines at various pitches corresponding to near-integer multiples of the block copolymer periodicity, L_0. The HSQ dimensions were measured in reference to the block copolymer periodicity and determined to be approx. 0.5 L_0 (10-12 nm, Table 7.1). The height of the HSQ lines was approximately 5 nm (Figure 7.4) as measured by atomic force microscopy (AFM). The as-cast thickness of the block copolymer layer was ca. 1 L_0 (22 nm) and the as-cast thickness of TC was ca. 20 nm. The samples were annealed at 190˚C in air for 10 minutes. Figure 7.3 (middle

row) shows the corresponding block copolymer domain pattern after the TC was removed using a TMAH-based developer and a subsequent oxygen etch. The block copolymer alignment is nearly perfect across the entire patterned area (3 μm by 4 μm) with density multiplications $\leq$ 4x. It is likely that the minor bridging observed between the block copolymer domains can be improved by optimization of the etch process. This hypothesis is supported by the excellent PS-PTMSS structures recently produced using advanced etch tools with highly optimized recipes.[70] At 5x and 6x density multiplications, the block copolymer alignment contained minor dislocations and disclinations, and the frequency of these defects scaled with the density multiplication. These defects are highlighted in the larger area images provided in Figures 7.5 and 7.6. The results are on par with chemo-epitaxy density multiplications reported elsewhere.[142,143]

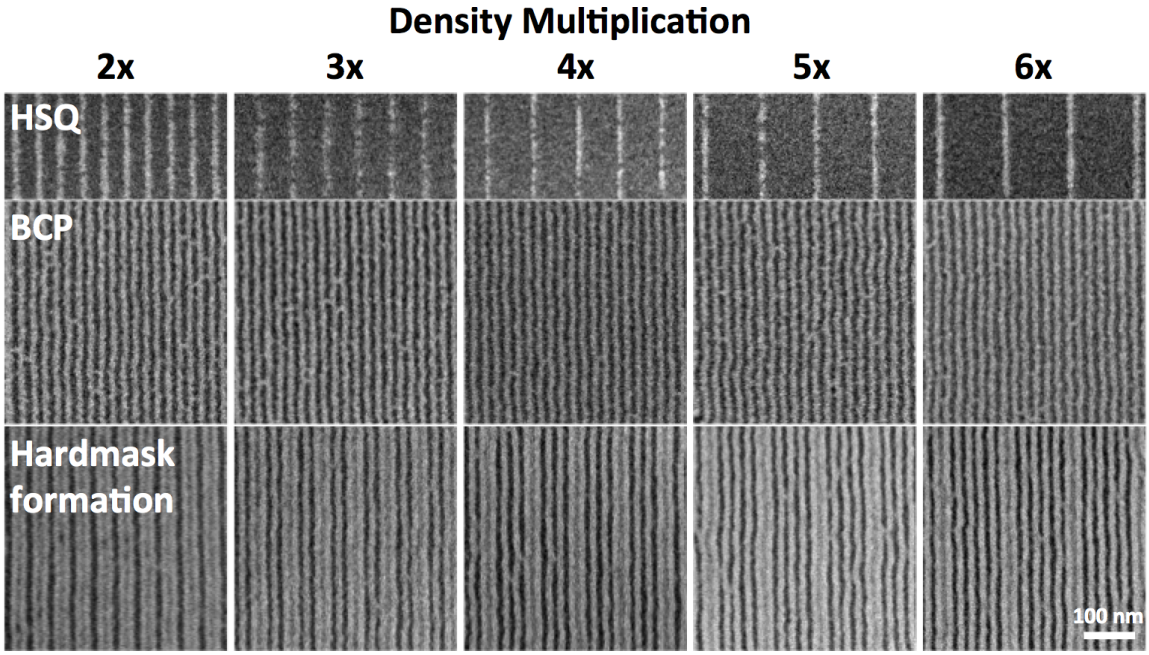

Figure 7.3: SEMs of HSQ guide lines (top), self-assembled block copolymer (middle), and hardmask after further etching (bottom). The block copolymer (thickness = 1 L_0, 22 nm) was annealed for 10 minutes at 190˚C. The scale bar is valid for all micrographs.

Table 7.1: Summary of HSQ features used for chemo-epitaxy.

Density Multiplication	HSQ Pitch (nm)	HSQ Line Width (nm)
2x	45	12.1
3x	67	11.3
4x	90	10.7
5x	115	12.0
6x	135	12.0

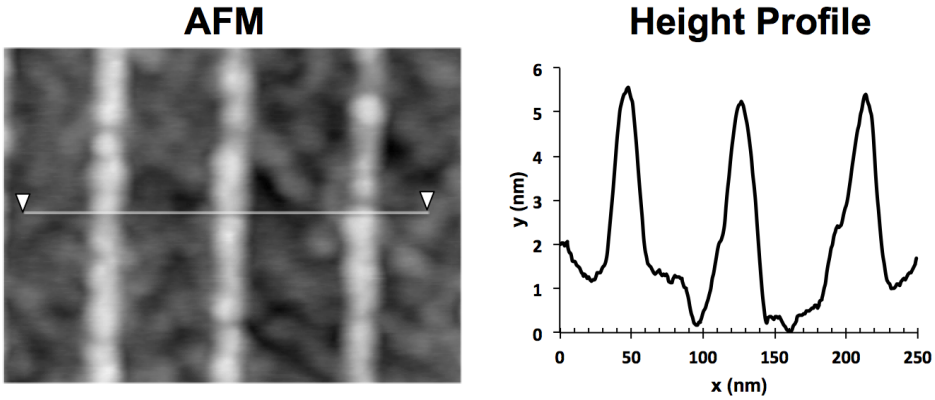

Figure 7.4: Representative atomic force micrograph of the HSQ guidelines produced for chemo-epitaxy.

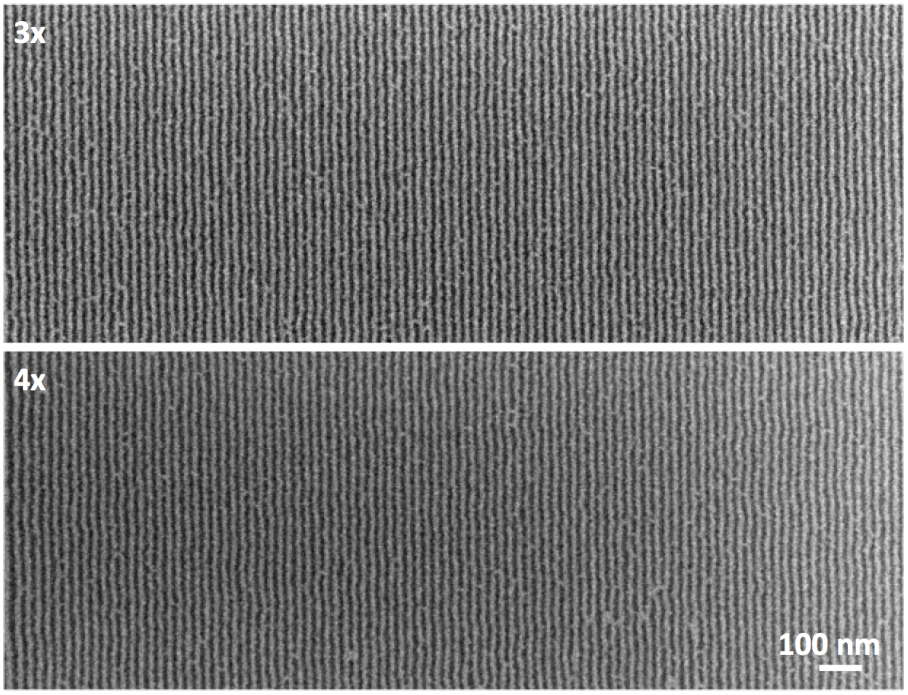

Figure 7.5: Larger view images of 3x-4x density multiplications for chemo-epitaxy. The scale bar is valid for all micrographs.

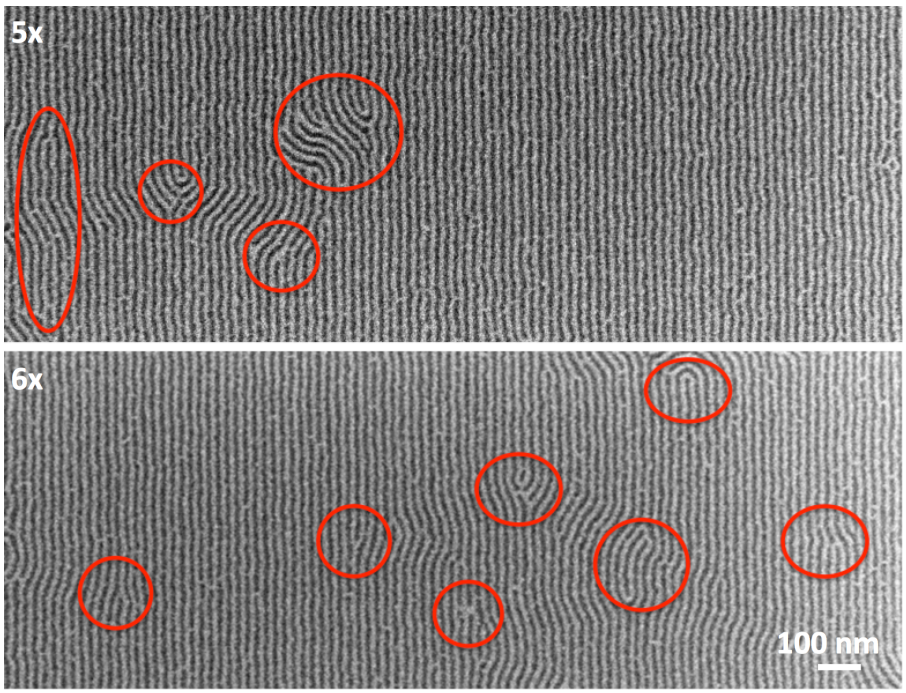

Figure 7.6: Larger view images of 5x-6x density multiplications for chemo-epitaxy. The scale bar is valid for all micrographs. The defects in the patterns have been highlighted.

Unlike previous efforts using HSQ-based chemical patterns to direct PS-PMMA,[133,141] it was not intuitively obvious which domain would be preferentially directed by the HSQ lines as neither the PS nor the PTMSS domains have polar or hydrogen bonding groups, which would strongly interact with the oxide-like HSQ lines. Figure 7.3 (bottom row) shows the hardmask after etching completely through the PS domain and the neutral layer. The most notable feature is the appearance of alternating lines that are either 11 nm or 33 nm wide. The 33 nm line arises from the apparent fusion of the HSQ and the two adjacent PTMSS domains (Both HSQ and PTMSS contain oxidized silicon after exposure to O_2 RIE). Since the PS block located on the HSQ is

removed, the exposed HSQ and two flanking PTMSS domains appear as a single "fused" domain as observed from the top-down. These data confirm that the HSQ has preferential affinity for the PS domains (which are less hydrophobic than the PTMSS domains). If PTMSS domains were aligned on top of the HSQ line, no 33 nm line would be observed, and Figure 7.3 (middle) and Figure 7.3 (bottom) would be identical.[133,134]

7.3 GRAPHO-EPITAXY

Grapho-epitaxy was also studied and demonstrated using trenches formed from HSQ. The process flow is outlined in Figure 7.7. Preparation of the samples was carried out in a manner similar to that desired for the chemo-epitaxy flow with several slight modifications. First, the XST was not purposefully skewed to favor the PTMSS block. Instead, a perfectly neutral XST was used (XST-52).[70] Second, a thicker layer of HSQ was used to form the physical pre-patterns. The result is a neutral surface bordered by PS preferential sidewalls. The trench subdivision is defined as the number of natural periods that span the width of the trench.

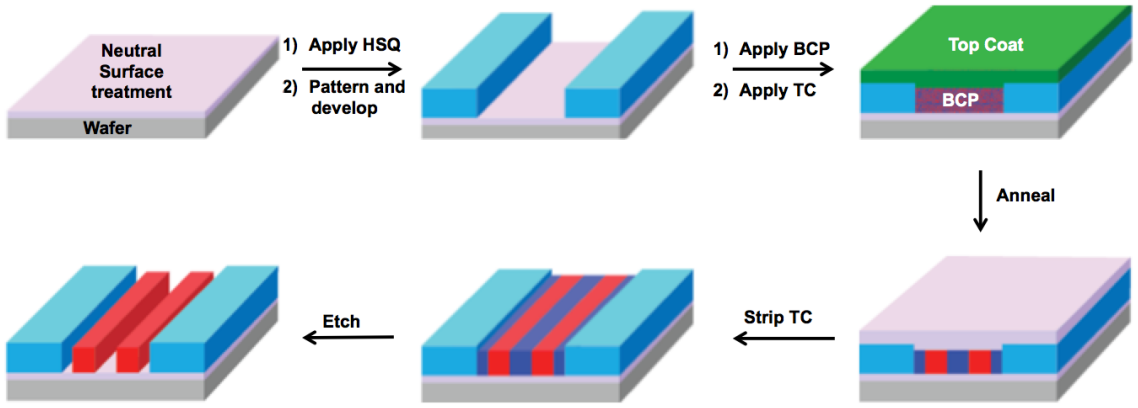

Figure 7.7: Schematic of the grapho-epitaxy flow using HSQ trenches

Figure 7.8 (top row) shows the physical trenches that were formed by patterning HSQ. The trenches are approximately 40 nm deep. Block copolymer was spin coated to partially fill the trench. Then, the sample was coated with top coat and annealed. The top coat was stripped, and the sample was etched. Figure 7.8 (bottom row) shows micrographs of 3x, 5x, and 7x DSA subdivision of HSQ trenches. In this example, the thickness of the block copolymer was approximately 25 nm (Figures 7.9 and 7.10). The DSA is nearly perfect with trench subdivisions ≤ 5x. At larger trench subdivisions, such as 7x, the system accommodates more defects, which have been highlighted in the larger area SEM images (Figure 7.11). Trenches that were commensurate in width (within approx. 5% of L_0, Table 7.2) to the natural periodicity were found to direct the alignment. Trenches incommensurate with the natural periodicity showed higher levels of defects and did not direct the alignment, which is in agreement with literature reports.[144]

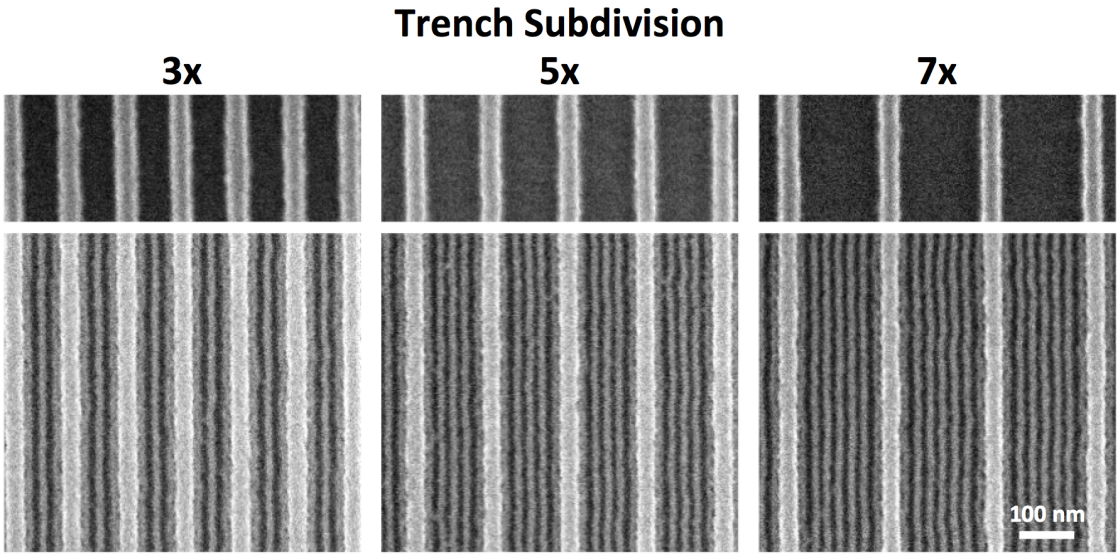

Figure 7.8: SEM micrographs of HSQ trenches (top) and grapho-epitaxy of the block copolymer (bottom). The scale bar is valid for all micrographs.

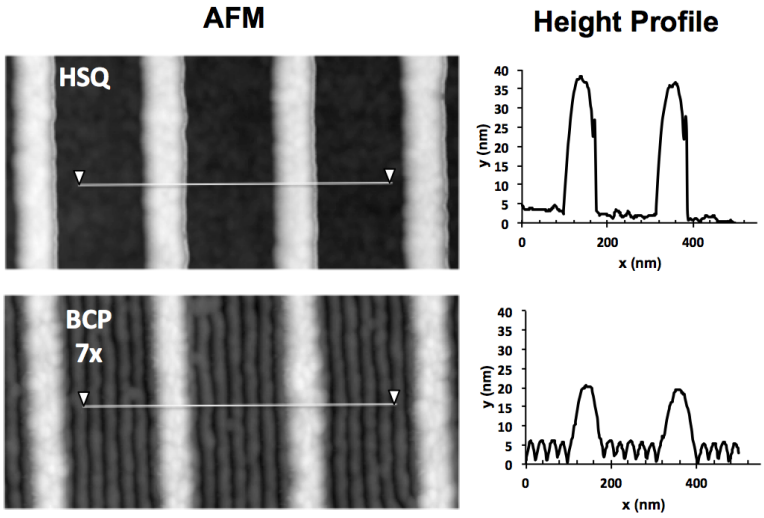

Figure 7.9: Atomic force micrograph of HSQ trenches (top) and corresponding grapho-epitaxy of block copolymer (bottom).

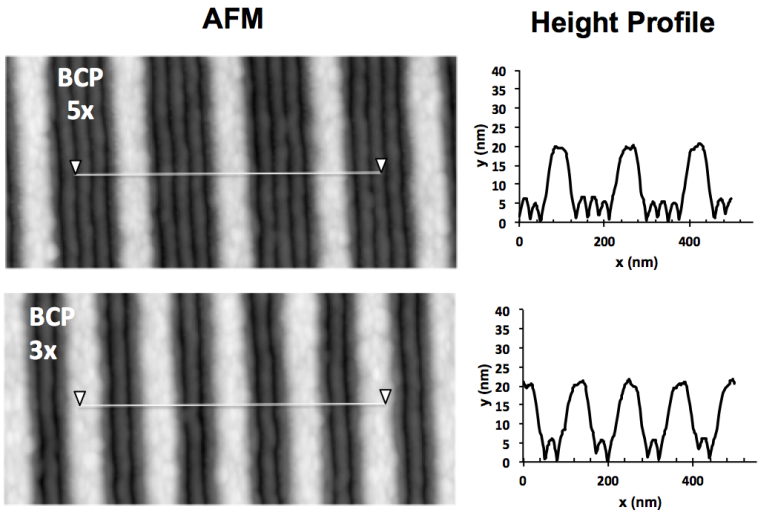

Figure 7.10: Atomic force micrographs of grapho-epitaxy with 5x (top) and 3x (bottom) density multiplications.

Table 7.2: Summary of HSQ grapho-epitaxy trenches. The L_0 of PS-PTMSS is 22 nm.

Density Multiplication	HSQ Pitch (nm)	Area between HSQ sidewalls (nm)
3x	110	69
5x	150	111
7x	195	151

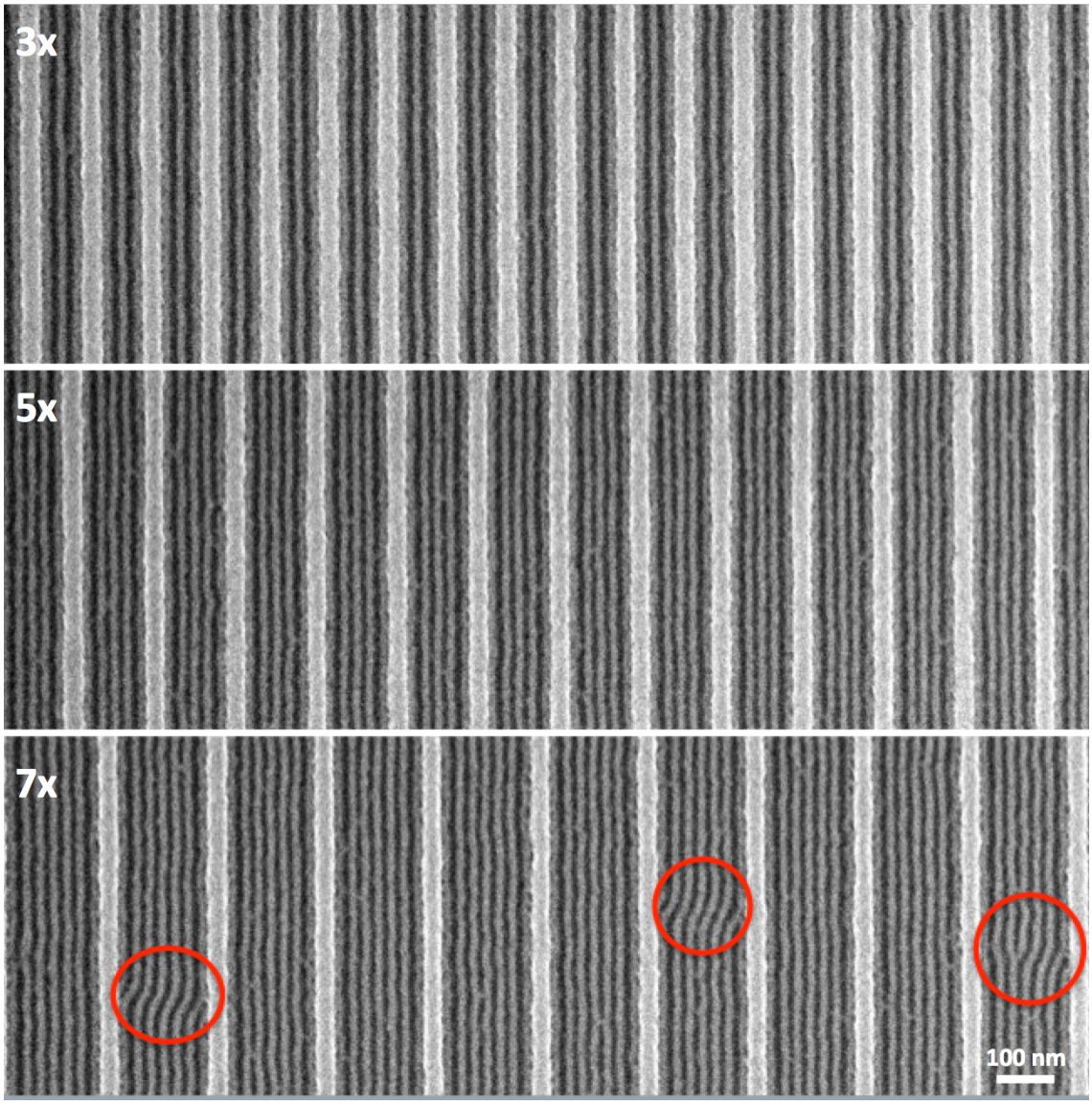

Figure 7.11: Large view images of grapho-epitaxy with density multiplications of 3x (top), 5x (middle) and 7x (bottom). The scale bar is valid for all the micrographs.

The DSA from the chemo-epitaxy and grapho-epitaxy are very similar. No qualitative differences were observed, which is important because it demonstrates that the class of block copolymers used herein is amenable to DSA *via* two leading techniques.

Although sections 7.2 and 7.3 provided evidence that the alignment of Si-containing block copolymers can be controlled, the overall patterning process is not scalable since it relies on e-beam patterning. Sections 7.4 and 7.5 discusses collaborations with HGST and Imec where efforts were focused on designing processes that are amenable to high volume manufacturing.

7.4 Side-wall DSA Collaboration with HGST

Up to this point, the grapho-epitaxy and chemo-epitaxy was demonstrated using PS-PTMSS, which has a relative low χ value. A collaboration with HGST and their DSA research team was initiated with the intention of achieving two goals: 1) demonstrate DSA of PMOST-PTMSS (higher χ than PS-PTMSS) and 2) generate imprint templates for bit patterned media. Using the materials synthesized at the University of Texas at Austin, HGST developed a new DSA strategy that uses chemically oxidized sidewalls for guiding self-assembly, which is shown in Figure 7.12a. First, crosslinkable polystyrene (X-PS) is crosslinked on a substrate. Then, a photoresist is patterned on top of X-PS using e-beam lithography. An oxidative etch is used to transfer the pattern down to the surface of the wafer. During the etch, the side walls of the X-PS mat are oxidized, which makes them *more* preferential to PMOST than unoxidized X-PS. The photoresist is stripped and a brush is grafted in the interstitial region. The brush was hydroxy-terminated PS brush (PS-OH), which is intermediate in surface energy between PMOST and PTMSS (but not neutral). This brush material reacts with the wafer surface, but it

does not graft to X-PS or the etched sidewall of X-PS. After grafting the brush in the interstitial regions, the block copolymer and top coat are spin coated. The sample is thermally annealed and the top coat is removed. A series of etch steps can be used to transfer the DSA pattern into the substrate.

The major distinguishing feature of the sidewall DSA process is that two interfaces with chemical contrast are created for every patterned line. In classical DSA schemes (Figure 7.12b), chemically patterned surfaces produced one line of chemical contrast per every patterned line. Figure 7.12c shows the chain orientation of the sidewall DSA process, which essentially combines shallow trench grapho-epitaxy with chemo-epitaxy. The consequence of this scheme is that the patterning dimensions are relaxed by a factor of two. In Section 7.2, the chemo-epitaxy guide lines needed to have a critical dimension on the order of 0.5 L_0. With the sidewall approach, the shallow trenches are 1 L_0 in critical dimension. As the L_0 of the target block copolymer scales below L_0 = 10 nm, physically patterning 0.5 L_0 guidelines becomes nearly impossible. However, patterning 1 L_0 guide lines remains feasible using e-beam lithography. Furthermore, the sidewall guiding DSA scheme is not limited to a 1:1 patterning scheme as shown in Figure 7.12a. Recent calculations show that up 8x density multiplications may be possible.[145]

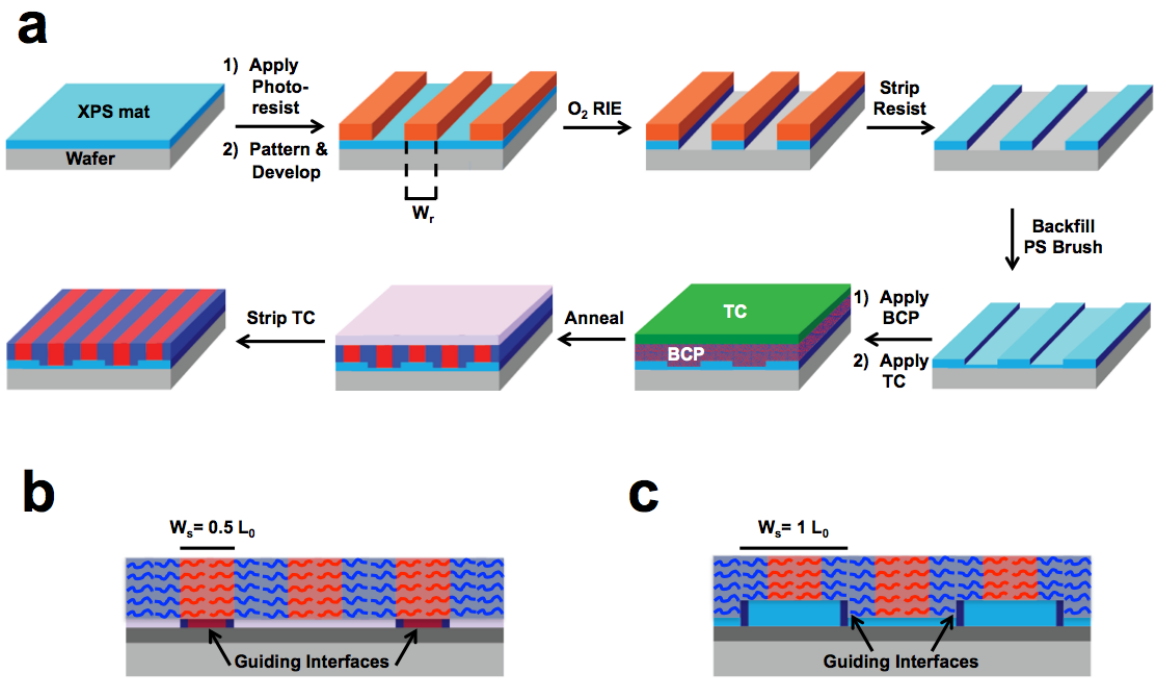

Figure 7.12: a) Process flow for creating the mat lines with oxidized sidewalls that serve as guiding interfaces and block copolymer self-assembly. b) The orientation of individual polymer chains in the LiNe flow. c) The orientation of individual polymer chains in sidewall guiding DSA flow.

The process in Figure 7.12a was carried out using PMOST-PTMSS (L_0 = 20 nm). A silicon substrate coated with 17 nm of diamond-like carbon (DLC) and 8 nm of X-PS. E-beam resist (ZEP) was deposited on top of X-PS and was patterned using a rotary e-beam tool. The exposed patterns consisted of line/space arrays with a pitch of 2 L_0. The domains of PMOST-PTMSS were aligned by thermal annealing with a top coat, and the line pattern was transferred into the underlying silicon substrate through a series of RIE steps.[146] First, the resulting pattern was transferred into DLC using an oxidative etch. Then, the pattern was transferred in the silicon substrate using a CHF_3/CF_4 etch process.

A final oxidative etch step was performed to remove any residual DLC on top of the silicon features. The final result of the pattern-transferred image is shown in Figure 7.13. Overall, the quality of the image transfer is very high, and in particular, the line edge roughness is very low despite using unoptimized conditions. The process used non-neutral X-PS and PS-OH. Future experiments were aimed at using neutral materials, which are anticipated to result in fewer defects.[145] Unfortunately, HGST cancelled their DSA program, and no further experiments were performed to optimize the process.

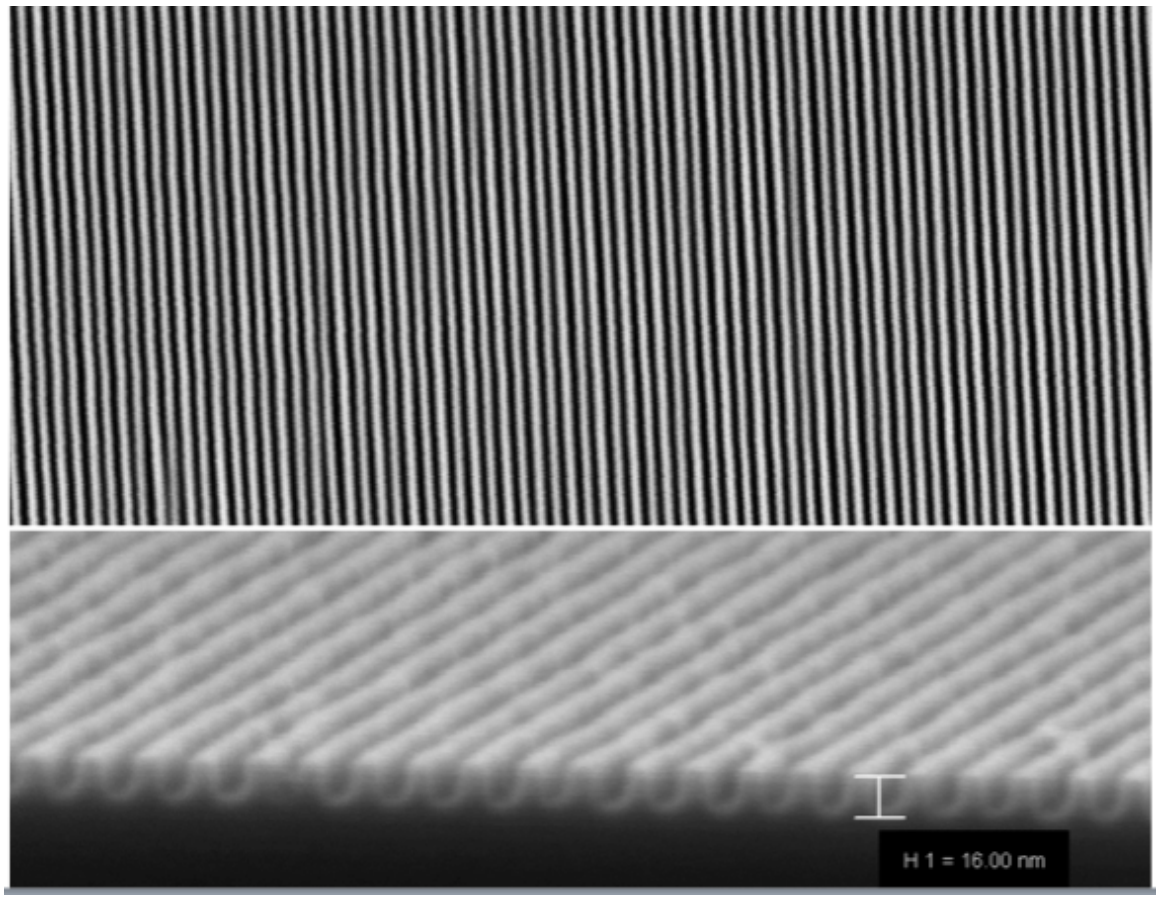

Figure 7.13: Pattern transferred images of PMOST-PTMSS in a silicon substrate. The pitch of the line/space pattern is 19.9 nm.

7.5 COLLABORATION WITH IMEC

Shortly after the first DSA attempts were demonstrated, a student in the Willson and Ellison Groups, Gregory Blachut, had a unique opportunity to spend time at Imec, which is a major microelectronics research center in Leuven, Belgium. His goal was to apply the orientation strategy developed at the University of Texas at Austin with the DSA strategy (LiNe process) developed by Paul Nealey's group and IMEC.[64] Access to research at IMEC is a key step towards taking block copolymers from "lab to fab." All of Blachut's work was performed on 300 mm wafers using processes amenable to high volume manufacturing. The DSA strategy shown in Figure 7.14. The only difference is that Blachut used crosslinkable poly(4-methoxystyrene) (XPMOST) as the "mat" and controlled the orientation with a top coat.

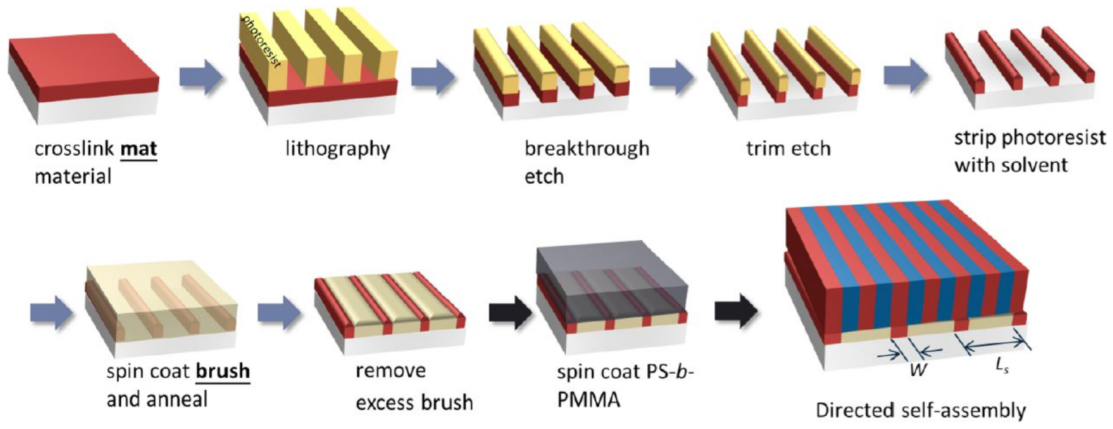

Figure 7.14: LiNe process used at IMEC for the DSA of PS-PMMA. Reprinted with permission from Liu et al. *Macromolecules* **2013**, 46, 1415-1424. Copyright 2013 American Chemical Society.

The materials that were used at Imec are summarized in Figure 7.15. One of the best DSA results is shown in Figure 7.16. The XPMOST guide line was 0.8 L_0 and the pitch of the guidelines was approximately 4 L_0. The sample was annealed at 205˚C for 5 minutes prior to etching. The DSA looks very promising. However, there are still too many defects for full scale manufacturing. The DSA process is complex and relies on the interplay of many variables including the guideline chemistry, backfill brush chemistry, guideline height, etc. Recent results from Imec show that the DSA mechanism is not fully understood and that the cartoon representations are highly oversimplified.[69] Future work is aimed at understanding how the block copolymer interacts with the guideline and interstitial region to create DSA patterns with no defects.

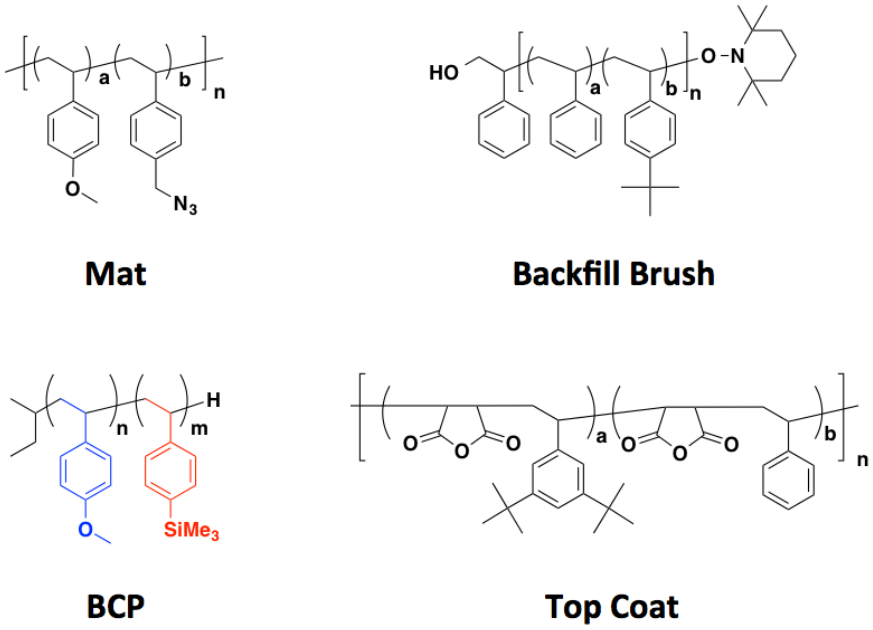

Figure 7.15: Summary of materials used at Imec for these experiments.

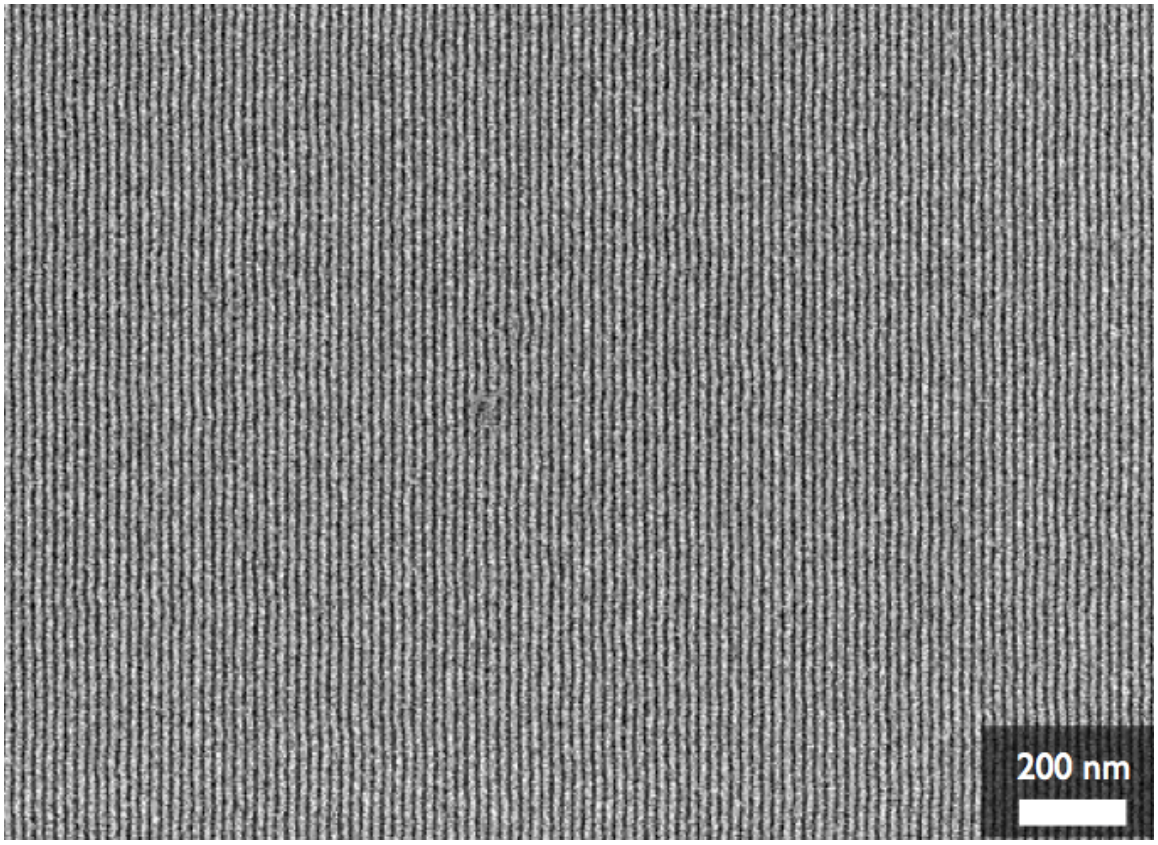

Figure 7.16: One of the best DSA results at Imec. The guideline width was 0.8 L_0 and the pitch was 80 nm. The sample was annealed at 205˚C for 5 min.

7.6 CONCLUSIONS

Chemo- and grapho-epitaxy of perpendicularly oriented lamellae of PS-PTMSS were demonstrated using chemical contrast from HSQ. This resulted in density multiplications and trench subdivision up to 6x and 7x, respectively. The DSA of a higher χ block copolymer, PMOST-PTMSS, was demonstrated using the "LiNe" process at Imec and a sidewall guiding process at HGST. The orientation control afforded by tailored top and bottom interfaces in conjunction with DSA schemes provides a satisfying

demonstration that silicon-containing block copolymers are amenable to DSA processes and can go beyond the resolution limits of PS-PMMA. Full integration of high-resolution patterning using PMOST-PTMSS is currently under investigation at Imec. The author hopes that extension of the underlying patterning methods to next-generation technology nodes will be facilitated by the principles, materials, and techniques described within this chapter.

7.7 EXPERIMENTAL

7.7.1 Instrumentation

Electron beam patterns were generated with a Vistec/Leica VB6 electron beam lithography tool running at 100 kV and using a beam current of 0.25 nA. XSTs and block copolymers were spin coated using a Brewer Cee spin coater. TCs were spin coated on a Headway Model PWM32 spin coater. Thin film thickness measurements were made on a NanoSpec 6100. Samples were annealed on a PMC Dataplate 732 series hot plate. Samples were etched using a Plasma-Therm Versaline. Atomic force micrographs were taken on a Bruker 3100 with Bruker OTESPA tips. Scanning electron micrographs were taken on a Leo 1550 using an accelerating voltage of 10 kV. Brightness and contrast on all SEMs were uniformly enhanced using commercial image editing software.

7.7.2 Reagents and Materials

Toluene, MIBK, and methanol were purchased from Sigma-Aldrich. Test-grade silicon wafers (100) were purchased from Silicon Quest International. All reagents were used without further purification unless stated. Full experimental procedures and characterization for the cross-linkable surface treatment (XST-64 and XST-52), PS-PTMSS (PS-PSTMSS, 22 nm) and top coat (TC-IR) can be found elsewhere.[70] The parentheses reflect the name of the material in the previous report. HSQ resist (2% XR-1541, a Dow Corning product) was purchased from MinoriTech Inc.

7.7.3 Reactive Ion Etching

The etching reported in Figure 7.3 and Figure 7.8 was performed using the following recipe: pressure= 6 mTorr, Rf1 power = 20 W, Rf2 power = 100 W, O_2 flow rate = 20 scmm, temperature = 20˚C.

7.7.4 Sample Preparation for Chemo-epitaxy

XST-64 was spin coated (0.5 wt% in toluene, 2000 rpm, 5000 rpm/s) to obtain a film ca. 20 nm in thickness. The sample was crosslinked by annealing at 250˚C for 5 minutes open to air. The sample was rinsed thoroughly with PGMEA. HSQ resist (2% XR-1541) was first diluted by mixing with methyl isobutyl ketone (MIBK) in a ratio of 1 part HSQ to 3.5 parts MIBK, spun at 5000 rpm and baked at 130˚C for 3 mins. This resist

was written with doses in the range 2000-6000 μC/cm^2 and developed in 0.26 N aqueous tetramethylammonium hydroxide solution for 40s. The HSQ lines were analyzed using AFM and SEM. Block copolymer was spin coated (0.75 wt% in MIBK, 2000 rpm, 5000 rpm/s) on the patterned substrate to yield a film thickness of approx. 22 nm (1 L_0). The trimethylammonium salt of the top coat was spin coated (0.6 wt% in methanol, 2500 rpm, 5000 rpm/s) directly onto the block copolymer film. The sample was annealed in air at 190˚C for 10 minutes, rapidly quenched to room temperature, and the top coat was then removed by placing in a solution of 3 parts 0.26 N TMAH and 1 part isopropyl alcohol for 1 minute. The sample was rinsed with deionized water and dried with a gentle stream of nitrogen. Figure 7.3 (middle row) was produced after etching the sample for 8 seconds using the etch conditions described above. Figure 7.3 (bottom) was produced after etching the sample for 16 seconds using the etch conditions described above.

7.7.5 Sample Preparation for Grapho-epitaxy

XST-52 was spin coated (0.5 wt% in toluene, 2000 rpm, 5000 rpm/s) to obtain a film ca. 20 nm in thickness. The sample was crosslinked by annealing at 250˚C for 5 minutes open to air. The sample was rinsed thoroughly with PGMEA. HSQ resist (2% XR-1541) was used without dilution, spun at 5000 rpm, and baked at 130˚C for 3 mins. This resist was written with doses in the range 2000-3000 μC/cm^2 and developed in 0.26 N aqueous tetramethylammonium hydroxide solution for 40 s. The sample was rinsed with deionized water and dried with a gentle stream of nitrogen. Block copolymer was

spin coated (0.75 wt% in MIBK, 2000 rpm, 5000 rpm/s) on the patterned substrate. The TMA salt of the top coat was spin coated (0.6 wt% in methanol, 2500 rpm, 5000 rpm/s) directly onto the block copolymer film. The sample was annealed, open to air, at 190˚C for 10 minutes, rapidly quenched to room temperature, and the top coat was removed by placing in a solution of 3 parts 0.26 N TMAH and 1 part isopropyl alcohol for 1 minute. The sample was rinsed with deionized water and dried with a gentle stream of nitrogen. The sample was etched for 8 seconds using the etch conditions described in the instrumentation section.

7.7.6 Sidewall DSA Preparation

The guiding lines used in the chemical patterns were written by an Elionix rotary e-beam tool on 50 nm ZEP resist which was coated on 8 nm crosslinked polystyrene mat provided by AZ materials. The mat had been cross-linked by heating to 290ºC for 2 hours on top of a 17 nm thick layer of diamond-like carbon (DLC) on a silicon substrate. After writing the circumferential line pattern on the resist, developing it, and etching the exposed areas to the DLC with an O_2 RIE, hydroxyl-functionalized polystyrene from Polymer Source with a molecular weight of 1.2 kDa was grafted to the oxidized DLC at 200ºC for 30 minutes. PMOST-PTMSS characterization data can be found in a report that used the same materials.[13] The block copolymer materials were annealed beneath a spin-coatable top coat using a procedure developed previously. The block copolymers were spin cast on chemical contrast patterns from 1 wt% solutions in MIBK at various spin

speeds to control film thickness. Approximately 30 nm thick top coats were spin coated from methanol. Samples were then annealed at 200ºC for 1.5 minutes on a hot plate in air. Top coats were removed by rinsing the sample with a 5:1 methanol:40% trimethylamine solution in water solution and then subsequently rinsed thoroughly with methanol. RIE was performed using a Plasma herm tool. SEM images were collected on a Zeiss Supra SEM.

7.7.7 Brush Initiator Characterization

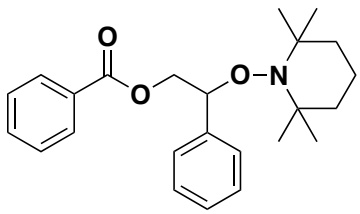

2-phenyl-2-((2,2,6,6-tetramethylpiperidin-1-yl)oxy)ethyl benzoate: The procedure used for this monomer was found in the literature.[147] The crude product was passed through a plug of silica using dichloromethane as the solvent. The solvent was removed by rotary evaporation and the monomer crystalized over time. Recrystallization was not performed. MP: 68-71°C. ^{1}H-NMR (400 MHz; $CDCl_3$): δ 7.93-7.91 (m, 2H), 7.57-7.27 (m, 8 H), 5.06 (dd, *J* = 6.2, 5.1 Hz, 1H), 4.82 (dd, *J* = 11.2, 5.0 Hz, 1H), 4.52 (dd, *J* = 11.2, 6.3 Hz, 1H), 1.58-0.99 (m, 18H). HRMS (ESI) m/z $[M+H]^+$ calcd for $C_{24}H_{31}NO_3$ 382.2377; found 382.2376.

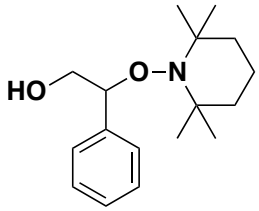

2-phenyl-2-((2,2,6,6-tetramethylpiperidin-1-yl)oxy)ethan-1-ol: The procedure reported in the literature was used.[148] The crude product was used without further purification. ^{1}H-NMR (400 MHz; $CDCl_3$): δ 7.39-7.27 (m, 5H), 5.91-5.87 (b, 1H), 5.32-5.28 (m, 1H), 4.22 (dd, *J* = 12.2, 9.6 Hz, 1H), 3.72 (dd, *J* = 12.2, 2.7 Hz, 1H), 1.6-1.11 (m, 18H). HRMS (ESI) m/z $[M+H]^+$ calcd for $C_{17}H_{27}NO_2$ 278.2115; found 278.2113.

7.7.8 Brush Synthesis

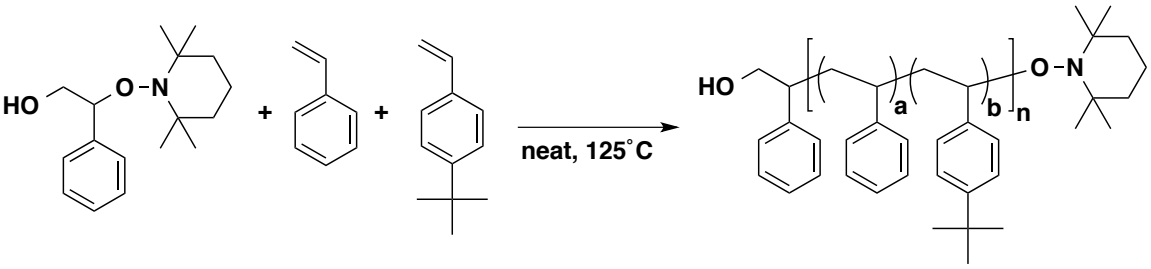

This procedure is representative of that used for the hydroxyl terminated brushes. Inhibitor was removed from all monomers with basic alumina. A round bottom flask equipped with a condenser was charged with a stir bar, the NMP initiator (0.38 g, 1.66 mmol, 1 eq.), styrene (8.30 g, 8.30 mmol, 47.9 eq.) and 4-*tert*-butylstyrene (25.49 g, 147.9 mmol, 88.3 eq.). The solution was degassed by sparging with nitrogen for 30 minutes. The degassed solution was then placed in an oil bath and stirred at 125˚C. After 18.6 hrs, the reaction vessel was quenched to 0˚C. The polymer solidified upon cooling. Approximately 150 g of THF was added to dissolve the polymer. Precipitation two times in 1200 mL of methanol resulted in a fine white powder. The polymer was dried at 60˚C under vacuum overnight. The mass of the recovered polymer was 19.6 g (57%).

Table 7.3: Brush feed ratio and molecular weights

	Feed Ratios (mol%)		Molecular Weight (kDa)**		
Entry	**S***	**t-BS***	**M_n***	**M_w***	**Đ**
1	27.7	72.3	17.6	21.7	1.23
2	35	65	16.26	20.6	1.27
3	42	58	17.2	21.4	1.24
4	50.6	49.4	18.6	23	1.24
5	60	40	15.3	18.8	1.23
6	69.6	30.4	16.9	19.6	1.16
7	75	25	16.7	19.9	1.19
8	80	20	15.9	18.7	1.18
9	86	14	16.9	19.6	1.16

*Abbreviations: S = Styrene, t-BS = 4-*tert*-butylstyrene
**Molecular weights are relative to PS standards in THF

7.8 ACKNOWLEDGEMENTS

The DSA of PS-PTMSS was performed at the IBM Almaden Research Center. Dr. Dan Sanders, Dr. Joy Cheng, and Dr. Charles Rettner contributed to the DSA portions. Dr. Jane Frommer helped with AFM. Elizabeth Lofano helped capture SEMs. Amy Bowers helped etch the samples. Dr. Julie Cushen and Dr. Ricardo Ruiz performed the DSA of PMOST-PTMSS at HGST. Gregory Blachut performed the DSA work at imec in collaboration with Dr. Roel Gronheid.

Chapter 8: Photopatternable Interfaces

The material reported in this chapter has been reproduced in part with permission from Maher, M. J.; Bates, C. M.; Blachut, G.; Carlson, M. C.; Self, J. L.; Janes, D. W.; Lane, A. P.; Ellison, C. J.; Willson, C. G. "Photopatternable Interfaces for Block Copolymer Lithography." *ACS Macro Lett*. **2014**, 824–828. Copyright 2014 American Chemical Society.[149] Portions of Section 8.6 have been reproduced with permission from Lane, A. P.; Maher, M. J.; Willson, C. G.; Ellison, C. J. "Photopatterning of Block Copolymer Thin Films." *ACS Macro Lett*, **2016**, *5*, 460-465. Copyright 2016 American Chemical Society.

8.1 Background

Advanced microelectronic architectures require complex custom patterns. For example, bit patterned media needs rectangular bits and distinct servo regions[150] while semiconductors require isolated and discontinuous line/space arrays. These patterns can be produced using DSA in tandem with other processing steps, such as multiple block copolymer layers,[151] cut masks,[33] imprint lithography,[32,37] and/or select pattern transfer blocking.[152] Blocking pattern transfer is appealing because it can potentially be achieved using parallel and perpendicular block copolymer domains within the same film. Achieving control over both perpendicular and parallel domains within the same film has been most commonly explored by altering the surface chemistry at the substrate interface to create select areas of neutral and preferential regions.[153-155] The perpendicular domains only appear in the areas where the block is confined by neutral interfaces. Parallel features, which cannot be pattern transferred, appear only in the preferential regions.[53]

Photopatternable interfaces in which the chemistry can be changed using light are attractive because they can be transformed in an area selected manner. The author is aware of only three papers detailing directly patternable orientation layers: one is based on inherently electron-beam sensitive materials,[155] a process that lacks scalability due to notoriously slow e-beam patterning rates, and a second that is based on self-assembled monolayers,[62] which undergo ill-defined changes in surface chemistry upon exposure to X-rays. A third photo-patternable polymer system captures some of the principles embodied in the system reported herein but does not definitively establish preferential interfacial (or non-preferential) interactions or demonstrate two-dimensional orientation control in a single layer.[156] A material and process that precisely tunes block copolymer interactions using traditional lithographic practices (*e.g.* a high throughput and economical process based on optical exposure sources) would therefore be a valuable addition to lithography by directed self-assembly (DSA).[24]

In this chapter, photo-patternable interfaces are introduced. These materials change surface chemistry upon exposure to light in either one of two ways; 1) an inherently neutral surface can be rendered preferential by exposure (herein denoted "N2P"), or 2) a preferential surface can be made neutral by exposure ("P2N"). Poly(styrene-*block*-4-trimethylsilylstyrene) (PS-PTMSS, L_0 = 22 nm) is used as a model block copolymer to demonstrate the principles found in this chapter.

8.2 Material Design

These photo-patternable orientation layers follow a previously reported design,[70] and are terpolymers composed of maleic anhydride, 4-*tert*-butoxystyrene, and 3,5-di-*tert*-butylstyrene formulated with a photo-acid generator (PAG). Maleic anhydride forms

alternating copolymers with styrenic derivatives,[117] and the relative ratio of the two styrene derivatives in the terpolymers determines the nature of the interfacial interactions with a block copolymer.[70] Incorporation of PAG allows for direct photo-patterning of these materials because exposure generates a latent image and subsequent heating induces the acid catalyzed thermolysis of 4-*tert*-butoxystyrene to generate isobutylene and a more polar phenol (Scheme 8.1).[157]

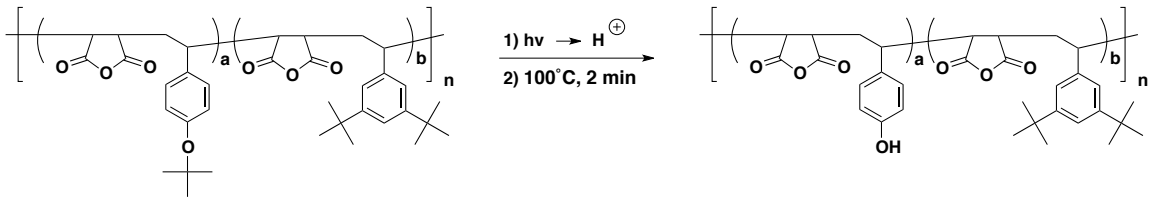

Scheme 8.1: Acid-catalyzed deprotection of the materials used as GSTs and TCs.

Up to this point, all of the maleic anhydride-containing polymers have been used as top coats. However, the top coats can also function as grafted surface treatments (GSTs). Covalent bonding can be accomplished by nucleophilic acyl substitution reactions between the maleic anhydride and amine functionalized surfaces,[158] which enables these photo-patternable materials to function both as top coats and GSTs. The grafting procedure is shown below in Figure 8.1. First, a wafer can be amine-functionalized by silylating with (3-aminopropyl)triethoxysilane (APTES). Then, the GST is spin coated onto amine-functionalized wafer and annealed for 1-5 minutes at 180°C. After annealing, excess, ungrafted material can be removed by rinsing the wafer with solvent. For these GSTs, the average remaining film is only 3-5 nm thick.

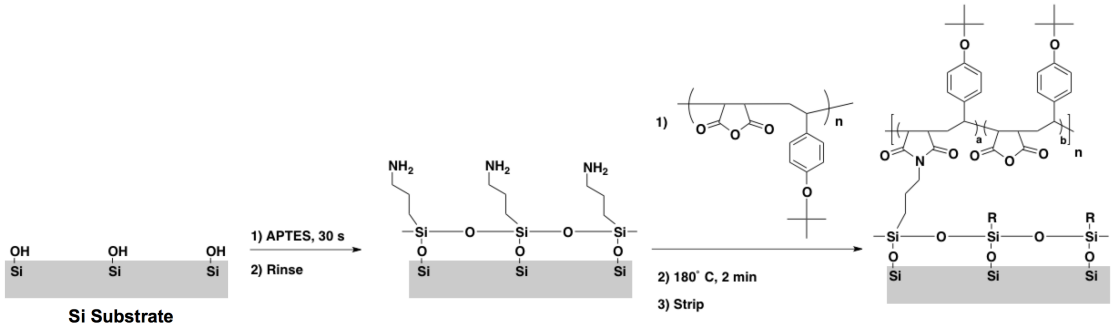

Figure 8.1: Illustration of the grafting procedure.

8.3 SURFACE IDENTIFICATION

8.3.1 Neutral to Preferential (N2P)

The island/hole test that was discussed in Chapter 4 was used to identify a neutral GST, which will be referred to as GST-N. The results of the island/hole test are shown in Figure 8.2. The block copolymer was annealed at various film thicknesses (L_{avg}), and the resulting topography was analyzed by optical and atomic force microscopy (AFM). The 0.5 L_0 topography that forms is characteristic of a neutral surface.[115] The composition of GST-N is 49% 4-*tert*-butoxystyrene and 51% maleic anhydride.

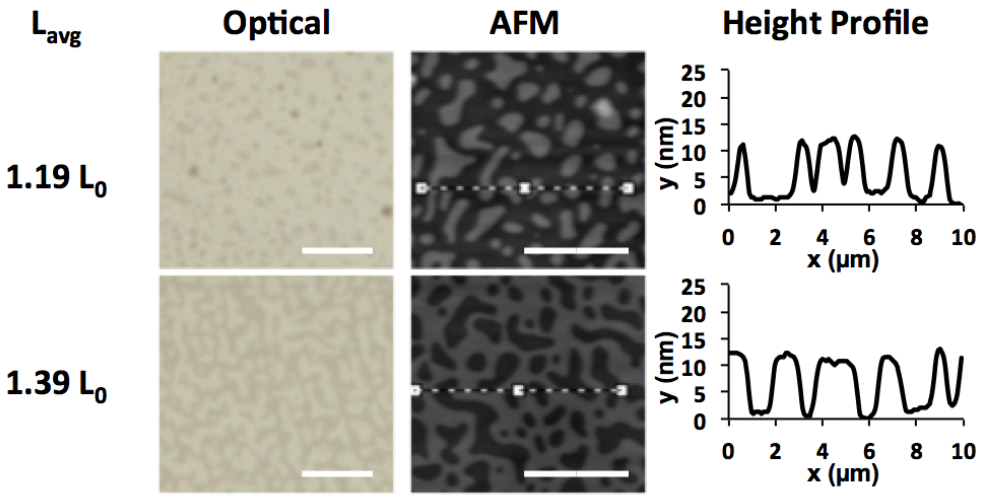

Figure 8.2: Optical and atomic force micrographs of PS-PTMSS (L_0 = 22 nm) annealed on GST-N for 10 minutes at 180˚C. Scale bars are 5 μm. Note: at these film thicknesses, in the optical micrographs dark spots are thicker (islands) and light spots are thinner (holes).

An IR study was performed to study the deblocking reaction of 4-*tert*-butoxystyrene in thin films. A 300 nm thick film of GST-N containing 5% triphenylsulfonium nonaflate (a common photoacid generator) was spin coated onto a silicon wafer. Figure 8.3A (blue curve) shows the IR spectrum of the as cast film after being annealed at 180˚C for 1 minute. The asymmetric and symmetric carbonyl stretches of the maleic anhydride moiety appear at 1855 and 1782 cm^{-1}, respectively. The CH_3 bend of the *tert*-butyl group appears as an asymmetric doublet at 1390 and 1369 cm^{-1}. The characteristic *tert*-butyl ether C-O-C stretching modes at 1242 and 1163 cm^{-1} appear and are in agreement with aryl alkyl ether assignment.[121] The presence of the *tert*-butyl ether and lack of a phenolic OH stretch at ~3500 cm^{-1} suggests that no thermal deblocking occurred under the grafting conditions. Figure 8.3B (red curve) shows the IR spectrum of the film after exposure to approx. 15 mJ/cm^2 of 254 nm light and annealing

at 100˚C for 2 minutes. The acid-catalyzed deblocking of the *tert*-butyl ether is evidenced by the appearance of the phenolic OH stretch at 3500 cm^{-1}. Additionally, there is significant reduction in the *tert*-butyl CH_3 bend and nearly complete disappearance of the C-O-C stretching modes. The two aromatic C-C stretches shift from 1606 to 1612 cm^{-1} and 1508 to 1516 cm^{-1}, which provides further support of a local change in the environment of the aromatic ring.

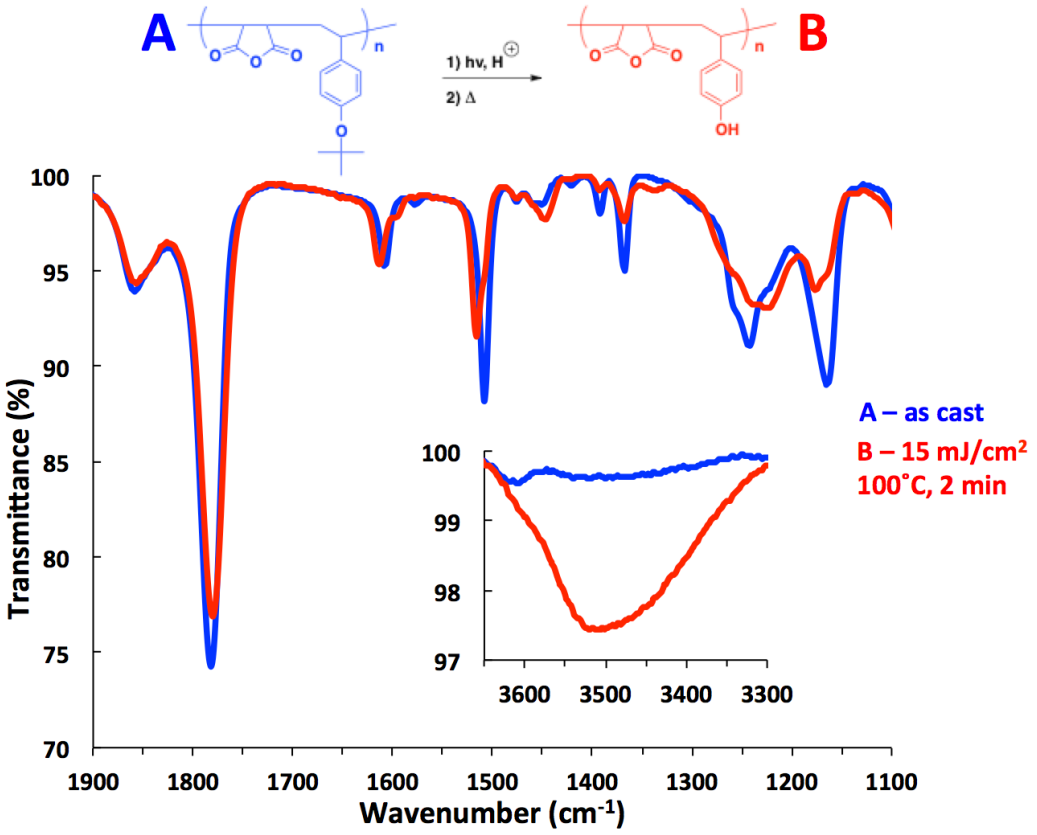

Figure 8.3: Thin film IR data demonstrates light-induced chemical modification of a GST-N. (A) Blue curve: cast from methyl isobutyl ketone with 5% triphenylsulfonium nonaflate (B) Red curve, exposed with ca. 15 mJ/cm^2 of 254 nm light and heated at 100˚C for 2 min.

After confirming that GST-N can be deprotected in thin films, focus was aimed at patterning the film in select areas. Since the chemistry is changing at the interface to a more polar species, the exposed regions of the film should be preferential to PS. Figure 8.4 illustrates the photopatterning process. A thin film of GST-N (ca. 50 nm) containing PAG was grafted to an amine-functionalized wafer and exposed (before rinsing) using a line/space photomask. In the areas of the film that were exposed, acid was generated. Heating the film induced the acid-catalyzed deprotection of the *tert*-butyl ether only in the exposed regions, which changes the chemistry from neutral to preferential. The un-grafted GST was then stripped with organic solvent to leave a chemically patterned surface with an average thickness of 3-4 nm. No significant topography between the exposed and unexposed regions was observed (Figure 8.5). After patterning and rinsing the GST, the block copolymer was deposited to a thickness (L_{avg}) between 1.0 L_0 and 1.5 L_0 and thermally annealed. Since L_{avg} was incommensurate to both symmetric and asymmetric wetting [$L_{avg} \neq$ n L_0 and $L_{avg} \neq$ (n+ 0.5) L_0], thickness quantization generated topography on the surface of the film, which was inspected by optical microscopy and AFM.[88,89]

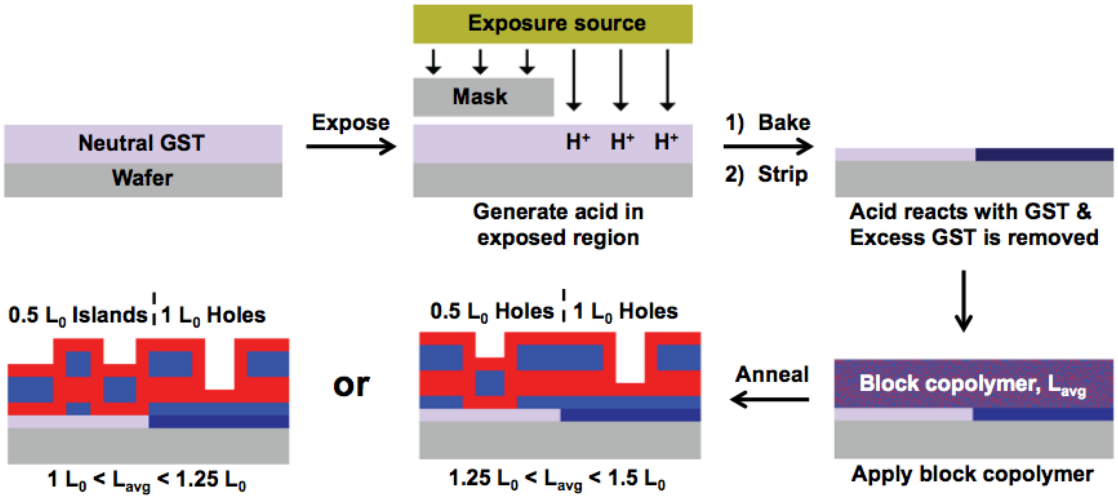

Figure 8.4: Island and hole formation on a chemically patterned GST-N.

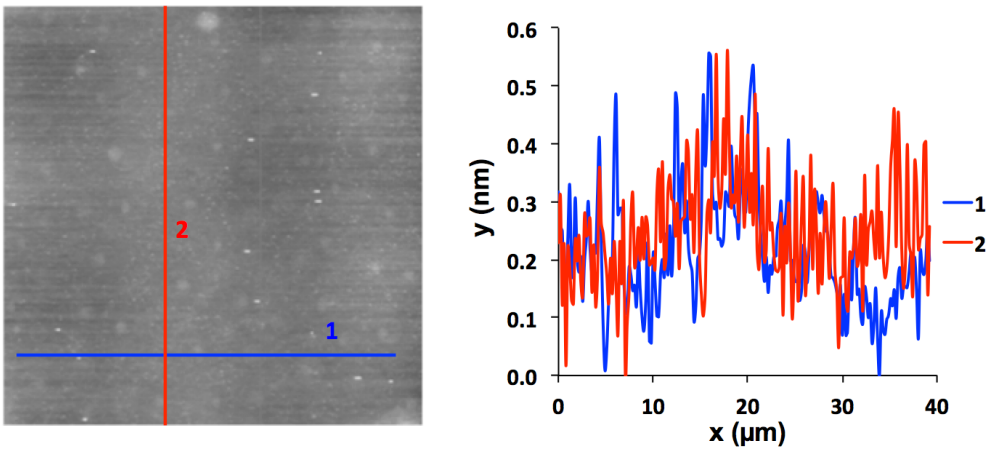

Figure 8.5: AFM micrograph of patterned GST-N. Unexposed and exposed regions have no significant differences in thickness after removing excess GST.

Figure 8.6 shows the optical and AFM images of PS-PTMSS annealed on chemically patterned GST-N. In the unexposed regions, 0.5 L_0 features are present. However, in the exposed regions, 1 L_0 holes appear. At this film thickness, this indicates asymmetric wetting, which suggests that GST-N has become preferential to PS. This makes sense because the surface is becoming more polar after deprotection of the *tert*-butyl ether. A control sample was run to confirm that the wetting preference change was due to the deprotection reaction and not exposure to light alone. GST-N was blanket exposed in the absence of PAG. Figure 8.7 shows 0.5 L_0 features, which suggests that the light alone is not changing the chemistry of GST-N.

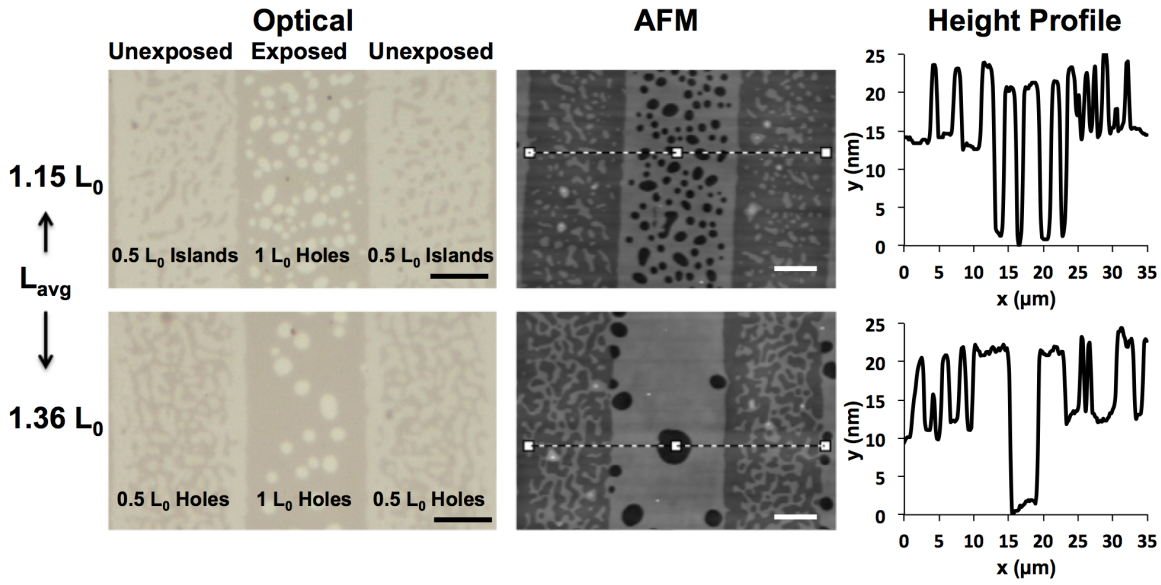

Figure 8.6: N2P process: Optical and AFM micrographs of PS-PTMSS (L_0=22 nm, L_{avg}=1.15 and 1.35 L_0) annealed at 180°C for 10 min on chemically patterned GST-N. Scale bars are 5 μm.

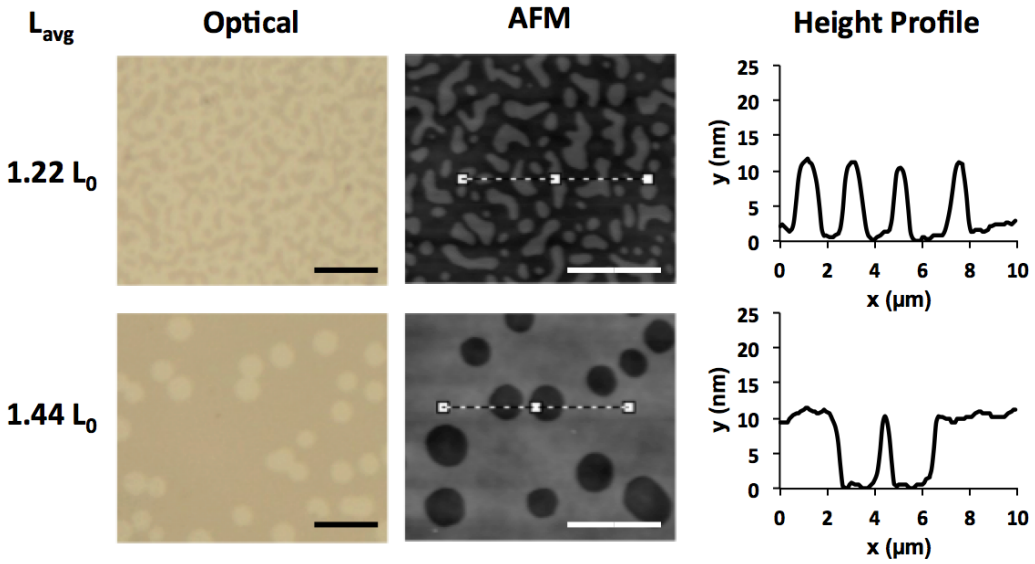

Figure 8.7: N2P controls. Optical micrographs of PS-*b*-PTMSS (L_0=22 nm, L_{avg}=1.15 and 1.35 L_0) annealed at 180˚C for 10 min on GST-N (exposed with approx. 15 mJ/cm^2 254 nm light with no photoacid generator). Scale bars are 5 μm.

8.3.2 Preferential to Neutral (P2N)

Identifying a P2N interface was not as simple as identifying a N2P surface. Recall that GST-N contained approximately 50% 4-*tert*-butoxystyrene and 0% 3,5-di-*tert*-butylstyrene. Increasing the amount of 3,5-di-*tert*-butylstyrene increases the hydrophobicity and makes the GSTs increasingly preferential to PTMSS. However, increasing 3,5-di-*tert*-butylstyrene also decreases the amount of 4-*tert*-butoxystyrene and thus the amount of polarity change upon deprotection. There is no guarantee that any combination of 3,5-di-*tert*-butylstyrene and 4-*tert*-butoxystyrene would become neutral upon deprotection. Each preferential GST had to be patterned and tested according to Figure 8.8. The process for patterning the P2N GST (GST-P) is the same as patterning

GST-N except that the exposed regions should be neutral, and 0.5 L_0 features should appear in those regions.

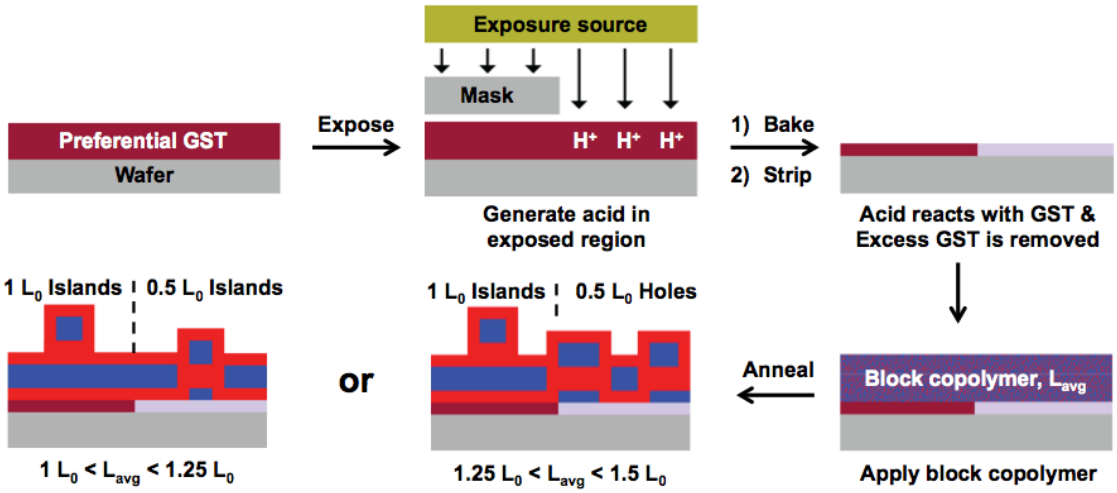

Figure 8.8: Island and hole formation on a chemically patterned GST-P.

After screening several GSTs, a P2N material was found. GST-P was found to contain 24% 4-*tert*-butoxy styrene and 26% 3,5-di-*tert*-butylstyrene. The results of the island/hole test are shown in Figure 8.9. In the unexposed regions, full islands are observed that have 1 L_0 topography. With initial film thicknesses between 1-1.5 L_0, island topography indicates symmetric wetting. This suggests that GST-P is preferential to PTMSS since PTMSS is known to wet the air interface. However, upon exposure to photoacid, the exposure regions show half features. The flip from half islands to half holes about a film thickness of 1.25 L_0 indicates that deprotected GST-P is neutral.

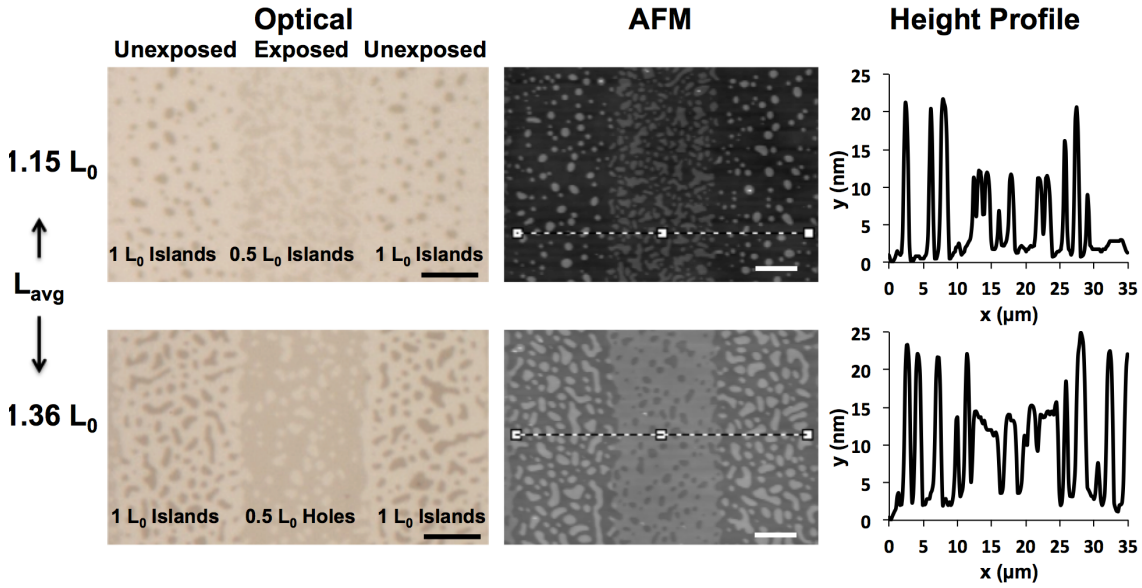

Figure 8.9: P2N process: Optical and atomic force microscopy micrographs of PS-PTMSS (L_0=22 nm, L_{avg}=1.15 and 1.35 L_0) annealed at 180˚C for 10 min on chemically patterned GST-P. Scale bars are 5 μm.

8.4 Orientation Results

The GSTs used in this chapter have been summarized by Figure 8.10. All of the wetting preference experiments are in good agreement with the initial predications. Since the GSTs have maleic anhydride, they can also be used as top coats. Theoretically, the top coat can also be patterned. However, this is more challenging because the top coat TMA salts can quench the photoacid. Patterning both the GST and top coats is the subject of future work.

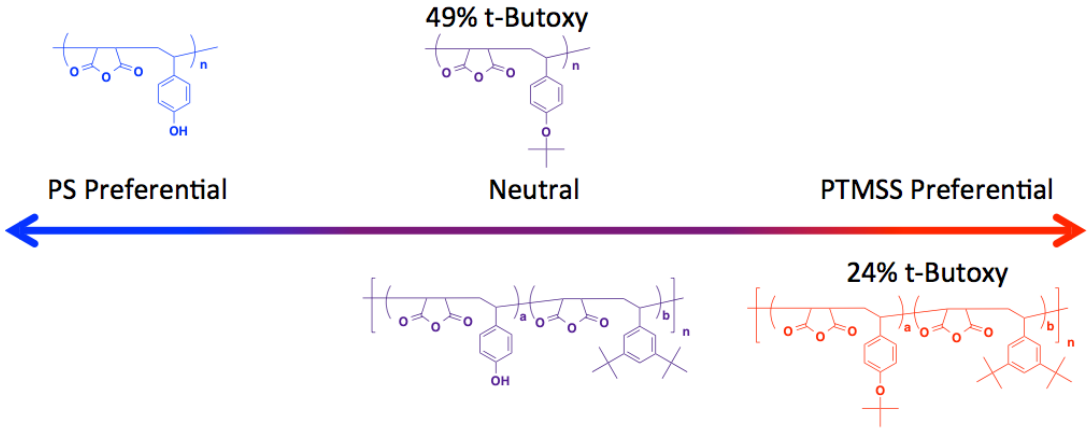

Figure 8.10: Summary of GSTs used in this chapter.

The ultimate goal is to demonstrate spatial orientation control of perpendicular and parallel domains using the photopatterned GSTs. Coupling the photo-patternable GST substrate surfaces with a proper top coat provides the ability to produce areas of arbitrary shape in which there are perpendicular lamellae orientation while the lamellae in the rest of the film are oriented parallel to the substrate. Figure 8.11 illustrates the strategy used to produce alternating regions of perpendicular and parallel lamellae by both N2P and P2N patterning processes. The N2P process produced perpendicular lamellae only in the unexposed regions region. In contrast, the P2N process produced perpendicular lamellae only in the exposed regions.

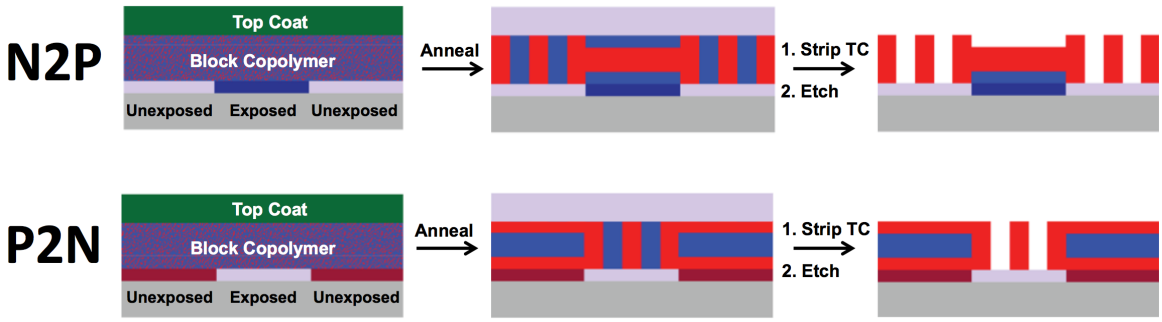

Figure 8.11: Illustration of two-dimensional spatial control of block copolymer orientation using the N2P and P2N processes. Top: a chemically patterned GST-N with neutral unexposed regions and PS-preferential exposed regions. Bottom: chemically-patterned GST-P with PTMSS-preferential unexposed regions and neutral exposed regions.

Figure 8.12 shows scanning electron micrographs (SEMs) of PS-PTMSS annealed between patterned GST-N or GST-P and a near-neutral top coat. The films were patterned with a crude contact photomask to yield sub-micron line-space patterns. PS-PTMSS with a thickness of 3 L_0 was deposited and annealed under a near-neutral top coat (TC-24, containing 24% 4-*tert*-butoxystyrene). The near-neutral TC-24 was slightly PTMSS preferential and was chosen to promote the formation of parallel lamellae in regions of the film overlaying preferential GST. A perfectly neutral top coat did not completely orient lamellae parallel at the free surface in as-designed preferential regions, as a consequence of its non-preferential block copolymer interactions. Unexposed regions (for N2P with GST-N) and exposed regions (for P2N with GST-P) produce perpendicular lamellae since the block copolymer is confined by one neutral and one near-neutral interface. These perpendicular features are independent of film thickness (Figure 8.13) and a large majority appears to span the entire film thickness, even at 3 L_0, when confined between exposed GST-P (neutral) and a near-neutral top coat (Figure 8.14). In contrast,

the exposed regions (for N2P with GST-N) and unexposed regions (for P2N with GST-P) are featureless, suggestive of parallel block copolymer domains that form in the presence of a strongly preferential interface. The boundaries between the exposed and unexposed regions are ill defined along the interface, which is most likely due to low-resolution contact printing.

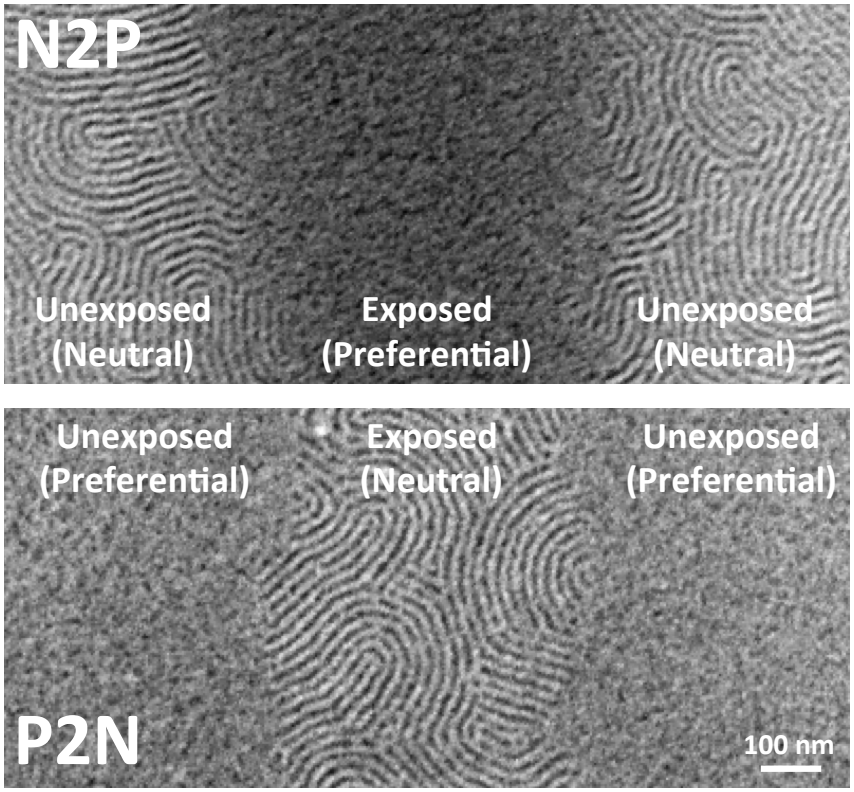

Figure 8.12: Scanning electron micrographs of PS-PTMSS (L_0 = 22 nm, L_{avg} = 3 L_0) annealed at 180˚C for 10 minutes confined between top coat TC-24 and chemically patterned GST-N (top) or GST-P (bottom). The top coat was stripped and the samples were etched with O_2 plasma.

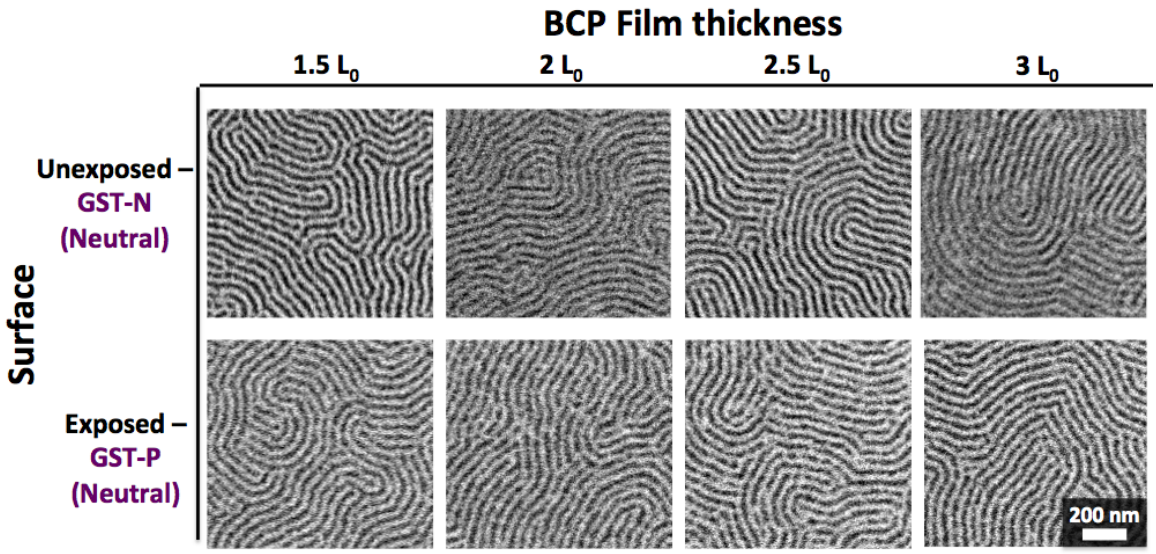

Figure 8.13: Film thickness study. Samples were annealed between a neutral GST and a near-neutral top coat for 10 mins at 180˚C. The samples were stripped of the top coats, etched, and imaged using SEM.

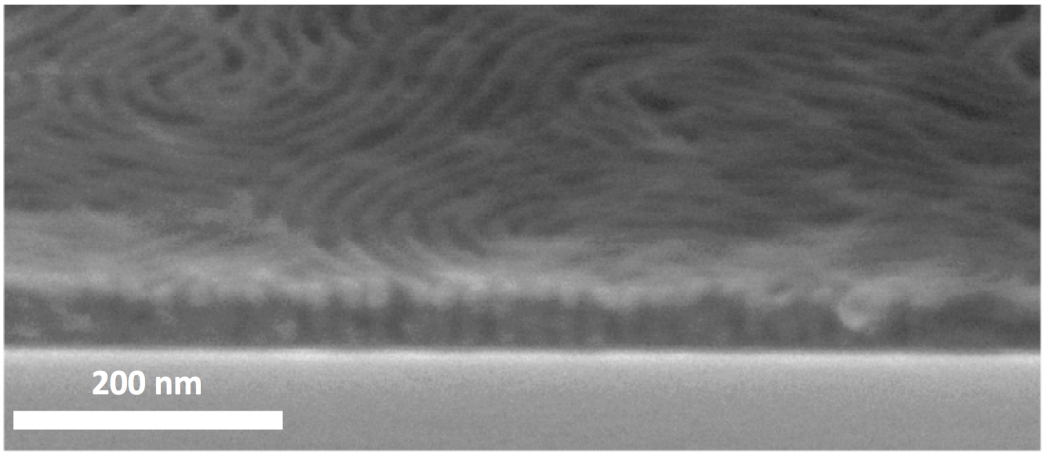

Figure 8.14: Tilted SEM of etched PS-PTMSS annealed between exposed GST-P (neutral) and a near-neutral top coat. The as-cast block copolymer thickness was 3 L_0 (66 nm). The tilted SEM shows perpendicular features throughout the film.

8.5 Patterning with High Resolution 193 nm and E-beam Lithography

In the previous sections, photopatterning with crude contact printing provided little control over the line edge roughness between regions of perpendicular and parallel domains.[149] The purpose of this section is to study the orientation control on patterned surfaces near the resolution limits of 193nm and e-beam lithography. Figure 8.15 shows the results of the N2P and P2N processes using 193nm lithography to pattern the surfaces a 1:1 line/space pattern with a pitch of 400 nm. In the top image, perpendicular domains are observed in the areas that were not exposed to photoacid. In the bottom image, however, perpendicular domains appear only in the exposed areas. The interfaces are relatively sharp and are much improved compared to previous reports.[149] This technique offers the ability to selectively control the spatial orientation of domains with well-defined boundaries using one exposure in either exposed or unexposed areas. Compared to the N2P process, the P2N process has less well-defined boundaries. This could be due to an inherent difference in the amount of chemical contrast between the neutral and preferential regions. For example, the N2P process utilizes a GST that contains 50% *tert*-butoxystyrene whereas the P2N process uses a GST with 24% *tert*-butoxystyrene.[149] We hypothesize that larger chemical contrast between the two areas would result in more precisely defined interfaces. The rest of the concepts demonstrated in this chapter will be focus on the N2P process because it results in much sharper interfaces.

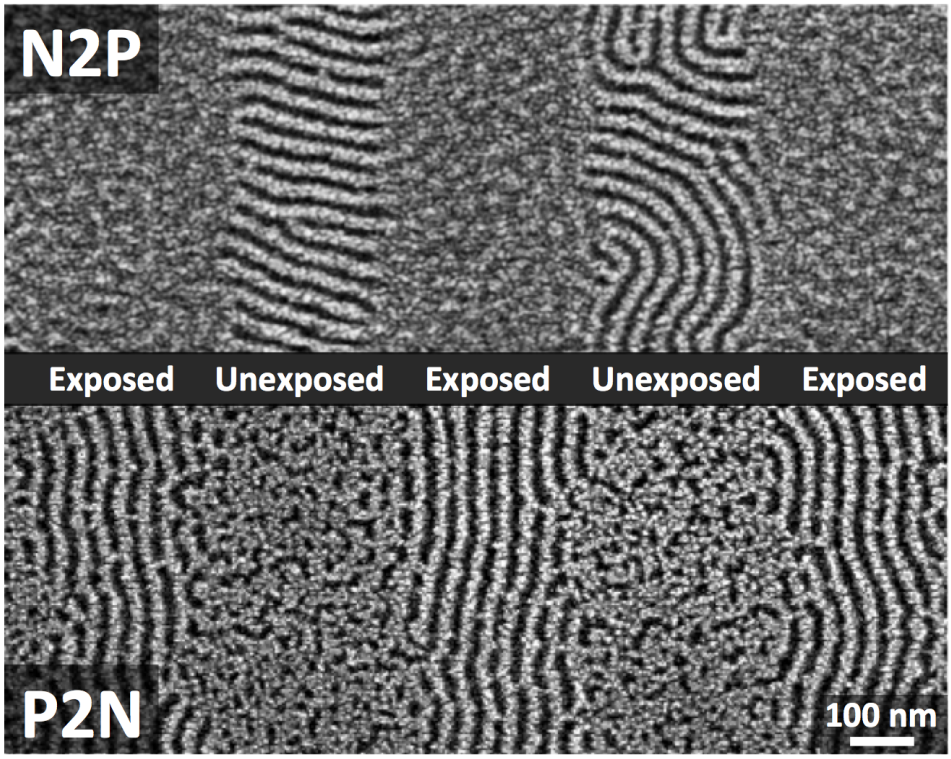

Figure 8.15: SEM images of the N2P and P2N results. The pitch of the line/space array was 400 nm.

The dimensions (line width) of the line/space pattern are related to the dose of exposure, and either underexposure or overexposure should produce line/spaces that are not 1:1. An exposure dose study with two different pitches, 200 and 400 nm, was performed with the N2P process. Figure 8.16 shows the results as the exposure dose was varied from 1 mJ/cm^2 to 5 mJ/cm^2. Again, only the areas that were not exposed yield perpendicular domains. However, as dose is increased, the exposed area becomes much larger and effectively shrinks the areas of perpendicular domains systematically.

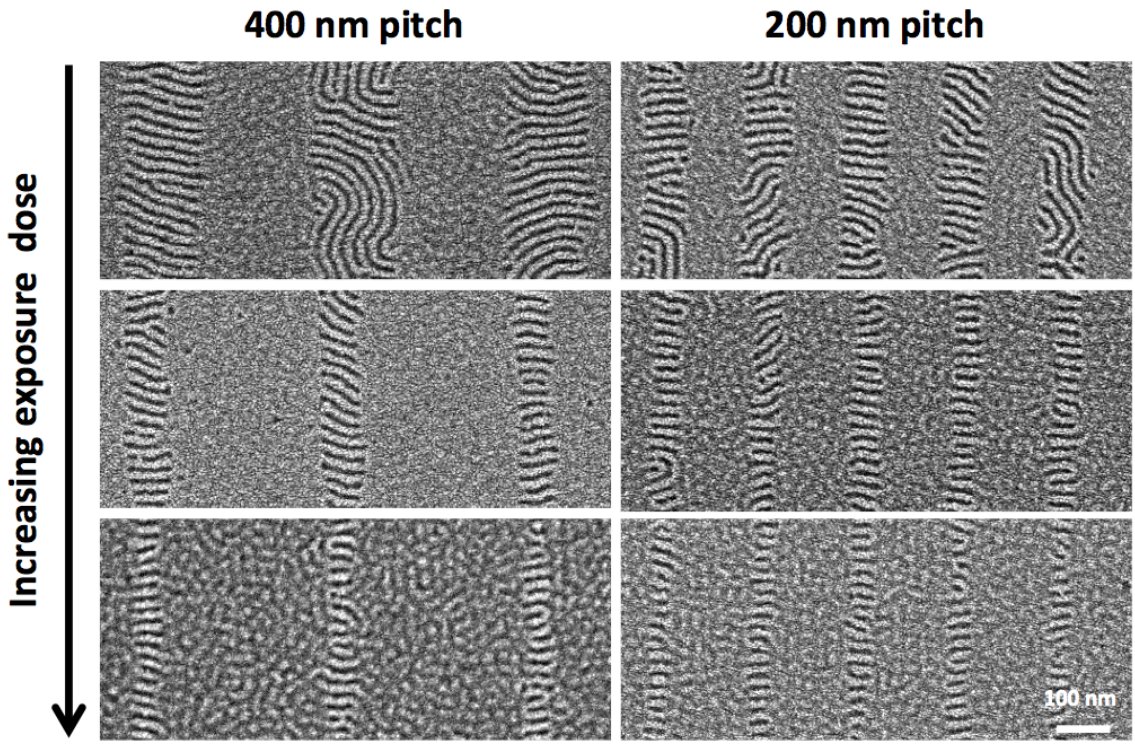

Figure 8.16: Exposure dose study of the N2P process with two different pitches. Dose increases from 1 mJ/cm^2 to 5 mJ/cm^2.

Interestingly, the perpendicular domains in Figure 8.16 spontaneously adopt a ladder-like arrangement stacked normal to the exposed regions as the normalized neutral area dimension (t/L_0) is reduced. The perpendicular domains traverse the width of the unexposed regions instead of running parallel to the length of the exposed, preferential regions. This observation is in good agreement with a reports by Stoykovich *et al*. and Shin *et al*. using PS-PMMA, [30,153] and theoretical calculations demonstrate that the ladder-like (linearly stacked) arrangement is more favorable than parallel lines.[159] Figure 8.17 shows a graph that plots the percent of domains in the linearly stacked, ladder-like arrangement as a function of normalized neutral width. This was quantified as the percent

of line/spaces that completely traverse the entire width of neutral area. As the width of the neutral area decreases from approx. 180 nm to approx. 40 nm, the percent laddered quickly approaches 100%. Intuitively, this makes sense because there is less latitude for random walk, especially since there is an energetic penalty for forming lines parallel to the exposed, preferential regions.

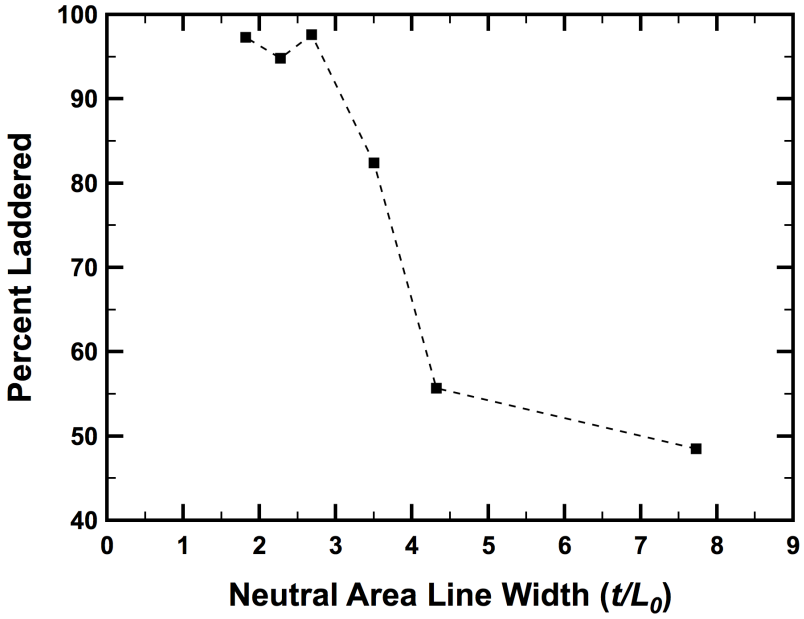

Figure 8.17: Plot of domains adopting a ladder-like arrangement as a function of neutral area width.

Another observation from Figure 8.16 is that some of the line/spaces do not traverse the entire width of the neutral region and may also bifurcate into more than one line and/or form "S"-like or "C"-like structures. In this chapter, these structures were defined as defects. Block copolymer domains that did not terminate at both ends of the patterned line or failed to traverse the entire patterned line were counted as a single defect. Additionally, any branching points or "S"-like or "C"-like structures were counted

as a single defect. Figure 8.18 displays a graph of the defects per each neutral area (line) as a function of normalized neutral area line width. There are a large number of defects when the line width is large, which was expected. However, the density of defects quickly drops as the line width decreases. The defects are minimal when the line width is approximately 2 L_0 in thickness.

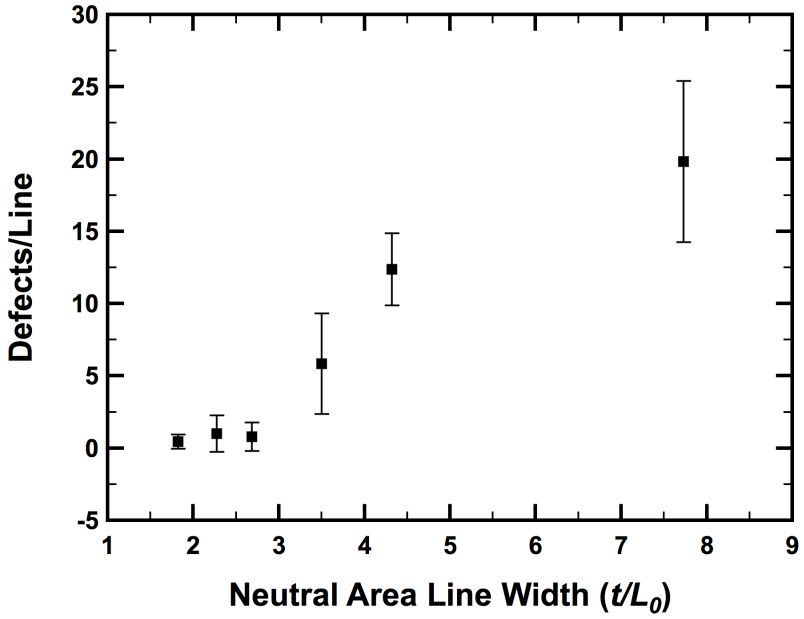

Figure 8.18: Plot of the defects per each line. The error bars represent one standard deviation.

The rectangular structures may be potential candidates for use in bit-patterned media. Currently, these type of structures are highly desired, but require multiple, complex processing steps.[33,34] By using photopatternable interfaces, these rectangular structures form spontaneously in one exposure step. However, the defects would need to be minimized before application, which is outside the scope of this work. It is promising

that the defects significantly decrease as the neutral area approaches the dimensions required for bit-patterned media.

The N2P process was also performed using e-beam lithography as the radiation source. E-beam lithography offers the ability to pattern much smaller, higher resolution areas. First, the previous results of alternating perpendicular and parallel domains within the same film were reproduced in Figure 8.19A. Then, the width of the patterned area was decreased to approximately 35 nm (~1.6 L_0). Two hypotheses were made about the reduction of preferential area critical dimension: 1) the spatial arrangement of the perpendicular domains would run parallel to the exposed line as opposed to adopting the ladder-like, linearly stacked arrangement. 2) The orientation of domains in the exposed, preferential region would be perpendicular and not parallel since the critical dimension of the exposed line is less than 2 L_0. The result of the experiment is shown in Figure 8.19B. Contrary to the hypotheses, the perpendicular domains still have the ladder-like arrangement and no parallel spatial arrangements are evident. Additionally, the block copolymer domains in the exposed area still have a parallel orientation, which indicates that a mix of parallel and perpendicular domains within the same film is achievable on length scales that approach L_0. The width of the preferential region in which the domains do not adopt a parallel orientation and remain perpendicular is not clear, but apparently it must be less than 1.6 L_0. In addition to a straight line/space array, the e-beam tool was used to more complex areas such as the concentric circles shown in Figures 8.19C and 8.19D. Interestingly, the ladder-like structures are still evident and follow the curvature. This suggests that complex, non-linear structures may also be generated using this patterning technique.

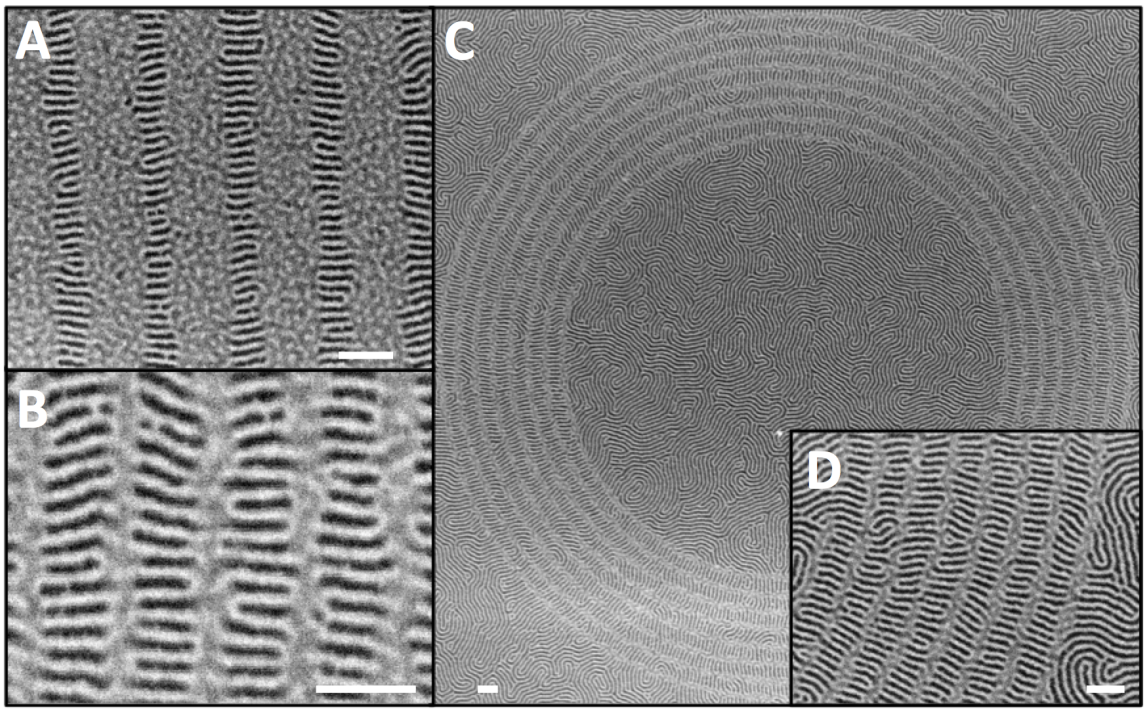

Figure 8.19: SEM results of the N2P process using e-beam lithography; **A)** Approx. 100 nm wide exposed lines with a pitch of 150 nm; **B)** Approx. 40 nm exposed lines with a pitch of 130 nm; **C)** Approx. 35 nm exposed lines with a pitch of approx. 120 nm arranged in a circular pattern; **D)** Higher magnification region of C. Scale bars are 100 nm.

8.6 OUTLOOK

In this chapter, the spatial control of block copolymer domains was demonstrated using interfaces that were photopatternable. The author envisions that these photopatternable interfaces could be used to simplify the current DSA schemes and avoid additional processing steps. A hypothetical DSA scheme that could be highly valuable is shown in Figure 8.20. Here, a P2N surface treatment is exposed, and the exposed area is rendered neutral. During this transformation, the photoacid diffuses laterally in the film and reacts with areas that were initially not exposed, which effectively shrinks the

unexposed areas. Since the unexposed areas are preferential, there is potential that they can be shortened in width to the order of 0.5-1.5 L_0 and function as guidelines. Whereas most DSA schemes focus on patterning the guideline, this scheme focuses on patterning the interstitial region between the unexposed guidelines. This creates two advantages: 1) It significantly relaxes the patterning requirements, and 2) it eliminates the trim etch process step. While material sets for this type of process exist, DSA using this technique has yet to be demonstrated. However, the realization of this process would be incredibly valuable and it can be combined with spatial orientation control to form custom block copolymer designs.

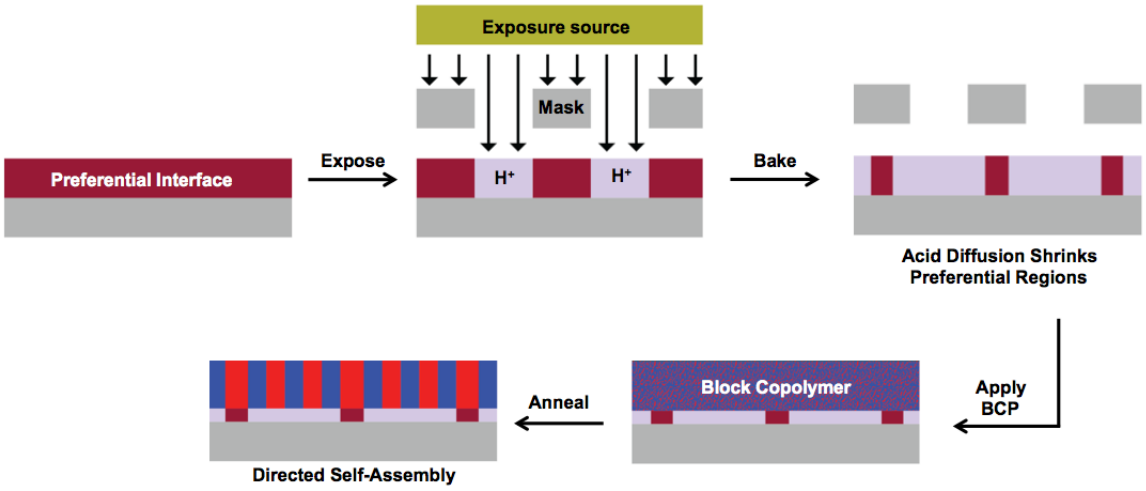

Figure 8.20: Theoretical directed self-assembly technique. A photoacid-labile surface treatment containing photoacid generator is exposed and photoacid is generated. Photoacid reacts with the surface treatment to produce areas of neutral region. Lateral acid diffusion shrinks the unexposed areas. Block copolymer is applied and the unexposed areas act as guidelines and direct the self-assembly during thermal annealing.

8.7 EXPERIMENTAL

8.7.1 Instrumentation:

Size exclusion chromatography (SEC) data for the GST/TCs were collected on an Agilent 1200 Series Isopump and Autosampler with an Agilent Technologies 1100 RI detector. One PLgel 5 μm, 100 Å column and one PLgel 5 μm, 1000 Å column were used with DMF (with 0.01 M LiBr) as an eluent at 70°C and a flow rate of 1 mL/min. The refractive index response of the top coats was compared to polystyrene (PS) standards, which were used to calibrate the instrument by refractive index response (conventional calibration). A Brewer CEE 100CB Spincoater was used to coat all thin films. Ellipsometry was performed with a J.A. Woollam Co, Inc. VB 400 VASE Ellipsometer with wavelengths from 382 to 984 nm and a 65° angle of incidence. A Zeiss Supra 40 VP scanning electron microscope operating at 3 kV with the in-lens detector and a working distance of 2-5 mm was used to collect all SEM data. Brightness and contrast for all SEMs were uniformly enhanced using commercial image editing software. The exposure source was an EXFO Novacure 2100 spot curing system (mercury arc lamp). The 254 nm bandpass filter and chrome deposited Ronchi Rulings used for contact printing were purchased from Edmund Optics. Doses were measured using a Coherent FieldMaxII-TO equipped with a PowerMax PM3 detector. Atomic force micrographs were taken with an Asylum MFP-3D AFM. Thermogravimetric analysis was performed on a Mettler Toledo TGA/DSC 1 STAR. Digital scanning calorimetry was performed on a TA Instruments Q100. Combustion analysis was performed by Midwest Microlab, LLC.

The following instruments were used in Section 8.5 and later. The 193nm exposure source was a solid-state 193 nm laser.[160] The pitch of the line/space pattern was set at either 200 or 400 nm using a variable angle prism. The ratio of the exposed to unexposed areas was 1:1. Electron beam patterns were generated with a Vistec/Leica VB6 electron beam lithography tool running at 100 kV and using a beam current of 0.25 nA. Thin film thickness measurements were made on a NanoSpec 6100. Samples were etched using a Plasma-Therm Versaline and coated with gold/palladium alloy prior to imaging. The gold/palladium was sputter coated using an Emitech K550X using 20 mA for 30 sec. Scanning electron micrographs were captured on a Leo 1550 using an accelerating voltage of 10 kV. Brightness and contrast on all SEMs were uniformly enhanced using image-editing software.

8.7.2 Reagents

Maleic anhydride, 50 wt.% aq. Trimethylamine and aminopropyltriethoxysilane (APTES) were purchased from Acros. Styrene (99%), 4-*tert*-butoxystyrene, N,N-dimethylformamide (CHROMASOLV Plus, for HPLC) and azobisisobutyronitrile (AIBN) were purchased from Sigma-Aldrich. Test grade silicon wafers with ca. 1.5 nm native oxide were purchased from Addison Engineering. Methanol (HPLC grade), tetrahydrofuran (HPLC grade), methyl isobutyl ketone (MIBK), and basic alumina were purchased from Fisher Scientific. Triphenylsulfonium nonaflate was purchased from Clariant. All materials were used without further purification unless otherwise stated. AIBN was recrystallized from methanol. Crosslinked polystyrene was synthesized according to a previous report.[61] 3,5-di-*tert*-butylstyrene was synthesized using a previously reported method.[70]

8.7.3 GST and TC Synthesis:

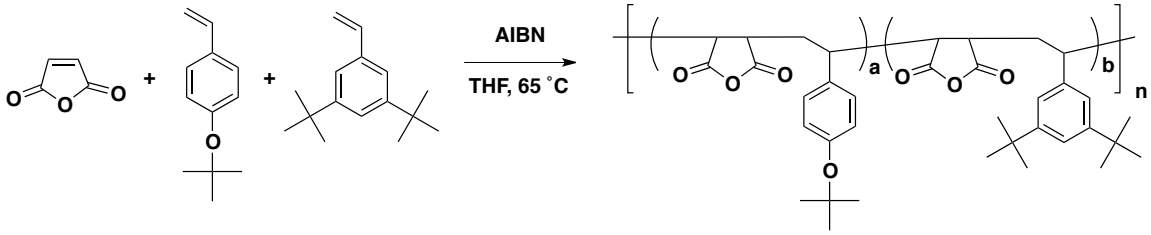

The following procedure is representative of all GST/TC syntheses. Monomers containing inhibitor were stirred over basic alumina for 20 minutes and filtered prior to use. A 3-neck round bottom flask equipped with a condenser, rubber stoppers, and a magnetic stir bar was charged with maleic anhydride (2.43 g, 24.8 mmol, 0.50 eq.), 4-*tert*-butoxystyrene (1.92 g, 10.9 mmol, 0.22 eq.), 3,5-di-*tert*-butylstyrene (3.00 g, 13.7 mmol, 0.28 eq.), AIBN (0.081 g, 0.500 mmol, 0.01 eq.), and THF (40 mL). Nitrogen was bubbled through the solution for 30 minutes to remove oxygen. After purging, the flask was immersed in an oil bath at 65°C and heated under dynamic nitrogen for 18 hrs. The reaction was cooled by immersion in an ice-water bath for 10 minutes. The polymer was precipitated in approx. 400 mL of methanol, isolated by filtration, redissolved in THF and precipitated again in methanol. The polymer was dried *in vacuo* at 75°C overnight, yielding 4.55 g (62%) of isolated product. The polymer was characterized by TGA, DSC, IR, and elemental analysis.

Table 8.1: GST composition summary[a]

	Feed Ratio (mol%)			Actual (mol%)[b]		
GST-	**MA**	**tBuOSty**	**ditBuSty**	**MA**	**tButoxySty**	**ditBuSty**
N	50	50	0	51	49	0
P	50	22	28	50	24	26

[a]Abbreviations: MA (Maleic anhydride), tBuOSty (4-*tert*-butoxystyrene), ditBuSty (3,5-di-*tert*-butylstyrene). [b]Calculated from combustion analysis.

Table 8.2: GST characterization summary

	Molecular Weight (Da)[a]					
GST-	**M_n (Da)**	**M_w (Da)**	**Đ**	**T_g (˚C)**	**T_d (˚C)**	**Yield[b]**
N	16400	51800	3.16	199	216	49%
P	20100	67000	3.33	205	232	62%

[a]Calculated by SEC relative to polystyrene standards. [b]Based on recovered mass.

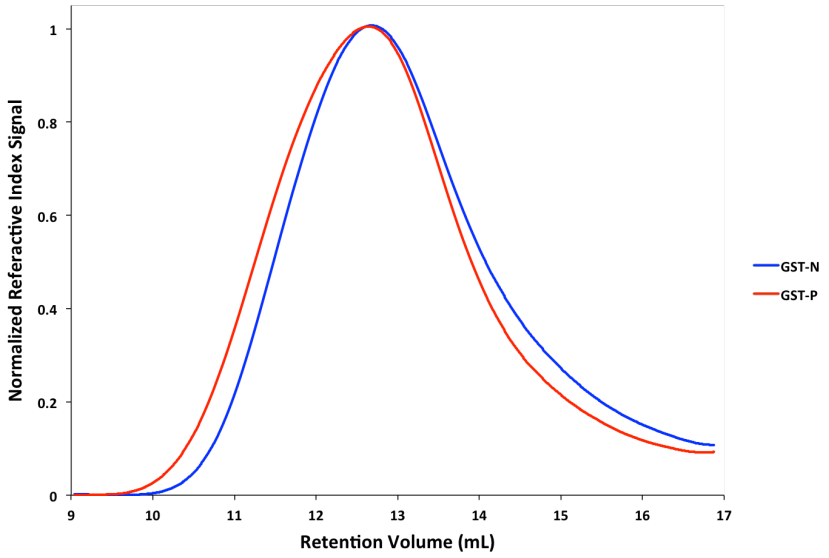

Figure 8.21: GST size exclusion chromatograms.

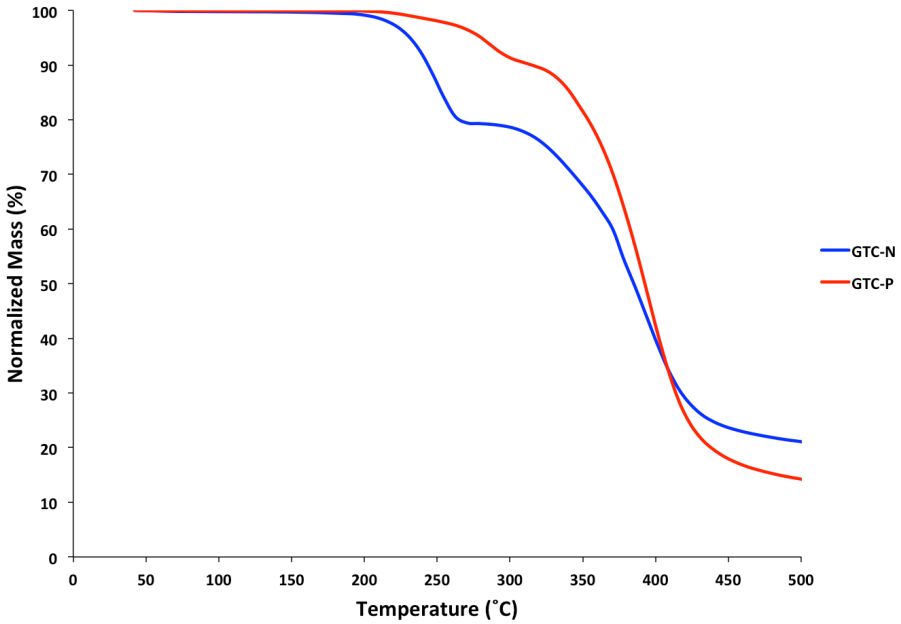

Figure 8.22: Thermogravimetric analysis of the GSTs. Samples were heated to 500˚C at a rate of 10˚C/min.

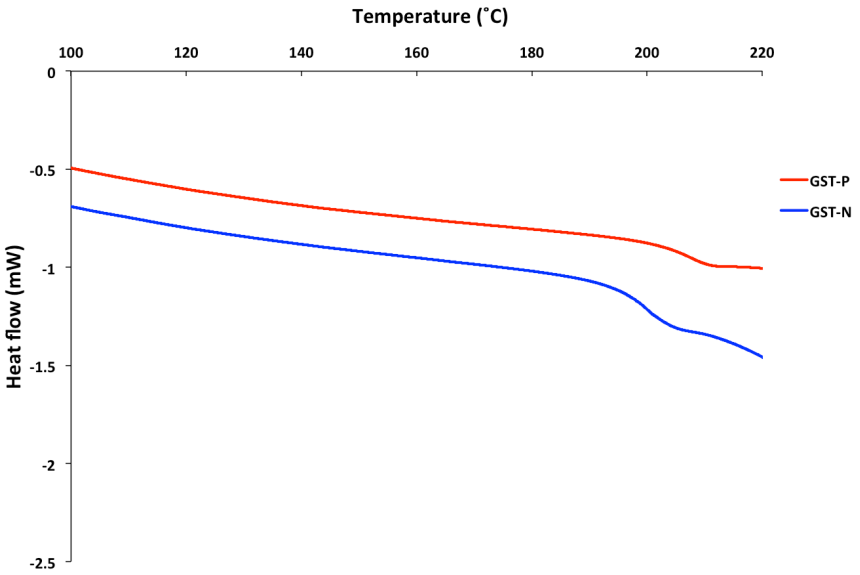

Figure 8.23: GST differential scanning calorimetry data. Samples were heated to 220˚C at 10˚C/min for 2 cycles. The second heating cycle is shown.

8.7.4 TC TMA Salt Formation:

The preparation of TMA salts followed a modification of a previously reported procedure.[70] Approx. 1 g of each polymer was dissolved in approx. 7 g of 50 wt.% aq. TMA. After complete dissolution, the viscous solution was poured into 50 mL of THF. The THF and water were removed via rotary evaporation at 40˚C, and the solid was dried *in vacuo*.

8.7.5 Amination of Silicon Wafer Surface:

A silicon wafer was covered with neat aminopropyltriethoxysilane (APTES). After 30 sec, the wafer was washed repeatedly with tetrahydrofuran. The wafer was

subsequently annealed at 120˚C for 1 min to remove residual solvent. The thickness of the APTES layer was measured to be ca. 1 nm by ellipsometry.

8.7.6 General Grafting Procedure:

GSTs (1 wt.% in MIBK) were spin coated on a silicon wafer that had been treated with APTES. The resulting film was initial ca. 20 nm thick. The wafer was heated at 180˚C for 1 minute. The residual material was stripped with tetrahydrofuran. The remaining thickness was approx. 3 nm thick (for the N2P process) or 4 nm thick (for the P2N).

8.7.7 Analysis of Substrate Surface Wetting:

Solutions of PS-PTMSS (0.75-1.5 wt.% in MIBK) were spin coated onto the GST. Film thicknesses were measured by ellipsometry. Samples were heated at 180˚C for 10 minutes. The resulting topography was observed using optical microscopy, and the topographic profile was measured using AFM.

8.7.8 IR Sample Preparation:

A 10 wt.% solution of GST-N containing 5% triphenylsulfonium nonaflate (relative to polymer mass) was spin coated onto a silicon wafer and heated at 180˚C for 1 min. The film thickness was approx. 300 nm. An initial IR spectrum was recorded. The film was then blanket exposed to approx. 15 mJ/cm^2 of 254 nm light using a broadband light source equipped with a 254 nm bandpass filter. Immediately after exposure, the wafer was heated at 100˚C for 2 min and another IR spectrum was recorded.

8.7.9 N2P and P2N Patterning Processes:

For the N2P process, a 2 wt.% solution GST-N containing 5 wt.% triphenylsulfonium nonaflate (relative to polymer mass) in MIBK was spin coated at 2500 rpm. For the P2N process, a 2 wt.% solution GST-P containing 10 wt.% triphenylsulfonium nonaflate (relative to polymer mass) in MIBK was spin coated at 2500 rpm. Annealing at 180˚C for 1 minute was applied to yield film thicknesses of ca. 55 nm. A 40 lines-per-millimeter Ronchi ruling and a 254 nm bandpass filter were placed directly on the film for contact printing. The film was exposed with a broadband UV light source from a distance of 33 mm. The dose was approximately 30 mJ/cm^2. After exposure, the wafer was annealed at 100˚C for 2 minutes and rapidly quenched to room temperature. The surface treatment that did not graft to the substrate was removed by stripping with MIBK and THF. The resulting GST was approximately 3 nm thick (N2P) or 4 nm thick (P2N).

8.7.10 SEM Sample Preparation using Ronchi Rulings

A modified procedure from a previous report was used to prepare the samples for SEM.[70] The GSTs were the chemically patterned with a 600 lines-per-mm Ronchi ruling. The block copolymer thickness was approx. 66 nm. The thin film stacks were annealed at 180˚C for 10 minutes. Top coats were removed by immersing in a solution of methanol and 50% aq. TMA solution (1:1 by volume). The samples were then etched with O_2 RIE for 25 seconds using previously reported conditions.[70]

8.7.11 Sample Preparation for High-resolution Patterning

Aminopropyltriethoxysilane treated wafers were prepared.[149,161] A solution of neutral or preferential surface treatment (1 wt% in MIBK with 10% triphenylsulfonium nonaflate) was spin coated at 1500 rpm and annealed at 180˚C for 1 minute. Exposure doses were approximately 1-5 mJ/cm^2. Samples were post-exposure baked at 100˚C for 1 minute. The samples were rinsed with MIBK to remove ungrafted material. PS-PTMSS was spin coated out of MIBK to form films approximately 1 L_0 in thickness. A neutral top coat salt was spin coated out of methanol and annealed at 180˚C for 10 minutes.[70] The top coat was removed by immersion in 3 parts TMAH (0.26 N) and 1 part 2-propanol (by volume). Samples were rinsed with DI water and dried with a gentle stream of nitrogen. Samples were etched and coated with gold/palladium under previously reported conditions.[162]

8.8 Acknowledgements

Dr. Christopher Bates helped synthesize the various GSTs used in this chapter. Matt Carlson helped evaluate the photopatternable GSTs. Gregory Blachut synthesized PS-PTMSS. William Durand helped obtain the cross-sectional image. Dr. Charles Rettner at IBM performed the e-beam patterning.

Chapter 9: Tin-Containing Block Copolymers

9.1 Pattern Transfer

Most organic block copolymers exhibit limited block-block dry etch selectivity. Two general strategies have emerged to improve the etch contrast between the blocks to facilitate pattern development. Sequential infiltration synthesis (a manifestation of atomic layer deposition) injects etch resistant metals into one block copolymer domain to increase etch selectivity,[40,42] but the process is slow, requires specialized instrumentation, and alters the dimensions of the block copolymer domains.[43] The second approach, the direct synthesis of block copolymers containing inorganic monomers[44-49] imparts inherent etch contrast.[50] The latter technique is clearly preferable with all other considerations being equal. Both methods of generating etch contrast are reasonably controllable and well understood although pattern transfer challenges still remain with high-resolution sub-10 nm domains.[77]

Patterned quartz templates for imprint lithography are needed to produce ultra-high density data storage devices (i.e. bit patterned media).[32,163] DSA directing features could be patterned directly on quartz wafers via e-beam lithography or molecular transfer printing[164,165] or indirectly by transferring silicon-features into quartz via UV curing.[37,166]

Recently, the latter method was used to generate high quality quartz nanoimprint templates via directed self-assembly (DSA) but that process included a series of complex steps.[37] A ubiquitous difficulty in pattern transfer derives from a lack of oxygen *and* fluorinated plasma etch selectivity. Consequently, generation of templates for imprint lithography requires patterning an intermediate layer (typically chromium) that is impervious to fluorine-based etches required to pattern quartz. It was reasoned that if tin could be incorporated into one block of a lamellae-forming block copolymer, the tin block could serve as an oxygen etch mask for development because tin oxides are not volatile. Subsequent transfer of the developed pattern into quartz could be possible because tin fluorides are not volatile. This would greatly simplify the production of imprint templates.

In this chapter, a novel family of tin-containing polymers are designed to be resistant to fluorinated etch chemistries used to etch inorganic oxides. Since tin-containing polymers are reportedly resistant to both oxidizing and fluorine etch conditions,[167] the incorporation of tin directly into a carefully designed block copolymer should produce high-resolution patterns with facile subsequent pattern development *and* pattern transfer processes. To the best of the author's knowledge, there are only a few reports describing the synthesis of tin-containing block copolymers[168-170] and no reports on their etch properties or lithographic potential. In the first part of this chapter, the synthesis of poly(4-trimethylstannylstyrene-*block*-styrene) (PSnS-PS) and poly(4-trimethylstannylstyrene-*block*-4-methoxystyrene) (PSnS-PMOST) are described. Well-defined block copolymers with periodicities (L_0) ranging from 18-34 nm were successfully synthesized using reversible addition-fragmentation chain-transfer (RAFT) polymerization. Later in the chapter, thermally-induced thin-film self-assembly and direct pattern transfer into SiO_2 are demonstrated.

9.2 TIN-CONTAINING STYRENE AND ANIONIC FAILURE

The monomer 4-trimethylstannylstyrene (SnS) contains 44 wt% Sn, which far exceeds the minimum (~10 wt%) needed to form a sufficient etch barrier.[167] The monomer was readily synthesized in high yields from the Grignard reaction of 4-chloromagnesium styrene and trimethyltin chloride.

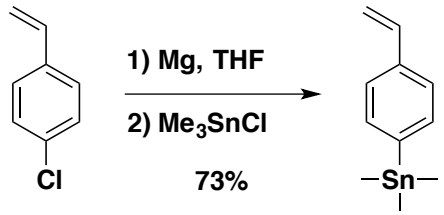

Scheme 9.1: Synthesis of 4-trimethylstannylstyrene (SnS).

Anionic polymerization of the monomer is desirable since it opens the door to block copolymers with controlled molecular weights, narrow dispersities, and well defined macromolecular structures, but was ultimately unsuccessful. Direct initiation of the monomer with *sec*-butyllithium in THF at -78 ˚C formed an insoluble residue (Scheme 9.2). Polymerization in cyclohexane at 40 ˚C yielded an ill-defined polymer with broad molar mass dispersity and uncontrolled molar mass (Scheme 9.3, Figure 9.1).

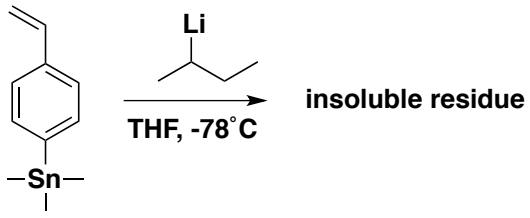

Scheme 9.2: Anionic polymerization attempt in tetrahydrofuran.

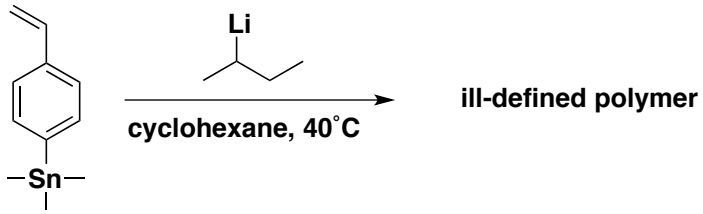

Scheme 9.3: Anionic polymerization attempt in cyclohexane.

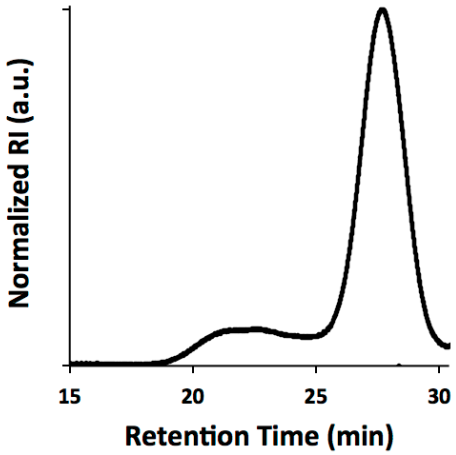

Figure 9.1: SEC trace of the polymer resulting from Scheme 9.3. The major peak had an M_n = 4.6 kDa and $Đ$ = 1.30 whereas the minor peak had M_n = 59.6 kDa and Đ = 1.78.

Attempts to grow a PSnS block from living PS were also unsuccessful. Living polystyrene was synthesized according to Scheme 9.4. The polystyrene aliquot was well defined (M_n = 22.9 kDa, Đ = 1.05). However, addition of SnS to the living anion resulted in an ill-defined polymer. The SEC chromatographs of the aliquot and block copolymer are shown in Figure 9.2.

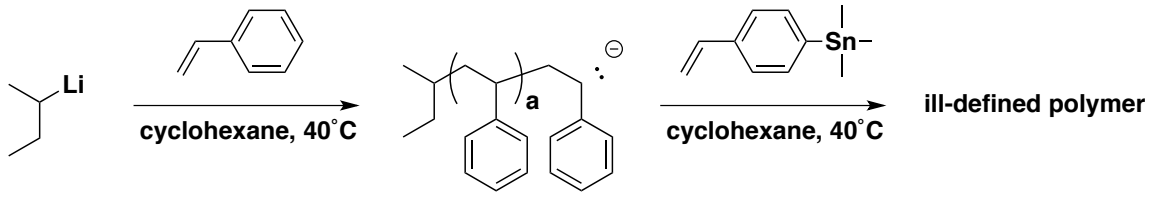

Scheme 9.4: Attempt to polymerize poly(styrene-*block*-4-trimethylstannylstyrene) via anionic polymerization.

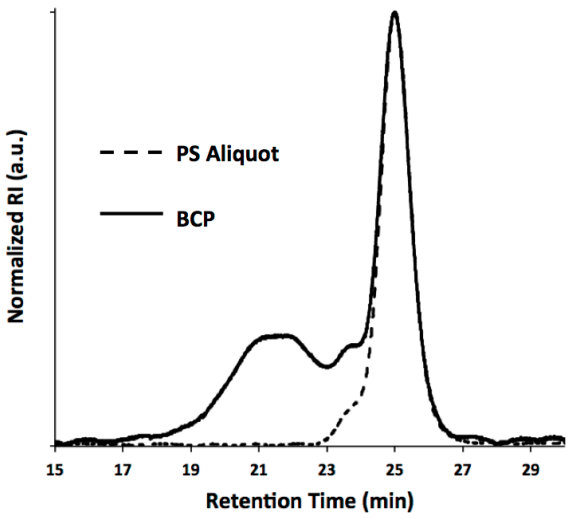

Figure 9.2: SEC traces of the polystyrene aliquot (dashed line) and resulting block copolymer formed after the addition of SnS (solid line).

In analogy to similar reports with 4-triphenylstannylstyrene,[171] the SnS monomer may not be stable towards anionic conditions. To test this hypothesis, a model compound, trimethyl(phenyl)tin, was exposed to *sec*-butyllithium and quenched with methanol (Scheme 9.5). Approximately 2% of the trimethyl(phenyl)tin was converted to the tin hydride, dimethyl(phenyl)stannane. This suggests that the monomer undergoes chain transfer side reactions that prevent controlled polymerization.

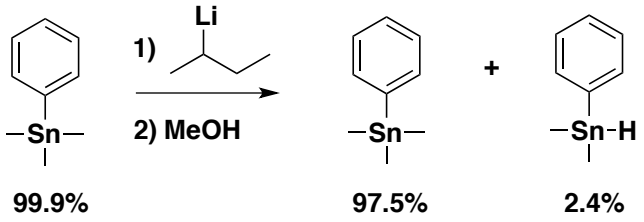

Scheme 9.5: Reaction of trimethyl(phenyl)tin with *sec*-butyllithium followed by quenching with methanol.

9.3 RAFT Polymerization of Tin-containing Block Copolymers

RAFT was used to circumvent the undesired chain transfer reactions observed in anionic polymerization.[172] Homopolymerization of SnS using RAFT is shown in Scheme 9.6. Homopolymers with controlled molecular weights were achieved by adjusting the initiator to monomer ratio (Table 9.1). The homopolymers had mass dispersities (*Đ*) <1.20 and monomodal molar mass distributions (Figure 9.3).

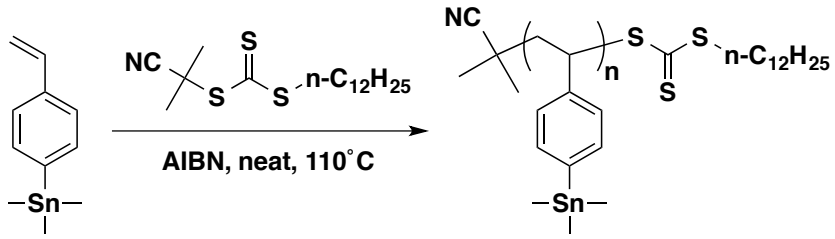

Scheme 9.6: Homopolymerization of SnS *via* RAFT.

Table 9.1: Homopolymer synthesis details.

Entry	Method[a]	SnS/Initiator[b]	Time (hr)	M_n (kDa)[c]	$Đ$	Yield
1	B	315	24	36.3	1.12	33%
2	A	225	19	30.9	1.12	65%
3	A	110	22	15.4	1.20	50%
4	A	97	23	13.9	1.13	74%
5	A	93	20	12.9	1.04	79%
6	A	76	23	11.8	1.01	75%
7	A	75	18	10.8	1.04	67%
8	A	56	17	7.6	1.04	72%
9	A	37	22	5.1	1.07	77%

a: Method refers to polymerization conditions. See experimental (Section 9.8.4)
b: Mol ratio
c: Determined by SEC in THF using a dn/dc value of 0.2027

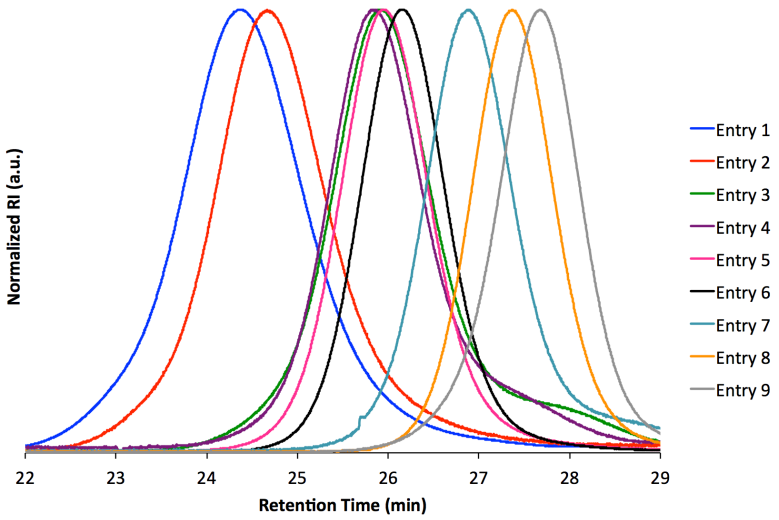

Figure 9.3: SEC traces of PSnS homopolymers synthesized via RAFT.

A second block (either PS or PMOST) was grown from several PSnS homopolymers to create tin-containing block copolymer analogous to silicon-containing block copolymers synthesized previously with known lithographic properties. The

reactive end groups were removed using AIBN to prevent thermal coupling (Scheme 9.7).[59] SEC traces (Figure 9.4) demonstrate controlled block copolymer synthesis; a detailed synthetic experimental procedure is in the experimental section.

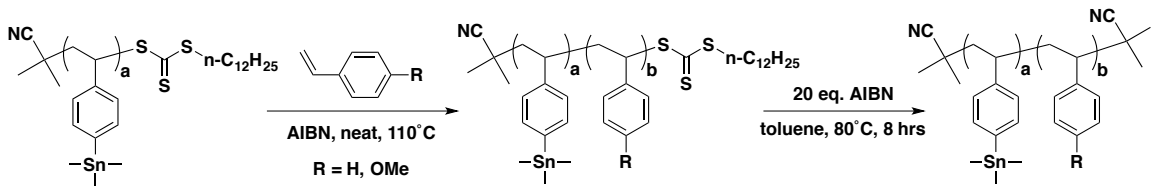

Scheme 9.7: Synthesis of PSnS-PS and PSnS-PMOST.

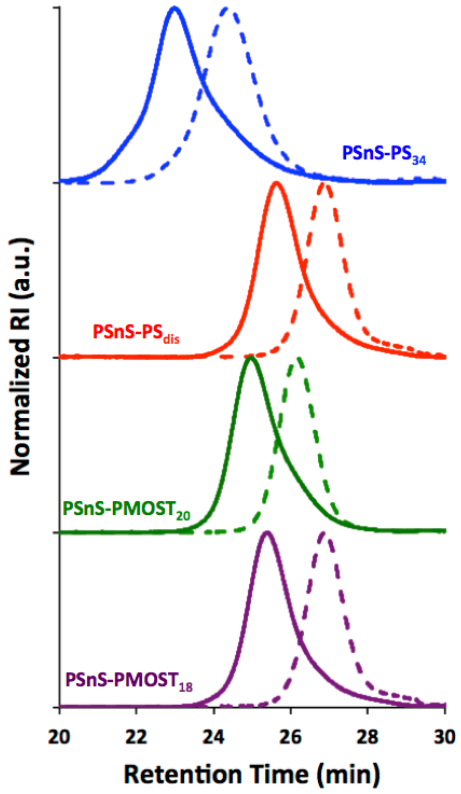

Figure 9.4: SEC traces of the PSnS-PS or PSnS-PMOST (solid lines) and their corresponding homopolymers (dashed lines).

Table 9.2 tabulates block copolymer characterization data for the polymers used in subsequent lithographic studies. PSnS-PS_{34}, PSnS-$PMOST_{20}$, and PSnS-$PMOST_{18}$ are ordered as evidenced by a sharp primary Bragg reflection (q*) at scattering wave vectors $q < 0.04$ Å^{-1} (Figure 9.5) in the small angle x-ray scattering experiment. Each sequence of higher order reflections (2q*, 3q*) is consistent with a lamellar morphology; PSnS-PS_{34} and PSnS-$PMOST_{20}$ exhibit the characteristic 2q* structure factor extinction expected for perfectly symmetric lamellae.[173] The lamella periodicity (L_0) was extracted from reciprocal space using the relationship derived from Bragg's law, $L_0=2p/q^*$. Herein, block copolymers are distinguished by their periodicity (e.g., PSnS-PS_{34}). While χ values were not measured for these polymers, the fact that PSnS-PS_{dis} and PSnS-$PMOST_{18}$ have nearly equivalent molar masses but different order parameters qualitatively suggests that PSnS-PMOST has the larger χ. This conclusion is comparable to the structure-property relationships elucidated with analogous silicon-containing block copolymers.[49]

Table 9.2: PSnS-PS and PSnS-PMOST characterization data

			Block Copolymer		
Sample	**PSnS M_n (kDa)[a]**	**PS or PMOST M_n (kDa)[b]**	**$Đ$**	**ϕ_{PSnS}[c]**	**L_0 (nm)**
PSnS-PS_{34}	36.3	24.5	1.31	0.54	34
PSnS-PS_{dis}	10.8	7.1	1.24	0.55	disordered
PSnS-$PMOST_{20}$	11.8	9.1	1.07	0.51	20
PSnS-$PMOST_{18}$	10.8	8.5	1.18	0.51	18

a: Determined by SEC
b: Determined by ^{1}H NMR
c: Calculated using $\rho_{PSnS} = 1.335$ g/cm^3, $\rho_{PS} = 1.050$ g/cm^3, $\rho_{PMOST} = 1.113$ g/cm^3

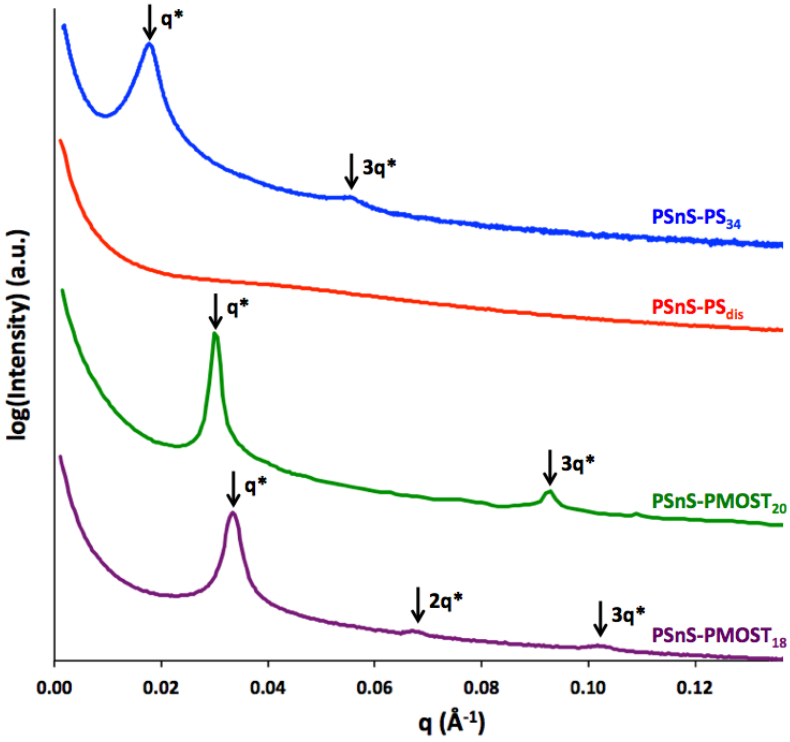

Figure 9.5: Synchrotron small angle x-ray scattering profiles of the block copolymers listed in Table 9.2.

9.4 Thin Film Self-Assembly

Similar to most block copolymers, tin-containing block copolymers do not spontaneously form perpendicular domains when annealed in thin films due to disparate surface energies of the two components. Therefore, thin film self-assembly was first optimized since perpendicular domain orientation is a requisite for subsequent pattern transfer. Figure 9.6A provides a summary of the materials utilized for orientation control. These materials are equivalent in chemistry but different in composition to those previously used for silicon-containing block copolymers. Neutral substrate surface treatments (XSTs) and top coats (TCs) were identified using established island/hole

methodologies (see experimental).[70,115] Figure 9.6B illustrates the process used to control block copolymer domain orientation. A brief oxygen etch was used to remove the organic domains and produce contrast for SEM inspection. SEM micrographs (Figure 9.7) reveal a perpendicular orientation of block copolymer domains for PSnS-PS_{34}, PSnS-$PMOST_{20}$, and PSnS-$PMOST_{18}$ over a range of film thicknesses (1.5-2.0 L_0).

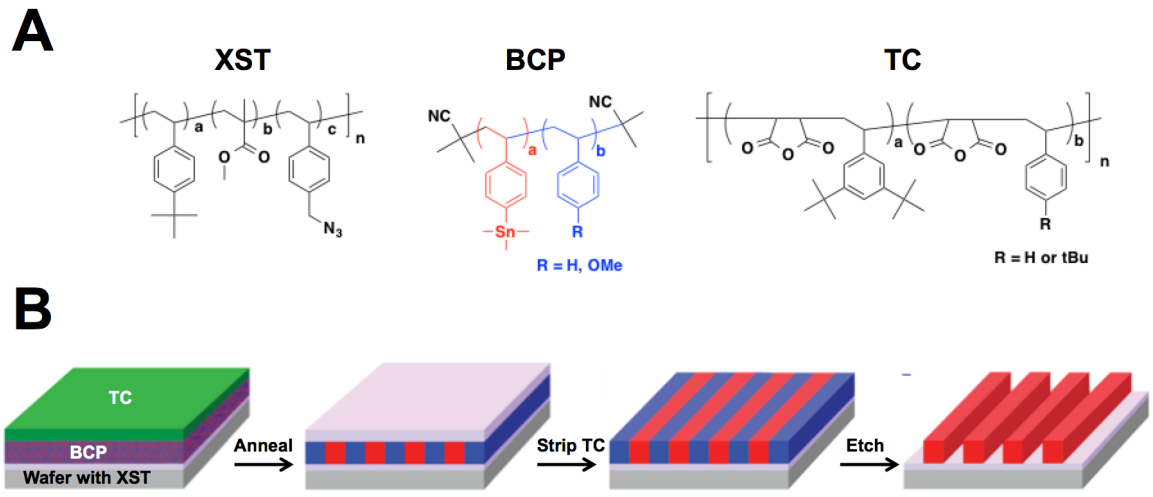

Figure 9.6: **(A)** Materials used in the present study. **(B)** Schematic of the process flow to develop block copolymer features for top down imaging.

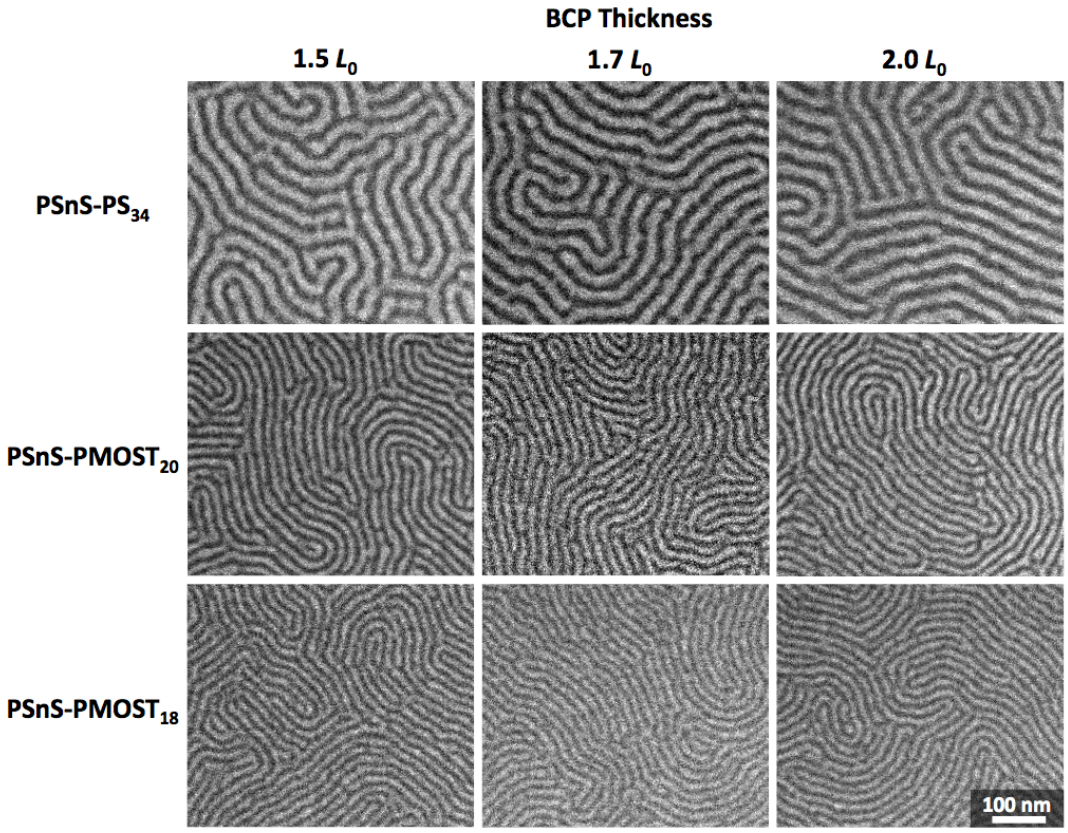

Figure 9.7: Top down SEM micrographs of block copolymer self-assembly. Samples were annealed at 180˚C for 10 min. The scale bar is valid for all micrographs.

9.5 ETCH PROPERTIES

The primary purpose of incorporating tin into the block copolymer was to create a robust etch mask to aid pattern transfer into an inorganic oxide. For this to be realized, PSnS must demonstrate etch resistance to both oxidizing (to remove the organic block) and fluorine (to transfer the pattern into SiO_2) plasma chemistries. Homopolymer etch studies were used to guide the development of block copolymer etch recipes, which were later optimized for dry development and pattern transfer. Etch studies of PS, PMOST,

PSnS, and poly(4-trimethylsilylstyrene) (PTMSS) using the same etch recipes that are later used with the block copolymers are reported in Figure 9.8. Importantly, comparisons are drawn with a silicon-containing polymer (PTMSS). PTMSS is analogous in structure to PSnS and was used in lieu of the more commonly studied poly(dimethylsiloxane) (PDMS), which is not glassy at room temperature and is known to be etchable when exposed to fluorine-containing plasmas.[44,174] Under oxidizing etch conditions (Figure 9.8A), both PTMSS and PSnS form etch barriers upon oxidation and show high steady-state etch selectivity relative to PS and PMOST. This implies that complete selective removal of the organic block from either PSnS or PTMSS block copolymers is possible, both confirming previous studies on Si-block copolymers and establishing equivalent performance with Sn-containing polymers. In order to efficiently transfer the relief pattern into SiO_2, oxidized block copolymer domains must etch slower than SiO_2 when exposed to fluorine-containing etch chemistry. Therefore, the etch rates under fluorine etch conditions were studied after a brief oxidative etch to simulate pattern transfer conditions (Figure 9.8B). SiO_2 etches faster than all four homopolymers and PSnS etches the slowest (Table 9.3). The improved selectivity of PSnS relative to Si-containing and organic polymers shows that PSnS is the best candidate to directly pattern SiO_2.

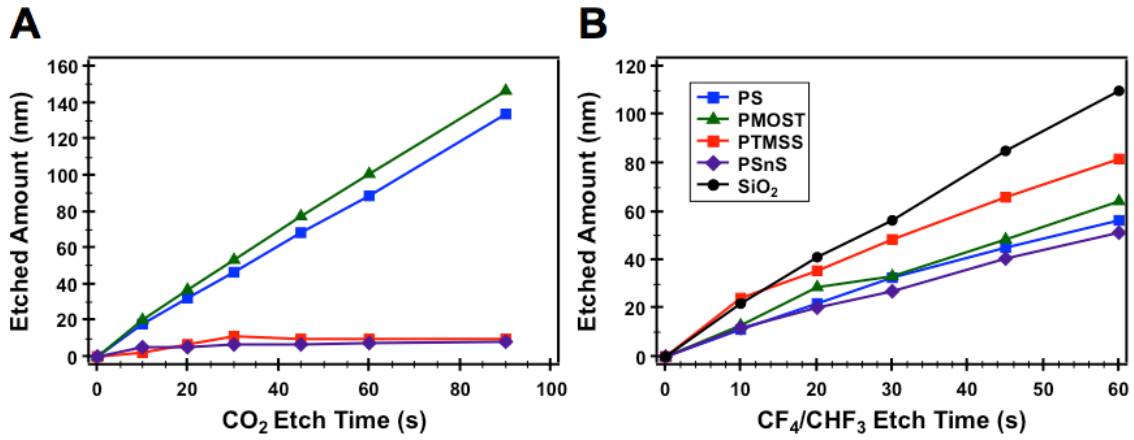

Figure 9.8: **A)** Homopolymer etch plot with oxidative (CO_2) etch conditions. **B)** Homopolymer etch plot with CF_4/CHF_3 plasma after a brief CO_2 etch.

Table 9.3: Homopolymer steady-state etch rates compared to SiO_2

Polymer	CO_2 Etch Rate (nm/s)*	CF_4/CHF_3 Etch Rate (nm/s)*	Selectivity to SiO_2
PS	1.44 ± 0.02	0.90 ± 0.12	2.0
PMOST	1.58 ± 0.03	0.98 ± 0.21	1.8
PTMSS	0.07 ± 0.14	1.15 ± 0.08	1.5
PSnS	0.04 ± 0.03	0.79 ± 0.06	2.2
SiO_2	N/A	1.76 ± 0.09	1.0

*Calculated at 95% confidence.

X-ray photoelectron spectroscopy (XPS) was used to quantify the elemental surface composition *before* and *after* the plasma exposure. After oxidation with CO_2, the surface exhibits an enrichment of Sn and oxygen and a sharp decrease in carbon in the PSnS sample (Figure 9.9). XPS spectra reveal the formation of tin oxides (SnO_x) at the surface (Figure 9.10), which explains the effective etch barrier observed during CO_2 etching. Note that a small amount of fluorine is detected on the surface even though no

fluorine-containing gas was used. This is a common artifact that arises from etch chamber cross-contamination with fluorine-containing gases used in separate experiments. Figure 9.8 also shows the elemental composition after exposure to CO_2 followed by CF_4/CHF_3 etch chemistries. The increase in fluorine at the surface is larger than the artifact observed in the non-fluorine-containing etch runs. The F-bonding state exists predominately as the fluoride and fluorocarbon, which is known to be deposited during CF_4/CHF_3 etching as a polymerization (Figure 9.11). The percent composition at the surface provides evidence that there are significant quantities of sub-fluorides forming on the surface (SnF_x and $SnOF_x$) but probably not appreciable levels of SnF_4. The etch barrier formed by sub-fluorides could explain why the etch rate for PSnS is less than PTMSS and PS during the CF_4/CHF_3 etch. However, the fact that a complete etch stop is not formed seemingly implies that the sub-fluorides are less stable or are more porous to the etch conditions than presumably solid SnF_4. Further increasing the etch performance of Sn-containing polymers should be possible by changing the process gases to bias the production of SnF_4. Regardless, PSnS provides a significant advantage in etch selectivity versus all tested materials, including oxygen-resistant PTMSS.

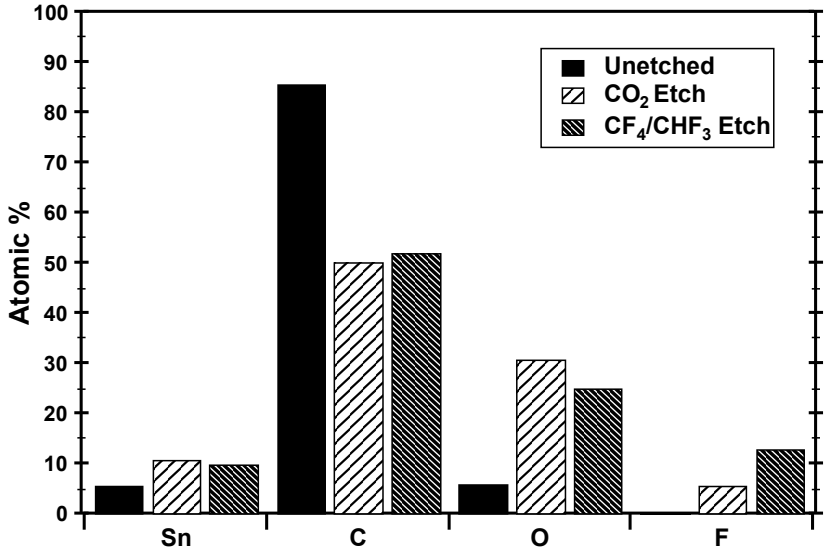

Figure 9.9: Elemental compositions at the surface of PSnS films determined by XPS. Films before and after exposure to CO_2 oxidative and fluorine-containing chemistries.

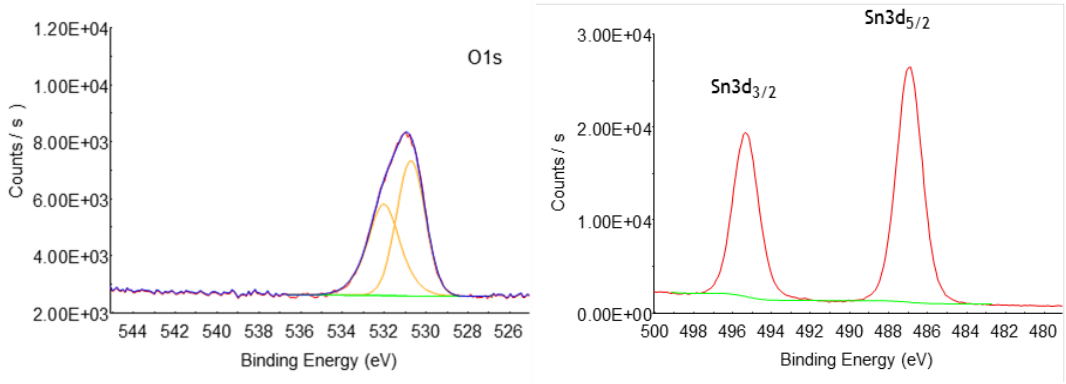

Figure 9.10: High energy resolution O1s and Sn3d XPS spectra provide additional insight about surface chemistry after CO_2 etch process. Binding energies and peak shapes are consistent with the formation of SnO_x species at the surface.

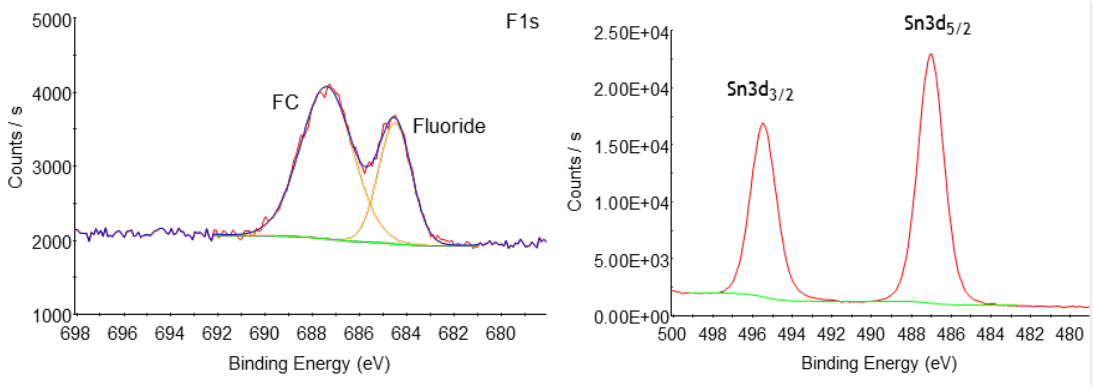

Figure 9.11: High energy resolution F1s and Sn3d XPS spectra are shown after the CF_4/CHF_3 etch step. Evidence of fluorocarbon and metal fluorides are observed. Binding energies and peak shapes are consistent with SnF_x, SnO_xF_y, and SnO_x formation.

9.6 Pattern Transfer Attempt

A two-step etch process was used to pattern transfer PSnS-PS_{34}, PSnS-$PMOST_{20}$, PSnS-$PMOST_{18}$ into a thick layer of silicon oxide (ca. 160 nm, prepared by deposition of tetraethylorthosilicate). The 10 nm XST thickness was not optimized in this study; to minimize the effects of etch rate differences and/or etch isotropy, the thickness could be further reduced to circa 3–5 nm.[149] Additionally, the C:F ratio in the plasma can be tuned to protect the sidewalls during the etch. The block copolymer thicknesses were 1.5 L_0 for PSnS-PS_{34} and PSnS-$PMOST_{20}$ and 2.0 L_0 for PSnS-$PMOST_{18}$. A CO_2 oxidizing etch was used to completely remove the PS or PMOST domains and underlying neutral layer. Tilted SEMs demonstrate residual tin etch mask remaining after the CO_2 etch (Figure 9.12, left side). Exposed SiO_2 in the trenches confirms that the oxidizing etch has cleared the organic block copolymer block. A CF_4-enriched etch was subsequently used to etch into the SiO_2. Evidence of full pattern transfer is shown on the right side of Figure 9.12. The pattern depth transferred was approx. 50 nm for PSnS-PS_{34} and approx. 20-25 nm for

PSnS-PMOST$_{20}$ and PSnS-PMOST$_{18}$ before the remaining block copolymer etch mask was sputtered away. The width of each trench was measured to be approximately 0.5 L_0. The sidewall profile shows good pattern transfer fidelity for all three pitches and the quality of the transfer is similar to that observed with Si-containing block copolymers produced with image transfer layers.[146] In the smaller pitches, the top of the features shows some roughness, which would need to be improved if used for fabrication. Any residual tin-block can be removed via hydrogen-containing plasmas. A hydrogen-containing clean etch did not change the image quality of Figure 9.12, which suggests that the tin etch mask was completely depleted during the pattern transfer. Overall, these results demonstrate the proof of concept that tin-containing block copolymers are capable of serving as an etch mask for pattern transfer into SiO_2.

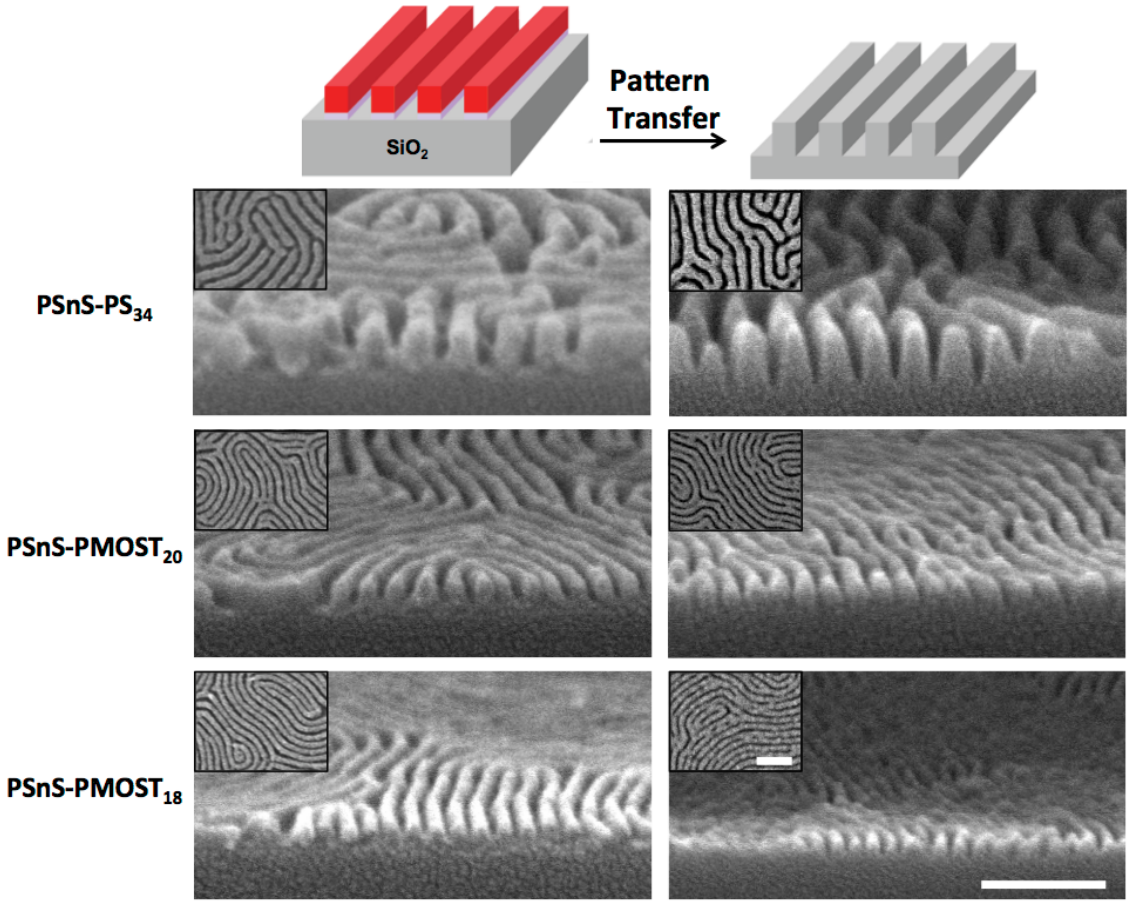

Figure 9.12: Schematic and SEMs of the pattern transfer step of the block copolymers used in this study. **Left)** SEMs after complete removal of the organic domains via CO_2 etch. **Right)** SEM after transfer into SiO_2 with $CF_4/CHF_3/Ar/O_2$ etch conditions. **In-sets)** Top down SEM images. Scale bars represent 100 nm and are valid for each tilted or top down SEM, respectively.

9.7 Conclusions

A series of new tin-containing block copolymers was synthesized by RAFT polymerization. These polymers form lamellar features with bulk periodicities spanning 18-34 nm. The orientation of the domains was controlled via thermal annealing between

neutral bottom and top interfaces. The tin-containing block is more resistant to both oxidizing and fluorine-based etch chemistries than organic and Si-containing polymers, and the products of the etch process were studied by XPS. A two-step etch process using CO_2 and $CF_4/CHF_3/Ar/O_2$ was developed to enable pattern transfer of PSnS-$PS_{34,}$ PSnS-$PMOST_{20}$, and PSnS-$PMOST_{18}$ into SiO_2. Oxide aspect ratios ≥3:1 prove the feasibility of using tin-containing block copolymers for pattern transfer and foreshadow improvements in lithographic patterning processes aided by new material design strategies.

9.8 EXPERIMENTAL

9.8.1 Instrumentation

Gel permeation Chromatography (GPC) measurements were performed on an Agilent 1100 Series Isopump and Autosampler with a Viscotek Model 302 TETRA detector. Tetrahydrofuran was used as the eluent, and the flow rate was 1 mL/min. SAXS data were conducted at Argonne National Lab on beamline 12-ID. SEM images were taken with a Zeiss Supra 40 VP. ^{1}H and ^{13}C NMR spectra were collected on a VARIAN 400 MHz instrument. Thin film IR transmission spectra were collected on a Nicolet Avatar 360 FT-IR. Molecular distributions are relative to PS standards. The dn/dc value used was 0.2027, which corresponds to the PSnS homopolymer.

9.8.2 Reagents

4-Chlorostyrene was purchased from Synquest. Magnesium, magnesium sulfate, trimethyltin chloride, trimethyl(phenyl)tin, styrene, 2-cyano-2-propyl dodecyl trithiocarbonate, 2-phenyl-2-propyl benzodithioate and 2,2'-azobis(2-methylpropionitrile)

were purchased from Sigma-Aldrich. 1,2-Dibromoethane was purchased from Lancaster. 4-Methoxystyrene was purchased from Alfa Aesar. Hexane, methanol, and THF were purchased from Fisher Scientific. All chemicals above were used without further purification unless otherwise noted. 4-Chlorostyrene was purified by distillation. Monomers were passed through basic alumina columns to remove inhibitor. Tetrahydrofuran was filtered through an activated alumina column.

9.8.3 Monomer Synthesis

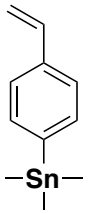

4-trimethylstannylstyrene- A 1-liter 3-neck round bottom glass flask was equipped with a 250 mL addition funnel and a condenser under nitrogen. Magnesium (8.3 g, 0.341 mol), dibromoethane (0.2 mL) and anhydrous tetrahydrofuran (50 mL) were added to the flask. The solution was stirred at 60 °C for 1.5 hours. A solution of 4-chlorostyrene (31.5 g, 0.227 mol) in tetrahydrofuran (150 mL) solution was added via addition funnel slowly for 1 hr. under a constant flow of nitrogen gas. The solution was stirred at 60 °C for additional 1.5 hr. The solution was cooled gradually at 0 °C. Trimethylstannyl chloride (43.0 g, 0.216 mol) in tetrahydrofuran (30 mL) solution was added to the solution slowly for 0.5 hr. The solution was warmed to room temperature and stirred for an additional 1.5 hr. The solution was cooled back to 0˚C and water (100 mL) was added slowly to the solution. The solution was warmed to room temperature and hexane (200 mL) was added. The solution was stirred for 15 min and filtered. The organic layer was separated and washed two times with water (30 mL), and then dried over magnesium sulfate, and concentrated via rotary evaporation. The crude product was purified by distillation at 1 Torr and 105

°C to give 44.4 g of 4-trimethylstannylstyrene as a colorless liquid. GC spectra showed 99.5% purity. The yield of the reaction was 73 %. ^{1}H NMR ($CDCl_3$): δ = 7.39 (m, 1H), 6.70 (dd, J = 20 Hz, J = 12 Hz, 1H), 5.77 (d, J = 20 Hz, 1H), 5.24 (d, J = 12 Hz, 1H), 0.28 (t, J = 24 Hz, 9H). ^{13}C NMR ($CDCl_3$): δ = 142.09, 137.47, 136.94, 136.00, 125.75, 113.79, -9.57. HRMS (CI) m/z for $[M]^+$ calcd for $C_{11}H_{16}Sn$ 268.0274; found for 268.0283(^{120}Sn), also found for 264.0256 (^{116}Sn) and 266.0273(^{118}Sn).

9.8.4 Homopolymer Synthesis

Poly(4-trimethylstannyl styrene) (PSnS). Method A: A mixture of 4-trimethylstannylstyrene (3.30 g, 12.4 mmol), 2-cyano-2-propyldodecyltrithiocarbonate (19.0 mg, 0.055 mmol), and 2,2'-azobis(2-methylpropionitrile) (1.1 mg, 0.006 mmol) was added to a 25 mL round bottom flask with a condenser and degassed by two freeze-pump-thaw cycles. The solution was stirred at 110 °C under nitrogen for 24 hours. The reaction mixture was dissolved in tetrahydrofuran (3 mL), precipitated into methanol (250 mL) twice, and dried to give PSnS as a white powder (2.15 g, 65% yield). The dn/dc value was determined to be 0.2027 by GPC.

Poly(4-trimethylstannyl styrene) (PSnS). Method B: A mixture of 4-trimethylstannyl styrene (3.02 g, 11.3 mmol), and 2-cyano-2-propyldodecyltrithiocarbonate (12.5 mg, 0.036 mmol) was added to a 250 mL round bottom flask and degassed by two freeze-pump-thaw cycles. The solution was stirred at 110 °C under nitrogen, and *tert*-butyl peroxybenzoate (0.3 mg, 0.002 mmol) dissolved in 0.5 g *p*-xylenes was slowly added to the solution with syringe pump for 3 hours and then stirred for 21 hours. The reaction mixture was dissolved in tetrahydrofuran (20 mL),

precipitated into methanol (500 mL) twice, and dried to give PSnS a white powder (1.00 g, 33% yield).

9.8.5 Block Copolymer Synthesis

Poly(4-trimethylstannyl styrene)-*b*-polystyrene (PSnS-PS). A mixture of PSnS (0.760 g), styrene (1.527 g, 14.7 mmol), and 2,2'-azobis(2-methylpropionitrile) (0.2 mg, 0.001 mmol) was added to 25 mL round bottom flask with a condenser, and then were degassed by two freeze-pump-thaw cycles, was stirred at 110 °C under nitrogen for 7 hours. The solidified reaction mixture was dissolved in tetrahydrofuran (5 mL) and precipitated into methanol (100 mL) two times, and then dried to give PSnS-PS (1.21 g) as white powder. The M_w and Đ were 85.4 kDa and 1.31, respectively.

Poly(4-trimethylstannylstyrene)-*b*-poly(4-methoxystyrene) (PSnS-PMOST). A mixture of PSnS (0.392 g), 4-methoxystyrene (0.745 g, 5.55 mmol), and 2,2'-azobis(2-methylpropionitrile) (0.7 mg, 0.004 mmol) was added to 25 mL round bottom flask with a condenser and was degassed by two freeze-pump-thaw cycles. Then, the solution was stirred at 110 °C under nitrogen for 2 hours. The solidified reaction mixture was dissolved in tetrahydrofuran (2 mL) and precipitated into methanol (100 mL) two times, and dried to give PSnS-PMOST (0.53 g) as white powder. The M_w was calculated to be 21.4 kDa, and the Đ of 1.18.

Removal of RAFT End Groups. The RAFT end groups were removed for thin film studies using a previously reported method[59]. Approximately 1 g of block copolymer was dissolved in toluene with 20 eq. of AIBN. The solution was heated to 80°C for 8 hrs.

The solution was cooled to room temperature, precipitated in methanol, filtered and dried *in vacuo*.

Table 9.4: Additional block copolymer synthetic details and characterization data

				block copolymer				
Sample	**PSnS M_n[a]**	**(Mon2/ PSnS)[b]**	**Time (hr)**	**Yield**	**PS/PMOST M_n[c]**	**Đ**	**T_g (˚C)**	**T_d (˚C)**
PSnS-PS_{34}	36.3	2.0	7	53%	24.5	1.31	107, 115	297
PSnS-PS_{dis}	10.8	1.5	2.5	51%	7.1	1.24	105, 115	260
PSnS-$PMOST_{20}$	11.8	2.0	2	60%	9.1	1.07	100, 115	261
PSnS-$PMOST_{18}$	10.8	2.0	2	46%	8.5	1.18	106, 114	257

a: Determined by SEC
b: Mon2 is either styrene or 4-methoxystyrene. Mass ratio
c: Determined by NMR

9.8.6 Neutral XST and TC Composition

Table 9.5: Composition of the neutral interfaces

	XST Composition (%)*			**TC Composition (%)***			
Block copolymer	tBuSty	Sty	VBzAz	MA	tBuSty	ditBuSty	Sty
PSnS-PS	46	46	8	52	0	12	36
PSnS-PMOST	34	60	6	50	50	0	0

*determined by combustion
Abbreviations: tBuSty = 4-*tert*-butylstyrene, Sty = styrene, VBzAz = 4-vinylbenzylazide, MA = maleic anhydride, ditBuSty = 3,5-di-*tert*-butylstyrene

9.8.7 Neutral XST Screening

Neutral top and bottom interfaces were found using previously reported materials and methodology.[70,115]

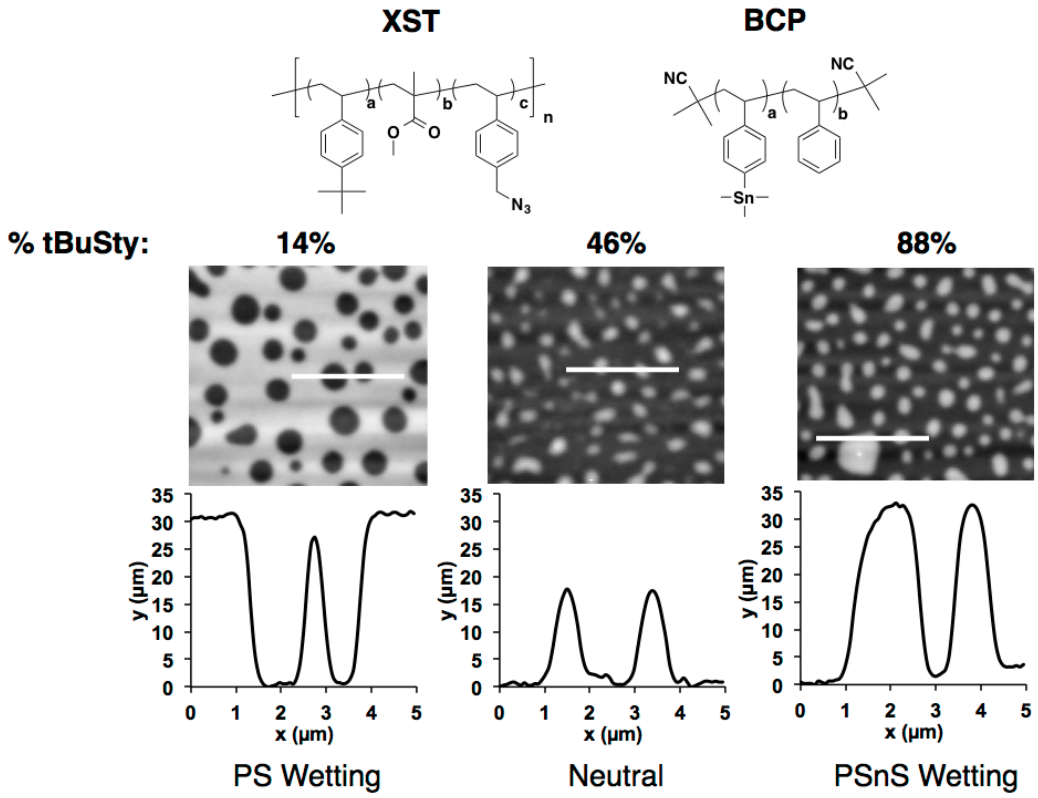

Figure 9.13: Atomic force micrographs of the surface topography formed after annealing PSnS-PS_{34} on different XST surface treatments. The height profiles collected using tapping mode are shown. The block copolymer film thicknesses are between 1-1.5 L_0 and were baked at 180˚C for 10 minutes. The "half" islands formed on the 46% tBuSty XST are indicative of a neutral surface.

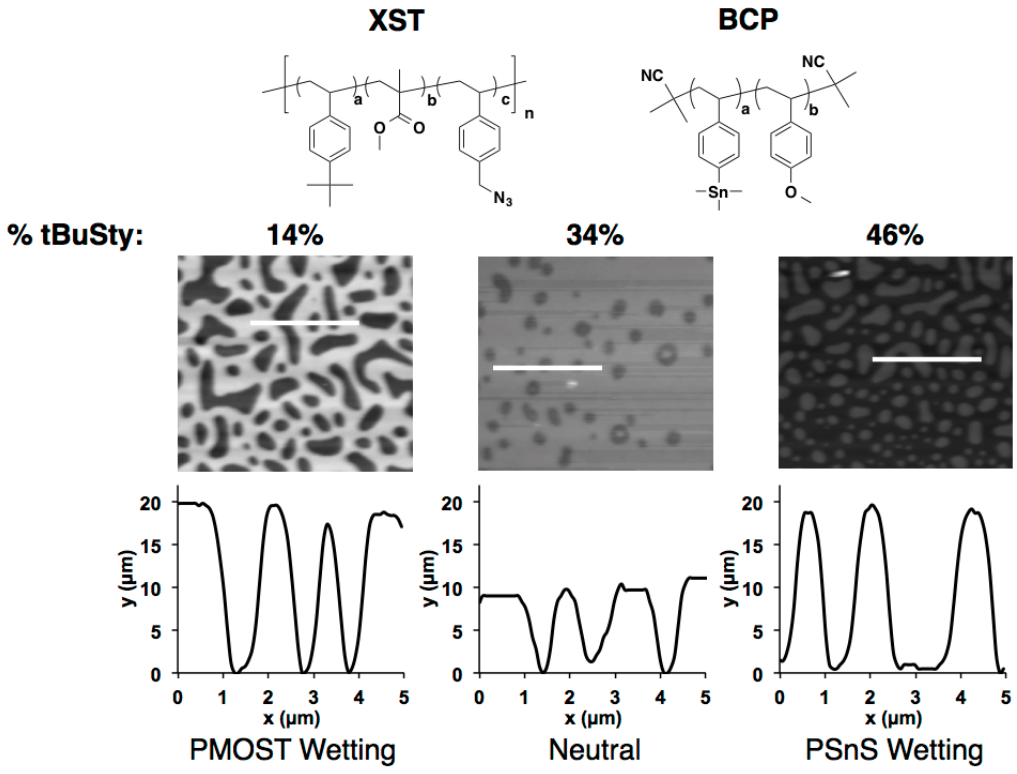

Figure 9.14: Atomic force micrographs of the surface topography formed after annealing PSnS-PMOST$_{20}$ on different XST surface treatments. The height profiles collected using tapping mode are shown. The block copolymer film thicknesses are between 1-1.5 L_0 and were baked at 180˚C for 10 minutes. The "half" holes formed on the 34% tBuSty XST are indicative of a neutral surface.

9.8.8 Etching

Plasma etching was performed on a commercial 300mm capacitively coupled plasma reactor, Lam Research Exelan® Flex45™, which contains confined plasma technology and multisource RF frequencies applied to the bottom electrode. For etch rate and block copolymer pattern transfer tests, coupons (2000 mm^2) coated with either homopolymer or assembled block copolymer patterns were thermally pasted (Type 120

Silicone, Wakefield Solutions) onto the center of 300mm 248nm DUV resist carrier wafers. SiO_2 coupons were prepared in a similar fashion. For pattern transfer tests using block copolymer masks, CF_4-rich plasma chemistry was used for all of the samples. For the largest pitch block copolymer sample, CHF_3 was added to the CF_4. For the smallest pitch samples, Ar and O2 were added and the gas ratios were adjusted in order to obtain an acceptable profile.

9.8.9 XPS

Angle resolved x-ray photoelectron spectroscopy (ARXPS) was used to explore post etch surface chemistry modifications of block copolymers. XPS spectra were collected using a Thermo Fisher Scientific Theta 300 ARXPS instrument utilizing a monochromatic Al ka x-ray source (hn=1486.6eV) and an electron energy analyzer operating in a high energy resolution mode with a constant pass energy of 50eV.

9.9 ACKNOWLEDGEMENTS

The work in this chapter has been in development for a very long time. Jeff Strahan initiated this project. Kazunori Mori found synthetic conditions for the tin-containing block copolymers. Special recognition must be given to Kazu for his hard work, which led to the first demonstration of orientation control of tin-containing block copolymers thin films. Andrew Dinhobl significantly contributed to the monomer and block copolymer synthesis in this chapter. Steve Sirard from Lam developed etch recipes for the pattern transfer experiments. Emir Gurer from Lam provided the XPS data.

Chapter 10: Summary and Outlook

10.1 SUMMARY

In Chapter 1, a series of goals was presented for this dissertation. These goals were aimed at overcoming the material design and process challenges associated with block copolymer lithography. A summary of these goals is listed below:

- Synthesize high-χ silicon-containing block copolymers that form sub-10 nm domains
- Synthesize surface treatments to control the interfacial interactions between the block copolymer domains and the substrate
- Develop a strategy to control the interfacial interactions between the block copolymer and free interface
- Develop methods to determine surface treatment and top coat wetting preference
- Demonstrate etch selectivity and pattern transfer of the block copolymer domains
- Control the long-range alignment of block copolymer domains by directed self-assembly techniques

The work presented in this dissertation has been the result of a large collaborative effort, and the author is extremely grateful to all those who contributed to the success of these projects. The author is also proud to report that all of the aforementioned goals have been successfully achieved. Silicon-containing block copolymers that have L_0 values as low as 10 nm have been reported. Neutral surface treatments and top coats were

identified for these block copolymers using island and hole methodology. Then, orientation control of block copolymer domains was achieved by annealing the block copolymer between these neutral surface treatments and top coats. Importantly, orientation control was demonstrated on the sub-1 minute timescale via thermal annealing. The process is fast and relies on equipment/processes that already exist in nanofabrication facilities. Collaborative efforts with industrial partners have shown that the silicon-containing block copolymers synthesized at the University of Texas at Austin can be aligned by directed self-assembly (DSA) using techniques amenable to high volume manufacturing. The self-assembled block copolymers can be used as an etch mask, and successful pattern transfer of some of the smallest lamellar features to date have been reported herein.

10.2 OUTLOOK

Over the past decade, major advances in the field are facilitating a transition from "lab to fab." However, there are still major challenges with block copolymer lithography. The goal of this section is to briefly report some of the remaining challenges to be addressed in the field.

10.2.1 Defectivity

The successful integration of block copolymer lithography with high volume microelectronic manufacturing depends highly on defect reduction. Currently, the number of defects per unit area is too high. However, the critical tolerance level of defects per area is not well-defined. Standardization of the critical number of defects per area must be agreed upon within the lithographic community. Another challenge is

identifying and quantifying the number of defects per area. Currently, the metrology used for block copolymer lithography is premature. To further complicate the matter, the block copolymer domains form structures that are near the resolution limit of most scanning electron microscopes.

10.2.2 Understanding the DSA Mechanism

Understanding how the block copolymer domains interact with guiding features is critical for optimizing DSA and minimizing defects. In this dissertation, chemo-epitaxy was demonstrated using HSQ guidelines that were approximately 0.5 L_0 in width. As in the case of all chemo-epitaxy demonstrations, the guide lines were not perfectly planar and had topography. The topography complicates the DSA mechanism because there are now sidewalls to consider. The DSA is a result of a combination of shallow trench grapho-epitaxy and chemical affinity for each surface. Currently, cross-sectional transmission electron microscopy (TEM) in tandem with electron energy loss spectroscopy (EELS) is being used to study the block copolymer and guide line interactions. In particular, this provides a way to study the through-film profile of the domains. The goal is to better understand these interactions in order to optimize guideline dimensions (shape, width, height, sidewall profile, sidewall chemistry, etc.).

Another challenge that faces the block copolymer lithographic community is determining neutral layers for the interstitial regions between guide lines. On neutral surfaces, both block copolymer domains make contact with the substrate. For DSA, the surface between the guide lines needs to be neutral. However, unequal block coverage (e.g. three A domains and two B domains) occurs in these interstitial regions, which means slightly off-neutral materials are needed. Methods that could determine neutrality

for regions that have unequal block cover coverage would be of tremendous value. These methods would need to consider the degree of preference with the guide line as well. The interfacial properties of the guide line and interstitial region combined need to be neutral.

Most DSA strategies use "preferential" guide lines to direct long range alignment. The term "preferential" is perhaps misleading. The nomenclature implies that the guideline prefers to interact with one of the block copolymer domains. However, this does not necessarily mean that it is energetically favorable for the guide line to interact with one of the block copolymer domains. More correctly, "preferential" to one domain means that one of the domains pays a smaller energetic penalty for forming a surface on the guide line. There is a *positive* interaction parameter (χ) between both block copolymer domains and the guide line. It would be interesting to study DSA using guidelines that exhibit a *negative* interaction parameter, which would mean that it would be energetically favorable for interaction between one of the domains and the guide line. Guide lines of this type might create more thermodynamically favored DSA, which could potentially lead to less defects and faster defect annihilation times.

10.2.3 Block Copolymer Uniformity

There are some concerns about block copolymer batch-to-batch uniformity. No two batches of polymer are the same even if all the characterization data are identical. The effect of polymer dispersity and molecular weight needs to be studied further. If a new batch of block copolymer is introduced, do all of the processes need to be adjusted to obtain uniform nanostructures with low defectivity? This problem will certainly need to be addressed prior to industrial adaptation.

10.2.4 DSA for sub-5 nm Features

The DSA of block copolymer domains will not replace optical lithography. However, it can be used to supplement lithography and possibly be used to achieve feature sizes that are far too expensive to pattern otherwise. The ultimate goal is to demonstrate DSA of sub-5 nm features. In this dissertation, a polymer that could form sub-5 nm lamellae was reported. This polymer could be selectively etched with excellent pattern fidelity. Achieving the DSA of these features is currently being explored, which is a major challenge because guide lines on the order of 0.5 L_0 are not possible. The DSA will likely require combining chemo-epitaxy with grapho-epitaxy. Recently, imprint lithography was used to demonstrate the DSA of these sub-5 nm features. These results are anticipated to be published in the near feature. When reported, this will be the DSA of the smallest lamellar block copolymer using a patterning method amenable to high volume manufacturing.

Bibliography

(1) Copeland, B. J. "Colossus: Its Origins and Originators." *IEEE Annals of the History of Computing* **2004**, *26*, 38–45.

(2) Sale, A. E. "The Rebuilding of Colossus at Bletchley Park." *Annals of the History of Computing* **2005**, *27*, 61–69.

(3) Hoddeson, L. "The Discovery of the Point-Contact Transistor." *Hist. Stud. Phys. Sci.* **1981**, *12*, 41–76.

(4) Kilby, J. S. "Invention of the Integrated Circuit." *IEEE Trans. Electron Devices* **1976**, *23*, 648.

(5) Mack, C. "Fifty Years of Moore's Law." *IEEE Trans. Semicon. Manufact.* **2011**, *24*, 202–207.

(6) Ferain, I.; Colinge, C. A.; Colinge, J.-P. "Multigate Transistors as the Future of Classical Metal–Oxide–Semiconductor Field-Effect Transistors." *Nature* **2011**, *479*, 310–316.

(7) Mack, C. *Fundamental Principles of Optical Lithography: the Science of Microfabrication*; John Wiley & Sons: London, 2007.

(8) Wagner, C.; Harned, N. "EUV Lithography: Lithography Gets Extreme." *Nature Photonics* **2010**.

(9) Mallik, A.; Ryckaert, J.; Mercha, A. "Maintaining Moore's Law: Enabling Cost-Friendly Dimensional Scaling." *Proc. SPIE* **2015**, *9422*, 94221N.

(10) Pirati, A.; Peeters, R.; Smith, D.; Lok, S.; Minnaert, A.; van Noordenburg, M.; Mallmann, J.; Harned, N.; Stoeldraijer, J.; Wagner, C.; Zoldesi, C.; van Setten, E.; Finders, J.; de Peuter, K.; de Ruijter, C.; Popadic, M.; Huang, R.; Lin, M.; Chuang, F.; van Es, R.; Beckers, Ml; Brandt, D.; Farrar, N.; Schafgans, A.; Brown, D.; Boom, H.; Meiling, H.; Kool, R. "Performance Overview and Outlook of EUV Lithography Systems." *Proc SPIE* **2015**; *9422*, 94221P.

(11) Yaegashi, H.; Oyama, K.; Hara, A. "Recent Progress on Multiple-Patterning Process." *Proc. SPIE* **2015**, *9425*, 942502.

(12) Bates, F. S.; Fredrickson, G. H. "Block Copolymer Thermodynamics: Theory and Experiment." *Annu. Rev. Phys. Chem.* **1990**, *41*, 525–557.

(13) Bates, C. M.; Maher, M. J.; Janes, D. W.; Ellison, C. J.; Willson, C. G. "Block Copolymer Lithography." *Macromolecules* **2014**, *47*, 2–12.

(14) Matsen, M. W. "The Standard Gaussian Model for Block Copolymer Melts." *J. Phys. Condens. Matter* **2002**, *14*, R21–R47.

(15) Cochran, E. W.; Garcia-Cervera, C. J.; Fredrickson, G. H. "Stability of the Gyroid Phase in Diblock Copolymers at Strong Segregation." *Macromolecules* **2006**, *39*, 2449–2451.

(16) Sinturel, C.; Vayer, M.; Morris, M.; Hillmyer, M. A. "Solvent Vapor Annealing of Block Polymer Thin Films." *Macromolecules* **2013**, *46*, 5399–5415.

(17) Ouk Kim, S.; Solak, H. H.; Stoykovich, M. P.; Ferrier, N. J.; de Pablo, J. J.; Nealey, P. F. "Epitaxial Self-Assembly of Block Copolymers on

Lithographically Defined Nanopatterned Substrates." *Nature* **2003**, *424*, 411–414.
(18) Morkved, T. L.; Lu, M.; Urbas, A. M.; Ehrichs, E. E.; Jaeger, H. M.; Mansky, P.; Russell, T. P. "Local Control of Microdomain Orientation in Diblock Copolymer Thin Films with Electric Fields." *Science* **1996**, *273*, 931–933.
(19) Rockford, L.; Liu, Y.; Mansky, P.; Russell, T. P.; Yoon, M.; Mochrie, S. G. J. "Polymers on Nanoperiodic, Heterogeneous Surfaces." *Phys. Rev. Lett.* **1999**, *82*, 2602–2605.
(20) Bodycomb, J.; Funaki, Y.; Kimishima, K.; Hashimoto, T. "Single-Grain Lamellar Microdomain From a Diblock Copolymer." *Macromolecules* **1999**, *32*, 2075–2077.
(21) Segalman, R. A.; Yokoyama, H.; Kramer, E. J. "Graphoepitaxy of Spherical Domain Block Copolymer Films." *Adv. Mater.* **2001**, *13*, 1152–1155.
(22) Cheng, J. Y.; Ross, C. A.; Thomas, E. L.; Smith, H. I.; Vancso, G. J. "Fabrication of Nanostructures with Long-Range Order Using Block Copolymer Lithography." *Appl. Phys. Letters* **2002**, *81*, 3657–3659.
(23) Yang, X. M.; Peters, R. D.; Nealey, P. F.; Solak, H. H.; Cerrina, F. "Guided Self-Assembly of Symmetric Diblock Copolymer Films on Chemically Nanopatterned Substrates." *Macromolecules* **2000**, *33*, 9575–9582.
(24) Ruiz, R.; Kang, H.; Detcheverry Francois, A.; Dobisz, E.; Kercher, D. S.; Albrecht, T. R.; de Pablo, J. J.; Nealey, P. F. "Density Multiplication and Improved Lithography by Directed Block Copolymer Assembly." *Science* **2008**, *321*, 936–939.
(25) Tsai, H.; Pitera, J. W.; Miyazoe, H.; Bangsaruntip, S.; Engelmann, S. U.; Liu, C.-C.; Cheng, J. Y.; Bucchignano, J. J.; Klaus, D. P.; Joseph, E. A.; Sanders, D. P.; Colburn, M. E.; Guillorn, M. A. "Two-Dimensional Pattern Formation Using Graphoepitaxy of PS-*b*-PMMA Block Copolymers for Advanced FinFET Device and Circuit Fabrication." *ACS Nano* **2014**, *8*, 5227–5232.
(26) Yi, H.; Bao, X.-Y.; Zhang, J.; Bencher, C.; Chang, L.-W.; Chen, X.; Tiberio, R.; Conway, J.; Dai, H.; Chen, Y.; Mitra, S.; Wong, H. S. P.; "Flexible Control of Block Copolymer Directed Self-Assembly Using Small, Topographical Templates: Potential Lithography Solution for Integrated Circuit Contact Hole Patterning." *Adv. Mater.* **2012**, *24*, 3107–3114.
(27) Doise, J.; Bekaert, J.; Chan, B. T.; Gronheid, R.; Cao, Y.; Hong, S.; Lin, G.; Fishman, D.; Chakk, Y.; Marzook, T. "Implementation of Surface Energy Modification in Graphoepitaxy Directed Self-Assembly for Hole Multiplication." *J. Vac. Sci., B* **2015**, *33*, 06F301.
(28) Lille, J.; Patel, K.; Ruiz, R.; Wu, T. W.; Gao, H.; Wan, L.; Zeltzer, G.; Dobisz, E.; Albrecht, T. R. "Imprint Lithography Template Technology for Bit Patterned Media (BPM)." *Proc. SPIE* **2011**, *8166*, 816626.
(29) Stoykovich, M. P.; Mueller, M.; Kim, S. O.; Solak, H. H.; Edwards, E. W.; de Pablo, J. J.; Nealey, P. F. "Directed Assembly of Block Copolymer Blends Into Nonregular Device-Oriented Structures." *Science* **2005**, *308*, 1442–1446.

(30) Stoykovich, M. P.; Kang, H.; Daoulas, K. C.; Liu, G.; Liu, C.-C.; de Pablo, J. J.; Müller, M.; Nealey, P. F. "Directed Self-Assembly of Block Copolymers for Nanolithography: Fabrication of Isolated Features and Essential Integrated Circuit Geometries." *ACS Nano* **2007**, *1*, 168–175.

(31) Costner, E. A.; Lin, M. W.; Jen, W.-L.; Willson, C. G. "Nanoimprint Lithography Materials Development for Semiconductor Device Fabrication." *Annu. Rev. Phys. Chem.* **2009**, *39*, 155–180.

(32) Yang, X.; Xiao, S.; Hu, W.; Hwu, J.; van de Veerdonk, R.; Wago, K.; Lee, K.; Kuo, D. "Integration of Nanoimprint Lithography with Block Copolymer Directed Self-Assembly for Fabrication of a Sub-20 nm Template for Bit-Patterned Media." *Nanotechnology* **2014**, *25*, 395301.

(33) Ruiz, R.; Dobisz, E.; Albrecht, T. R. "Rectangular Patterns Using Block Copolymer Directed Assembly for High Bit Aspect Ratio Patterned Media." *ACS Nano* **2011**, *5*, 79–84.

(34) Wan, L.; Ruiz, R.; Gao, H.; Patel, K. C.; Lille, J.; Zeltzer, G.; Dobisz, E. A.; Bogdanov, A.; Nealey, P. F.; Albrecht, T. R. "Fabrication of Templates with Rectangular Bits on Circular Tracks by Combining Block Copolymer Directed Self-Assembly and Nanoimprint Lithography." *J. Micro/Nanolithogr., MEMS, MOEMS* **2012**, *11*, 031405.

(35) Park, S.; Lee, D. H.; Xu, J.; Kim, B.; Hong, S. W.; Jeong, U.; Xu, T.; Russell, T. P. "Macroscopic 10-Terabit–Per–Square-Inch Arrays From Block Copolymers with Lateral Order." *Science* **2009**, *323*, 1030–1033.

(36) Zhao, Y.; Sivaniah, E.; Hashimoto, T. "SAXS Analysis of the Order–Disorder Transition and the Interaction Parameter of Polystyrene-*block*-Poly(methyl methacrylate)." *Macromolecules* **2008**, *41*, 9948–9951.

(37) Wan, L.; Ruiz, R.; Gao, H.; Patel, K. C.; Albrecht, T. R.; Yin, J.; Kim, J.; Cao, Y.; Lin, G. "The Limits of Lamellae-Forming PS-*b*-PMMA Block Copolymers for Lithography." *ACS Nano* **2015**, *9*, 7506–7514.

(38) Liu, Y.; Longo, D. M.; Hull, R. "Ultrarapid Nanostructuring of Poly(Methylmethacrylate) Films Using Ga^+ Focused Ion Beams." *Appl. Phys. Lett.* **2003**, *82*, 346.

(39) Jurgensen, C. W.; Shugard, A.; Dudash, N.; Reichmanis, E.; Vasile, M. J. "Experimental Tests of the Steady-State Model for Oxygen Reactive Ion Etching of Silicon-Containing Polymers." *J. Vac. Sci. Technol., A* **1988**, *6*, 2938–2944.

(40) Park, M.; Harrison, C.; Chaikin, P. M.; Register, R. A.; Adamson, D. H. "Block Copolymer Lithography: Periodic Arrays of ~1011 Holes in 1 Square Centimeter." *Science* **1997**, *276*, 1401–1404.

(41) Hempenius, M. A.; Lammertink, R. G. H.; Péter, M.; Vancso, G. J. "Poly(Ferrocenylsilanes) as Etch Barriers in Nano and Microlithographic Applications." *Macromol. Symp.* **2003**, *196*, 45–56.

(42) Peng, Q.; Tseng, Y.-C.; Darling, S. B.; Elam, J. W. "Nanoscopic Patterned Materials with Tunable Dimensions via Atomic Layer Deposition on Block

Copolymers." *Adv. Mater.* **2010**, *22*, 5129–5133.
(43) Ruiz, R.; Wan, L.; Lille, J.; Patel, K. C.; Dobisz, E.; Johnston, D. E.; Kisslinger, K.; Black, C. T. "Image Quality and Pattern Transfer in Directed Self Assembly with Block-Selective Atomic Layer Deposition." *J. Vac. Sci. Technol., B* **2012**, *30*, 06F202.
(44) Jung, Y.-S.; Ross, C. A. "Orientation-Controlled Self-Assembled Nanolithography Using a Polystyrene-Polydimethylsiloxane Block Copolymer." *Nano Lett.* **2007**, *7*, 2046–2050.
(45) Ross, C. A.; Jung, Y. S.; Chuang, V. P.; Ilievski, F.; Yang, J. K. W.; Bita, I.; Thomas, E. L.; Smith, H. I.; Berggren, K. K.; Vancso, G. J.; Cheng, J. Y.; "Si-Containing Block Copolymers for Self-Assembled Nanolithography." *J. Vac. Sci. Technol., B* **2008**, *26*, 2489–2494.
(46) Cushen, J. D.; Bates, C. M.; Rausch, E. L.; Dean, L. M.; Zhou, S. X.; Willson, C. G.; Ellison, C. J. "Thin Film Self-Assembly of Poly(Trimethylsilylstyrene-*b*-D, L-Lactide) with Sub-10 nm Domains." *Macromolecules* **2012**, *45*, 8722–8728.
(47) Cheng, J. Y.; Ross, C. A.; Chan, V. Z. H.; Thomas, E. L.; Lammertink, R. G. H.; Vancso, G. J. "Formation of a Cobalt Magnetic Dot Array via Block Copolymer Lithography." *Adv. Mater.* **2001**, *13*, 1174–1178.
(48) Kim, S. Y.; Gwyther, J.; Manners, I.; Chaikin, P. M.; Register, R. A. "Metal-Containing Block Copolymer Thin Films Yield Wire Grid Polarizers with High Aspect Ratio." *Adv. Mater.* **2014**, *26*, 791–795.
(49) Durand, W. J.; Blachut, G.; Maher, M. J.; Sirard, S.; Tein, S.; Carlson, M. C.; Asano, Y.; Zhou, S. X.; Lane, A. P.; Bates, C. M.; Ellison, C. J.; Willson, C. G.; "Design of High-X Block Copolymers for Lithography." *J. Polym. Sci., Part A: Polym. Chem.* **2015**, *53*, 344–352.
(50) Nunns, A.; Gwyther, J.; Manners, I. "Inorganic Block Copolymer Lithography." *Polymer* **2013**, *54*, 1269–1284.
(51) Chang, J.-B.; Son, J. G.; Hannon, A. F.; Alexander-Katz, A.; Ross, C. A.; Berggren, K. K. "Aligned Sub-10-nm Block Copolymer Patterns Templated by Post Arrays." *ACS Nano* **2012**, *3*, 2071-2077.
(52) Seshimo, T.; Bates, C. M.; Dean, L. M.; Cushen, J. D.; Durand, W. J.; Maher, M. J.; Ellison, C. J.; Willson, C. G. "Block Copolymer Orientation Control Using a Top-Coat Surface Treatment." *J. Photopolym. Sci. Technol.* **2012**, *25*, 125–130.
(53) Walton, D. G.; Kellogg, G. J.; Mayes, A. M.; Lambooy, P.; Russell, T. P. "A Free Energy Model for Confined Diblock Copolymers." *Macromolecules* **1994**, *27*, 6225–6228.
(54) Mansky, P.; Liu, Y.; Huang, E.; Russell, T. P.; Hawker, C. "Controlling Polymer-Surface Interactions with Random Copolymer Brushes." *Science* **1997**, *275*, 1458–1460.
(55) Mansky, P.; Russell, T. P.; Hawker, C. J.; Pitsikalis, M.; Mays, J. "Ordered

Diblock Copolymer Films on Random Copolymer Brushes." *Macromolecules* **1997**, *30*, 6810–6813.

(56) Huang, F.; Tian, Y.; Chen, C. Y.; Cheng, Y. J.; Young, C. A.; Jen, A. K. Y. "Cross-Conjugated Polymers with Large Two-Photon Absorption Cross-Sections for Metal Ion Sensing." *J. Phys. Chem. C* **2007**, *111*, 10673–10681.

(57) In, I.; La, Y.-H.; Park, S.-M.; Nealey, P. F.; Gopalan, P. "Side-Chain-Grafted Random Copolymer Brushes as Neutral Surfaces for Controlling the Orientation of Block Copolymer Microdomains in Thin Films." *Langmuir* **2006**, *22*, 7855–7860.

(58) Ryu, D. Y.; Shin, K.; Drockenmuller, E.; Hawker, C. J.; Russell, T. P. "A Generalized Approach to the Modification of Solid Surfaces." *Science* **2005**, *308*, 236–239.

(59) Bang, J.; Bae, J.; Löwenhielm, P.; Spiessberger, C.; Given-Beck, S. A.; Russell, T. P.; Hawker, C. J. "Facile Routes to Patterned Surface Neutralization Layers for Block Copolymer Lithography." *Adv. Mater.* **2007**, *19*, 4552–4557.

(60) Han, E.; Gopalan, P. "Cross-Linked Random Copolymer Mats as Ultrathin Nonpreferential Layers for Block Copolymer Self-Assembly." *Langmuir* **2010**, *26*, 1311–1315.

(61) Bates, C. M.; Strahan, J. R.; Santos, L. J.; Mueller, B. K.; Bamgbade, B. O.; Lee, J. A.; Katzenstein, J. M.; Ellison, C. J.; Willson, C. G. "Polymeric Cross-Linked Surface Treatments for Controlling Block Copolymer Orientation in Thin Films." *Langmuir* **2011**, *27*, 2000–2006.

(62) Peters, R. D.; Yang, X. M.; Kim, T. K.; Sohn, B. H.; Nealey, P. F. "Using Self-Assembled Monolayers Exposed to X-Rays to Control the Wetting Behavior of Thin Films of Diblock Copolymers." *Langmuir* **2000**, *16*, 4625–4631.

(63) Bencher, C.; Yi, H.; Zhou, J.; Cai, M.; Smith, J.; Miao, L.; Montal, O.; Blitshtein, S.; Lavi, A.; Dotan, K.; Dai, H.; Cheng, J. Y.; Sanders, D. P.; Tjio, M.; Holmes, S. "Directed Self-Assembly Defectivity Assessment. Part II." *Proc. SPIE*, **2012**, *8323*, 83230N.

(64) Liu, C.-C.; Thode, C. J.; Rincon Delgadillo, P. A.; Craig, G. S. W.; Nealey, P. F.; Gronheid, R. "Towards an All-Track 300 mm Process for Directed Self-Assembly." *J. Vac. Sci., B* **2011**, *29*, 06F203.

(65) Delgadillo, P. A. R.; Gronheid, R.; Thode, C. J.; Wu, H.; Cao, Y.; Somervell, M.; Nafus, K.; Nealey, P. F. "All Track Directed Self-Assembly of Block Copolymers: Process Flow and Origin of Defects." *Proc. SPIE*, **2012**; *8323*, 83230D.

(66) Delgadillo, P. R.; Gronheid, R.; Thode, C. J.; Wu, H.; Yi, C.; Neisser, M.; Somervell, M.; Nafus, K.; Nealey, P. F. "Implementation of a Chemo-Epitaxy Flow for Directed Self-Assembly on 300-mm Wafer Processing Equipment." *J. Micro/Nanolithogr., MEMS, MOEMS* **2012**, *11*, 031302.

(67) Nagpal, U.; Müller, M.; Nealey, P. F.; de Pablo, J. J. "Free Energy of Defects in Ordered Assemblies of Block Copolymer Domains." *ACS Macro Lett.* **2012**, *1*, 418–422.

(68) Hur, S.-M.; Thapar, V.; Ramírez-Hernández, A.; Khaira, G.; Segal-Peretz, T.; Rincon Delgadillo, P. A.; Li, W.; Müller, M.; Nealey, P. F.; de Pablo, J. J. "Molecular Pathways for Defect Annihilation in Directed Self-Assembly." *Proc. Nat. Acad. Sci.* **2015**, *112*, 14144–14149.

(69) Williamson, L. D.; Seidel, R. N.; Chen, X.; Suh, H. S.; Rincon Delgadillo, P.; Gronheid, R.; Nealey, P. F. "Three-Tone Chemical Patterns for Block Copolymer Directed Self-Assembly." *ACS Appl. Mater. Interfaces* **2016**, *8*, 2704–2712.

(70) Maher, M. J.; Bates, C. M.; Blachut, G.; Sirard, S.; Self, J. L.; Carlson, M. C.; Dean, L. M.; Cushen, J. D.; Durand, W. J.; Hayes, C. O.; Ellison, C. J.; Willson, C. G. "Interfacial Design for Block Copolymer Thin Films." *Chem. Mater.* **2014**, *26*, 1471–1479.

(71) Jastrzebski, L. "Heavy Metal Contamination During Integrated-Circuit Processing: Measurements of Contamination Level and Internal Gettering Efficiency by Surface Photovoltage." *Mater. Sci. Eng., B* **1989**, *4*, 113-121.

(72) Clarson, S. J.; Semlyen, J. A. *Siloxane Polymers*; Prentice-Hall: Englewood Cliffs, NJ, 1993.

(73) Cushen, J. D.; Otsuka, I.; Bates, C. M.; Halila, S.; Fort, S.; Rochas, C.; Easley, J. A.; Rausch, E. L.; Thio, A.; Borsali, R.; Willson, C. G.; Ellison, C. J.; "Oligosaccharide/Silicon-Containing Block Copolymers with 5 N=nm Features for Lithographic Applications." *ACS Nano* **2012**, *6*, 3424–3433.

(74) Hirao, A.; Ando, Y.; Ishizone, T.; Nakahama, S. "Anionic Polymerization of p-pentamethyldisilyl-, p-heptamethyltrisilyl-, and p-nonamethyltetrasilylstyrenes 1." *Macromolecules* **2003**, *36*, 5081–5087.

(75) Gabor, A. H.; Lehner, E. A.; Mao, G.; Schneggenburger, L. A.; Ober, C. K. "Synthesis and Lithographic Characterization of Block Copolymer Resists Consisting of Both Poly(Styrene) Blocks and Hydrosiloxane-Modified Poly(Diene) Blocks." *Chem. Mater.* **1994**, *6*, 927–934.

(76) Colburn, M.; Grot, A.; Choi, B. J.; Amistoso, M.; Bailey, T.; Sreenivasan, S. V.; Ekerdt, J. G.; Willson, C. G. "Patterning Nonflat Substrates with a Low Pressure, Room Temperature, Imprint Lithography Process." *J. Vac. Sci. Technol, B* **2001**, *19*, 2162–2172.

(77) Gu, X.; Gunkel, I.; Russell, T. P. "Pattern Transfer Using Block Copolymers." *Philos. Trans. R. Soc.* **2013**, *371*, 20120306.

(78) Matsen, M. W.; Thompson, R. B. "Equilibrium Behavior of Symmetric ABA Triblock Copolymer Melts." *J. Chem. Phys.* **1999**, *111*, 7139–7146.

(79) Matsen, M. W. "Architectural Effect on the Surface Tension of an ABA Triblock Copolymer Melt." *Macromolecules* **2010**, *43*, 1671–1674.

(80) Khanna, V.; Cochran, E. W.; Hexemer, A.; Stein, G. E.; Fredrickson, G. H.; Kramer, E. J.; Li, X.; Wang, J.; Hahn, S. F. "Effect of Chain Architecture and Surface Energies on the Ordering Behavior of Lamellar and Cylinder Forming Block Copolymers." *Macromolecules* **2006**, *39*, 9346–9356.

(81) Ji, S.; Nagpal, U.; Liu, G.; Delcambre, S. P.; Müller, M.; de Pablo, J. J.;

Nealey, P. F. "Directed Assembly of Non-Equilibrium ABA Triblock Copolymer Morphologies on Nanopatterned Substrates." *ACS Nano* **2012**, *6*, 5440–5448.
(82) Khaira, G. S.; Qin, J.; Garner, G. P.; Xiong, S.; Wan, L.; Ruiz, R.; Jaeger, H. M.; Nealey, P. F.; de Pablo, J. J. "Evolutionary Optimization of Directed Self-Assembly of Triblock Copolymers on Chemically Patterned Substrates." *ACS Macro Lett*. **2014**, *3*, 747–752.
(83) Cushen, J. D. High Interaction Parameter Block Copolymers for Advanced Lithography, The University of Texas at Austin, 2013.
(84) Durand, W. J. Design, Synthesis, and Engineering of Advanced Materials for Block Copolymer Lithography, The University of Texas at Austin, 2015.
(85) Hayes, L. J. "Surface Energy of Fluorinated Surfaces." *J. Fluorine Chem*. **1976**, *8*, 69–88.
(86) Owens, D. K.; Wendt, R. C. "Estimation of the Surface Free Energy of Polymers." *J. Appl. Polym. Sci*. **1969**, *13*, 1741–1747.
(87) Anslyn, E. V.; Dougherty, D. A. *Modern Physical Organic Chemistry*; University Science Books: Sausalito, CA, 2006.
(88) Coulon, G.; Ausserre, D.; Russell, T. P. "Interference Microscopy on Thin Diblock Copolymer Films." *J. Phys. France* **1990**, *51*, 777–786.
(89) Coulon, G.; Collin, B.; Ausserre, D.; Chatenay, D.; Russell, T. P. "Islands and Holes on the Free Surface of Thin Diblock Copolymer Films. I. Characteristics of Formation and Growth." *J. Phys. France* **1990**, *51*, 2801–2811.
(90) Coulon, G.; Collin, B.; Chatenay, D.; Gallot, Y. "Kinetics of Growth of Islands and Holes on the Free Surface of Thin Diblock Copolymer Films." *J. Phys. II France* **1993**, *3*, 697–717.
(91) Andersen, T. H.; Tougaard, S.; Larsen, N. B.; Almdal, K.; Johannsen, I. "Surface Morphology of PS–PDMS Diblock Copolymer Films." *J. Electron Spectrosco. Relat. Phenom*. **2001**, *121*, 93–110.
(92) Turner, M. S. "Equilibrium Properties of a Diblock Copolymer Lamellar Phase Confined Between Flat Plates." *Phys. Rev. Lett*. **1992**, *69*, 1788–1791.
(93) Bates, C. M.; Seshimo, T.; Maher, M. J.; Durand, W. J.; Cushen, J. D.; Dean, L. M.; Blachut, G.; Ellison, C. J.; Willson, C. G. "Polarity-Switching Top Coats Enable Orientation of Sub-10 nm Block Copolymer Domains." *Science* **2012**, *338*, 775–779.
(94) Durand, W. J.; Carlson, M. C.; Maher, M. J.; Blachut, G.; Santos, L. J.; Tein, S.; Ganesan, V.; Ellison, C. J.; Willson, C. G. "Experimental and Modeling Study of Domain Orientation in Confined Block Copolymer Thin Films." *Macromolecules* **2016**, *49*, 308–316.
(95) Vu, T.; Mahadevapuram, N.; Perera, G. M.; Stein, G. E. "Controlling Domain Orientations in Thin Films of AB and ABA Block Copolymers." *Macromolecules* **2011**, *44*, 6121–6127.
(96) US 13/922,011
(97) Duda, J. L. "Molecular Diffusion in Polymeric Systems." *Pure Appl. Chem.*

1985, *57*, 1681–1690.
(98) Houlihan, F. M.; Wallow, T. I.; Nalamasu, O.; Reichmanis, E. "Synthesis of Cycloolefin–Maleic Anhydride Alternating Copolymers for 193 nm Imaging." *Macromolecules* **1997**, *30*, 6517–6524.
(99) Pye, P. J.; Rossen, K.; Weissman, S. A.; Maliakal, A.; Reamer, R. A.; Ball, R.; Tsou, N. N.; Volante, R. P.; Reider, P. J. "Crystallization-Induced Diastereoselection: Asymmetric Synthesis of Substance P Inhibitors." *Chem. - Euro. J.* **2002**, *8*, 1372–1376.
(100) Pasquale, A. J.; Allen, R. D.; Long, T. E. "Fundamental Investigations of the Free Radical Copolymerization and Terpolymerization of Maleic Anhydride, Norbornene, and Norbornene tert-Butyl Ester: in-Situ Mid-Infrared Spectroscopic Analysis." *Macromolecules* **2001**, *34*, 8064–8071.
(101) Welander, A. M.; Kang, H.; Stuen, K. O.; Solak, H. H.; Müller, M.; de Pablo, J. J.; Nealey, P. F. "Rapid Directed Assembly of Block Copolymer Films at Elevated Temperatures." *Macromolecules* **2008**, *41*, 2759–2761.
(102) Clark, D. T.; Peeling, J.; O'malley, J. M. "Application of ESCA to Polymer Chemistry. VIII. Surface Structures of AB Block Copolymers of Polydimethylsiloxane and Polystyrene." *J. Polym. Sci. Polym. Chem. Ed.* **1976**, *14*, 543–551.
(103) Han, E.; Stuen, K. O.; La, Y.-H.; Nealey, P. F.; Gopalan, P. "Effect of Composition of Substrate-Modifying Random Copolymers on the Orientation of Symmetric and Asymmetric Diblock Copolymer Domains." *Macromolecules* **2008**, *41*, 9090–9097.
(104) Han, E.; Stuen, K. O.; Leolukman, M.; Liu, C.-C.; Nealey, P. F.; Gopalan, P. "Perpendicular Orientation of Domains in Cylinder-Forming Block Copolymer Thick Films by Controlled Interfacial Interactions." *Macromolecules* **2009**, *42*, 4896–4901.
(105) Bates, C. M. Advanced Materials for Block Copolymer Lithography, The University of Texas at Austin, 2013.
(106) Mayo, F. R.; Walling, C. Copolymerization. *Chem. Rev.* **1950**, *46*, 191–287.
(107) Lieber, E.; Rao, C.; Chao, T. S. "Infrared Spectra of Organic Azides." *Anal. Chem.* **1957**, *29*, 916-918.
(108) Jørgensen, J. K.; Ommundsen, E.; Stori, A.; Redford, K. "Synthesis, Characterisation and Decomposition of 1, 3-Benzene Disulfonyl Azide; a Cross-Linking Agent for Polyolefins." *Polymer* **2005**, *46*, 12073-12080.
(109) Janes, D. W.; Maher, M. J.; Carroll, G. T.; Saylor, D. M.; Ellison, C. J. "Modulating Solubility and Enhancing Reactivity of Photo-Cross-Linkable Poly(Styrene Sulfonyl Azide-*alt*-Maleic Anhydride) Thin Films." *Macromolecules* **2015**, *48*, 8361–8368.
(110) Peters, R. D.; Yang, X. M.; Kim, T. K.; Nealey, P. F. "Wetting Behavior of Block Copolymers on Self-Assembled Films of Alkylchlorosiloxanes: Effect of Grafting Density." *Langmuir* **2000**, *16*, 9620–9626.
(111) Coulon, G.; Collin, B.; Chatenay, D.; Gallot, Y. "Kinetics of Growth of Islands

and Holes on the Free Surface of Thin Diblock Copolymer Films." *J. Phys. II France* **1993**, *3*, 697–717.
(112) Lambooy, P.; Russell, T.; Kellogg, G.; Mayes, A.; Gallagher, P.; Satija, S. "Observed Frustration in Confined Block Copolymers." *Phys. Rev. Lett.* **1994**, *72*, 2899–2902.
(113) Kellogg, G. J.; Walton, D. G.; Mayes, A. M.; Lambooy, P.; Russell, T. P.; Gallagher, P. D.; Satija, S. K. "Observed Surface Energy Effects in Confined Diblock Copolymers." *Phys. Rev. Lett.* **1996**, *76*, 2503–2506.
(114) Collin, B.; Chatenay, D.; Coulon, G.; Ausserre, D.; Gallot, Y. "Ordering of Copolymer Thin Films as Revealed by Atomic Force Microscopy." *Macromolecules* **1992**, *25*, 1621–1622.
(115) Kim, S.; Bates, C. M.; Thio, A.; Cushen, J. D.; Ellison, C. J.; Willson, C. G.; Bates, F. S. "Consequences of Surface Neutralization in Diblock Copolymer Thin Films." *ACS Nano* **2013**, *7*, 9905–9919.
(116) Stasiak, P.; McGraw, J. D.; Dalnoki-Veress, K.; Matsen, M. W. "Step Edges in Thin Films of Lamellar-Forming Diblock Copolymer." *Macromolecules* **2012**, *45*, 9531–9538.
(117) Trivedi, B. C.; Culbertson, B. M. *Maleic Anhydride*; Plenum Press: New York, NY, 1982.
(118) Lin, J. W. P.; Dudek, L.P.; Majumdar, D. "Wetting Properties of Homopolymers and Copolymers of Pentafluorostyrene and Methylacrylate and Homopolymer Blends." *J. Appl. Polym. Sci.* **1987**, *33*, 657–667.
(119) Moore, E. "Properties of Styrene-Maleic Anhydride Copolymers." *Ind. Eng. Chem. Prod. Res. Dev.* **1986**, *25*, 315–321.
(120) Liu, C.-C.; Ramírez-Hernández, A.; Han, E.; Craig, G. S. W.; Tada, Y.; Yoshida, H.; Kang, H.; Ji, S.; Gopalan, P.; de Pablo, J. J.; Nealey, P.F. "Chemical Patterns for Directed Self-Assembly of Lamellae-Forming Block Copolymers with Density Multiplication of Features." *Macromolecules* **2013**, *46*, 1415–1424.
(121) Silverstein, R. M.; Webster, F. X.; Kiemle, D. J. *Spectrophotometric Identification of Organic Compounds*; 7 ed.; John Wiley & Sons: Hoboken, NJ, 2005.
(122) Cushen, J. D.; Wan, L.; Pandav, G.; Mitra, I.; Stein, G. E.; Ganesan, V.; Ruiz, R.; Grant Willson, C.; Ellison, C. J. "Ordering Poly(Trimethylsilylstyrene-*block*- D, L-Lactide) Block Copolymers in Thin Films by Solvent Annealing Using a Mixture of Domain-Selective Solvents." *J. Polym. Sci., Part B: Polym. Phys.* **2014**, *52*, 36-45.
(123) Delgadillo, P. R.; Suri, M.; Durant, S.; Cross, A.; Nagaswami, V. R.; Heuvel, D. V. D.; Gronheid, R.; Nealey, P. "Defect Source Analysis of Directed Self-Assembly Process." *J. Micro/Nanolithogr., MEMS, MOEMS* **2013**, *12*, 031112.
(124) Welander, A. M.; Craig, G. S. W.; Tada, Y.; Yoshida, H.; Nealey, P. F. "Directed Assembly of Block Copolymers in Thin to Thick Films." *Macromolecules* **2013**, *46*, 3915–3921.

(125) Israelachvili, J. N. *Intermolecular & Surface Forces*; 2nd ed.; Academic Press: San Diego, CA, 1992.
(126) Brandrup, J.; Immergut, E. H.; Grulke, E. A.; Abe, A. *Polymer Handbook*; John Wiley and Sons, 2005.
(127) Albrecht, T. R.; Bedau, D.; Dobisz, E.; Gao, H.; Grobis, M.; Hellwig, O.; Kercher, D.; Lille, J.; Marinero, E.; Patel, K.; Ruiz, R.; Schabes, M. E.; Wan, L.; Weller, D.; Wu, T-W. "Bit Patterned Media at 1 Tdot/in^2 And Beyond." *IEEE Trans. Magn.* **2013**, *49*, 773–778.
(128) Keen, I.; Yu, A.; Cheng, H.-H.; Jack, K. S.; Nicholson, T. M.; Whittaker, A. K.; Blakey, I. "Control of the Orientation of Symmetric Poly (Styrene)-*block*-Poly (D, L-Lactide) Block Copolymers Using Statistical Copolymers of Dissimilar Composition." *Langmuir* **2012**, *28*, 15876–15888.
(129) Kim, S.; Nealey, P. F.; Bates, F. S. "Decoupling Bulk Thermodynamics and Wetting Characteristics of Block Copolymer Thin Films." *ACS Macro Lett.* **2012**, *1*, 11–14.
(130) Li, H.; Gu, W.; Li, L.; Zhang, Y.; Russell, T. P.; Coughlin, E. B. "Synthesis of Semicrystalline/Fluorinated Side-Chain Crystalline Block Copolymers and Their Bulk and Thin Film Nanoordering." *Macromolecules* **2013**, *46*, 3737–3745.
(131) Kennemur, J. G.; Yao, L.; Bates, F. S.; Hillmyer, M. A. "Sub-5 nm Domains in Ordered Poly(Cyclohexylethylene)-*block*-Poly(Methyl Methacrylate) Block Polymers for Lithography." *Macromolecules* **2014**, *47*, 1411–1418.
(132) Bates, C. M.; Pantoja, M. A. B.; Strahan, J. R.; Dean, L. M.; Mueller, B. K.; Ellison, C. J.; Nealey, P. F.; Willson, C. G. "Synthesis and Thin-Film Orientation of Poly(Styrene-*block*-Trimethylsilylisoprene)." *J. Polym. Sci., Part A: Polym. Chem.* **2012**, *51*, 290–297.
(133) Doerk, G. S.; Liu, C.-C.; Cheng, J. Y.; Rettner, C. T.; Pitera, J. W.; Krupp, L. E.; Topuria, T.; Arellano, N.; Sanders, D. P. "Pattern Placement Accuracy in Block Copolymer Directed Self-Assembly Based on Chemical Epitaxy." *ACS Nano* **2013**, *7*, 276–285.
(134) Doerk, G. S.; Cheng, J. Y.; Rettner, C. T.; Balakrishnan, S.; Arellano, N.; Sanders, D. P. "Deterministically Isolated Gratings Through the Directed Self-Assembly of Block Copolymers." *Proc. SPIE* **2013**, *8680*, 86800Y.
(135) Chang, J.-B.; Choi, H. K.; Hannon, A. F.; Alexander-Katz, A.; Ross, C. A.; Berggren, K. K. "Design Rules for Self-Assembled Block Copolymer Patterns Using Tiled Templates." *Nat. Commun.* **2014**, *5*, 3305.
(136) Cheng, J. Y.; Sanders, D. P.; Truong, H. D.; Harrer, S.; Friz, A.; Holmes, S.; Colburn, M.; Hinsberg, W. D. "Simple and Versatile Methods to Integrate Directed Self-Assembly with Optical Lithography Using a Polarity-Switched Photoresist." *ACS Nano* **2010**, *4*, 4815–4823.
(137) Liu, C.-C.; Nealey, P. F.; Raub, A. K.; Hakeem, P. J.; Brueck, S. R. J.; Han, E.; Gopalan, P. "Integration of Block Copolymer Directed Assembly with 193 Immersion Lithography." *J. Vac. Sci. Technol., B* **2010**, *28*, C6B30.

(138) Gronheid, R. "Frequency Multiplication of Lamellar Phase Block Copolymers with Grapho-Epitaxy Directed Self-Assembly Sensitivity to Prepattern." *J. Micro/Nanolithogr., MEMS, MOEMS* **2012**, *11*, 031303.
(139) Mansky, P.; Russell, T. P.; Hawker, C. J.; Mays, J.; Cook, D. C.; Satija, S. K. "Interfacial Segregation in Disordered Block Copolymers: Effect of Tunable Surface Potentials." *Phys. Rev. Lett.* **1997**, *79*, 237–240.
(140) Grigorescu, A. E.; van der Krogt, M. C.; Hagen, C. W.; Kruit, P. "10nm Lines and Spaces Written in HSQ using Electron Beam Lithography." *Microelectron. Eng.* **2007**, *84*, 822–824.
(141) Cheng, J. Y.; Rettner, C. T.; Sanders, D. P.; Kim, H.-C.; Hinsberg, W. D. "Dense Self-Assembly on Sparse Chemical Patterns: Rectifying and Multiplying Lithographic Patterns Using Block Copolymers." *Adv. Mater.* **2008**, *20*, 3155–3158.
(142) Hinsberg, W.; Cheng, J.; Kim, H.-C.; Sanders, D. P. "Self-Assembling Materials for Lithographic Patterning: Overview, Status, and Moving Forward." *Proc. SPIE* **2010**, *7637*, 76370G.
(143) Farrell, R. A.; Hosler, E. R.; Schmid, G. M.; Xu, J.; Preil, M. E.; Rastogi, V.; Mohanty, N.; Kumar, K.; Cicoria, M. J.; Hetzer, D. R.; Devilliers, A. J. "Manufacturability Considerations for DSA." *Proc. SPIE* **2014**, *9051*, 90510Z.
(144) Park, S. M.; Stoykovich, M. P.; Ruiz, R.; Zhang, Y.; Black, C. T.; Nealey, P. F. "Directed Assembly of Lamellae- Forming Block Copolymers by Using Chemically and Topographically Patterned Substrates." *Adv. Mater.* **2007**, *19*, 607–611.
(145) Pandav, G.; Durand, W. J.; Ellison, C. J.; Willson, C. G.; Ganesan, V. "Directed Self Assembly of Block Copolymers Using Chemical Patterns with Sidewall Guiding Lines, Backfilled with Random Copolymer Brushes." *Soft Matter* **2015**, *11*, 9107–9114.
(146) Cushen, J. D.; Wan, L.; Blachut, G.; Maher, M. J.; Albrecht, T. R.; Ellison, C. J.; Willson, C. G.; Ruiz, R. "Double-Patterned Sidewall Directed Self-Assembly and Pattern Transfer of Sub-10 nm PTMSS-*b*-PMOST." *ACS Appl. Mater. Interfaces* **2015**, *7*, 13476–13483.
(147) Ghani, M. A. A.; Abdallah, D.; Kazmaier, P. M.; Keoshkerian, B.; Buncel, E. "Multi-Armed, TEMPO-Functionalized Unimolecular Initiators for Starburst Dendrimer Synthesis via Stable Free Radical Polymerisation. 2. Tris (1,3,5)Benzyloxy Unimers." *Can. J. Chem.* **2004**, *82*, 1403–1412.
(148) Hawker, C. J.; Hedrick, J. L. "Accurate Control of Chain Ends by a Novel "Living" Free-Radical Polymerization Process." *Macromolecules* **1995**, *28*, 2993–2995.
(149) Maher, M. J.; Bates, C. M.; Blachut, G.; Carlson, M. C.; Self, J. L.; Janes, D. W.; Durand, W. J.; Lane, A. P.; Ellison, C. J.; Willson, C. G. "Photopatternable Interfaces for Block Copolymer Lithography." *ACS Macro Lett.* **2014**, 824–828.
(150) Lille, J.; Ruiz, R.; Wan, L.; Gao, H.; Dhanda, A.; Zeltzer, G.; Arnoldussen, T.;

Patel, K.; Tang, Y.; Kercher, D. "Integration of Servo and High Bit Aspect Ratio Data Patterns on Nanoimprint Templates for Patterned Media." *IEEE Trans. Magn.* **2012**, *48*, 2757–2760.

(151) Tavakkoli K G, A.; Gotrik, K. W.; Hannon, A. F.; Alexander Katz, A.; Ross, C. A.; Berggren, K. K. "Templating Three-Dimensional Self-Assembled Structures in Bilayer Block Copolymer Films." *Science* **2012**, *336*, 1294–1298.

(152) Doerk, G. S.; Cheng, J. Y.; Singh, G.; Rettner, C. T.; Pitera, J. W.; Balakrishnan, S.; Arellano, N.; Sanders, D. P. "Enabling Complex Nanoscale Pattern Customization Using Directed Self-Assembly." *Nat. Commun.* **2014**, *5*, 5805.

(153) Shin, D. O.; Kim, B. H.; Kang, J.-H.; Jeong, S.-J.; Park, S. H.; Lee, Y.-H.; Kim, S. O. "One-Dimensional Nanoassembly of Block Copolymers Tailored by Chemically Patterned Surfaces." *Macromolecules* **2009**, *42*, 1189–1193.

(154) Liu, G.; Thomas, C. S.; Craig, G. S. W.; Nealey, P. F. "Integration of Density Multiplication in the Formation of Device-Oriented Structures by Directed Assembly of Block Copolymer-Homopolymer Blends." *Adv. Funct. Mater.* **2010**, *20*, 1251–1257.

(155) Han, E.; Leolukman, M.; Kim, M.; Gopalan, P. "Resist Free Patterning of Nonpreferential Buffer Layers for Block Copolymer Lithography." *ACS Nano* **2010**, *4*, 6527–6534.

(156) Cheng, J.; Lawson, R. A.; Yeh, W.-M.; Tolbert, L. M.; Henderson, C. L. "Developing Directly Photodefinable Substrate Guiding Layers for Block Copolymer Directed Self-Assembly (DSA) Patterning." *Proc. SPIE* **2011**, *7972*, 79722I.

(157) Conlon, D. A.; Crivello, J. V.; Lee, J. L.; O'Brien, M. J. "The Synthesis, Characterization, and Deblocking of Poly(4-tert-Butoxystyrene) and Poly(4-tert-Butoxy-α-Methylstyrene)." *Macromolecules* **1989**, *22*, 509–516.

(158) Pompe, T.; Zschoche, S.; Herold, N.; Salchert, K.; Gouzy, M.-F.; Sperling, C.; Werner, C. "Maleic Anhydride Copolymers: A Versatile Platform for Molecular Biosurface Engineering." *Biomacromolecules* **2003**, *4*, 1072–1079.

(159) Jeong, S.-J.; Moon, H.-S.; Shin, J.; Kim, B. H.; Shin, D. O.; Kim, J. Y.; Lee, Y.-H.; Kim, J. U.; Kim, S. O. "One-Dimensional Metal Nanowire Assembly via Block Copolymer Soft Graphoepitaxy." *Nano Lett.* **2010**, *10*, 3500–3505.

(160) Merriam, A. J.; Bethune, D. S.; Hoffnagle, J. A.; Hinsberg, W. D.; Jefferson, C. M.; Jacob, J. J.; Litvin, T. "A Solid-State 193-nm Laser with High Spatial Coherence for Sub-40 nm Interferometric Immersion Lithography." *Proc. SPIE* **2007**, *6520*, 65202Z.

(161) Maher, M. J.; Bates, C. M.; Durand, W. J.; Blachut, G.; Janes, D. W.; Cheng, J. Y.; Sanders, D. P.; Willson, C. G.; Ellison, C. J. "Interfacial Layers with Photoswitching Surface Energy for Block Copolymer Alignment and Directed Self-Assembly." *J. Photopolym. Sci. Technol.* **2015**, *28*, 611–615.

(162) Maher, M. J.; Rettner, C. T.; Bates, C. M.; Blachut, G.; Carlson, M. C.; Durand, W. J.; Ellison, C. J.; Sanders, D. P.; Cheng, J. Y.; Willson, C. G.

"Directed Self-Assembly of Silicon-Containing Block Copolymer Thin Films." *ACS Appl. Mater. Interfaces* **2015**, *7*, 3323–3328.

(163) Albrecht, T. R.; Arora, H.; Ayanoor-Vitikkate, V.; Beaujour, J.-M.; Bedau, D.; Berman, D.; Bogdanov, A. L.; Chapuis, Y.-A.; Cushen, J.; Dobisz, E. E.; Doerk, G.; Gao, H.; Grobis, M.; Gurney, B.; Hanson, W.; Hellwig, O.; Hirano, T.; Jubert, P-O.; Kercher, D.; Lille, J.; Liu, Z.; Mate, C. M.; Obukhov, Y.; Patel, K. C.; Rubin, K.; Ruiz, R.; Schabes, M.; Wan, L.; Weller, D.; Wu, T-W.; Yang, E. "Bit-Patterned Magnetic Recording: Theory, Media Fabrication, and Recording Performance." *IEEE Trans. Magn.* **2015**, *51*, 1–42.

(164) Janes, D. W.; Thode, C. J.; Willson, C. G.; Nealey, P. F.; Ellison, C. J. "Light-Activated Replication of Block Copolymer Fingerprint Patterns." *Macromolecules* **2013**, *46*, 4510–4519.

(165) Inoue, T.; Janes, D. W.; Ren, J.; Suh, H. S.; Chen, X.; Ellison, C. J.; Nealey, P. F. "Molecular Transfer Printing of Block Copolymer Patterns Over Large Areas with Conformal Layers." *Adv. Mater. Interfaces* **2015**, *2*, 1500133.

(166) Resnick, D. J.; Sreenivasan, S. V.; Willson, C. G. "Step & Flash Imprint Lithography." *Mater. Today* **2005**, *8*, 34–42.

(167) Labadie, J. W.; MacDonald, S. A.; Willson, C. G. "Organotin Polymer: Synthesis and Resist Properties." *Journal of Imag. Sci.* **1986**, *30*, 169–173.

(168) Sankaran, V.; Cohen, R. E.; Cummins, C. C.; Schrock, R. R. "Morphology of Diblock Copolymers of Norbornene and Organometallic Derivatives of Norbornene." *Macromolecules* **1991**, *24*, 6664–6669.

(169) Cummins, C. C.; Beachy, M. D.; Schrock, R. R.; Vale, M. G.; Sankaran, V.; Cohen, R. E. "Synthesis of Norbornenes Containing Tin(II), Tin(IV), Lead(II), and Zinc(II) and Their Polymerization to Give Microphase-Separated Block Copolymers." *Chem. Mater.* **1991**, *3*, 1153–1163.

(170) David-Quillot, F.; Duchêne, A.; Catala, J. M.; Balland-Longeau, A.; Thibonnet, J. "Living Radical Polymerization of Styrene Derivatives Containing Trialkylmetal Groups." *J. Macromol. Sci., Part A* **2010**, *47*, 461–467.

(171) Yamazaki, N.; Nakahama, S.; Hirao, A.; Goto, J.; Shiralshi, Y.; Martinez, F.; Phung, H. M. "Anionic Polymerization of P Triphenyltin Styrene." *J. Macromol. Sci., Chem.* **1981**, *16*, 1129–1144.

(172) Mori, K.; Blachut, G.; Bates, C. M.; Maher, M. J.; Strahan, J. R.; Sirard, S. M.; Durand, W. J.; Ellison, C. J.; Willson, C. G. "A Study of Tin-Containing Block Copolymers." *J. Photopolym. Sci. Technol.* **2014**, *27*, 445–448.

(173) Roe, R.-J. *Methods of X-Ray and Neutron Scattering in Polymer Science*; 1st ed.; Oxford University Press: New York, 2000.

(174) Garra, J.; Long, T.; Currie, J.; Schneider, T.; White, R.; Paranjape, M. "Dry Etching of Polydimethylsiloxane for Microfluidic Systems." *J. Vac. Sci. Technol., A* **2002**, *20*, 975–982.